INFORMATION TO USERS

NOTE TO USERS

The original manuscript received by UMI contains pages with slanted print. Pages were microfilmed as received.

This reproduction is the best copy available

UMI

University of Alberta

A Multi-Yield Surface Model in Reference State Soil Mechanics for Cohesionless Soils and Liquefaction Problems

by

Manouchehr Latifi Namin   ©

A thesis submitted to the Faculty of Graduate Studies and Research in partial fulfillment of the requirements for the degree of Doctor of Philosophy

in

Geotechnical Engineering

Department of Civil and Environmental Engineering

Edmonton, Alberta

Spring 1998

The author has granted a non-exclusive licence allowing the National Library of Canada to reproduce, loan, distribute or sell copies of this thesis in microform, paper or electronic formats.

The author retains ownership of the copyright in this thesis. Neither the thesis nor substantial extracts from it may be printed or otherwise reproduced without the author's permission.

L'auteur a accordé une licence non exclusive permettant à la Bibliothèque nationale du Canada de reproduire, prêter, distribuer ou vendre des copies de cette thèse sous la forme de microfiche/film, de reproduction sur papier ou sur format électronique.
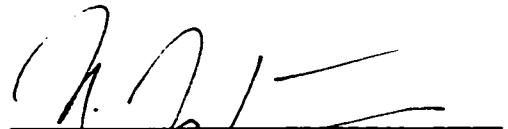
L'auteur conserve la propriété du droit d'auteur qui protège cette thèse. Ni la thèse ni des extraits substantiels de celle-ci ne doivent être imprimés ou autrement reproduits sans son autorisation.

0-612-29060-3

Canada
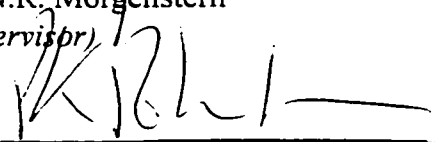
University of Alberta

Faculty of Graduate Studies and Research

The undersigned certify that they have read. and recommend to the Faculty of Graduate Studies and Research for acceptance, a thesis entitled **A Multi-Yield Surface Model in Reference State Soil Mechanics for Cohesionless Soils and Liquefaction Problems** submitted by **Manouchehr Latifi Namin** in partial fulfillment of the requirements for the degree of Doctor of Philosophy in Geotechnical Engineering.

Dr. N.R. Morgenstern
(Supervisor)

Dr. P.K. Robertson
(Co-Supervisor)

Dr. D. Chan
(Co-Supervisor)

Dr. T.M. Hrudey

Dr. A.W. Lipsett

Dr. J.H. Prevost
(External Examiner)

Date: 26 Sept 1997

To My Wife, Our Children and
To My Father and Mother

ABSTRACT

Liquefaction of cohesionless soils is a phenomenon that has caused a number of catastrophic events in the past. The term "liquefaction" has been used by different researchers to define both flow liquefaction in strain-softening soils and cyclic liquefaction caused during cyclic loading with shear reversal. During the last decades, different approaches have been proposed to analyze these catastrophic phenomena. Empirical criteria based on field observations, total stress analysis and effective stress analysis are the three main approaches in this area. It is believed that effective stress analysis, using constitutive models, is the most powerful tool to determine permanent deformations during and after liquefaction. None of the elements in the effective stress approach is as important as the constitutive model.
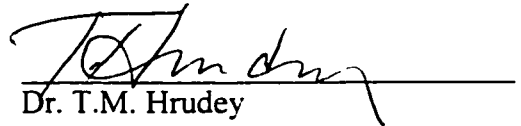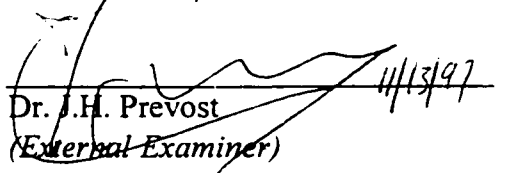
The state of the soil has a significant effect on its behavior. In most existing constitutive models for cohesionless soils, this important factor has been overlooked. As a result, these models can be used only for a small range of stresses and void ratios for which the model has been calibrated. In this study, after showing the limitation of models with no reference, a framework, termed "Reference State Soil Mechanics," is proposed. In this framework the multi-yield surface theory is extended to embrace "Reference State Soil Mechanics". The modified model is capable of predicting drained and undrained responses of loose and dense sands under both monotonic and cyclic loading with a unique set of parameters. At large strains, this model shows the same ultimate state condition for both loose and dense sands. The model can also represent the effects of

initial cross-anisotropy and induced anisotropy. Two different hardening rules have been used and compared with each other for specimens at different states. Validation of the model has been achieved using comprehensive comparisons of the model predictions with experimental observations on different sands with various physical properties under both monotonic and cyclic loading. It is shown that this model is capable of handling both flow liquefaction and cyclic liquefaction in a unique framework.

ACKNOWLEDGEMENTS

TABLE OF CONTENTS

Page

LIST OF TABLES

LIST OF FIGURES

Page

CHAPTER 1

CHAPTER 2

CHAPTER 3

CHAPTER 4

CHAPTER 5

APPENDIX

Chapter 1

INTRODUCTION

1.1. Introduction

Liquefaction of soils and associated ground failure have been the main cause of extensive damage to public facilities. life lines and residential buildings during some of the past major earthquakes. Especially after the two major earthquakes of March 27, 1964 in Anchorage. Alaska and of June 16, 1964 in Nigata. Japan. geotechnical engineers have started to study the mechanism of liquefaction and its consequences in relation to the stability of structures constructed with or on cohesionless soils.

Soil liquefaction is a phenomenon by which a soil mass transforms from a solid state to a nearly liquid state. Liquefaction has been observed in granular soils whose shear strength is primarily based on the frictional resistance of grains. It is believed that if an element of saturated cohesionless soil with relatively low permeability is subjected to a rapid distortion, the behavior will be undrained controlled mainly by the tendency of the soil skeleton to contract or dilate. If the initial state of confining pressure and relative density cause the soil skeleton to undergo a contractive response. it is expected that this

contractive tendency will be counteracted by a pore pressure increase in a situation with no volume change.

Despite a lot of research over the past three decades, there are still conflicting opinions concerning the critical aspects of the phenomenon of soil liquefaction, including the definition of "liquefaction".

It seems the term "liquefaction" was used for the first time in a paper by Hazen (1920) in which the failure of the hydraulic fill sands in the Calaveras Dam was described. On March 24, 1918, the upstream toe of the Calaveras Dam which was under construction suddenly flowed and approximately 730,000 m^3 of material moved around 90 m. Apparently at the time of the failure, no special disturbance was noticed. Hazen stated that if the pressure of the water in the pores of a sandy soil is great enough, it will have the effect of holding the particles apart, producing a condition that is practically equivalent to that of quick clay.

At present the term "liquefaction" is used in a broad sense for several phenomena in which either loss in strength or reduction in stiffness takes place in a cohesionless soil resulting in large deformations.

On the one hand, the phenomenon of liquefaction is associated with a condition of zero effective stress caused by progressive increases in pore water pressure which result from the tendency towards densification of the sand structure subjected to cyclic undrained loading (Seed and Lee, 1966; Lee and Seed, 1967). The condition of zero effective stress may be temporary during each loading cycle, but the associated shear strains may be so large that the consequences can be catastrophic.

On the other hand, the term "liquefaction" has been used to describe the strain softening behavior of loose sands sheared under undrained conditions (Castro, 1969; Casagrande, 1975). Loading a loose sand under undrained condition beyond the peak

point of the stress-strain curve results in a marked reduction in strength with increasing strain until the stress stabilizes at an ultimate or residual strength (Castro, 1969; Bishop, 1971; Hanzawa, 1980).

In 1975, Casagrande stated that the term "liquefaction" was used in the literature until 1966 to describe the response of saturated loose sands to strains or shocks which resulted in flow slides. He implied that with the development of the cyclic triaxial test in connection with earthquake research, liquefaction was used to describe a specific response of sand in cyclic triaxial tests. Casagrande insisted that this was a separate phenomenon which describes the response of a dilatant sand to cyclic loading in a triaxial test when the peak pore pressure rises momentarily in each cycle to the confining pressure.

This difference between definitions used by the Berkeley group (Seed and Lee, 1966) and Casagrande (1975) was not only a discussion over terminology, but also over practical significance. Based on the Berkeley group's concept, the higher the initial or static shear stress, the more resistant the sand will be to the development of liquefaction. Castro (1969), however, showed that with the increase of the shear stress, the possibility of liquefaction increased. Subsequently, Rollins and Seed (1988) modified the Berkeley approach by recognizing that for loose sands the increase of static stress increases liquefaction susceptibility.

In the terminology which has been suggested by Robertson (1994), liquefaction can be classified into three categories: 1) flow liquefaction 2) cyclic liquefaction and 3) cyclic mobility .

Flow liquefaction has been observed in loose saturated cohesionless soils. Its main features are the large amount of soil involved in the failure, the short time of its occurrence and the very flat slope that is finally reached. This kind of liquefaction can be triggered either by monotonic effects, such as rapid construction or over steepening of a

slope, or by cyclic effects, such as earthquake, blasting or pile driving. This kind of liquefaction requires a strain softening response in undrained shear loading, resulting in a constant shear resistance at large strains. It also requires that in-situ shear stresses be greater than the ultimate or residual undrained shear strength. For failure of a soil structure to occur, such as a slope, a sufficient volume of material must strain soften. The resulting failure can be a slide or a flow depending on the material characteristics and slope geometry. The resulting movements are the result of internal causes and can arise after the trigger mechanism occurs. It can occur in any metastable saturated soil, such as very loose granular deposits, very sensitive clays and loess (silt) deposits. The schematic triggering condition for flow failure is illustrated in Figure 1.1.

In cyclic liquefaction (see Figure 1.2), pore pressures increase under undrained cyclic loading with shear stress reversal and the effective confining stress can reach zero. At the point of zero effective confining stress, no shear stress can exist. When shear stress is applied, pore pressures drop and a very soft initial stress-strain response can develop resulting in large deformations. Soil will strain harden with increasing shear strain.

This kind of liquefaction requires undrained cyclic loading where shear stress reversal or zero shear stress can develop: in other words, where in-situ static gravitational shear stress is low compared to the cyclic shear stresses. In addition, the number of cycles or strain must be sufficient to allow the effective confining stress to reach zero.

Deformations during cyclic loading when the effective stress is approximately zero can be large, but deformations generally stabilize when cyclic loading stops. The resulting movements are primarily the result of external causes and occur only during the cyclic loading. Subsequent movements can occur due to pore pressure redistribution. However, this will depend on ground conditions and soil stratigraphy.

Cyclic liquefaction can occur in almost all sands, provided the size and duration of cyclic loading is sufficiently large. For dense sands the size and duration of cyclic

loading must be large: hence. the condition of zero effective confining stress may not always be achieved. Clays can also experience cyclic liquefaction. but deformations at zero effective stress may be small due to the possible cohesive strength.

Cyclic mobility also requires undrained cyclic loading (see Figure 1.3). but no shear stress reversal develops. As a result. zero effective stress does not develop. Deformation during cyclic loading will stabilize. The resulting movements are the result of external causes and only occur during the cyclic loading. Clays can also experience cyclic mobility.

Since flow liquefaction involves a loss in strength. in general. it can be more catastrophic than the other two kinds of liquefaction. There are several case histories where flow failure have been observed. The failures of the Calaveras Dam (Hazen. 1920). Fort Peck Dam (Middlebrooks. 1942: Casagrande. 1965). Lower San Fernando Dam (Seed et al.. 1975: Castro et al.. 1985). the Norwegian fjords (Bjerrum. 1971). the Nerlerk berm (Sladen et al.. 1985-b: Been et al.. 1987-b) and the Fraser River delta of British Columbia (Chillarige et al.. 1994: Chillarige. 1995) are some of these cases.

Several major catastrophic phenomena. especially over the last 30 years. have heightened our awareness of the technical shortcomings for evaluating soil response during and after liquefaction. The 1964 earthquakes at Nigata and Anchorage and the resulting slide in the Lower San Fernando Dam (1971) may be the three most important events since 1964 in advancing our knowledge and understanding of the seismic behavior of soils. Awareness of the need for more sophistication in earthquake engineering was high during the mid-1960s. and technical advances were made at a rapid rate. Throughout the 1970s and 1980s researchers learned a great deal about the liquefaction susceptibility of various soil types. Procedures to predict liquefaction based on a combination of analytical techniques. laboratory tests and empirical data were developed. modified and simplified during this period. Other important advances were made in effective stress analysis and the estimation of large permanent deformations.

The intent of the next section is to trace developments from the late 1960s. when we were using very crude methods to evaluate whether or not liquefaction could occur. through the 1970s and 1980s. when we learned a great deal about the liquefaction susceptibility of various kinds of soils. to today, when we are predicting deformations that might occur following liquefaction.

1.2. Analysis of liquefaction

In this section the different methods for evaluating the various phenomena which have been called liquefaction will be briefly reviewed. For the sake of clarity. cyclic liquefaction and flow liquefaction will be discussed separately.

1.2.1. Cyclic liquefaction

The methods which have been proposed to evaluate the cyclic liquefaction potential of ground may be classified as follows:

- Empirical criteria based on field observations
- Total stress approach
- Effective stress approach

1.2.1.1. Empirical criteria based on field observations

Following the Nigata earthquake, a number of Japanese engineers (Kishida. 1966: Koizumi, 1966: Ohsaki, 1966) studied the areas in Nigata where liquefaction had and had not occurred and developed criteria. based primarily on the Standard Penetration Test (SPT) resistance of the sand deposits, for differentiating between liquefiable and nonliquefiable conditions in that city (Figure 1.4). It should be recognized. however. that

the results are not likely to be applicable to other areas where shaking intensities may be stronger or water tables may be at different depths than that in the Nigata area.

Subsequently, Seed and Peacock(1971) presented a more comprehensive collection of site conditions at various locations where some evidence of liquefaction or no liquefaction was known to have taken place. This study was used as a basis to determine the relationship between field values of cyclic stress ratio and the relative density of the sand, as determined from the SPT. Liquefaction was assumed to have occurred based on the presence of observable surface features such as sand boils and ground cracks. This collection of field cases has subsequently been used by others. often supplemented by a few additional site studies (e.g.. Castro. 1975; Christian and Swiger. 1975). to determine other correlations between liquefaction producing parameters and penetration resistance.

The earthquake induced cyclic shear stress ratios acting on the soil at depth can be estimated from the ground surface acceleration using the following simplified equation (Seed and Idriss. 1971):

$$\frac{\tau_{av}}{\sigma_0} \approx 0.65 \frac{a_{max}}{g} \frac{\sigma_0}{\sigma_0'} r_d \qquad (1\text{-}1)$$

where a_{max}. σ_0. σ_0' and r_d are maximum acceleration at the ground surface. total overburden pressure on sand layer under consideration. effective overburden pressure on sand layer and a stress reduction factor. respectively. Therefore. the possibility of cyclic liquefaction. for any given site and a given value of maximum ground surface acceleration. can be obtained on an empirical basis using a chart by measuring the values of N_1 for the sand layer involved.

In his later publication of 1985, Seed, based on the recommendation of Kovacs et al. (1983) and Kavazanjian et al. (1983), considered an energy ratio of 60% as the average energy delivered by hammers for standardizing the N_1-value. Hence. at present $(N_1)_{60}$ value is used instead of N_1 value in measuring liquefaction resistance. Seed recognized

that dense sands ($(N_1)_{60} > 15$) generally experienced less deformation for a given cyclic loading than loose sands.

To include the influence of fines content, Seed et al. (1985) developed the correction further as shown in Figure 1.5. This correlation shows that for the same cyclic resistance ratio, the penetration resistance in silty sands is smaller. This is probably due to the greater compressibility and decreased permeability of silty sands which reduces penetration resistance and moves the penetration process toward an undrained penetration. At the recent NCEER workshop (1996) a correction curve based on fines content was also developed and recommended for use in practice as shown in Figure 1.6.

Figure 1.5 is based on an earthquake magnitude of M=7.5, an effective overburden pressure of 100 kPa (1 tsf) and level ground conditions. The latter condition signifies that there are no static shear stresses on horizontal planes. The popularity of the Seed method for assessing liquefaction has resulted in it being applied outside the conditions on which the curve in Figure 1.5 was based. In recent years it has been applied to embankment dams and their foundations. In these situations, overburden pressures are much higher and large static shear stresses exist on potential failure planes. These applications have challenged engineers and researchers to adapt the basic liquefaction resistance curve to these changed conditions and to other earthquake magnitudes. This has resulted in corrections being applied to the cyclic resistance ratio by means of correction factors K_m, K_σ, and K_α: K_m for earthquake magnitude, K_σ for overburden pressure effects and K_α for static shear stress effects. Different researchers have proposed varying correction factors.

Scaling factors, K_m, are used to modify the original curve for other earthquake magnitudes. Seed and Idriss (1982) proposed factors which were based on data from large-scale laboratory simple shear tests. It has been recognized in recent years that these

scaling factors may be somewhat conservative for M<7.5 . Ambraseys (1988) proposed much larger scaling factors based on analysis of field data. More recently. Arango (1996) has studied this issue again. His factors are also much larger than the Seed and Idriss (1982) factors. and are generally somewhat less than those of Ambraseys. The NCEER committee (1996) selected tentative scaling factors which are very similar to the lowest factors proposed by Arango (1996) (see Figure 1.7).

A further correction must be made to the cyclic resistance ratio for overburden pressure. K_σ. Although the curve proposed by Seed and Harder (1990) is used widely in practice. research during recent years has demonstrated that using this curve can be very conservative. The NCEER committee has reviewed the research by Vaid and Chern (1985); Vaid and Thomas (1995); Koester (1992) and Arango (1996) and has recommended a new K_σ curve for practice that leads to substantially smaller corrections to the cyclic resistance (Figure 1.8).

A review of the available data suggests that K_σ depends to some extent on the soil type and grading. Therefore. for high hazard structures. it is recommended that site specific K_σ be determined by testing high quality undisturbed samples such as coring samples from frozen ground. Although this is an expensive process. reliable estimates of K_σ may lead to major savings in remediation costs.

The most controversial correction to the basic curve is the correction for static shear using K_α. The K_α factors which are currently used in practice are those recommended by Seed and Harder (1990). Boulanger et al.(1991) have suggested a revised version of the Seed and Harder (1990) curve which has a much narrower range of K_α values. It is limited to pressures less than 300 kPa. The NCEER committee (1996) has tentatively recommended that the Boulanger et al. (1991) correlation for effective overburden pressures less than 300 kPa be adopted in practice. However. the 300 kPa is a relatively low limit for analysis of dams. Besides. the effect of static shear is also

dependent on the level of confining pressure and. therefore. it is not adequate to relate the values of K_α only to the static shear stress ratio.

In addition to implied corrections. based on discussions at the NCEER workshop (1996). the Seed et al. (1985) SPT curve was modified to avoid the extrapolation to zero cyclic resistance ratio at zero penetration resistance.

Other SPT based methods have also been developed (for example Tokimatsu and Yoshimi. 1983; Fear and McRoberts. 1995). but the correlation by Seed et al. (1985) appears to remain the most popular. especially in North America.

Although the method initially proposed by Seed is simple. it has many problems. Fear and McRoberts (1995) reviewed the Berkeley trigger criterion. They showed that the basis for the selection of N in the Berkeley database was not clear and the methodology used in the Berkeley database was not explicitly stated nor consistently followed. Fear and McRoberts' study found that the $(N_1)_{60}$ in the Berkeley catalog was a minimum value only in some cases: for many other cases. it could be considered an average value over some portion of the borehole and. in a few cases. it was a high value. According to Fear and McRoberts' study. the Berkeley interpretations are generally more conservative. particularly at higher values of cyclic stress ratio. Besides. the results of their study indicate a zone in which liquefaction may or may not occur. whereas the more conservative Berkeley plot indicates no such zone (see Figure 1.9).

Empirical charts of this type do not take into account all the significant factors affecting cyclic liquefaction. Because of the unreliable nature of the SPT. all methodologies based on this test cannot be considered as a complete criterion for evaluating the susceptibility of a site for liquefaction. The main factors affecting the SPT tests have been reviewed in various papers such as Seed et al.. 1985; Skempton. 1986 and Robertson et al.. 1983. among others. Some correction factors for the modification of the

SPT results for overburden pressure. delivered rod energy. borehole diameter. rod length and sampling method have been proposed (Skempton. 1986). Also a summary of the recommended procedure for performing the SPT has been recommended by Seed and Harder (1990).

It seems the SPT is used primarily because of the voluminous database available. Despite numerous corrections and recommendations provoked by the inherent problems and poor reliability associated with the SPT, the Cone Penetration Test is becoming the in situ test of choice. The CPT provides continuous profiles of penetration resistance which are useful for identifying soil stratigraphy and providing continuous profiles of estimated cyclic resistance ratio.

Considering the previous discussions. although professional and regulatory practice often adopts this method as a design method. the designer should not rely solely on such a simplistic approach. The predictions offered by SPT and CPT can be either useful at a screening level or complementary to other design findings. The point is that even if one can neglect all the deficiencies of these methods. finally they cannot give complete information about the deformation which is the most important criterion for reliability of a soil structure affected by liquefaction.

1.2.1.2. Total stress approach

Seed and Idriss (1967) proposed an analytical procedure for evaluating the cyclic liquefaction potential of a sand deposit. This procedure involves two determinations:

1- An evaluation of the cyclic stresses induced at different levels in the deposit by the earthquake shaking.

2- A laboratory investigation to determine the cyclic stress which, at given confining pressures representative of specific depth in the deposit, will cause the soil to develop a peak cyclic pore pressure ratio of 100% or undergo various degrees of cyclic strain.

This procedure may be outlined as follows:

1- Choose a representative base motion which is likely to be developed in the base rock at the site under investigation.

2- Determine the response of the overlying soils to the selected base motion, assuming a vertical propagation of shear waves.

3- Idealize the shear stress history at the various depths to determine the significant number of stress cycles and the equivalent uniform cyclic shear stress developed at each level.

4- Determine, by means of cyclic load tests on representative samples of sand from the site, the cyclic shear stress required to cause liquefaction for the sand in the significant number of cycles.

5- Compare the results of sections 3 and 4 at each depth to determine whether or not liquefaction will occur.

One of the important steps in the application of this procedure was the necessity to compute the shear stress time history. In the early application of this procedure, linear elastic finite element analysis was the best available analytical tool for a stress computation problem. But it was known that a considerable amount of energy would be absorbed in the system as a result of inelastic deformation. Considering this fact, Seed and his coworkers started to apply the incremental method in the evaluation of shear stress time history in the soil deposits. They used the linear elastic finite element

procedure but simply adjusted the soil moduli and damping ratio to be compatible with the level of shear strain which a specific element of the soil has experienced during the step by step solution. In this method during the analysis. the nonlinear stress-strain behavior of the soil is accounted for by iteratively adjusting the modulus and damping values until a reasonable consistency is obtained between the selected parameters and the computed strain level. This method was later named the "equivalent linear method" or "quasi-nonlinear method".

After applying their method over a period of time. Seed and Idriss (1971) proposed a simplified technique for evaluating induced stresses in the soil deposit by using the maximum ground surface acceleration. It was claimed that the simplified method is sufficiently accurate for many practical purposes. The main formula in this method has been presented in the previous section (equation 1-1).

Due to the elastic nature of the method used by Seed et al. (1975). no permanent deformation could be computed during the analysis. Since 1975. this method has been extensively applied in the evaluation of liquefaction stability of many geotechnical structures. A significant number of these applications has been reported in the literature (Seed et al.. 1985).

It is believed that the total stress approach which has been initially proposed by Seed and his co-workers was affected significantly by considering elastic behavior for soil. Although the mechanical response of soils is well known to be distinctly plastic. this approach always relied primarily on elastic analysis with iterative adjustment of the modulus and damping values to achieve compatibility with strain levels. The effective stress approach. which will be discussed in the next section. could address this deficiency.

1.2.1.3. Effective stress approach

Another way of attacking the problem of predicting the behavior of soil structures during and after liquefaction is to try to approach the problem by way of the fundamental soil properties. That is, to view soils as assemblages of particles and to construct constitutive models on that basis. In this approach, which employs Biot's theory (Biot, 1941) and finite element method, effective stresses at different elements of a soil structure are determined and, using constitutive models, predictors can relate stresses to strains.

The appearance of this approach for solving deformation problems in soil mechanics arose from attempts to solve Biot's equation of consolidation using finite element method. Zienkiewicz et al. (1982) was one of the first groups that tried to simulate the Lower San Fernando Dam behavior during the 1971 earthquake using effective stress method. A Mohr-Coulomb plasticity model was used to represent cyclic behavior of the soils. Some discrepancies between the results of analysis and the field observations were found. Noticeable permanent deformation was predicted at the upstream shell after 10 seconds from the start of shaking, but field observations had shown that most of the motion of the slide occurred sometime after the cessation of earthquake due to a redistribution of pore pressure.

Analysis of the Lower San Fernando Dam by Zienkiewicz et al. (1982) was one of the first attempts to evaluate the performance of an effective stress analysis in simulation of a practical earthquake problem. This study revealed that a proper constitutive model plays a major role in the success of such analysis. This important issue has been the subject of extensive research in the recent years. Nowadays, it is believed that none of the factors affecting the prediction of soil behavior during liquefaction has the significance of the constitutive model used in the analysis.

Due to the complexity of the effective stress approach, geotechnical engineers at large have not yet accepted it as an alternative to the total stress approach. However, available evidence shows that effective stress analysis with proper constitutive models which can capture loading and unloading and dilative and contractive behavior are necessary to accurately evaluate the consequences of soil liquefaction.

1.2.2. Flow liquefaction

The approaches discussed thus far have been developed primarily to determine the response of the soil structures in cyclic liquefaction. Although the phenomenon of flow liquefaction had been observed and entered the literature earlier than cyclic liquefaction, the methods for its analysis have not been developed to the some extent as those for cyclic liquefaction. The triggering condition for this kind of liquefaction has been recognized recently (Sladen et al., 1985-a: Ishihara, 1993: Sasitharan et al., 1994: Skopek et al., 1994) that will be discussed in detail in the second chapter. However, the existing analysis methods in particular for determining deformation caused by flow failure are not mature. Generally two approaches are in use:

- Considering the problem as a stability failure
- Determining the deformation caused by flow liquefaction

In the first approach, it is assumed that liquefaction analysis is a stability analysis for which shear strength in the numerator of the factor of safety equation is the undrained steady state strength, S_{us}, and the denominator is the driving shear stress. The term "driving" refers to those shear stresses that are required for static equilibrium. Steady state strength is difficult to determine accurately because it is so sensitive to void ratio. Therefore, a major portion of the steps in the analysis, which will be discussed in the next chapter, relate to the measurement of this strength (Poulos et al., 1985).

Using conventional stability analysis, the driving shear stress, τ_d, is computed. If its average value is less than the undrained steady state shear strength in all zones along the trial surface, then instability cannot occur and the soil remains in stable equilibrium. In such a case, an earthquake or other disturbance cannot cause a flow slide, regardless of its intensity. The strains that occur during an earthquake depend on earthquake intensity. Such strains stop, however, when the earthquake stops, unless stress redistribution after shock causes a significant part of the soil mass to undergo liquefaction. The factor of safety against liquefaction is:

$$F_L = \frac{S_{us}}{\tau_d} \qquad (1\text{-}2)$$

Since S_{us} is the minimum strength that a contractive soil mass can have at the void ratio in situ, Poulos et al. suggested that a value of 1.1 for F_L can be considered safe for sands and silts if the highest in situ void ratios are known with sufficient confidence. When F_L is less than 1.0, the entire mass is in unstable equilibrium. Erosion at the toe of the slope, raising the ground water table, foundation movement, earthquake, blast or any other disturbance may cause liquefaction. It has been recommended that if a trial failure surface used in stability analysis passes through dilative and contractive soils, in zones where the soils are dilative, it is conservative to use the drained strength when estimating the factor of safety. As with all stability analysis methods, this approach does not give any information regarding deformation caused by liquefaction.

In the second approach, using finite element and constitutive models, deformation caused by liquefaction is evaluated. For example, Gu et al. (1993-a; 1993-b) used an undrained elastoplastic model to simulate the collapse of liquefied materials in the Lower San Fernando Dam and Wildlife site. They developed their model based on the critical-state boundary-surface theory, the concept of steady state strength and the undrained behavior of liquefiable soils. Their analysis considered the stress redistribution and reconsolidation caused by the development of liquefaction. Biot's theory was used to consider the effects of dissipation of excess pore water pressures. Gu et al. showed that

stress redistribution initiated by the strain softening of liquefied materials can occur in a short period and that it is the main reason for undrained flow failures of dams. slopes. and foundations. Considering this effect. they concluded that a postearthquake deformation analysis may be an essential component of liquefaction stability evaluations.

1.3. Objective and scope of this study

Despite the popularity of total stress methods. these analyses cannot take account directly the effects of pore pressure generation on the response of the soil mass. Total stress analysis provides only a crude means of assessing the overall permanent deformations of the soil structure. In order to model permanent deformations. inelastic behavior of soil obviously must be considered. Therefore. the total stress approach. which relied primarily on elastic analysis. is not able to determine this important consequence of liquefaction.

With more understanding of the liquefaction phenomenon in the last decade. it is believed that in particular whenever the problem necessitates a complete and accurate investigation. the effective stress analysis should be used. In this approach more research and development are needed to establish complete and efficient constitutive models. Nowadays. it is clear that the possibility of postearthquake failure must be taken seriously and included in the overall safety assessment. A number of dams failed after the passage a few hours after the earthquake. The failure of dike No. 2 of Mochikoshi gold mine in Japan that occurred 24 hours after the main earthquake (Ishihara. 1984) and the failure of Lower San Fernando Dam 30 seconds after the main shaking are two examples. The key to this delay appears to be in the generation of zones of high pore water pressure during the earthquake which in themselves may not be the cause of failure and a subsequent redistribution of such pressures by the consolidation process to a situation in which sliding will occur. The computation of such a pressure redistribution has to be made by the solution of consolidation equations which is possible only by means of effective stress approach.

This study has been motivated by the following factors:

- Most of the research to date has focused on developing methods for evaluating the possibility of liquefaction. It is now clear that design criteria based upon the probable occurrence of liquefaction can be excessively conservative and costly. There are requests for design approaches based upon deformation. However. deformation caused by liquefaction is still not a solved problem and should be the focus of research efforts.

- Considering the above mentioned discussions on the existing approaches which are most commonly used in analysis of soil liquefaction and its consequences. it seems that despite the complexity of the effective stress based procedures. they are more complete and exact if a deformation analysis is desired.

- Previous experience has shown that if one desires to achieve meaningful pore pressure and deformation in a boundary value problem involving liquefaction. it is extremely important to have a reasonable constitutive model. Much effort has been put into the development of constitutive models capable of assessing characteristics of soil behavior. but there still is no complete model.

- In spite of controversial ideas about liquefaction mechanism and its definition. both flow liquefaction and cyclic liquefaction are two real phenomena that may be seen in a soil structure. Often nobody can recognize that the damage caused by earthquake induced liquefaction is the effect of flow liquefaction or cyclic liquefaction. Therefore. it is important that a constitutive model be able to show the response of the soil in both flow and cyclic liquefaction.

- Apart from the liquefaction problem. one of the most important limitations of most existing constitutive models for sands is that their parameters depend on

soil state. As a result, the stress-strain-strength properties of a given sand at different initial states are characterized as two separate materials with different sets of parameters. This means that for a unique soil featuring two different states, two calibrations must be performed. As a result these models cannot adequately manage the response of the soil under loading in which the state of the soil changes. In the author's view, solving this problem, which generally exists in most existing constitutive models, is perhaps not less important than solving the liquefaction problem.

- Although there is significant evidence that sands exhibit not only inherent anisotropy but also induced anisotropy due to loading, most existing constitutive models for these soils are isotropic. This fact represents a significant shortcoming, especially in the case of predicting sand behavior under cyclic loading.

- In developing constitutive models for predicting soil response under cyclic loading, usually soil behavior under monotonic loading has been neglected and vice versa.

- As opposed to most existing models for cohesive soils, existing sand models, in general, do not describe ultimate state conditions.

Motivated by the above factors, the objective of this study is to present a framework for modelling the behavior of soils at different states. The multi-yield surface theory (Prevost, 1985) will be modified to consider the state of a soil. The model is able to show the response of the soil under monotonic and cyclic loading in drained and undrained conditions. This model, the calibration of which does not depend on a specific state, is able to show the response of the soil in flow and cyclic liquefaction in a unique framework.

Since the development of any constitutive model is not possible without considering the response of the soil under different conditions. Chapter 2 will discuss the behavior of cohesionless soils under monotonic and cyclic loading. In Chapter 3. after presenting a brief background on constitutive modelling for soils and clarifying that all models which do not consider the state of soil can work in a limited range of stresses and void ratios. the extension of Prevost's model to embrace "Reference State Soil Mechanics" will be presented. The procedure of its calibration will be shown. The validation of this model for monotonic and cyclic loading in different conditions for different soils will be demonstrated in Chapters 4 and 5. Finally. Chapter 6 represents the conclusion and recommendations for future studies.
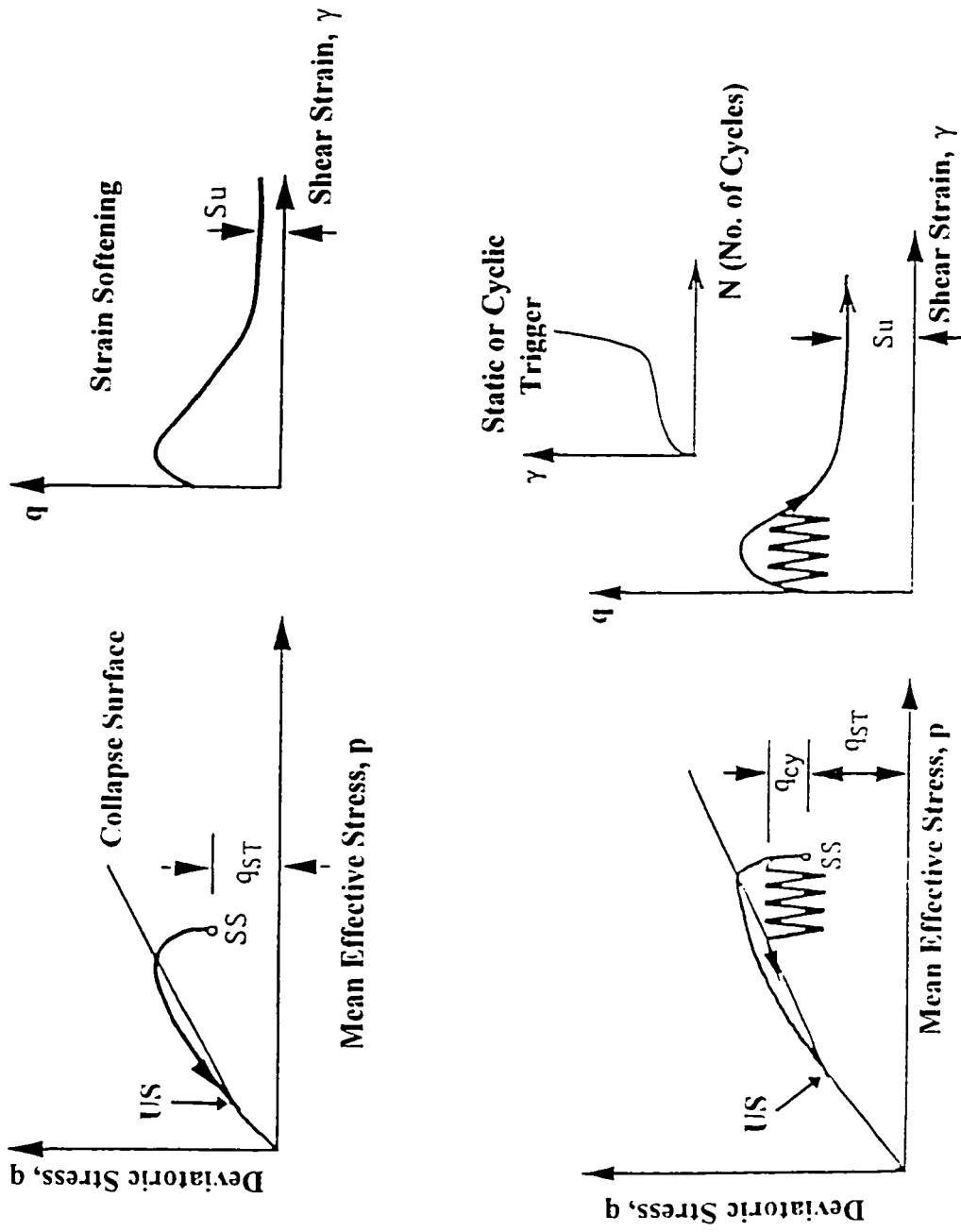
Figure 1.1. Schematic of undrained monotonic and cyclic behavior of sand illustrating flow liquefaction (modified after Robertson, 1994).
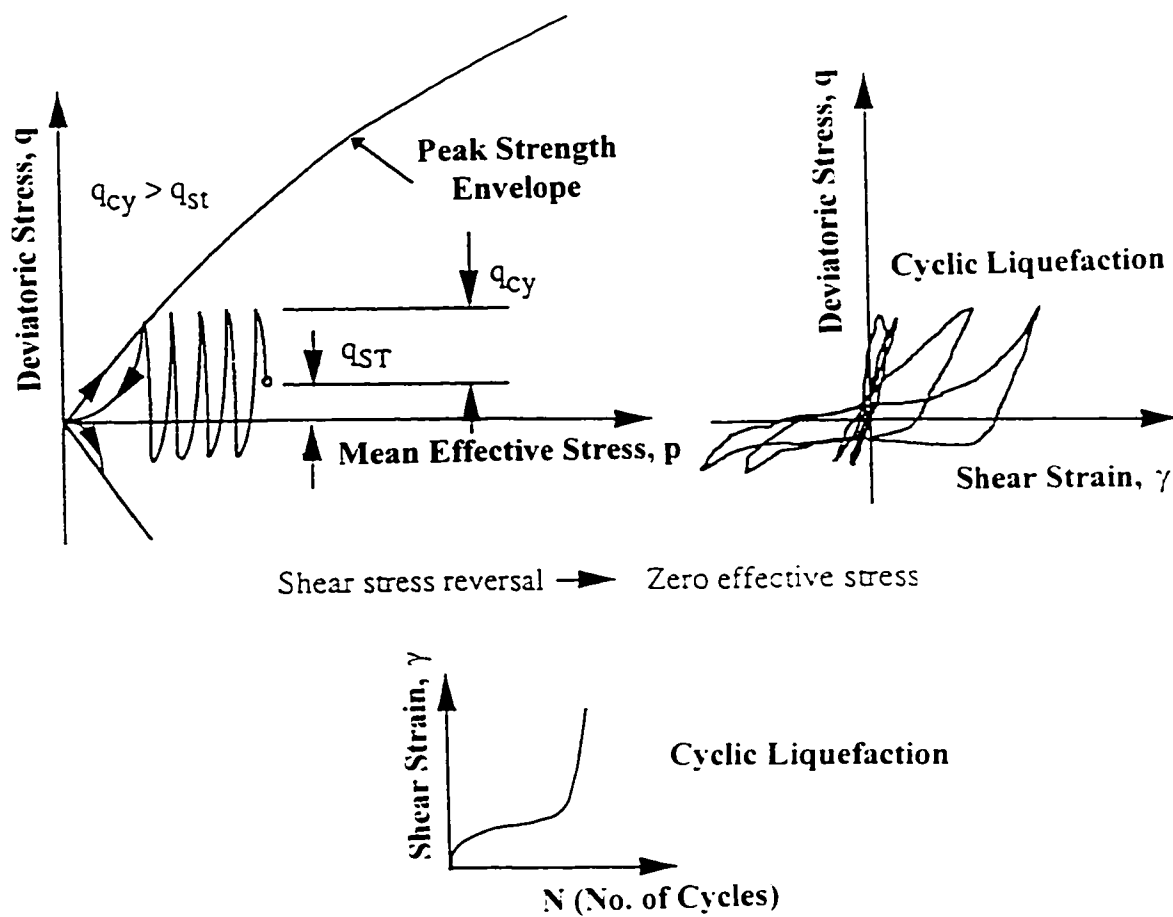
Figure 1.2. Schematic of undrained cyclic behavior of sand illustrating cyclic liquefaction (modified after Robertson. 1994).
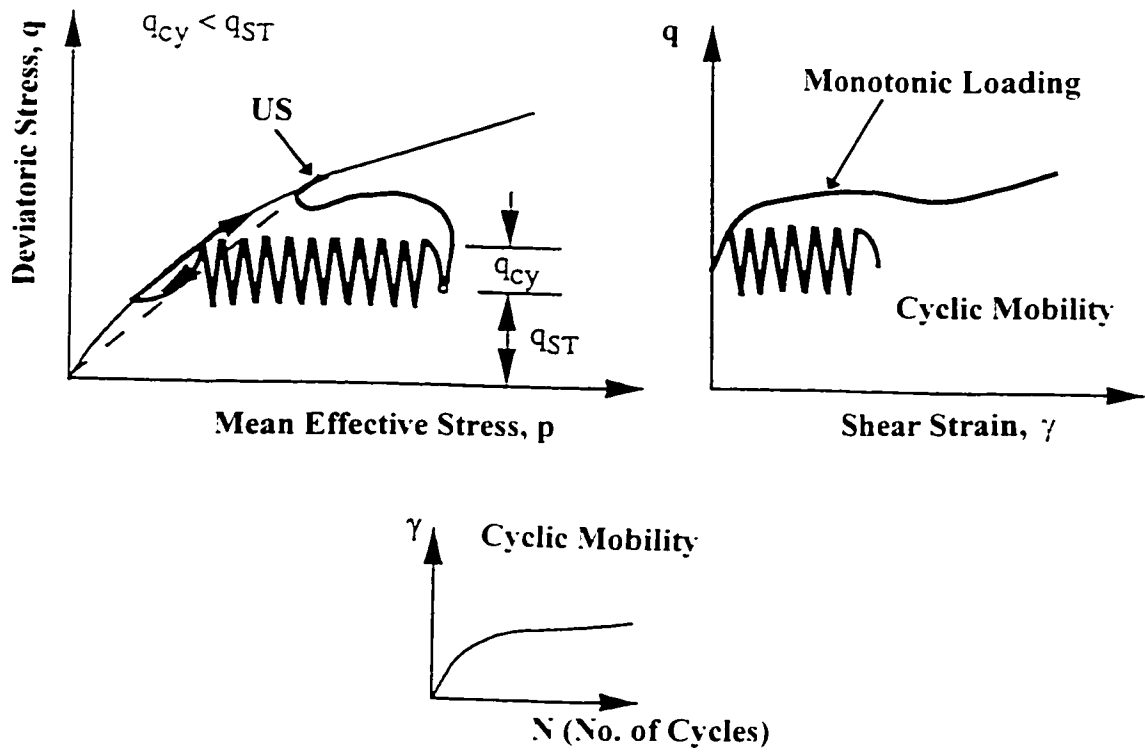
Figure 1.3. Schematic of undrained cyclic behavior of sand illustrating cyclic mobility (modified after Robertson. 1994).
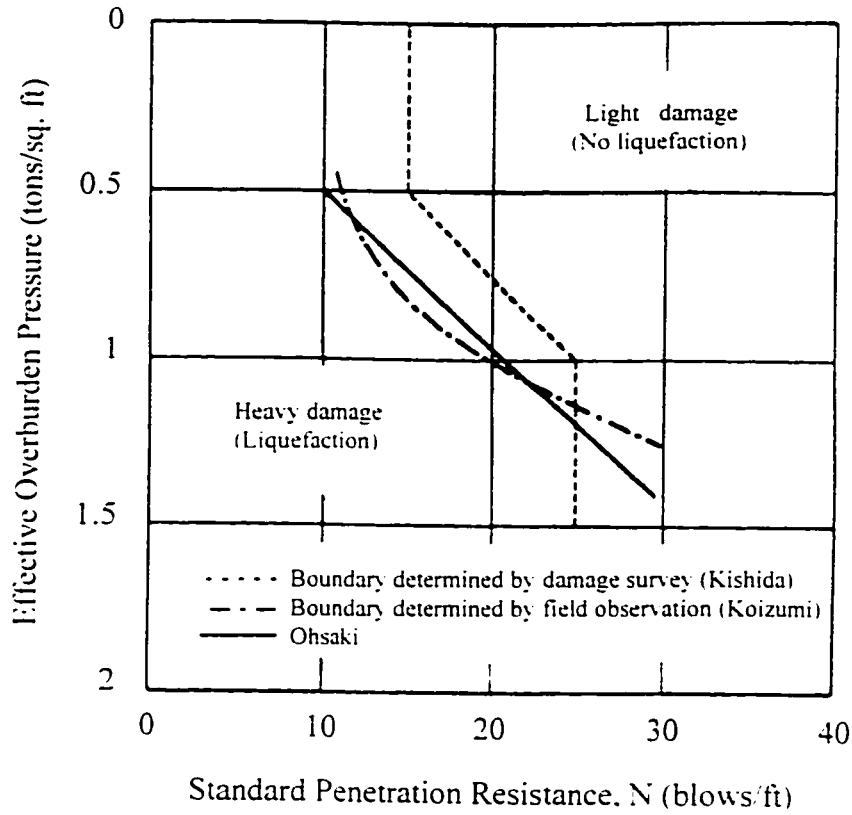
Figure 1.4. Analysis of liquefaction potential at Nigata for earthquake of 1994 (modified after Seed. 1979).
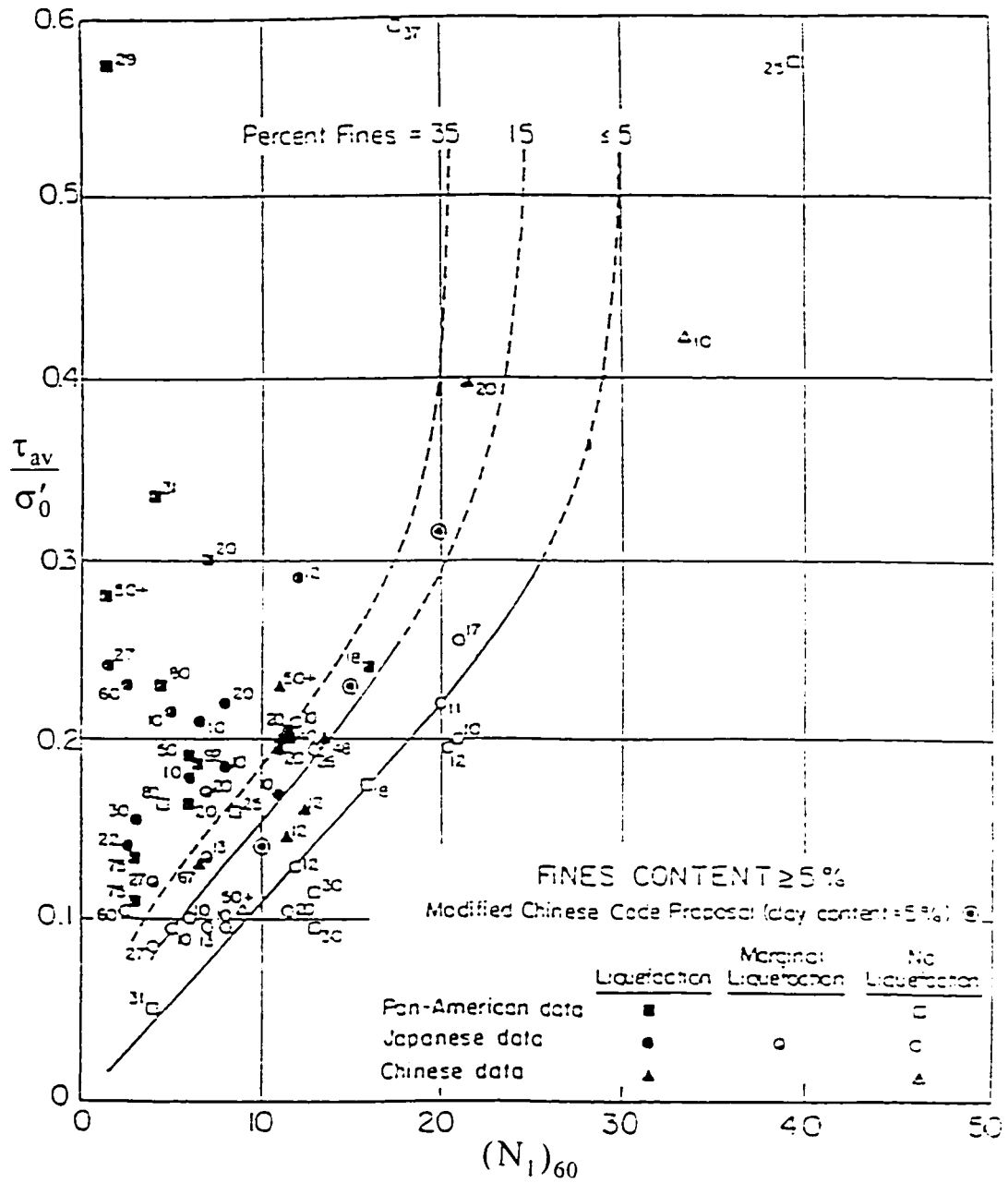
Figure 1.5. Relationship between stress ratios causing liquefaction and N -values for silty sands (after Seed et al.. 1985).
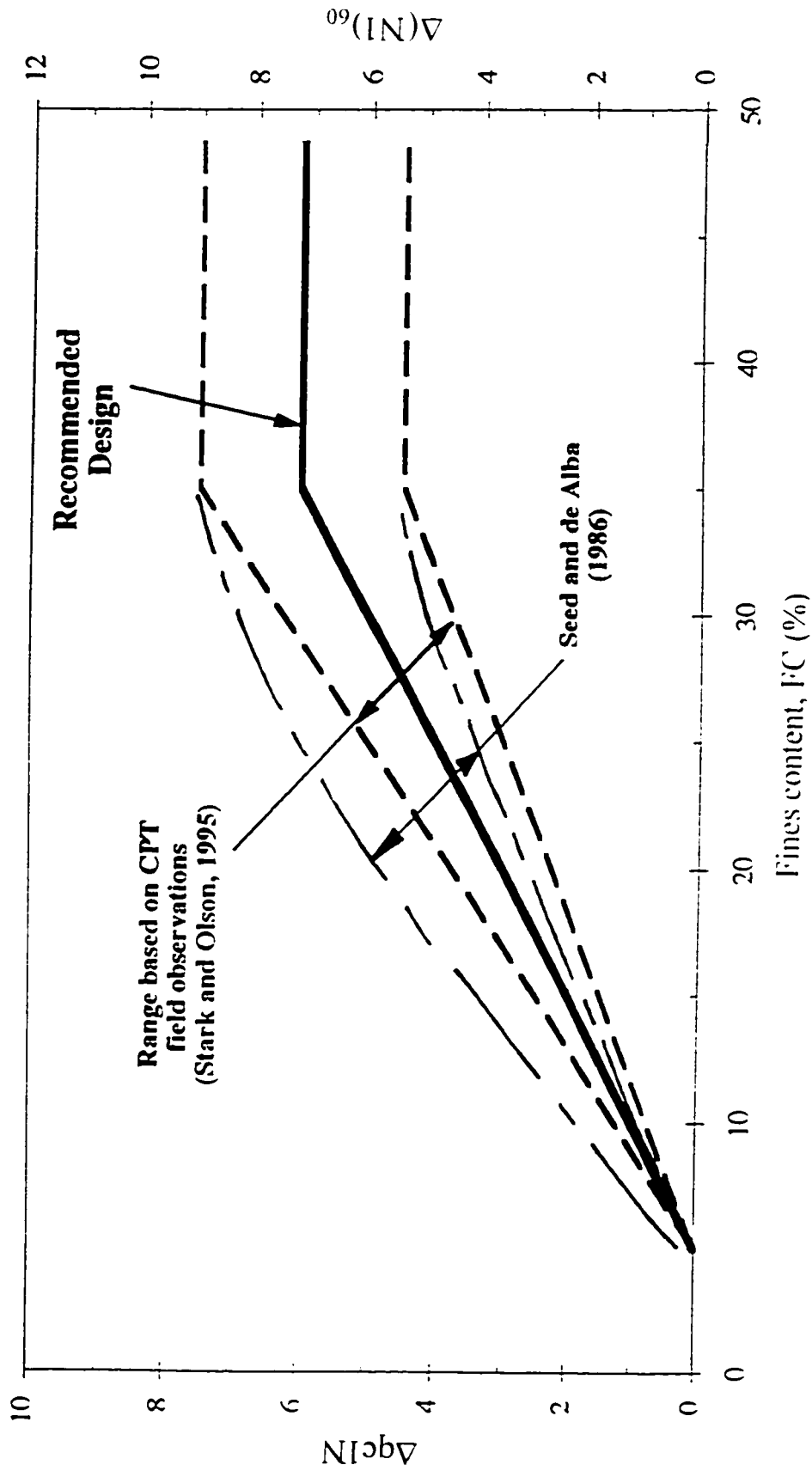
Figure 1.6. Recommended corrections to SPT and CPT values for fines content (after NCEER, 1996).
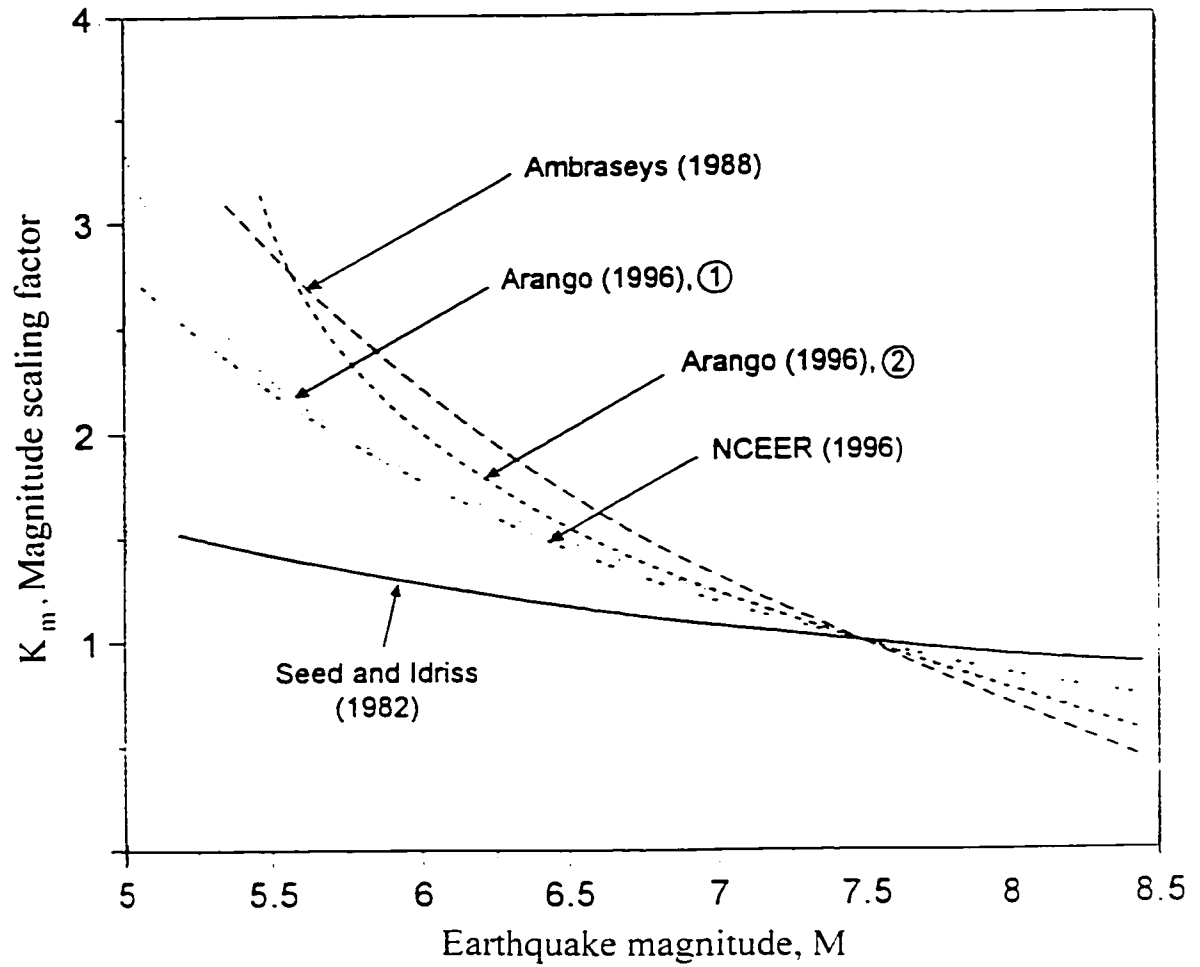
Figure 1.7. Recommended scaling factors. K$_m$. from various sources (after NCEER. 1996).
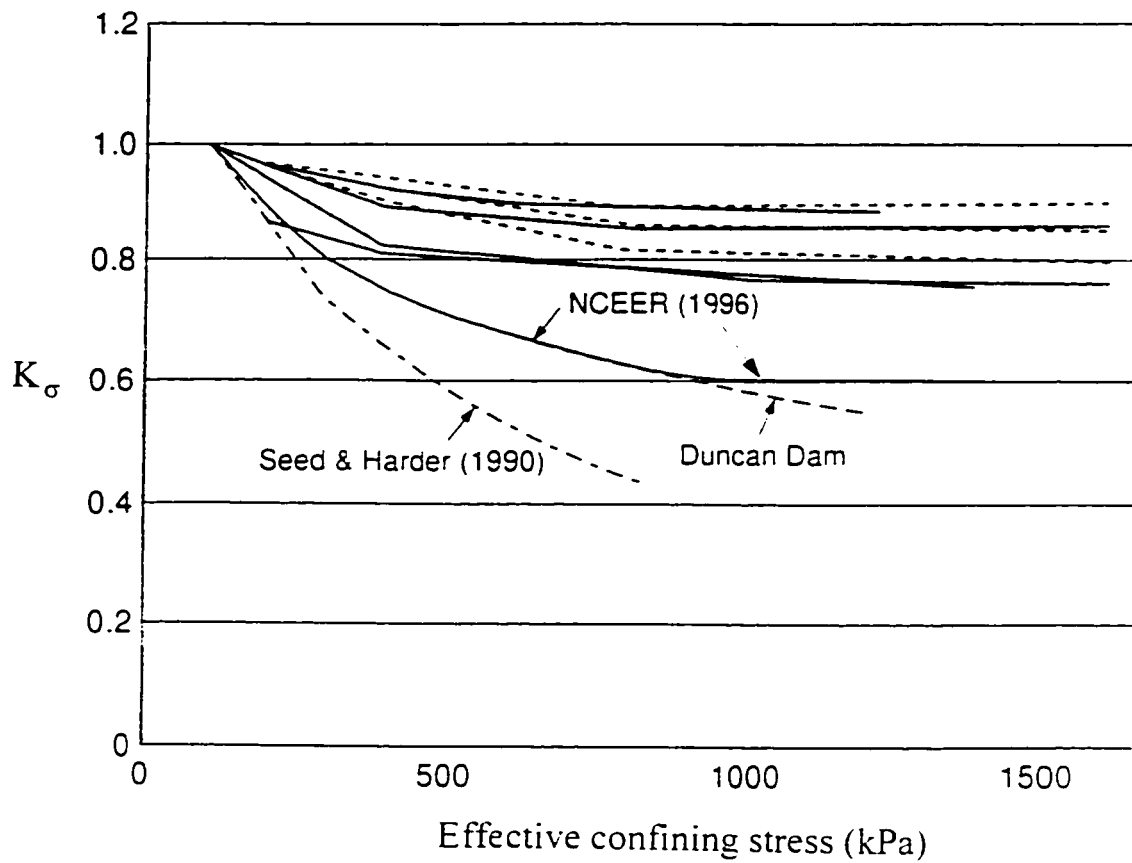
Figure 1.8. Recommended K_σ from various sources
(after NCEER. 1996).
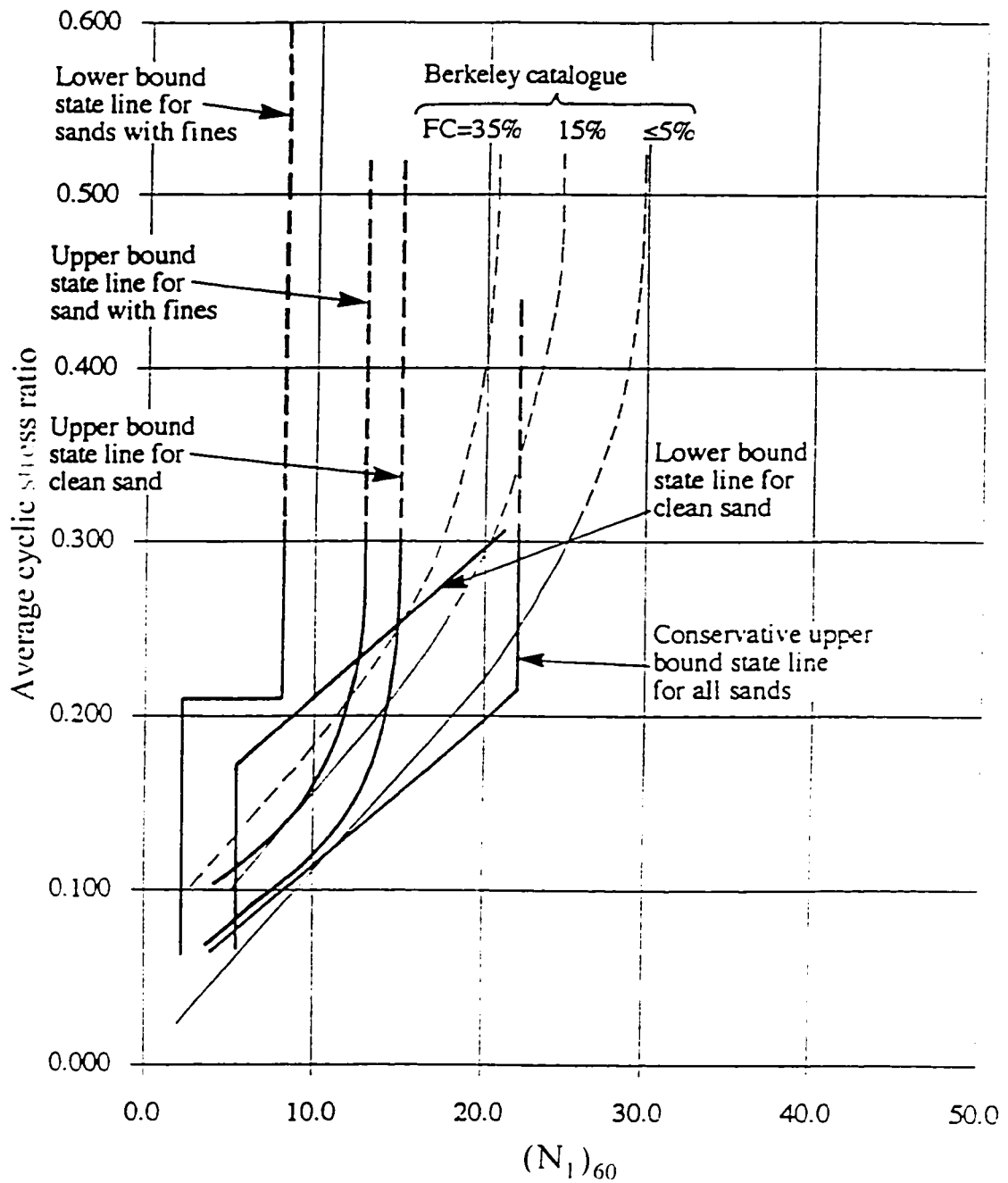
Figure 1.9. Summary of state boundary lines from Fear and McRoberts compared with original Berkeley interpretations (after Fear and McRoberts. 1995).

Chapter 2

BEHAVIOR OF COHESIONLESS SOILS

2.1. Introduction

During the last years. many researchers have worked to determine the behavior of cohesionless soils. Both monotonic and cyclic loading under different drainage conditions have been considered in these investigations. The interest cf researchers has increased. especially for understanding the behavior of these kinds of soils during and after liquefaction. For modelling the behavior of a material. an understanding of its response in different conditions is essential. Therefore in this chapter a review of experimental observations on cohesionless soil behavior will be presented.

2.2. Behavior of cohesionless soils under monotonic loading

Soil can develop large volume changes under loading. depending on the initial state of stress and void ratio. This tendency of volume change has a significant effect on the strength of the soil mass. Reynolds (1885) was the first person who pointed out the volume change in soil masses during loading. He showed that dense sands tend to expand when they are subjected to shear stress. Reynolds called this phenomenon "dilatancy". In the 1930s, Casagrande, based on his observations on the volume change in dense and

loose sands. realized the importance of volumetric strain in the deformation behavior of soil. He developed his famous concept of "critical density" or "critical void ratio".

The critical void ratio was first postulated by Casagrande in 1935 in a lecture to the Boston Society of Civil Engineering and published one year later in the journal of the same society (Casagrande. 1936). Using direct shear tests. Casagrande observed that during shearing. dense sand expands but loose sand reduces its volume.

Figure 2.1 shows the original diagram presented by Casagrande. In a dense sand. the grains are well interlocked and any deformation causes a loosening of the initial compact structure. On the other hand. very loose sand tends to contract in order to achieve a more stable structure.

Based on this observation. Casagrande concluded: when dense and loose sands are sheared in a drained condition. they change their void ratio until a common constant value is achieved (Casagrande. 1936; 1950; Casagrande and Fadum. 1942). This ultimate common void ratio was termed the "critical void ratio" by Casagrande. In this state. the soil continues to deform under constant strength and constant volume. thus the soil behaves as a frictional fluid.

Initially. Casagrande thought the critical void ratio was a unique constant value for a given soil. but later he realized it is a function of normal stresses. The greater the normal stress the smaller the critical void ratio. Then he showed that in the semi-log coordinate of void ratio (e) and confining pressure (σ_3), the critical void ratio can be represented by a single curve named "critical void ratio line" (Casagrande. 1975). Casagrande concluded that during undrained condition of shearing. any combination of void ratio and effective normal stress that is located to the left and below this line should develop a dilative response and. conversely, any initial state above this line should be contractive.

In 1958, using the simple shear test, Roscoe and his colleagues in Cambridge presented a conclusive study proving the concept of critical void ratio and extended it to clayey soils (Roscoe et al., 1958). Experimental data supporting the existence of the critical void ratio line have also been provided by Geuze (1948); Lindenberg et al. (1981) and Dieritchs and Forster (1985), among others.

Casagrande gradually evolved the concept that during flow failure, the grains of the soil are constantly rotating so as to offer a minimum frictional resistance. He called this special rearrangement of the grains "flow structure". Casagrande postulated that such structure exists only when the soil is flowing and the flow structure spreads out through the soil mass.

Three typical undrained triaxial compression behaviors of saturated sand are shown in Figure 2.2. The variations in stress - strain curves from type 1 to type 3 are associated with decreasing void ratio or decreasing normal effective stress. These types of response have been reported by different researchers such as Castro (1969); Castro et al. (1982); Lee and Seed (1970), among others. In type 1, the specimen exhibits a strain softening behavior. After the peak point of the stress - strain curve, which occurs at a small strain, there is a marked reduction in strength with increasing strain until the stress stabilizes at an ultimate or residual strength. The characteristic features of this type of response are continuous deformation at constant volume, constant confining pressure and constant shear stress, which has been called the "steady state" condition (Poulos, 1971).

In type 2, the specimen develops a partial drop in strength, but the sample ultimately starts to dilate and shear stress increases again. This kind of response was called "limited liquefaction" by Castro (1969) and the point in which the strength is minimum was called "quasi steady state" by Ishihara (1993).

The type 3 response represents strain hardening with no loss of shear strength. In this type, after a relatively small strain, the specimen begins to develop negative pore pressure. As a result, a high strength is mobilized in the specimen.

The difference of response presented by types 2 and 3 with type 1 is in the degree of strain softening. In cases 2 and 3, either the soil has a limited softening or it has no softening at all. In these types, after initial increase of pore pressure, the soil develops increasing shear resistance and decreasing pore pressure with further straining. This condition is reflected by a sharp turn around of the effective stress in mean effective normal stress-deviatoric stress (q - p) plane. The change in the response of the soil occurs on a line which was called "phase transformation" by Ishihara (1975).

The phase transformation line which was introduced by Ishihara et al. (1975) was initially defined from undrained monotonic test as the straight line in the (q - p) plane that joins the elbows of the effective stress paths where the response, due to shear stress, changes from positive to negative increments of pore water pressure. The same condition concerning the point of zero dilation was introduced later by Luong (1980) using drained triaxial tests. He called it "characteristic threshold". In this case, Luong defined it as the locus of states where the volumetric strains change from positive to negative. However, before Luong, Kirkpatrick (1961) showed that the lowest point on the volume change - axial strain curves corresponded to a constant stress ratio for the sand, irrespective of void ratio. Regarding the phase transformation line, it is important to point out that it is not a constant line in the (q - p) plane, but changes depending on the void ratio and initial effective mean stress. For specimens of medium dense sand (showing type 2 response), its slope is more than that in dense sand (showing type 3 response). However, for practical purposes in modelling sand behavior, it is usually assumed to be constant. This line also has an important effect on cyclic behavior of sands which will be discussed later.

The initial ideas of Casagrande on flow failure through the evaluation of the critical void ratio line were extended to a new concept, " steady state of deformation ".

"The steady state of deformation " was introduced into soil mechanics by Poulos (1971) who described this concept in the following way:

"The steady state of deformation for any mass of particles is that state in which the mass is continuously deforming at constant volume, constant normal effective stress, constant shear stress and constant velocity. The steady state of deformation is achieved only after all particle orientation has reached a statistically steady state condition and after all particle breakage, if any, is complete, so that the shear stress needed to continue deformation and the velocity of deformation remains constant".

Been et al. (1991) pointed out that the definition of the steady state does not require constant velocity. Available data suggests that the velocity of deformation has no effect on steady state conditions. The concept of steady state for sand is essentially the same as the critical state (Roscoe et al., 1958), although the development of the two concepts was apparently separated.

Referring to the above definition, it is clear that the presentation of the steady state line should be presented in a three dimensional space with three independent quantities. One of these quantities must show the degree of compaction of the soil, such as void ratio; another must indicate an effective normal stress, like the first invariant of the stress tensor; and the other must be a parameter which shows the level of shear stress attained by the soil mass, such as the deviator stress.

The steady state approach to liquefaction analysis has been described in a series of publications by Castro and associates (Castro, 1969; 1975; Castro and Poulos, 1977; Castro et al., 1982; Poulos, 1981). Ishihara, in his Rankine lecture (1993), also showed

that the steady state framework can be used over a wide range for the evaluation of soil response under drained, undrained, monotonic and cyclic loading condition. One of the advantages of this framework is that by considering the updated void ratio, one can follow the response of the soil from small initial strains to ultimate large strains.

Castro and his co-workers, see, for example, Castro (1987); Poulos et al. (1985; 1988) together with other researchers such as Been et al. (1985; 1991), have shown that the steady state condition is only a function of void ratio. They have indicated that steady state is independent of the initial effective confining pressure, fabric, rate of deformation and stress history.

However, other researchers have pointed out that the steady state is not only dependent on the void ratio of the soil mass, but is also affected by the effective consolidation stress, see, for example, Alarcon - Guzman et al. (1988); Konrad (1990a; 1990b; 1991); Chu (1992). Konrad's interpretation was that there is an upper and lower limit for the steady state condition and the steady state line would be taken as the average of these two limits.

Dobry and co-workers have tested specimens of silty sand prepared by sedimentation under water. This procedure results in a layered sample that is not uniform and likely represents to some extent hydraulic fill process in the field. Their results have indicated that steady state line is strongly affected by the sample preparation procedure (Dobry, 1991).

De Gregorio (1990) has shown experimental evidence suggesting that the location of the steady state line is affected by the sample preparation procedure and consequently by the initial fabric of the soil. The results of De Gregorio's tests indicated that dry pluviation technique provides a lower location for the steady state line in the $(e - \sigma_3)$ plane than the moist tamping method does. Marcuson et al. (1990) also found that the steady state line evaluated by samples performed by the wet pluviated technique was

slightly below the steady state line obtained through specimens prepared by moist tamping.

Regarding the stress path dependence of steady state condition. experimental results reported by Vaid et al. (1990) indicate that a sand is more contractive in extension than in compression triaxial test. Consequently. the position of the steady state line in extension is lower than that in compression. Similar results have been reported by Hanzawa (1980) and Riemer and Seed (1997). The last group has also claimed that the steady state to a lesser degree depends on the initial consolidation level prior to undrained shearing. They pointed out that the standard method of determining the steady state line for a given material seems unconservative. since triaxial compression testing of highly contractive samples yields the largest steady state strength and up to 50% stronger than those consolidated under much lower stresses. However. experimental results reported by Been et al. (1991) on Erksak sand have shown that the steady state lines evaluated from triaxial compression tests are identical to the steady state lines evaluated from triaxial extension tests. On the other hand. Pyke (1988). observing the fact that soil is an anisotropic material. has claimed that the steady state condition should be expected to be different in triaxial compression and extension. plane strain. simple shear and torsional shear tests.

In regard to the effect of the rate of deformation on the steady state. experimental results reported by Hird and Hassona (1990) on Leighton Buzzard sand have shown a different steady state of deformation in stress-controlled and strain-controlled conditions. Similar results have been presented by Casagrande (1975) for Banding sand. On the other hand, Poulos et al. (1988) have reported experimental evidence indicating that the effect of the rate of deformation on the steady state of deformation is negligible.

Considering the previous paragraphs related to the effect of different factors on the steady state line, it is concluded that there are many controversial experimental results about the uniqueness of the steady state condition. The influence of different factors on

steady state is not clear. and different researchers have obtained different results. The study of this fact is beyond the scope of the present study. However. it must be considered that without the definition of steady state. prediction of this ultimate state is not possible. Any model working in a steady state or critical state framework will finally show the ultimate state which is defined for it. As long as the variation of the steady state line with different parameters is not recognized and quantified. this is a weakness in all the existing constitutive models. In chapter 3. it will be shown that without considering the steady state line as a reference. the prediction of soil response in all conditions is not possible. It is clear that if this reference changes. the variations of that must be recognized. This subject demands future study. But the more important point is that having a reference with some error is always preferable to neglect the state of the soil. which will be shown has a very important effect on the soil response.

2. 3. Index properties in soil mechanics

Material indices include all properties that represent intrinsic features of the material itself and any change in them necessarily implies a change of the material. Size and shape of grains. maximum and minimum void ratio are some examples of these indices.

On the other hand. state indices describe the current state of the material which may be modified by external actions. Examples of these indices are void ratio. water content and degree of saturation. It has been recognized that the soil response is significantly affected by its initial state. A soil specimen under a different state of void ratio or level of confining stress can have completely different undrained or drained behavior. Therefore. in order to predict soil response. it is important that the state of the soil is defined using an appropriate state index.

The first attempt to introduce a state index for sand was the definition of "relative density." which is simply a linear interpolation for the current void ratio normalized

between maximum and minimum possible void ratio for a soil mass. It has been observed clearly that this parameter cannot show the complete state of the soil. Dense sands behave similarly to loose sands when the effective pressure is large (Bishop. 1966: Vesic and Clough. 1968). This similarity exists because the mechanical properties of sands are influenced by the possible volume change during shearing, not only by absolute magnitude of either void ratio or confining stress.

Overcoming this limitation of relative density. Been and Jefferies (1985) have introduced the "state parameter". ψ, which is the difference between current void ratio and void ratio on the steady state condition at the same mean effective normal stress. Been and Jefferies have assumed that soils with the same state parameter have the same characteristics. Their observations were similar to the conclusion reached by Roscoe and Poorooshasb (1963). They reported that: any two samples of a given soil. when subjected to a geometrically similar stress path. have the same strains provided that the difference between the initial void ratio and the void ratio at the critical state at the same normal stress is the same for each sample. Been and Jefferies (1985) reported the relationship between state parameter and different soil properties. As an example. Figure (2.3) shows the variation of the drained angle of shearing resistance with state parameter for Kogyuk sand. In the next chapter. it will be shown how the proposed model can represent the same behavior.

Although state parameter is preferred over relative density. it nonetheless has two limitations. First, it does not include the fabric of the sand which might have a considerable influence on the behavior of sands at small strains. especially under undrained conditions. Second, state parameter does not account for the effect of shear stress. Based on the author's knowledge. these two limitations still exist in all the state indices which already have been introduced by researchers.

Another parameter that has been used as a state index is "Brittleness Index". first presented by Bishop (1967). This index is represented as follows:

$$I_B = \frac{\tau_f - \tau_r}{\tau_f} * 100$$

where τ_f and τ_r represent the peak and residual shear strength.

Originally, Bishop presented the Brittleness Index as a parameter for clays in order to consider the percentage reduction in strength during the passage from the peak to residual state. This index was later used for sandy soils in which under undrained conditions of loading a drop in terms of strength is observed. In this case, the peak strength is equivalent to that observed in clay and the residual strength corresponds to the steady state strength. The results reported by Sladen et al. (1985-a) indicate that there is a good correlation between the Brittleness Index and the ratio (p_i'/p_s'), where p_i' and p_s' are the initial and steady state effective mean normal stress at the same void ratio, respectively.

Recently Robertson and Fear (1995) defined Brittleness Index as :

$$I_B = \frac{S_p - S_{min}}{S_p - S_i}$$

for triaxial compression, and as:

$$I_B = \frac{S_p - S_{min}}{S_p + S_i}$$

for triaxial extension, where S_p, S_{min} and S_i are peak shear strength, minimum shear strength and initial static shear stress, respectively. They pointed out that by using this definition of Brittleness Index, it is possible to quantify the loss in strength more clearly for anisotropically consolidated samples (i.e., $S_i > 0$).

One of the most important features of the Brittleness Index in the characterization of the undrained response of cohesionless materials is concerned with the identification of the occurrence and non - occurrence of a drop in terms of strength. In addition, when the value of I_B is known, it is possible to obtain a picture of the magnitude in the strength drop.

Ishihara (1993) claimed that the main assumption in the definition of state parameter. that is. that the behavior of soils with the same ψ is the same. is not always tenable. He noted that at high void ratios, the behavior of sand became more sensitive to a small variation in void ratio. Therefore. while ψ is useful for quantifying the behavior of medium to dense sand under relatively high confining stress. its usefulness decreases as the confining stress becomes smaller and the void ratio larger. In an effort to find an alternative index parameter, based on the upper and lower reference lines, he introduced "State Index". I_s. which has been defined as:

$$I_s = \frac{e_0 - e}{e_0 - e_s}$$

where e is the current void ratio. e_0 is a threshold void ratio above which soil exhibits zero residual shear strength when sheared undrained in triaxial compression. The value of e_0 can be determined by an extrapolation of the steady state line or quasi steady state line towards the zero point of confining stress. e_s is the void ratio in the lower reference line for the same effective mean normal stress. To capture the sand behavior in the medium strain range. Ishihara suggested taking the quasi steady state line as the second frame of reference.

Robertson and Fear (1995) proposed "Reference State Ratio". RSR. which is the ratio of the existing mean effective stress to the mean effective stress at ultimate state at the same void ratio. as a parameter to define the state of the soil. They mentioned that. because of small slope of ultimate state line in the ($p - e$) plane for very loose sands. state parameter (ψ) is not able to show the response of the soil in this zone.

Finally. it is important to emphasize that the behavior of cohesionless material is affected significantly by their states. In this section. we referred to previous efforts of different researchers to introduce a parameter for representing the state of the soil as complete as possible. However, in the author's opinion. none of the introduced parameters are yet complete. All of them have some limitations. It is more important.

however, that it is believed strongly (Poorooshasb, 1989) that to consider the state of a soil mass during loading is an essential and fundamental condition for predicting its real response. Chapter 3 includes a further discussion on this important factor.

2.4. Determination of in situ steady state strength

The key point in the application of the steady state approach is the determination of the steady state line and the in situ void ratio. Unfortunately, there are some difficulties in determining them. At a given site, a wide range of grain size distributions and of the shape of soil particles may exist. Therefore, there is not a uniform and unique soil in the site and finally a unique steady state line. On the other hand, because the steady state condition is affected by void ratio, the in situ void ratio must be determined accurately.

Poulos et al. (1985) have proposed a step-by-step method for determining the in situ state strength of a soil mass. They suggested using undisturbed samples from either fixed-piston sampling, freezing of the ground and coring or sampling in test pits. In situ void ratio can be determined by these samples. Poulos and his co-workers reported that should a sample be obtained even by the freezing method, the density increases during reconsolidation in the laboratory to in situ stresses. Such changes may cause a soil that is contractive in situ to become dilative in the laboratory. Therefore, a procedure is required for returning laboratory-measured steady state strengths to the in situ void ratio. Poulos et al. assumed that the slope of the steady state lines for the compacted specimens and undisturbed specimens in a semi-log plot is the same.

An alternative procedure to evaluate the in situ steady state strength has been proposed by Seed (1987). He suggested that the establishment of a relationship between residual strength and a given in situ soil characteristic such as penetration resistance may provide the most practical method. Using some case histories, Seed related the residual strengths of the liquefied sand to $(N_1)_{60}$ values for the soils involved. He pointed out the

scattering in the results. possibly reflecting different degrees of water content redistribution resulting from different degrees of soil stratification and, to some extent, whether the values were determined from conditions at the beginning of sliding or from conditions at the end of sliding.

Poulos (1988) has indicated that if the permeability of the soils is sufficiently high, it is reasonable to expect drainage to occur between SPT blows. In this case, the measured N - value would be associated with a drained steady state rather than undrained steady state. Poulos showed that for Lower San Fernando Dam, the blow count initially estimated can be reduced to one-third if it is assumed that the measured blow counts were closer to a drained condition. Besides, Davis et al. (1988) have shown that use of the post-failure cross section to back-figure the strength mobilized during liquefaction is not appropriate because the dynamic forces that are involved during the failure itself are not considered. Thus, the chart proposed by Seed should be used only as a first approximation.

Stark and Mesri (1992) provide an alternative approach to estimate S_{us} (strength at the ultimate state) and present a relationship between undrained strength ratio and equivalent $(N_1)_{60}$ in clean sand. The undrained strength ratio is defined as the mobilized S_{us} divided by initial effective vertical stress. This relationship is based on case histories used by Seed and Harder (1990) together with three additional case histories. The proposed relationship also consists of lower and upper bound lines and has the same problems as the plot by Seed.

Dobry and his co-workers have proposed a different approach for evaluating the undrained steady state in situ based on the simulation of the consolidation process that likely takes place in situ in the laboratory (Dobry, 1991; Baziar and Dobry, 1995).

Specimens are formed by pluviating equal weights of the sand-silt mixture sampled from the site into the triaxial preparation mold previously filled with water and then waiting long enough for full sedimentation to occur before pouring the next layer, typically in four layers. Due to the different rate of sedimentation, the specimens are not uniform and that factor, according to Dobry and co-workers, can represent to some degree the layered structure developed in the field. Baziar and Dobry (1995) have shown that the range of void ratio obtained by this sample preparation technique, in specimens consolidated under similar conditions in the field, is in agreement with the range of void ratio estimated by Poulos' procedure in the upstream slope of Lower San Fernando Dam. Dobry and his co-workers pointed out that by using the measured steady state strength of samples prepared by this method and effective consolidation pressure, the steady state strength of the soil in the field can be determined.

Been et al. (1986; 1987-a; 1987-b), using a correlation between the state parameter, ψ, and the CPT tip resistance, presented a method to estimate the state parameter in situ. They interpreted the existing data obtained from calibration chamber tests to provide the relationship of cone tip resistance to state parameter. A relationship between tip resistance, total mean stress, effective mean stress, slope of steady state line and state parameter was developed by Been et al. (1987-a). This relationship allows the interpretation of the in situ state of a soil mass, and as a result, using steady state line, the steady state strength of the soil.

Robertson (1990) presented a review of the relationship between S_{us} and normalized penetration resistance using relative density correlations with SPT $(N_1)_{60}$, correlations between normalized CPT $qc1$ and SPT $(N_1)_{60}$, published data on steady state relationships, field studies and large calibration chamber test results. Robertson found that the correlation by Seed (1987) represented a conservative lower bound correlation, especially at large values of $(N_1)_{60}$. He also investigated the correlation

suggested by Been and Jefferies. The results clearly suggested the lack of a unique relationship for all sands.

Fear and Robertson (1995) have combined critical state soil mechanics and shear wave velocity measurements in order to develop a framework which can be used to estimate the in situ ultimate undrained steady state shear strength of a sand. Shear wave velocity is an attractive parameter to use because it can easily be measured in both the field and the laboratory. The application of the proposed method relies on laboratory work to determine the parameters of the steady state line $\varphi'_s, \Gamma, \lambda$ (φ'_s, Γ and λ are steady state friction angle, intercept of the steady state line in e-log p space at p=1 and slope of the ultimate state line in e-log p space, respectively) and the parameters relating shear wave velocity to void ratio for a particular sand. Although the method appears quite promising, it is not without drawbacks. The level of accuracy in estimating S_{us} using shear wave velocity may present some problems and should be considered when applying the method. If the steady state line of a sand is relatively flat, it will not be possible to accurately determine S_{us} using shear wave velocity measurements or in situ penetration testing (Fear and Robertson1995).

The knowledge of in situ void ratio also is important for predicting soil response. Rather than using undisturbed sampling, this index parameter can be determined by in situ tests like SPT (Skempton, 1985). Using the results of these tests, relative density and void ratio can be determined. Cunning et al. (1994) also described a method to estimate in situ state of cohesionless soils from the in situ measurements of shear wave velocity. Based on both the relationship between void ratio, effective confining stress and shear wave velocity and the equation for the ultimate steady state line, they could estimate the in situ state of the sand. Using their method, the contractive / dilative behavior of a sand can be evaluated from in situ shear wave velocity and vertical effective stress with an estimate of K_0. The proposed method has the advantage that the shear wave velocity

measurement is independent of soil compressibility. unlike penetration test results. Its disadvantage. however. is that estimation of K_0 is not always easy.

In this section. different proposed methods for evaluating in-situ steady state (ultimate state) strength of the soil and void ratio have been briefly reviewed. The topic of which method in practice can be applied more efficiently and accurately is not the object of this research. What is important is that for having a complete prediction of the soil response in the field, the in situ state of the soil and its ultimate state conditions must be recognized. In the next chapters. the effect of this important factor in numerical analysis will be discussed in more detail.

2. 5. Behavior of cohesionless soils under cyclic loading

The Anchorage and Nigata earthquakes that occurred in 1964 in Alaska and Japan caused significant damage to structures on saturated sandy soil deposits. This damage was the result of excessive deformation that these materials underwent during and after the shock. Geotechnical researchers started to study the mechanism during which cohesionless soils lose their stiffness during and after earthquakes. It is believed that studies by Seed and his co-workers in the university of Berkeley (Seed and Lee. 1966: Lee and Seed. 1967; Peacock and Seed. 1968) provided significant insight into the behavior of saturated sands under cyclic loading.

They used cyclic triaxial tests on isotropically consolidated reconstituted specimens. In spite of their limitations (Castro, 1969; Seed. 1979). cyclic triaxial test results have provided a great deal of valuable information for the proper understanding of cyclic response of soils.

Figures 2.4 and 2.5 show typical results from undrained cyclic triaxial tests on isotropically consolidated samples at two loose and dense states. Relative density is an

important parameter which shows the volume change tendencies due to shearing. The greater the tendency towards volume contraction. the faster the pore pressure build up and hence. the higher potential of cyclic liquefaction. For example. in Figures 2.4 and 2.5. it is observed that almost ten cycles caused liquefaction in both cases. However. for the dense sand the deviator stress was 70 kPa. whereas for the loose sand it was only 39 kPa.

As can be seen. during the first cycles of loading. the specimens show no noticeable deformation. although the pore water pressure builds up gradually. However. after some cycles. the pore pressure suddenly increases to a value equal to the confining pressure. At this stage. the loose specimen develops large deformations which increase in amplitude under subsequent loading cycles.

For the dense sample. the axial strains accumulate at a slower rate with an increase in the number of cycles compared with those in the loose sand. In other words. the response of dense sands does not show the sudden development of large strain observed in the case of loose samples.

In cyclic triaxial tests. the pore pressure may become equal to the confining pressure. irrespective of the relative density of the sand. This zero effective stress condition always occurs at the moment that the deviator stress is zero. that is. when the specimen is subjected to an isotropic state of stress. However. the deformation induced in the specimen for each time a zero effective stress condition develops is dependent on the relative density of the specimen (Selig and Chang; 1981). Almost unlimited deformations may develop in loose specimens. whereas the corresponding deformations of dense specimens may be of limited magnitude.

From a set of experimental results carried out on cyclic triaxial tests similar to those explained above. Seed and Lee introduced new criteria to define "initial liquefaction", "partial liquefaction", "complete liquefaction" and "failure" (Seed and Lee. 1966; Lee and Seed. 1967). This terminology later caused some confusion that still exists

among geotechnical engineers regarding the distinction between liquefaction with loss of strength and liquefaction as a phenomenon that occurs in zero confining effective stress condition. The liquefaction analyzed by Seed and Lee is related mainly to a gradual increment of strains associated with the build up in pore pressure caused by cyclic loading. From these results. Seed and Lee concluded that the higher the confining pressure. the greater the cyclic stress amplitude required to induce failure. They also claimed that the higher the initial shear stress, the higher the resistance of soil against liquefaction. As can be observed. these results are exactly the opposite to those obtained from steady state concept. These contradictions between the conclusions obtained by steady state concept and Seed's cyclic triaxial tests led to Casagrande and Castro's decision to conduct some cyclic triaxial tests.

Castro (1969) and Casagrande (1975) carried out cyclic triaxial tests on medium to dense sands similar to those performed by Seed and Lee. These tests showed that during the implementation of cyclic loading. the samples deformed mainly at the top by alternate necking and bulging. For these tests Castro reported a significant redistribution of the density throughout the specimens. Castro's and Casagrande's findings questioned the results of cyclic triaxial tests. at least in the case of medium to dense sands.

Furthermore. Castro (1969) conducted cyclic triaxial tests with no stress reversal on very loose specimens. A typical result is shown in Figure 2.6. It is seen that after a number of cycles, the specimen suddenly flowed in the same way that occurred in monotonically loaded tests. Thus, in this case cyclic loading triggered flow liquefaction.

After the pioneering works of Seed and Lee from one side. and Castro and Casagrande from the other. many researchers attempted to clarify the cyclic undrained response of sandy soils. Different types of equipment. such as triaxial. simple shear. torsional shear and shaking table. have been used by different researchers. among them Ishihara et al. (1975); Ishihara and Yasuda (1975); Tatsuoka and Ishihara (1974-a;1974-

b): Vaid and Chern (1983: 1985): Ishihara (1985): Alarcon - Guzman et al. (1988): Hyodo et al. (1994).

Behavior similar to that observed in the cyclic triaxial tests is also observed in cyclic torsional tests (see Figures 2.7 and 2.8). As can be seen, when the cyclic effective stress path touches the phase transformation line, a significant change in the cyclic response takes place. During loading, the effective stress path is turned to higher effective confining stresses, indicating a dilative response, which during unloading is turned to the origin, which indicates a highly contractive behavior associated with a large increase in pore pressure. Once the phase transformation is crossed, this phenomenon is repeated, and at each cycle of loading and unloading the effective stress path moves upward and downward closely along the failure line and, if the soil is loose enough, starts to pass through the origin, indicating a condition of zero effective stress. The strain range within which the specimen remains in a liquefied state depends on the relative density of the sand. Dense sands can gain their strength in a small strain level, but loose sands, for showing a resistance, need to go to a high level of strain to gain resistance.

Ishihara (1985) reported that there is a threshold value of relative density above which the cyclic stress ratio that causes some amount of strain in a given number of cycles increases drastically.

As mentioned, Seed and his co-workers initially used isotropically consolidated samples in their studies. However, initial static shear stress has a significant influence on the occurrence of liquefaction and the mode of failure. Castro et al. (1982) and Vaid and Chern (1983; 1985) have initiated study on the effect of static shear stress or consolidation stress ratio on undrained cyclic loading behavior of sands.

In a number of tests conducted on Banding sand and a tailing sand, Castro et al. (1982) showed that during cyclic loading, specimens can show the same behavior as when monotonic loading condition and flow liquefaction occur in the tests. For occurring

cyclic liquefaction. existence of shear reversal during loading is an essential condition. Therefore. for a constant amplitude of cyclic loading. with increasing static shear stress. the strength of the soil against this kind of liquefaction will increase. This consists exactly with the results reported by Seed and his co-workers in Berkeley. As a result. it was often believed (Lee and Seed. 1967; 1970) that the soil element in a slope is more resistant to cyclic strain development than that under the level ground. Therefore. it was claimed that the critical initial state would correspond to isotropic consolidation. which represents an initially zero static shear. On the contrary. according to Castro and Poulos (1977) and Casagrande (1975). the resistance to strain development for soil element in the slope is always less than that under the level ground. Therefore. they suggested the use of anisotropically consolidated samples for simulating appropriate initial static shear.

Having conducted some tests on anisotropically consolidated samples of Ottawa sand and tailings sand. Vaid and Chern (1983; 1985) pointed out that the type of liquefaction determines the positive or negative effect of initial shear stresses. They observed that the resistance to cyclic strain development could decrease or increase depending on whether liquefaction or cyclic mobility is involved. They observed that the conclusion reported by Seed and associates is true only for soil elements which develop cyclic liquefaction. On the contrary. Castro and associate's conclusion is true only in the flow liquefaction case. They also showed that the influence of static shear stress on the undrained monotonic and cyclic loading behavior is the same.

Figure 2.9 shows the influence of the degree of anisotropy on the resistance of two soils under cyclic loading (Vaid and Chern. 1985). It should be noted that the increase of strength at low K_c ($K_c = 1/K_0$) ratio for sand in the figure is the result of the occurrence of flow liquefaction in the extension mode and not the development of cyclic liquefaction. Increasing the static shear in compression increases the cyclic load amplitude required to exceed the steady state shear strength in extension.

The undrained stability of a contractive sand under earthquake loading cannot be studied without considering the in situ effective stress path. This path actually determines the failure modes and the resulting deformations. Starting from an initial anisotropic state of stress, which is typical of most in situ conditions, a large strain can be developed in the soil, following different stress paths which depend not only on the initial state of the soil mass and the magnitude of the applied loads, but also on the boundary conditions. For example in deposits under level ground, cyclic liquefaction may develop after a sufficient number of cycles, irrespective of the initial state of stress, but flow liquefaction is unlikely. On the other hand, near the surface of sloping ground, the lateral strains are not constrained and the susceptibility to flow increases for loose sands with the inclination of the slope. In this case, cyclic liquefaction potential is low because the state of stress must remain anisotropic due to the shear stresses needed to maintain equilibrium imposed by geometry.

Furthermore, a combination of two mechanisms, flow liquefaction and cyclic liquefaction, may contribute to the failure of a complex structure, such as an earth dam. In different zones of a dam, two different phenomena can occur simultaneously. Even in one zone, during the process of liquefying, two mechanisms can exist at different times. But flow liquefaction, if there is any, will be observed before cyclic liquefaction (if it does not occur due to pore water pressure redistribution). This is because of the position of triggering the collapse surface compared to the phase transformation line.

The occurrence of liquefaction depends also on the amplitude and number of cycles in the series of stress applications. Consequently, cyclic undrained strength is usually defined as the combination of the constant amplitude cyclic shear stress and the corresponding number of cycles causing zero effective confining stress or a given level of shear strain.

It was seen that under cyclic loading, pore pressure in the soil increases and effective stress approaches zero. The rate of this increase depends on the relative density

of the soil. Loose soils liquefy at a small number of cycles compared to dense soils. Flow liquefaction can occur in the soil depending on density of the soil, static shear stress and amplitude of loading. The positive or negative effects of static shear stress in occurrence of liquefaction depend on the type of liquefaction. In practice, because different elements of a soil structure exist under various conditions, it is important that a model can show both of these phenomena in a unique framework.

2. 6. Collapse surface

The strain softening in undrained response of very loose sand, which causes a significant decrease in the strength of the soil and consequently flow liquefaction, begins on a surface named the "collapse surface" (Sladen et al., 1985-a; Sasitharan et al. 1994). Recognizing this important surface for any analysis of liquefaction is essential. In this section this important phenomenon will be discussed briefly.

Observations on the response of very loose sands under the undrained loading conditions have shown that these soils have a metastable structure. Sladen et al. (1985-a) reported the existence of a so-called "collapse surface". They saw that for a constant void ratio, the maximum points of stress paths in undrained triaxial tests stay on a straight line passing through the steady state point (see Figure 2.10). Sladen et al. pointed out that mechanistically the collapse surface can be imagined as the locus of soil states at which the destruction of a metastable sensitive soil structure is initiated by static loading until the steady state, which is analogous to a remolded condition, is reached.

The laboratory tests and back analyses (Sladen et al., 1985-b) for slides occurring during the hydraulic placement of an artificial island berm in the Beaufort sea have led to advancements in the understanding of the liquefaction potential of sand. Analyses of their undrained triaxial tests, undertaken in order to measure steady state parameters, suggest that there is a "collapse surface" in three dimensional void ratio - shear stress -

normal stress space (Figure 2.11.a). A necessary condition for liquefaction is that the soil state lie on this surface.

The collapse surface concept is fundamentally an extension of the steady state concept proposed by Poulos (1971) and in many respects follows the principles of critical state soil mechanics.

The results reported by Sladen et al. (1985-a) were only for monotonic loading. Alarcon - Guzman et al. (1988) conducted some monotonic and cyclic loading tests on Ottawa sand. Their experimental results suggest that the monotonic stress paths act as boundaries for cyclic stress paths. When cyclic stress paths touch the monotonic one. flow failure is triggered. Figure 2.12 shows typical results indicating the points where the flow failure was triggered. As can be seen. the effective stress path in monotonic undrained shear constitutes a state boundary that controls the initiation of flow liquefaction under undrained cyclic loading.

This state boundary depends on the sand fabric and the applied stress path. Depending on the initial state. the state boundary can either fully exhibit strain softening or have an elbow and then show strain hardening. Alarcon - Guzman et al. used the term "critical stress ratio (CSR) line". which had been introduced by Vaid and Chern (1983: 1985). for the curve showing the peak points on the state boundaries for a given initial void ratio. This line determines the initiation of strain softening behavior in monotonic undrained shear. They noted that. only for a constant state parameter. ψ. the CSR line may extrapolate back through the origin (as was claimed by Vaid and Chern). The results of Alarcon - Guzman et al.'s experiments showed that initiation of strain softening under cyclic loading, in general, does not occur at the CSR line determined from monotonic loading condition. Under cyclic loading. however, strain softening is determined by the state boundary corresponding to the same initial state. Ishihara et al. (1991) also confirmed that monotonic stress paths act as the boundary for the cyclic loading.

Using the results of triaxial tests. Sasitharan et al. (1994) showed that saturated very loose sand can show undrained collapse when loaded slowly under drained conditions following a certain stress path (Figure 2.13). They showed that the post peak portion of an undrained stress path defines the state boundary above which is not possible to have a stress state for a given void ratio and consolidation stress. Further, they showed that flow liquefaction under drained and undrained loading can occur when the stress path tries to cross the state boundary surface of the sand (see Figure 2.13). They pointed out that conventional slope stability analyses that use the ultimate friction angle in a limit state approach cannot account for the potential instability and strain softening behavior of soil elements close to the state boundary.

Gu et al. (1993-a). using an elasto plastic model for monotonic undrained condition after collapse and the finite element method, showed that the collapse of the Lower San Fernando Dam after the 1971 earthquake could be explained using a collapse surface concept similar to the state boundary surface presented by Sasitharan et al. (1994).

Skopek et al. (1994) undertook an interesting study on the collapse behavior of very loose dry Ottawa sand. It was demonstrated that very loose dry sand exhibited discontinuous behavior at stress states when flow liquefaction was triggered in an identical saturated sand (Figure 2.14). They showed that this discontinuous behavior was associated with increased compressibility presented as structural contraction and. occasionally, with vigorous stress independent contractive events named "structural collapse". They concluded that flow liquefaction is a result of a specific contractive response of a very loose sand structure and that this response is independent of drainage conditions and can be triggered by a loading path with no excess pore pressure. i.e.. drained.

The discontinuity reported by Skopek et al. has also been noticed in the tests performed by Anderson and Riemer (1995). They conducted some constant shear tests on

anisotropically consolidated samples of the Monterey # 0 sand. The initial conditions and state paths of five tests performed on this sand are shown in Figure 2.15. Two conclusions can be obtained by considering this figure. First, samples with different initial state show a different contractive or dilative response. Second, the ultimate state of specimens falls almost on a unique steady state line. As reported by Anderson and Riemer, the shown steady state line was determined by triaxial compression tests on isotropically consolidated specimens, and therefore the steady state condition is the same for both isotropically and anisotropically consolidated samples. They pointed out that only for very loose specimens was collapse observed before the failure envelope or steady state was reached. They emphasized that specimens subjected to this stress path behave differently than specimens of similar initial density and confining pressure subjected to typical compression stress paths. This observation also indicates the importance of the knowledge of stress path to accurately predict the collapse potential and thereby the potential for flow liquefaction.

The collapse surface concept, which was introduced initially by Sladen et al. (1985-a), and was studied by subsequent researchers, is a helpful approach for interpreting a lot of phenomena which could not be described by conventional methods. At the present time, it is clear that predicting the behavior of loose sands without considering the important collapse surface state boundary is not possible. Therefore, the consideration of this surface for developing any constitutive model is an essential condition. In this section, the collapse surface was discussed by using experimental results. In the next section, collapse will be reviewed as an instability phenomenon in the soil from a mechanical point of view.

2.7. Collapse, instability or flow

Loose sandy soils show a significant drop in shear stress when the stress path reaches the collapse surface under undrained loading (Figure 2.13). Considering the response of the soil between the peak shear stress and steady state point, we can write:

$$d^2 W_p = d\sigma_{ij} \, d\varepsilon_{ij}^p < 0$$

where W_p, $d\sigma_{ij}$ and $d\varepsilon_{ij}^p$ are the plastic work. an increment in stress and the corresponding plastic strain increment. respectively. Therefore. the second increment of the plastic work is negative. This means that Drucker's postulate (1959), referred to as stability in small (i.e.. the work done by the external agency during the application of the added set of forces on the changes in displacements it produces is positive or zero). is not satisfied.

The stability postulate formulated by Drucker appears to capture the behavior of solid metals with good approximation. Solid metals do not change volume during plastic deformation. and this leads to the normality condition with plastic increment vectors to the yield surface. i.e. associated flow is observed for solid metals.

On the other hand. experimental evidence obtained from tests on several types of sand have clearly indicated that the use of conventional associated flow rules results in unrealistic prediction of volumetric strain. Therefore. to characterize the volume change correctly. it is necessary to employ a nonassociative flow rule.

The application of nonassociative plastic flow rules for soil have resulted in questions regarding uniqueness and stability of such materials. Drucker's stability postulate is satisfied provided that associative plastic flow is employed in the construction of constitutive models involving convex. plastic yield surface.

Lade (1992: 1994) conducted a series of triaxial tests on fully saturated and partly saturated specimens under drained and undrained conditions to study the regions of stable and unstable behavior. The results of these experiments show that a positive value of the second increment of plastic work is neither a necessary nor a sufficient condition for stability of granular materials. This means that Drucker's postulate does not capture the conditions for stable and unstable behavior of these materials.

Experimental results have shown that the soil structure at the collapse condition exhibits such a degree of instability that a small disturbance is able to trigger a large amount of deformation. But this response is not the same as bifurcation in soil mechanics. In other words, the response of the soil between peak shear stress and steady state is unique, and if we repeat the tests with the same initial condition, the same response will always be obtained. Therefore, a mathematical solution describing the behavior of soil after the triggering of collapse can be established.

It is evident that flow liquefaction follows upon and necessitates instability, and instability requires employment of a nonassociated flow rule in the constitutive model. Nova (1991) has also shown theoretically that modeling of flow liquefaction within the framework of work-hardening plasticity with a single yield function requires the flow rule to be nonassociative. Therefore, in order to capture this phenomenon, the use of the non-associative flow rule in the constitutive model is essential.

Flow deformation is different from softening, because after the triggering of collapse until the steady state, the stress ratio is increasing. Besides, although a peak appears in the stress-strain curve, the hardening modulus is positive contrary to the softening condition.

Initiation of instability occurs at very low amounts of strain, whether under static or cyclic conditions. Once the instability has been triggered, it leads to flow liquefaction at large strains and steady state conditions. Steady state conditions, achieved at large strains, are not relevant to considerations dealing with the initiation of instability. However, in order to describe the sand behavior at large strains after initiation and during flow of the liquefied sand, analyses must be done based on steady state condition.

Based on the above discussions, one can conclude that, for modelling the sand behavior before and after collapse during flow liquefaction from small strains to large strains, a constitutive model in a steady state framework with a nonassociative flow rule

must be developed. Such a task is undertaken in this study. The details of the formulation will be presented in the next chapters.

2.8. Summary

In this chapter the behavior of cohesionless soils under monotonic and cyclic loading has been briefly reviewed. Because of the need to design safe soil structures against liquefaction phenomenon, the behavior of cohesionless soils has been investigated comprehensively. Depending on its initial state, the soil may show different responses, such as fully contractive, contractive-dilative or fully dilative behavior. The consideration of the soil state in predicting soil response is an essential condition that will be discussed in the next chapter.

Different characteristic surfaces such as collapse, phase transformation and steady state have a significant effect on soil response. Different state indices have been proposed by different researchers to characterize soil state. However, none of them is complete and in the general case a more complete frame must be considered. In practice, for capturing the real behavior of soil, the in situ state of the soil must be recognized. Since different researchers had worked on a limited range of possible conditions for the soil (for example, conducting triaxial cyclic tests only on either isotropically or anisotropically consolidated samples), they have reported some results which appear to contradict one another. The important point is that most of these reported responses are correct, but only in specific conditions. To capture these various soil responses in different conditions, a powerful framework must be applied. This was the focus of effort in this study.
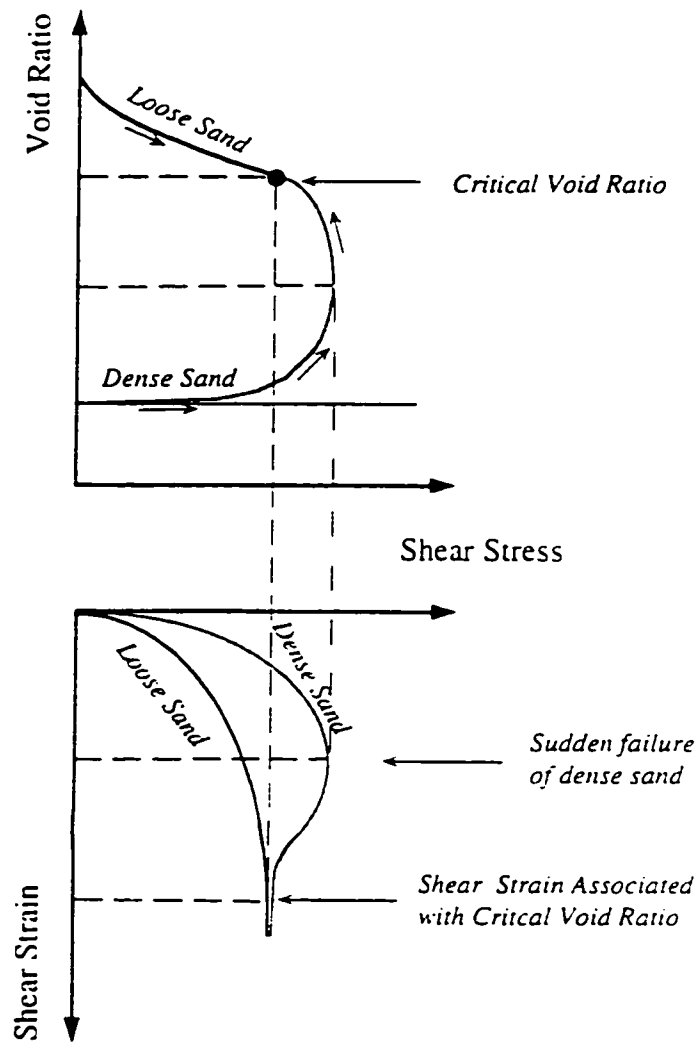
Figure 2.1. Effects of shearing on the volume of soils (modified after Casagrande. 1936).
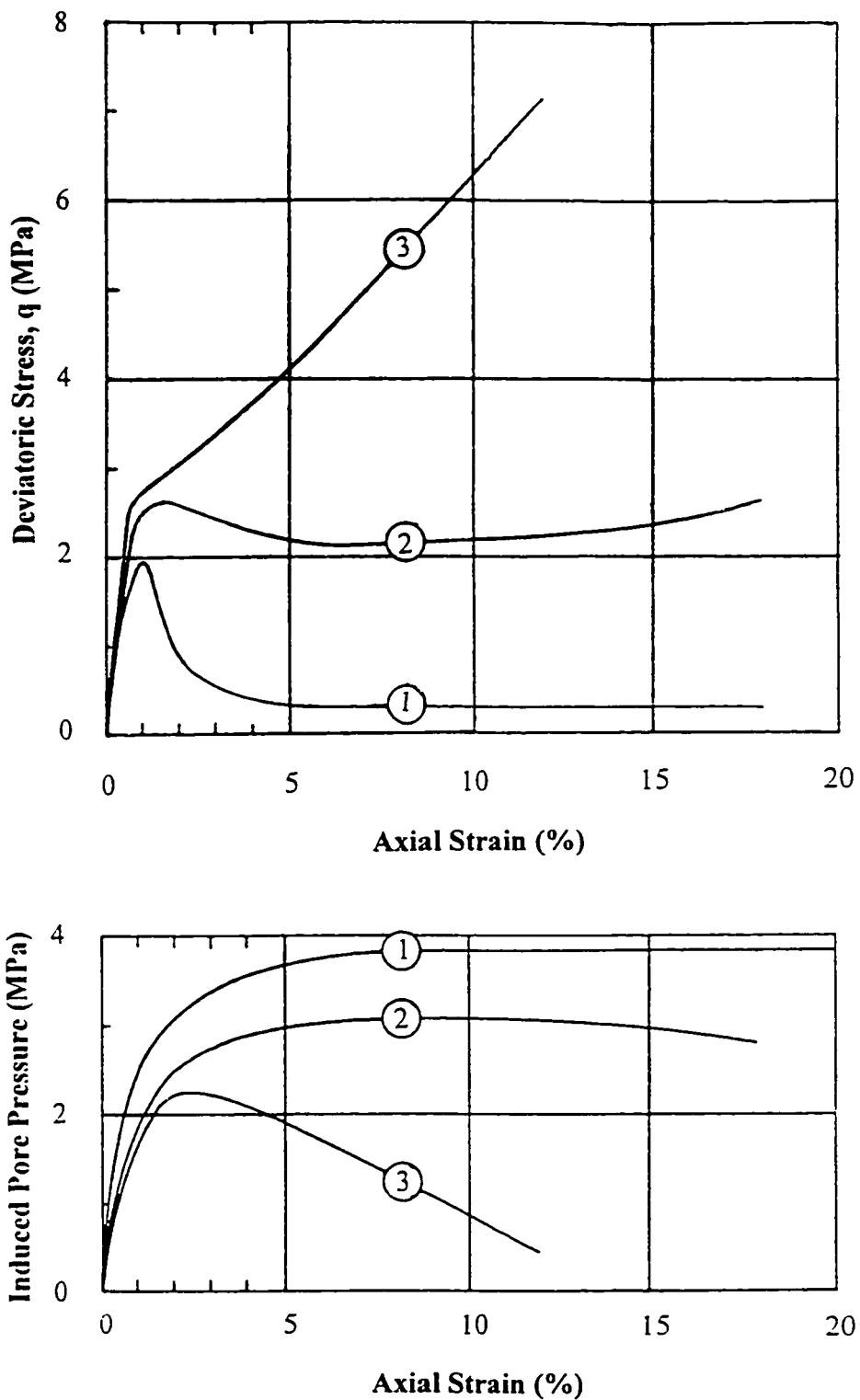
Figure 2.2. Typical undrained behavior of sands.
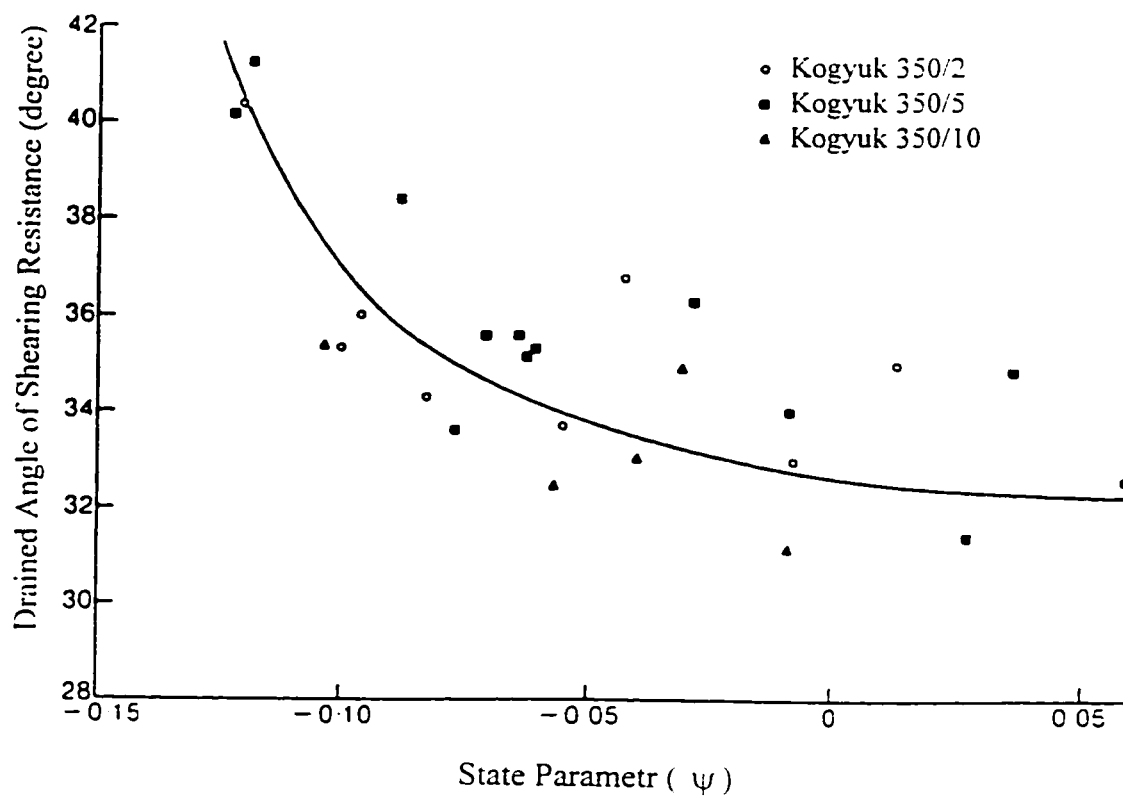
Figure 2.3. Peak angle of shearing resistance as a function of state parameter for Kogyuk 350 sands (modified after Been and Jefferies. 1985).
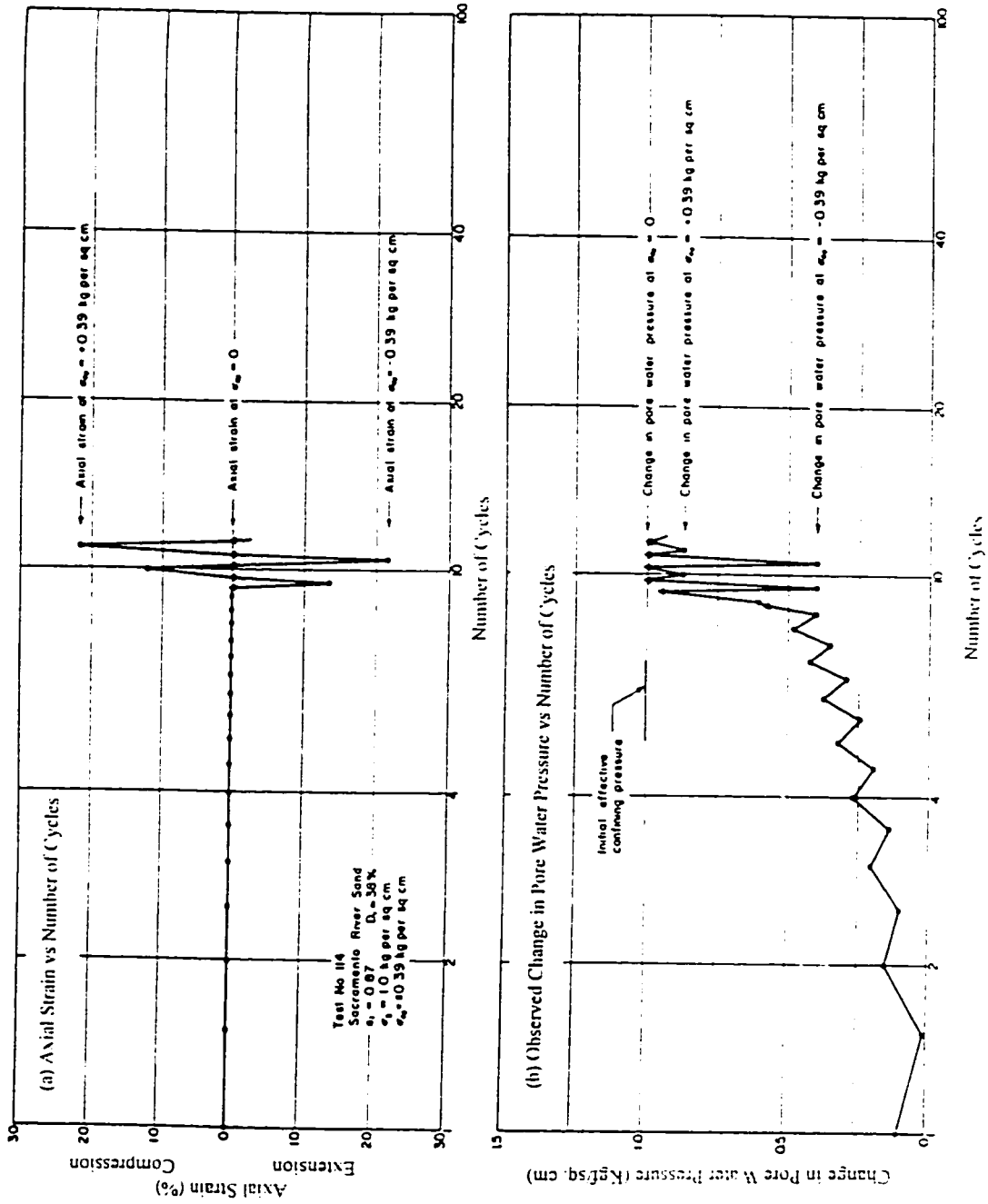
Figure 2.4. Typical results of cyclic triaxial tests on isotropically consolidated loose specimens (modified after Seed and Lee, 1966).
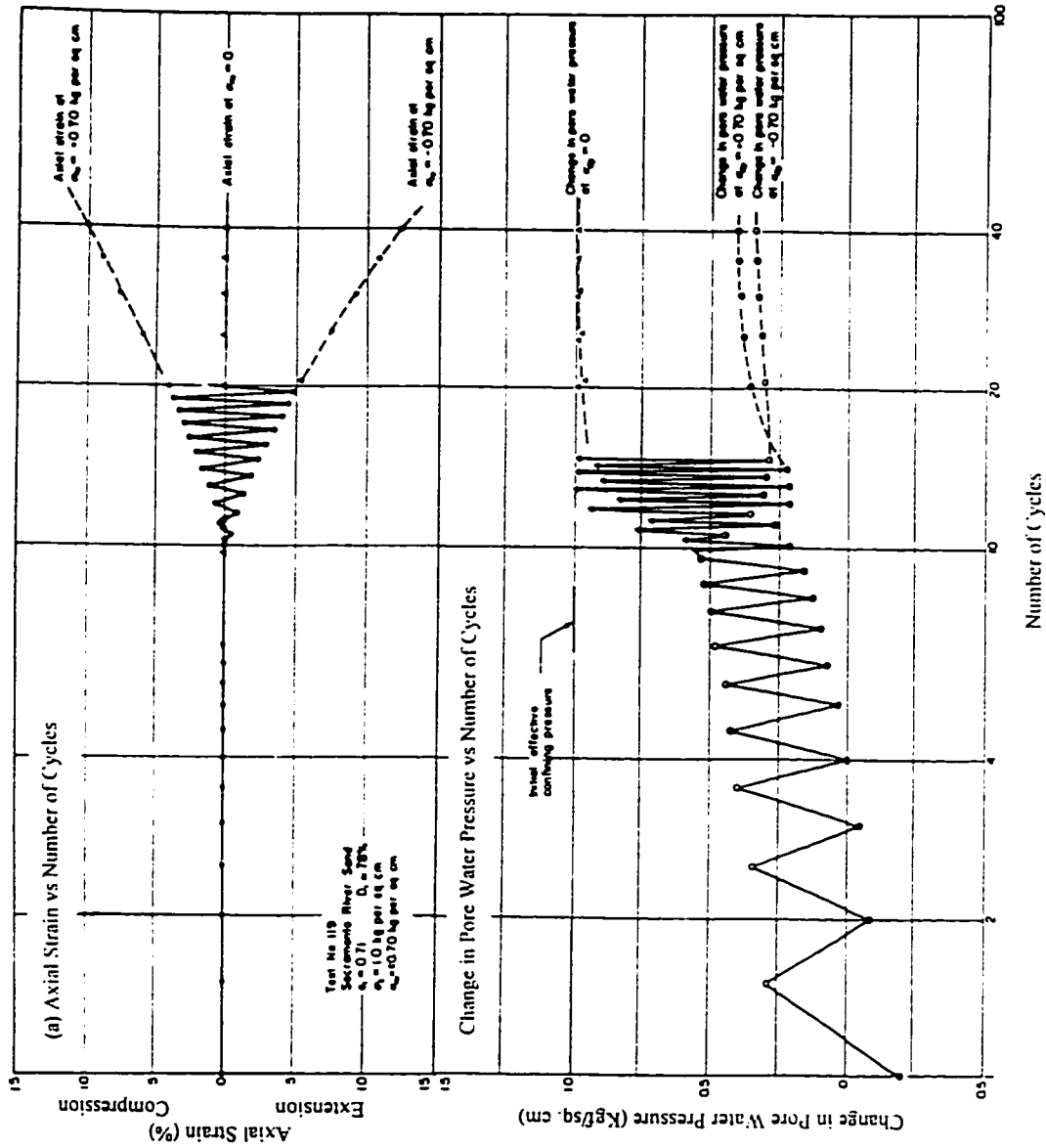
Figure 2.5. Typical results of cyclic triaxial tests on isotropically consolidated dense specimens (modified after Seed and Lee, 1966).

a) Banding Sand (Castro, 1969)

Deviatoric Stress, q (kPa)

Effective Normal Stress (kPa)

b) Banding Sand (Castro, 1969)

1st Cycle

3rd Cycle

Deviatoric Stress, q (kPa)
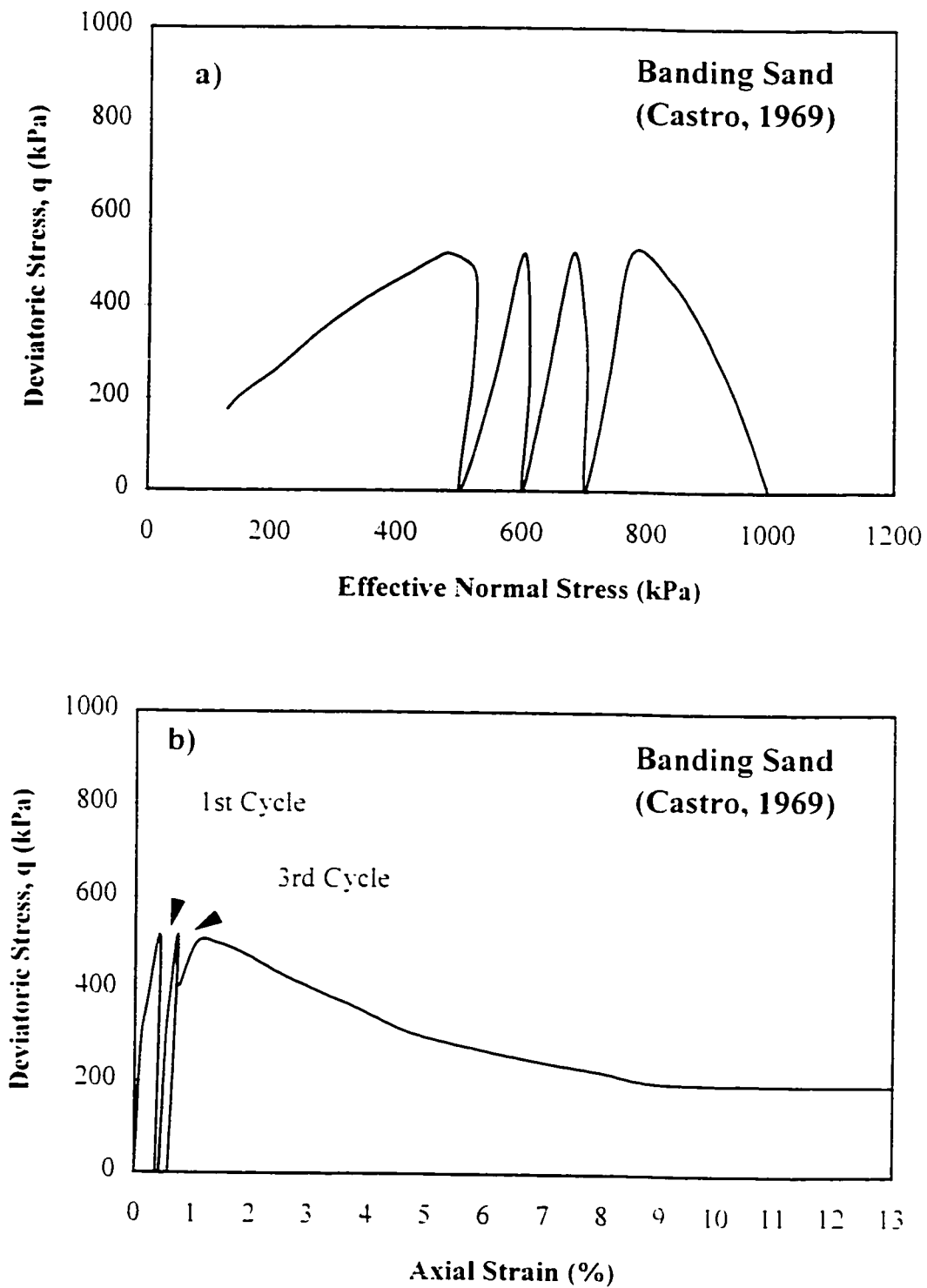
Axial Strain (%)

Figure 2.6. Typical stress path on stress-strain curves in cyclic test on loose sand (modified after Castro. 1969).

Torsional Shear Test

$\tau_d / \sigma_0 = 0.229$

$D_r = 47\%, \sigma_0 = 98$ KN/m ^{2}

γ (%)

a)

Stress - strain curve

Torsional Shear Test

$\tau_d / \sigma_0 = 0.229$

$D_r = 47\%, \sigma_0 = 98$ KN/m ^{2}

30   50   80 σ_0 100

Effective
confining stress
σ (kN/m²)

b)

Line of phase
transformation
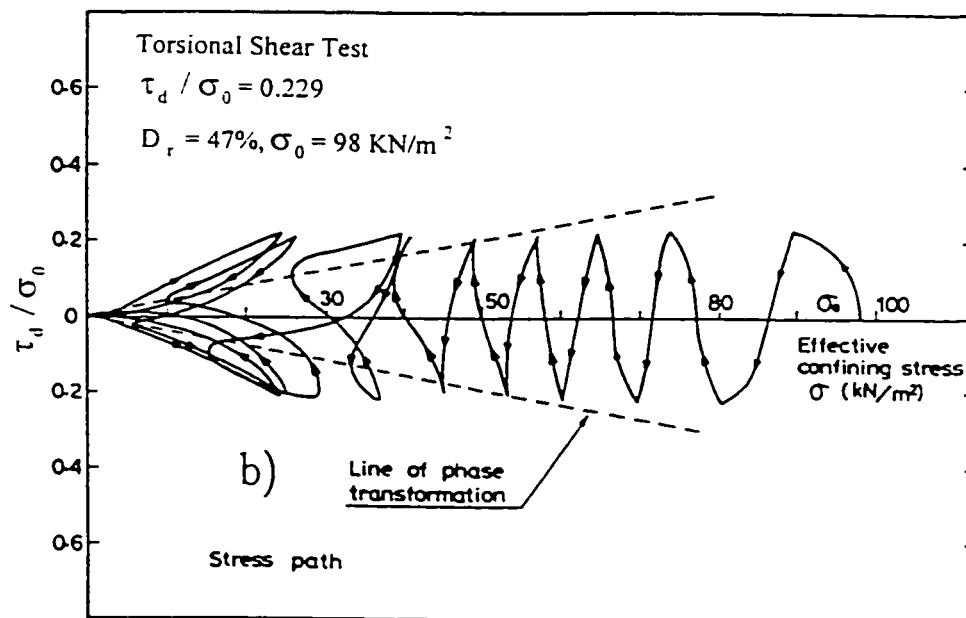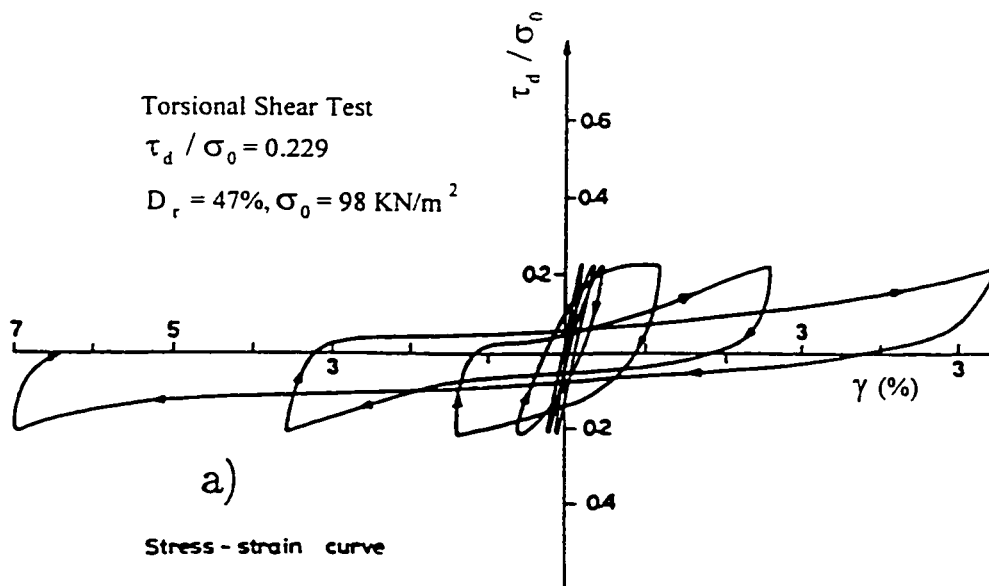
Stress path

Figure 2.7. Stress-strain curve and stress path in cyclic torsional test on
loose sand (modified after Ishihara, 1985).
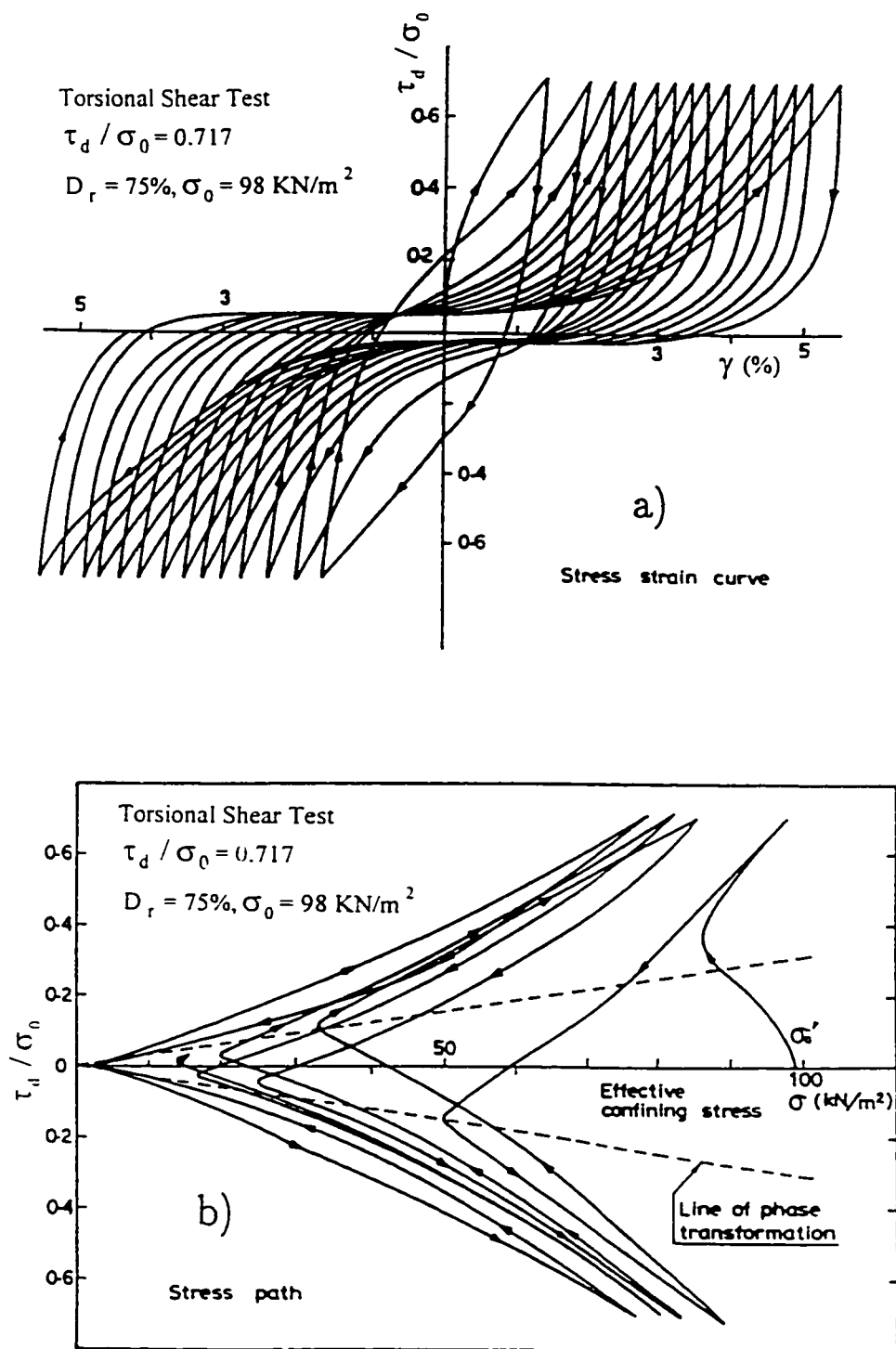
Figure 2.8. Stress-strain curve and stress path in cyclic torsional test on dense sand (modified after Ishihara, 1985).
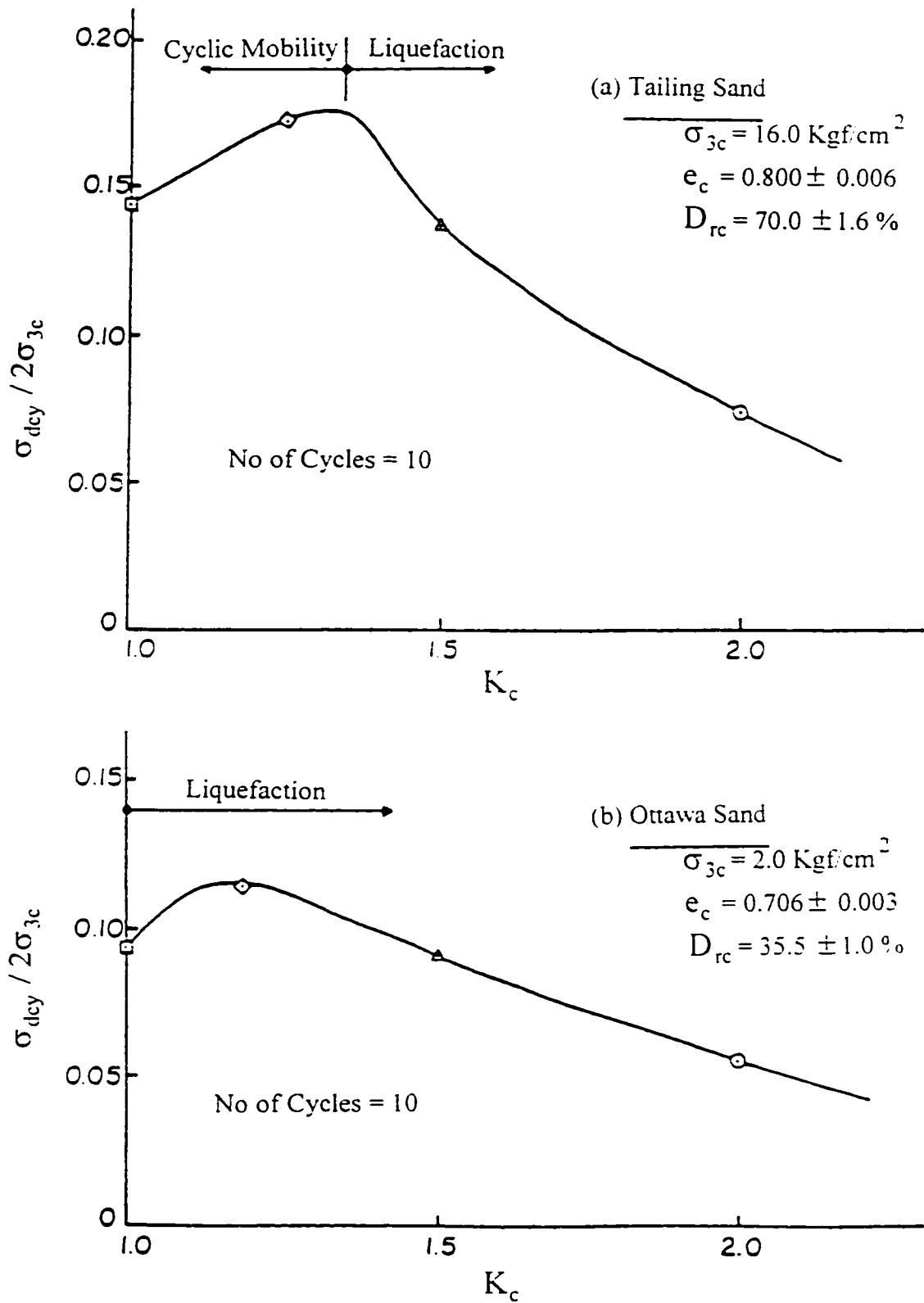
Figure 2.9. Effects of degree of anisotropy on cyclic strength of two sands (modified after Chern and Vaid. 1985).
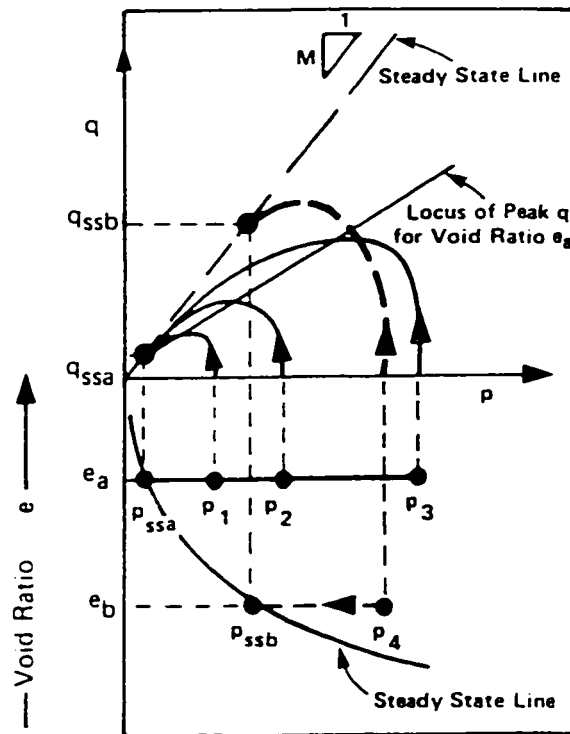
Figure 2.10. Schematic illustration of collapse surface (after Sladen et al.. 1985).
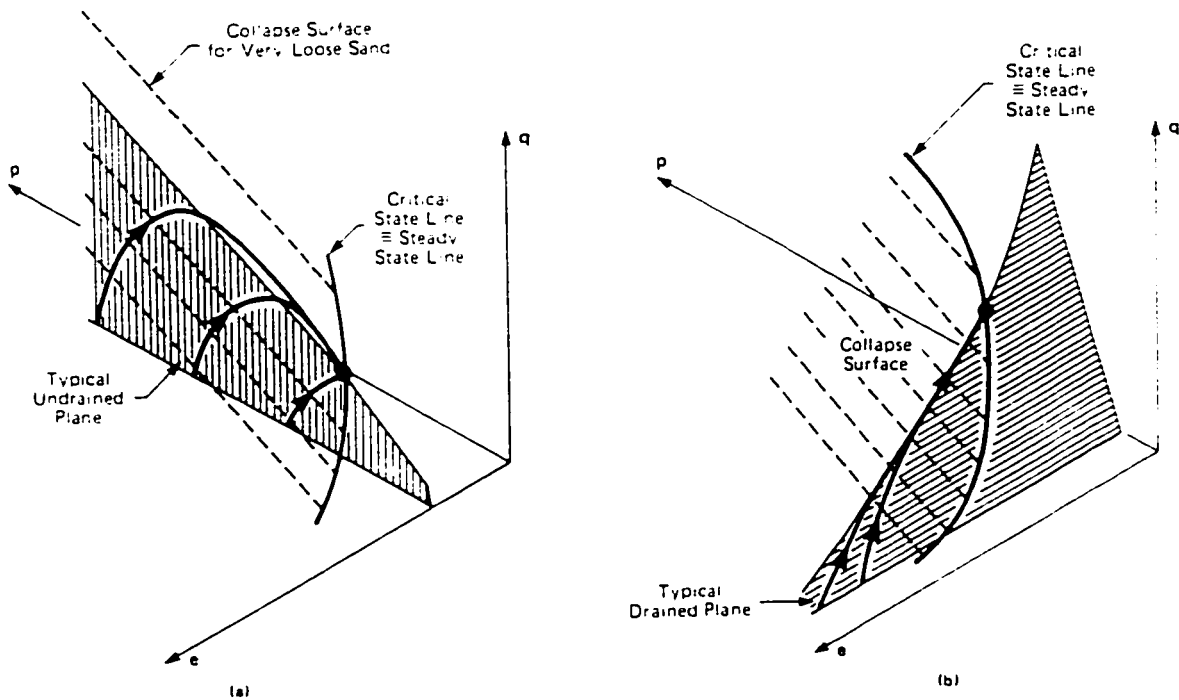
Figure 2.11. Collapse surface in p-q-e space (after Sladen et al.. 1985).
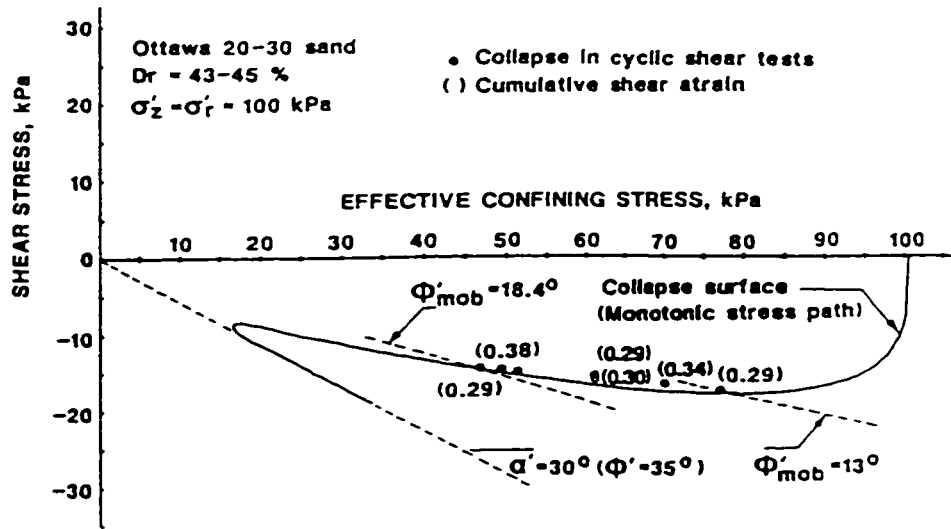
Figure 2.12. Stress conditions at initiation of flow liquefaction under cyclic loading (after Alarcon-Guzman et al., 1988).
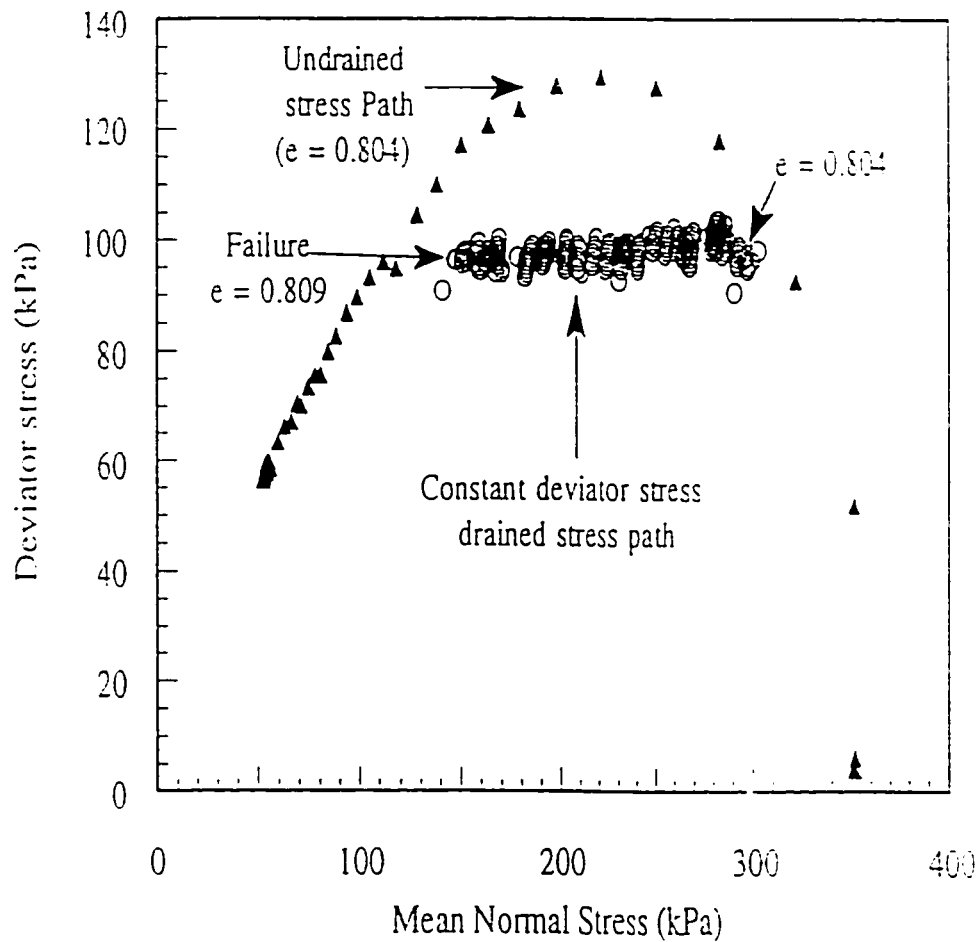
Figure 2.13. Undrained and drained collapse in saturated sand (after Sasitharan et al.. 1994).
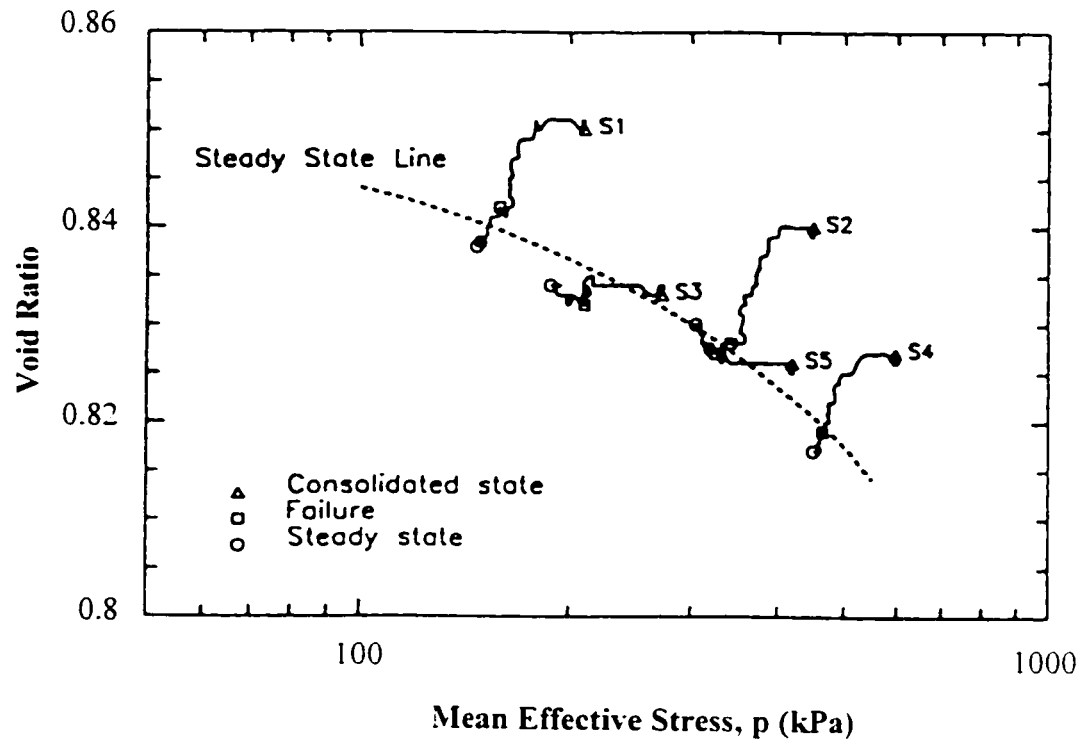
Figure 2.15. State paths at constant shear drained test on Monterey =0 sand (after Anderson and Riemer. 1995).
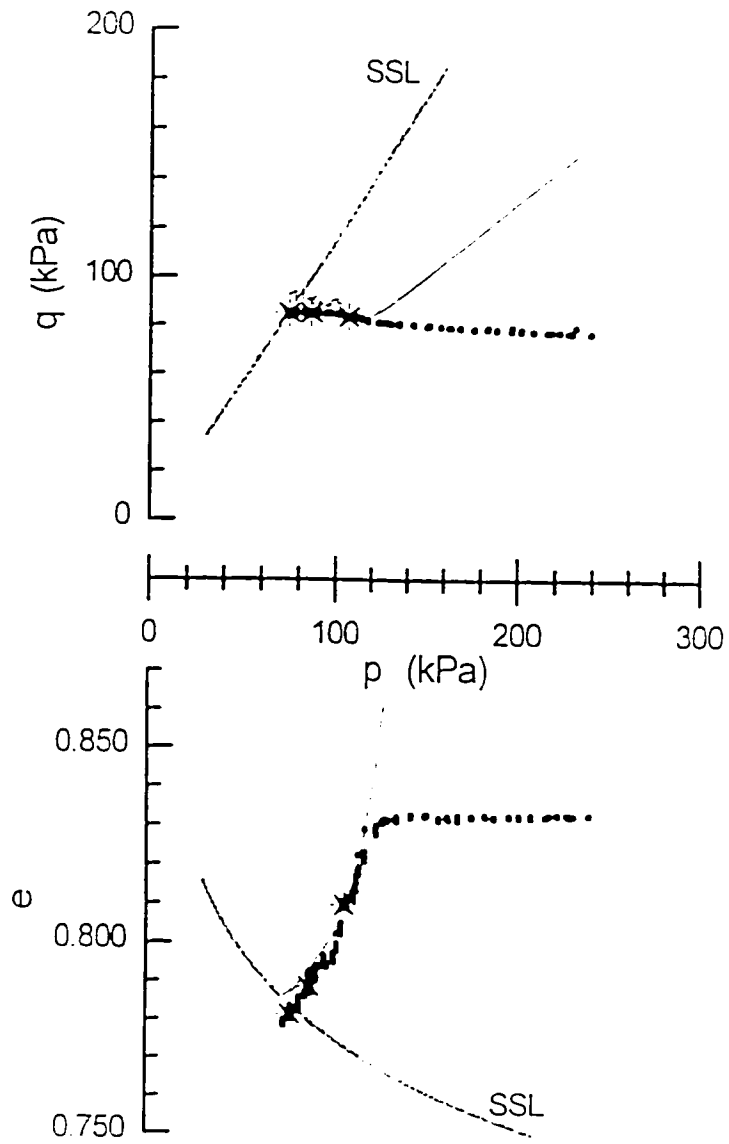
Figure 2.14. Collapse in dry soil (after Skopek et al.. 1994).

Chapter 3

A MULTI-YIELD SURFACE MODEL IN REFERENCE STATE SOIL MECHANICS FOR SAND

3.1. Introduction

The state of a soil has a significant effect on its behavior. In most existing constitutive models for cohesionless soils. this important factor has been neglected. As a result. these models can be used only for a small range of stresses and void ratios for which the model has been calibrated. In this chapter. after a brief review of plasticity in soil mechanics. and a demonstration of the limitation of models with no reference. a new framework. termed "Reference State Soil Mechanics." has been proposed. The multi-yield surface theory (Prevost. 1985) has been modified to embrace "Reference State Soil Mechanics." This model is capable of predicting drained and undrained response of loose and dense sands under both monotonic and cyclic loading with a unique set of parameters. At large strains. this model shows the same ultimate state condition for both loose and dense sands. The model can also capture the effects of initial cross-anisotropy and induced anisotropy. Two different hardening rules have been used and compared with each other for soil specimens at different states.

In chapter 2, the same terminology used by previous researchers was used. Poulos (1971), considering the similarity of soil behavior at large strains with steady state flow of fluids, chose this term to define the terminal state of the soil. From the other side, the Cambridge group, influenced by the critical void ratio concept of Casagrande, has chosen the term critical state to define this state. Although in terms of definition, there is apparently a difference between steady state and critical state regarding the velocity of deformation, these two terms refer to the same phenomenon and in the literature, researchers use them alternatively. It seems the term "ultimate state" represents better this terminal state (Poorooshasb, 1989). Therefore, from this point on in this thesis (except whenever discussion is about "critical state framework"), this term will be used.

3.2. Background

For a long time, soil mechanics has been based on linear elasticity for stress and deformation analysis when no failure of the soil was involved. On the other hand, the theory of perfect plasticity has been used to deal with the conditions of ultimate failure of a soil mass. Historically, the method of perfect plasticity was the most popular framework among traditional soil engineers. Problems of earth pressure, retaining walls, bearing capacity of foundations and stability of slopes are all considered in this category.

During the last few decades, advances in computer technology and numerical methods such as finite element or finite difference techniques have provided solutions for complex boundary value problems in geotechnical engineering. Further progress in analytical capabilities in geomechanics now depends upon consistent mathematical formulation of realistic material constitutive relations. Since the 1960's, considerable effort has been focused on developing simple or advanced constitutive models to capture stress-strain soil response under different loading conditions. The theory of plasticity has been the most successful and popular framework in this area.

The development of the modern theory of soil plasticity was strongly influenced by the theory of metal plasticity. The first major advance in the extension of metal plasticity to soil plasticity was made by Drucker and Prager (1952). who extended the Coulomb criterion to three dimensional soil mechanics problems. Motivated by the concept of work-hardening plasticity in metals (Drucker. 1950) and the experimental observations of the behavior of clays and sands. Drucker. Gibson and Henkel (1957) suggested that soil be treated as a work-hardening material which may finally reach the perfect plasticity state. They showed that by adopting a yield surface composed of a spherical cap on the open end of the Coulomb cone in the general stress space. it is possible to achieve qualitative agreements with the observed behavior of clays. Drucker et al. (1957) suggested that during a drained hydrostatic compression. due to a decrease in water content which leads to an increase in the soil strength. the spherical cap would be pushed farther. creating a new yield surface. This new concept of the use of current water content. or equivalently void ratio. as the hardening parameter and the introduction of the idea of a work-hardening cap are believed to be a landmark in the subsequent development of soil plasticity.

Considering the observations of Casagrande on critical void ratio. the Cambridge group under the leadership of Roscoe extended the basic concept of Drucker et al. (1957) and developed several plasticity-based soil models based on experimental data from triaxial tests. The ideas of the Cambridge group and the formulation of their famous model (Cam clay) led to the "Critical State Soil Mechanics" framework. Since the 1960's different formulations with varying degrees of sophistication have been developed to capture soil deformation behavior under different loading conditions.

Critical state (Roscoe et al.. 1958: Schofield and Wroth. 1968). bounding surface (Dafalias and Popov. 1975: Krieg. 1975) and multi-yield surface (Mroz. 1967: Prevost. 1978: 1985) are among the main formulations which have been proposed to construct constitutive models using plasticity theory. In spite of significant progress in constitutive

modelling. there is still no complete model representing soil behavior in all possible conditions.

The critical state framework is perhaps an exception. The critical state framework which divides soil behavior into wet and dry (normally consolidated and overconsolidated) or loose and dense. has attempted to capture the soil behavior on both wet and dry sides. In spite of the achievements using the critical state framework to model cohesive soils response. it has rarely been used for modelling the behavior of cohesionless soils.

Elasto-plastic theory requires consideration of three basic components: 1)Yield function 2)Flow rule and 3)Hardening rule.

- *Yield function* defines a surface in stress space that relates the highest stresses that a material can reach before any permanent deformations occur upon unloading. In the general case. the yield criterion depends on the current state of stress and should reflect the effects of past loading events on the microstructure of the material. This surface in practice is determined using experimental observations on a specific material. such as steel. clay or sand.

- *Flow rule* gives the direction of the plastic part of the strain increment. It is assumed in plasticity that the total strain increment ($\dot{\varepsilon}$) can be expressed as the sum of elastic ($\dot{\varepsilon}^e$) and plastic ($\dot{\varepsilon}^p$) strain increment. Especially in the past normality assumption (i.e.. the uniqueness of yield function and plastic potential function which shows the direction of plastic strain increment) has been a popular assumption.

- *Hardening rule* defines the variation of yield surface during loading. In general three cases can be considered:

- *Isotropic hardening*: In which the yield surface is assumed to expand uniformly but without any change in position in the stress space.

- *Kinematic hardening*: In which the yield surface moves but without any change in the size.

- *Isotropic-kinematic hardening*: In which both expansion and movement of the yield surface can occur.

Different researchers have worked to determine yield function and potential function for sand. Poorooshasb et al. (1966; 1967) were among the first groups who worked on yielding and flow of sands. Using the results of triaxial compression tests. they showed that sand is an elasto-plastic strain-hardening material. but does not conform to normality. They presented experimental verification for existence of a potential function which depended on stress and void ratio. On the other hand. the yield loci are found to be independent of void ratio and are only functions of the ratio of the second invariant of stress deviatoric tensor to the first invariant of the stress tensor. It is noted. therefore. that the normality condition is violated and in this respect the sand's behavior deviates from that of a classical plasticity body. Later. Poorooshasb (1971) modified his previous proposed functions for yield and hardening functions. The modified yield function was defined as:

$$f = \eta + m \ln p$$

where η . p and m are stress ratio (q / p). mean effective stress and a material parameter. respectively. Poorooshasb et al. (1966; 1967) carried out their tests mostly on dense sands. Following the work of Poorooshasb et al.. Tatsuoka and Ishihara (1974) investigated different kinds of stress paths with drained triaxial compression tests on Fuji River sand with different densities. The results of their tests showed that the yield loci change to some extent depending upon the density of the sample. so that under a constant mean stress. looser samples need higher deviatoric stress for yielding.

Apart from conventional triaxial tests. Lade and Duncan (1973) investigated the characteristics of cohesionless soils by performing cubical triaxial tests on both dense and

loose Monterey No. 0 sand. Examining the directions of plastic strain increment vectors. they concluded that the normality condition is not satisfied in the triaxial plane. but it is almost satisfied on the deviatoric plane. With this assumption that the mean effective stress has no influence on the shape of the failure surface in the deviatoric plane. they proposed an open cone which was dependent on the first and third stress tensor invariants for this surface. The yield surface enclosed by the failure surface has the same general shape as the failure surface and expands isotropically until reaching the failure condition.

Although isotropic hardening models have been widely used in soil mechanics because of their simplicity. these models are not adequate for the prediction of soil behavior under cyclic loading. The isotropic model predicts elastic behavior solely until the stress is fully reversed to the original state. However. it is observed in soil experiments that upon unloading. both elastic and plastic deformations occur well before the stress is fully reversed. Hence. an alternative approach to the isotropic hardening type of model is provided by kinematic hardening rules or a combination of isotropic and kinematic hardening rules. This approach has been employed by several researchers to provide a more realistic representation of soil behavior under reversed and particularly cyclic loading.

Iwan (1967) proposed a one dimensional plasticity model and showed that a collection of elasto-plastic units can effectively model the Bauschinger effect (which refers to directional anisotropy induced by the plastic deformations). This model had a significant improvement compared with previous kinematic hardening models which had been proposed for modelling the Bauschinger effect. In order to extend the model to three dimensional condition. Iwan (1967) and. independently. Mroz (1967) proposed a new framework within the theory of plasticity. Instead of using a single yield surface. they suggested the use of a family of yield surfaces with each surface translating independently in a pure kinematic manner. The translation of yield surfaces has been proposed so that they cannot intersect each other. Mroz/Iwan's models provided a general

framework called the "multi-yield surface plasticity" for modelling monotonic and especially cyclic behavior of metals.

The successful application of a multi-yield surface framework in modelling the cyclic response of metals encouraged some investigators to use this concept for monotonic and cyclic behavior of soils. Joyner and Chen (1976) were among the first who used the Mroz's multi-yield surface model in calculating the response of earth dams subjected to earthquake loading. Prevost (1977: 1978: 1985) developed three anisotropic hardening models within the multi-yield surface framework for clay and sand.

Multi-yield surface models are capable of representing anisotropic and cyclic behavior of soils. They offer great versatility and flexibility for describing any observed material behavior. They do not require the selection a priori to define the variation of plastic modulus in the stress space. Motivated by the versatility of multi-yield surface theory. this theory has been used in the present study.

3.3. Reference state soil mechanics

In this chapter a new framework. termed "Reference State Soil Mechanics". will be presented that can be used for modelling the behavior of both loose and dense soils. In "Reference State Soil Mechanics". soil behavior depends on the position of the soil state with respect to a reference state. Something close to this concept has been used by Poorooshasb (1989): Jefferies (1993) and Manzari and Dafalias (1997) for the description of the flow of sand and modelling of sand behavior .

Poorooshasb (1989) discussed the ultimate state concept for a unified approach to the formulation of the constitutive law for cohesionless granular media utilizing the state parameters. Poorooshasb (1989) mentioned that the state of a sample is defined by the complete set of the pertinent state parameters. He described a state parameter as a quantity that is associated with the sample and can be measured directly at the moment of

examination. A pertinent state parameter is a state parameter that is judged to influence. in some way. the behavior of the sample during the particular process to which it is subjected and its response examined. Poorooshasb (1989) assumed homogeneity and isotropy of the sample. Then it was judged that the void ratio (e) and the effective stress tensor (σ_{ij}) are state parameters. With these assumptions. ir the context of his discussions. the state of the sample is defined by the set of quantities (σ_{ij} . e). Therefore. based on Poorooshasb (1989). the state of a sample is defined by 7 parameters. Poorooshasb (1989) mentioned that the state of a sample can be represented by a point in an n dimensional space. This space was called the state space and the representative point the state point. Poorooshasb (1989) demonstrated the necessity of having to work in the state space (versus stress space).

Been and Jefferies (1985) presented a physical parameter. termed the state parameter (ψ). that combines the influence of void ratio and mean effective stress with reference to an ultimate state to describe sand behavior. Using the results of several tests under different conditions. they concluded that sands behave similarly if test conditions assure an equal initial proximity to the ultimate state. Later Jefferies used this parameter in developing "Nor-sand". a critical state model for sand. Jefferies (1993) postulated infinite number of isotropic normal consolidation loci. which force a separation of intrinsic state measured from overconsolidation. The state parameter (ψ) in Nor-Sand is used as a current variable which determines the current normal consolidation line. The condition of zero plastic volumetric strain occurs at only one point on each admissible yield surface and can be regarded as an image of the ultimate state. Although Nor-Sand can capture the influence of state on the constitutive behavior of sand. it suffers from a number of deficiencies. Normality has been used in Nor-Sand. Therefore. based on the discussion of Nova (1991). this model theoretically is not able to show the instability or collapse of the soil during the hardening process. Furthermore. Nor-Sand is an isotropic model and cannot work for cyclic loading.

Manzari and Dafalias (1997) coupled the two-surface formulation of plasticity with the state parameter (ψ) to construct a constitutive model for sands. The state parameter was used to define the peak and dilatancy stress ratios of sand.

In the present study, the state of a soil is defined by a complete set of independent state parameters. To define the state of a soil, one needs to know the current stress, position of the soil with respect to the ultimate state line (in $p - e$ plane) as a reference and history of loading. For the model in the thesis, the number of state parameters is 13. These parameters are six components of stress tensor (σ_{ij}), state parameter (ψ) and six components for determination of the position of the yield surface (α_{ij}) that shows the history of loading.

Regarding the difference between the "Reference State Soil Mechanics" framework and the "Critical State" framework, although both of them are the same in the definition of the ultimate state (or critical state) at large strains, there is an important distinction. In the "Critical State" framework, the focus is on the critical state that can be observed during the deformation at large strains. However, in the "Reference State Soil Mechanics" framework, each soil has a state that must be considered in the modelling of the behavior of that soil. The ultimate state is only a specific state in the "Reference State Soil Mechanics" framework. If a model is in the "Critical State" framework, it does not mean that it is necessarily in a "Reference State Soil Mechanics" framework. For example, if we believe that the dilatancy of a soil depends on both effective stress ratio and void ratio (or state parameter, ψ), both of these factors must be considered in the definition of the state of the soil and, as a result, in the modelling of its behavior. If a model does not consider completely the state of a soil during loading, it will miss some aspects of the behavior of the soil. In this case, the formulation of that model has not been defined completely in a "Reference State Soil Mechanics" framework, although it may show the correct ultimate state. With this definition, one may find some models in the "Critical State" framework that show the ultimate state correctly, but they are not in a

"Reference State Soil Mechanics" framework. since those models do not consider correctly the state of a soil before reaching the ultimate state.

It is believed that not only is the "Reference State Soil Mechanics" framework more general and can be used for both cohesive and cohesionless soils but that also without considering a reference state. complete modelling of soil behavior over a wide range of stresses and densities is not possible.

For choosing a parameter to define the current position of the soil element with respect to the ultimate state line. there are several options. The state parameter (ψ) was discussed. Ishihara (1993) pointed out that the main assumption in the definition of a state parameter. which is that the behavior of soils with the same ψ is the same. is not always correct. As an alternative he proposed "State Index". I_s. which has been defined using two upper and lower reference lines. He suggested to take the quasi-steady state line as the lower reference. Recently Robertson and Fear (1995) proposed "Reference State Ratio". RSR. which is the ratio of the existing mean effective stress to the mean effective stress at ultimate state at the same void ratio. as a parameter to define the state of the soil. They mentioned that for very loose sands. because of the small slope of the ultimate state line in the ($p-e$) plane. RSR works better than state parameter. The topic of which parameter can better represent the state of the soil is not the subject of this study. What is being argued is that considering soil state measured from a reference state is an essential condition for the complete constitutive modelling of soil behavior.

The point to note is that all the parameters. such as state parameter. ψ. State Index. I_s. or Reference State Ratio. RSR. which have been proposed by different researchers to define the state of the soil. are not complete for representing soil response in the general condition. To define the state of a soil sample at least seven quantities (σ_{ij}. e) plus history of loading must be used. This is an essential condition to capture the soil response in general stress-void ratio space. In the formulation of the presented model

in this thesis. these necessary parameters have been considered either directly or inherently.

Although the behavior of soils depends highly on their states. in most existing constitutive models. especially for cohesionless soils. this effect has not always been considered. As a result. the stress-strain properties of a given soil at different initial states are characterized as two separate materials with different sets of parameters. This means that for a unique soil with two different states. two calibrations must be performed and as a result. these models cannot handle well the response of the soils under drained or undrained conditions over a wide range of stresses and void ratios.

3.4. Models with no reference

As mentioned by different researchers. the state of soil has a significant effect on soil response. Therefore. models with no reference to follow the state of the soil during loading are not able to show this important effect. For observing the inability of models with no reference state. the results of ten conventional drained triaxial compression tests performed on loose and dense Toyoura sand (Verdugo and Ishihara. 1996) have been used. Toyoura sand is a standard sand which is composed of 75% quartz. 22% feldspar and 3% magnetite. It consists of subangular particles with a mean diameter $D_{50} = 0.17$ mm and a uniformity coefficient of $U_t = 1.7$. The maximum and minimum void ratio of this sand. determined by JSSMFE method. are 0.977 and 0.597 respectively with a specific gravity of 2.65 (Ishihara. 1993). The variation of void ratio with mean effective stress for these tests has been shown in Figure 3.1.

Each pair of these samples has been initially consolidated under the same mean effective stress and shear stress; the only difference was in the initial void ratio that causes different states for the samples. As can be seen. during drained shearing. loose samples contracted continuously until reaching the ultimate state at large strains.

However. soils denser than the ultimate state. after a small contraction. started to dilate and have reached the ultimate state condition at large strains. These tests illustrate how the state of soils can affect significantly their response under loading. All these samples have finally reached a unique ultimate state condition.

As an example of models with no reference. Prevost's model (1985) has been considered. This model is a multi-yield surface model that has been formulated in deviatoric stress space. For this study. the model was calibrated by using one of the contractive tests and then all the tests have been predicted using the same parameters. The results of the predictions are also illustrated in Figure 3.1. As can be seen. in spite of changes in the state of the samples. the model has also shown contraction for the dense specimens. Due to the lack of reference in this model. it could not separate the behavior of loose samples from that of dense ones. This inability can also be shown in undrained conditions. If two samples with different void ratios are taken with the same initial stresses. the model by Prevost will show exactly the same stress paths and stress-strain curves. However. experimental observations have shown that these two samples show completely different responses. The other problem that is observed in Figure 3.1 is the lack of a specific ultimate state condition for model predictions. These problems exist in all constitutive models with no reference state. Unfortunately at the present time. most of the existing constitutive models. for cohesionless soils. are in this category.

In the following. the formulation of a multi-yield surface model using a "Reference State Soil Mechanics" framework will be presented. This has been developed based on the Prevost's model (1985). The model is capable of predicting the behavior of both loose and dense sands in undrained and drained conditions under monotonic and cyclic loading with a unique calibration and set of parameters. The proposed model is calibrated easily by conventional laboratory tests and can capture the effect of both initial cross-anisotropy and induced anisotropy during loading. Using different parameters for compression and extension. the model can also show the effect of fabric in the soil response. Finally at large strains. the model shows a unique ultimate state. that depends

on void ratio. for both loose and dense samples. The formulation of the model will be presented in general stress space and then for the specific triaxial condition will be simplified.

3.5. Basic equations

All the stresses in the following equations are effective. Tensor quantities are shown by bold-faced characters. The stress tensor can be decomposed to deviatoric. s_{ij}. and spherical. $p\delta_{ij}$. parts. The assumption is that the increment of strain tensor. $\dot{\varepsilon}_{ij}$. can be decomposed into elastic. $\dot{\varepsilon}^e_{ij}$. and plastic. $\dot{\varepsilon}^p_{ij}$. parts. i.e..

$$\dot{\varepsilon}_{ij} = \dot{\varepsilon}^e_{ij} + \dot{\varepsilon}^p_{ij} \qquad (3-1)$$

The constitutive equation is written as:

$$\dot{\sigma}_{ij} = E_{ijkl}\dot{\varepsilon}^e_{kl} = E_{ijkl}(\dot{\varepsilon}_{kl} - \dot{\varepsilon}^p_{kl}) \qquad (3-2)$$

where σ_{ij} and E are effective stress tensor and isotropic elastic coefficient tensor. respectively. E is expressed as:

$$E_{ijkl} = (B - \frac{2G}{3})\delta_{ij}\delta_{kl} + G(\delta_{ik}\delta_{jl} + \delta_{il}\delta_{jk}) \qquad (3-3)$$

in which B . G and δ_{ij} are respectively bulk modulus. shear modulus and Kronecker delta. The increment of plastic strain is defined as:

$$\dot{\varepsilon}^p_{ij} = <\lambda> R_{ij} \qquad (3-4)$$

where λ is the so called "plastic loading function" . The symbol $< >$ denotes the Macauley bracket. i.e.. $<\lambda> = \lambda$ if $\lambda \geq 0$; otherwise $<\lambda> = 0$. R is a second order tensor which defines the direction of plastic strain increment in the stress space. The plastic loading function is defined as:

$$\lambda = \frac{1}{H}Q_{ij}\dot{\sigma}_{ij} \qquad (3-5)$$

in which H is the plastic modulus and Q is a unit second order tensor which defines the outer normal to the yield surface or loading direction. Combining equations (3-2), (3-4) and (3-5), we can write:

$$\lambda = \frac{1}{H + H_0}(Q_{ij}E_{ijkl})\dot{\varepsilon}_{kl} \qquad (3\text{-}6)$$

with

$$H_0 = Q_{ij}E_{ijkl}R_{kl} \qquad (3\text{-}7)$$

Incorporating equation (3-4) into equation (3-2) we have:

$$\dot{\sigma}_{ij} = E_{ijkl}(\dot{\varepsilon}_{kl} - <\lambda> R_{kl}) \qquad (3\text{-}8)$$

3.6. Yield surface

In accordance with the concept of multi-yield surface plasticity, the model consists of a set of yield surfaces. During past decades, considerable research has been conducted regarding the actual shape of the yield surface for cohesionless soils, e.g., Poorooshasb et al. (1966; 1967); Tatsuoka and Ishihara (1974); Yasufuku et al.(1991), among others. In particular, cones with their apex at the origin have been a popular chosen yield surface for modelling the soil response under loading. In this model the same shape has been selected for the yield surfaces. All the yield surfaces display kinematic hardening. The outermost yield surface acts as a failure surface and ultimate state surface simultaneously. This latter assumption with a pure kinematic hardening rule excludes any strain softening behavior for dense soils in drained conditions. In defining the hardening rule, a combination of isotropic-kinematic hardening will be used as an alternative by which this problem can be solved. Due to anisotropy, generally the center of the yield surface cones does not coincide with the hydrostatic axis in the stress space. The yield function that has been taken from Prevost (1985) is defined as:

$$f = \frac{3}{2}(s_{ij} - p\alpha_{ij})(s_{ij} - p\alpha_{ij}) - g^2(\theta)m_c^2 \ p^2 = 0 \qquad (3\text{-}9)$$

in which $p\alpha_{ij}$ is a deviatoric tensor that shows the position of center of cone on a deviatoric plane (see Figure 3.2) and m is a material parameter. α_{ij} is a variable that expresses the inherent and induced anisotropy of the soil.

The function $g(\theta)$ determines the shape of the cross section of the yield surface on the deviatoric plane. Considerable research has been performed regarding the actual shape of the failure surface in this plane. Using the results of cubical triaxial tests on Monterey No. 0 sand. Lade and Duncan (1973) have shown that the failure surface on the deviatoric plane is bigger than Mohr-Coulomb criterion and with a different friction angle (φ)for $b=0$ and $b=1$ conditions corresponding to triaxial compression and extension ($b=(\sigma_2-\sigma_3)/(\sigma_1-\sigma_3)$). Matsuoka and Nakai (1974: 1977). using the tests on Toyoura sand. pointed out that while φ is the same for $b=0$ and $b=1$. for $0<b<1$. it is more than what Mohr-Coulomb criterion shows.

In this model the function $g(\theta)$ has been chosen so that the shape of the ultimate state surface in the deviatoric plane is a rounded cornered hexagon of Mohr-Coulomb type. The advantage of the chosen shape to Lade and Duncan (1973) and Matsuoka and Nakai (1974. 1977) criteria is that the shape of the ultimate state surface has not been restricted to equal or unequal φ for $b=0$ and $b=1$ conditions. The process of calibration of the model is such that the model will illustrate the same or different φ for triaxial compression and extension based on what has been observed in the experiments. If experiments show that φ is the same in triaxial compression and extension. the ultimate state surface in the model will be close to Matsuoka-Nakai criterion (see Figure 3.3). However. if experiment results show unequal values for the friction angle in compression and extension (Lade and Duncan. 1973). the model will match with these results. A comparison of the ultimate state surface of the model with Mohr-Coulomb. Matsuoka-Nakai and Lade-Duncan criteria is shown in Figures (3.3) and (3.4). The function $g(\theta)$ which has been taken from Wang et al. (1990) is defined as:

$$g(\theta) = \frac{2m_k}{(1+m_k)-(1-m_k)\cos 3\theta} \qquad (3\text{-}10)$$

in which

$$m_k = -\frac{\eta_{uvl}}{\eta_{uvc}} \qquad (3\text{-}11)$$

$$\cos 3\theta = \frac{3\sqrt{3}}{2}\left(\frac{\bar{J}_3}{\bar{J}_2^{1.5}}\right) \qquad (3\text{-}12)$$

$$\bar{J}_2 = \frac{1}{2}\bar{s}_{ij}\bar{s}_{ji} \qquad (3\text{-}13)$$

$$\bar{J}_3 = \frac{1}{3}\bar{s}_{ij}\bar{s}_{jk}\bar{s}_{ki} \qquad (3\text{-}14)$$

$$\bar{s}_{ij} = s_{ij} - p\alpha_{ij} \qquad (3\text{-}15)$$

and η_{uvl} and η_{uvc} are the slope of ultimate state lines in $(q-p)$ plane in triaxial extension and compression. respectively. m_k also shows the ratio of the size of yield surface in triaxial extension and compression for all yield surfaces. The consideration of the constant m_k for all yield surfaces is an essential condition for keeping the uniqueness of the model at the contact point in the kinematic hardening which will be described later.

Considering the shape of the yield surfaces . one can see that for a constant stress ratio (η) loading. the stress path never crosses a yield surface. As a result. the performance of the model under such a loading is elastic. This problem can be solved by adding a cap to the yield surfaces following Vermeer (1978) or Lacy and Prevost (1987). The position and the size of this cap should be a function of volumetric strain. Since the behavior of dense and medium dense sands under this kind of loading. up to very high stresses where the breakage of grains occurs. is elastic (Ko and Scott. 1967). for simplicity in the application. it has not been added to the present model. For the range of stresses in which geotechnical engineers are interested. this is an acceptable assumption. For very loose sands. however. this assumption is not correct. Since application of this

kind of loading in practice is not frequent: considering only open cones does not make any important disadvantage for the present model.

The outer normal to the yield surface. Q. is determined as follows:

$$Q_{ij} = \frac{\dfrac{\partial f}{\partial \sigma_{ij}}}{\left(\dfrac{\partial f}{\partial \sigma_{kl}} \dfrac{\partial f}{\partial \sigma_{kl}}\right)^{0.5}} \qquad (3\text{-}16)$$

We can decompose Q to deviatoric. Q'. and spherical . Q'' . parts as:

$$Q_{ij} = Q'_{ij} + Q''\delta_{ij} \qquad (3\text{-}17)$$

3.7. Flow rule

Equation (3-4) defines the general form of the flow rule. For a specific definition we must define R . For convenience. we can decompose R to its deviatoric. R' . and spherical. $R''\delta_{ij}$. components as:

$$R_{ij} = R'_{ij} + R''\delta_{ij} \qquad (3\text{-}18)$$

where

$$R'' = \frac{1}{3} R_{ij} \qquad (3\text{-}19)$$

Lade and Duncan (1973) have shown that normality is satisfied in the deviatoric plane. Therefore we can assume:

$$R'_{ij} = Q'_{ij} \qquad (3\text{-}20)$$

R'' is determined mostly by the dilatancy of the soil. In most of the existing constitutive models. dilatancy depends only on stress ratio (η) and not on the individual values of deviator stress or mean effective stress.

To reflect the dependency of the shear dilatancy on the effective stress ratio (Rowe. 1962: Luong. 1980) and in the comparison of the existing stress ratio with

something similar to the slope of the phase transformation line (Ishihara et al., 1975). Prevost (1985) has suggested the following expression for R'' :

$$R'' = \frac{1}{3}\left[\frac{(\frac{\eta}{\bar{\eta}})^2 - 1}{(\frac{\eta}{\bar{\eta}})^2 + 1}\right]$$ (3-21)

where

$$\eta \quad = \text{mobilized stress ratio} = (\frac{3}{2}s_{ij}s_{ij})^{0.5} / p$$ (3-22)

and $\bar{\eta}$ or dilation parameter is a material parameter. In this model the same expression is used but with an important modification. Based on this flow rule, when $\eta < \bar{\eta}$, the model shows contraction and when $\eta > \bar{\eta}$, the model represents dilation. The case of $\eta = \bar{\eta}$ corresponds to no plastic volumetric strain.

The dilation parameter in Prevost's model is determined directly by the experimental results. Although it was suggested to use the average $\bar{\eta}$ for all yield surfaces, the average $\bar{\eta}$ is not effective . This problem can be seen if one uses the average values of $\bar{\eta}$ for prediction of the test which has been used for calibration of the model. On the other hand, the obtained $\bar{\eta}$ is related to a specific state of the soil that is usually contractive (which is used in calibration of the model). As a result, when the model is calibrated by a loose sample, it is not able to show the dilation behavior of a dense sample in drained conditions.

To solve this problem, the ultimate state surface has been used as a reference for the model. The rate and direction of volumetric strain depends on the position of the soil with respect to this surface compared with the condition which existed in a reference condition. Been and Jefferies (1985) showed that specimens with the same state parameter, ψ, have similar contractive or dilative characteristics. Also, they pointed out that approximately a unique relation between dilation and state parameter exists. Using

the results of a large number of tests which had been performed and reported for different kinds of sands. the following relationship is suggested for using in the model:

$$\overline{\eta} = \overline{\eta}_0 \exp\left[\frac{k_\alpha(\alpha_{_{//}}\alpha_{_{//}} - \alpha_{_{//}}^0\alpha_{_{//}}^0)}{g^2(\theta)m_c^2} + 5(\psi - \psi_{ref})|\eta^{\gamma}|\right] \qquad (3\text{-}23)$$

where $\overline{\eta}_0$ is the dilation parameter of the yield surface at a reference state parameter (ψ_{ref}) and position ($\alpha_{_{//}}^0$). k_α is a material parameter that affects the rate of volumetric strain with respect to the position of yield surface.

The second term in the bracket in equation (3-23) demonstrates that with changing the state of the soil. dilation parameter changes. In other words. loose soils have more tendency to contract than dense soils. This assumption corresponds with Been and Jefferies's (1985) observations. The shape of this function has been chosen so that. if soil has a bigger state parameter compared with the reference state ($\psi > \psi_{ref}$). the dilation parameter ($\overline{\eta}$) will be bigger than the reference dilation parameter ($\overline{\eta}_0$). As a result. soil will show more contraction. On the other side. if $\psi < \psi_{ref}$. the equation shows that $\overline{\eta} < \overline{\eta}_0$ and. therefore. soil will show less tendency to contract. The performance of the model in prediction of the behavior of dense. medium dense and loose samples of sands with a unique $\overline{\eta}_0$ and ψ_{ref} (which will be shown in the next chapter) confirms that the proposed formulation works.

The first term in the bracket in equation (3-23) has been defined to represent the effect of the position of yield surfaces on their dilation parameters. As will be seen in section (3.11) and the appendix. in calibration of the model. $\overline{\eta}_0$ is determined using the stress ratio (η) of each yield surface. For the first yield surfaces. because η is small. $\overline{\eta}_0$ will be small too. If this $\overline{\eta}_0$ is used for the prediction of the soil performance under unloading started at high stress ratio. since the existing η is higher than that which existed in the calibration. the model shows high dilation. For solving this problem. the first term has been considered in the bracket in equation (3-23). Because this problem

does not exist this much in the last yield surfaces. the term in the denominator has been added to decrease the effect of this part of the bracket for those yield surfaces. Considering this factor is particularly essential for modelling soil behavior under cyclic loading. Equation (3-23) is a key relationship that has a significant effect on the rate of plastic volumetric strain in the model.

The value of $\overline{\eta}$ in the general condition is determined by using the equation which has been suggested by Prevost (1985) as follow:

$$\overline{\eta} = \frac{\overline{\eta}_c + \overline{\eta}_k}{2} + \cos 3\theta \frac{\overline{\eta}_c - \overline{\eta}_k}{2}$$

(3-24)

where $\overline{\eta}_c$ and $\overline{\eta}_k$ are dilation parameters in compression and extension. respectively.

3.8. Hardening rule

In general. three kinds of hardening rules can be used in modelling soil behavior. isotropic. kinematic and combination of isotropic-kinematic hardening. It has been shown that to capture the cyclic response of the soils. kinematic hardening is an essential condition. In the present model. two different hardening rules are used. pure kinematic and isotropic-kinematic hardening.

Mroz (1967) has proposed a kinematic hardening rule. This rule is used to describe mathematically the motion of yield surfaces in the model. Assume that the surfaces $f^{(1)}$ to $f^{(i)}$ are in contact at point N . and the surface $f^{(i)}$ is translating towards the conjugate point T (see Figure 3.5). The translation of $f^{(i)}$ will occur along NT (or μ_n). where the lines connecting the center of the yield surface $f^{(i)}$ to N and the center of the yield surface $f^{(i-1)}$ to T are parallel. Since m_k is the same for all yield surfaces. they have a similar shape. For two yield surfaces $f^{(i)}$ and $f^{(i-1)}$ we have:

$$s_{ij}^{(l-1)} - p\alpha_{ij}^{(l-1)} = \frac{m_c^{(l-1)}}{m_c^{(l)}}(s_{ij}^{(l)} - p\alpha_{ij}^{(l)}) \qquad (3\text{-}25)$$

Therefore, the direction of translation, μ_{ij}, is determined as:

$$\mu_{ij} = \frac{m_c^{(l-1)}}{m_c^{(l)}}(s_{ij}^{(l)} - p\alpha_{ij}^{(l)}) - (s_{ij}^{(l)} - p\alpha_{ij}^{(l-1)}) \qquad (3\text{-}26)$$

The movement of center of yield surface (l) now can be determined by:

$$p\dot{\alpha}_{ij} = a\mu_{ij} \qquad (3\text{-}27)$$

where a is a scalar component that represents the amount of translation and can be determined by using of consistency condition as follow:

$$\dot{f} = \frac{\partial f}{\partial \sigma_{ij}}\dot{\sigma}_{ij} + \frac{\partial f}{\partial \alpha_{ij}}\dot{\alpha}_{ij} + \frac{\partial f}{\partial m_c}\dot{m}_c = 0 \qquad (3\text{-}28)$$

After the differentiating of equation (3-9), equation (3-28) can be written as:

$$Q_{ij}\left(\frac{\partial f}{\partial \sigma_{kl}}\frac{\partial f}{\partial \sigma_{kl}}\right)^{0.5}\dot{\sigma}_{ij} + \frac{\partial f}{\partial \alpha_{ij}}\dot{\alpha}_{ij} - 2g^2(\theta)m_c p^2\dot{m}_c = 0 \qquad (3\text{-}29)$$

and then

$$\dot{\alpha}_{ij} = \frac{Q_{ij}\left(\dfrac{\partial f}{\partial \sigma_{kl}}\dfrac{\partial f}{\partial \sigma_{kl}}\right)^{0.5}\dot{\sigma}_{ij} - 2g^2(\theta)m_c p^2\dot{m}_c}{-\dfrac{\partial f}{\partial \alpha_{ij}}} \qquad (3\text{-}30)$$

Combining equations (3-30), (3-27) and (3-5) we will have:

$$a = p\frac{\lambda H\left(\dfrac{\partial f}{\partial \sigma_{kl}}\dfrac{\partial f}{\partial \sigma_{kl}}\right)^{0.5} - 2g^2(\theta)m_c p^2\dot{m}_c}{-\dfrac{\partial f}{\partial \alpha_{ij}}\mu_{ij}} \qquad (3\text{-}31)$$

and then

$$\dot{\alpha}_{ij} = \frac{\lambda H\left(\dfrac{\partial f}{\partial \sigma_{kl}}\dfrac{\partial f}{\partial \sigma_{kl}}\right)^{0.5} - 2g^2(\theta)m_c p^2\dot{m}_c}{-\dfrac{\partial f}{\partial \alpha_{ij}}\mu_{ij}}\mu_{ij} \qquad (3\text{-}32)$$

Equations (3-26) and (3-32) describe completely the movement of yield surfaces in the stress space. For the pure kinematic hardening rule. the second term in the numerator of equation (3-32) is zero. In this case. because the last yield surface is also the ultimate state surface in the stress space. with the above kinematic hardening rule. the model is not capable of showing softening in drained conditions for dense sands. A lot of existing models have the same problem. Practically speaking. because dense sands are less problematic soils. usually designers are not interested in the behavior of sands in this region and some approximation is acceptable. However. in order to have a complete formulation for the model that can also model the behavior of dense sands more precisely. an isotropic hardening rule will be presented. A combination of the above kinematic hardening rule and an isotropic hardening rule can capture completely the behavior of very dense sands.

Been and Jefferies (1985) have shown that the peak angle of shearing resistance is a function of state parameter. ψ. Therefore. in constitutive modelling. the failure stress ratio cannot be regarded as a constant input soil parameter. Using this observation. Wood et al. (1994) linked the peak stress ratio with the current value of the state parameter through a simple linear expression:

$$\eta_{max} = \eta_{m} - k\psi \tag{3-33}$$

where k is a material constant and η_{m} is the ultimate state stress ratio. With this link. Wood et al. (1994) could capture the strain softening behavior of dense sands in drained conditions. Following Wood et al.(1994). Manzari and Dafalias (1997) added a Macauly bracket to the above equation and used it to define the variation of bounding stress-ratio in their model.

In the present work. the same relationship is adopted but for changing the size of yield surfaces as a function of state parameter. i.e..

$$m_{cd} = m_{c} + k < -\psi > \tag{3-34}$$

in which m_{ud} represents the size of the yield surface on the side that is denser than the ultimate state and must be used in place of m_u in the formulation of the model for the dense side. The parameter k is a material parameter. Using Macauly bracket $< >$ shows that for soils looser than the ultimate state. ψ is positive and the second part of the right side of equation (3-34) is zero: hence the size of yield surfaces are constant. For soils denser than the ultimate state. based on the value of ψ. the size of yield surfaces changes. and by approaching the ultimate state. the second part converges to zero. Finally for both loose and dense soils. the model shows the same ultimate state.

In the present model. the assumption is that all yield surfaces are under kinematic hardening except the last yield surface. For this yield surface all the elements of the tensor of $\dot{\alpha}$ are zero. Therefore. considering equation (3-32). the plastic modulus for the last yield surface is determined by:

$$H = \frac{2g^2(\theta)m_u p^2 \dot{m}_u}{\lambda \left(\dfrac{\partial f}{\partial \sigma_{ij}} \dfrac{\partial f}{\partial \sigma_{ij}} \right)^{0.5}}$$

(3-35)

Equation (3-35) illustrates that. if the model is under only kinematic hardening (i.e.. $\dot{m}_u =$ 0). the plastic modulus for the last yield surface theoretically will be zero. In general conditions. considering equation (3-34). one can write:

$$\dot{m}_{ud} = -k\psi < -\frac{\psi}{|\psi|} >$$

(3-36)

Considering Macauly bracket in equation (3-36). one can see that only for the state that is denser than the ultimate state. $\dot{m}_{ud}$ is not equal to zero. Therefore. $\dot{m}_{ud}$ shows the variation of the size of yield surface in the dense side. Also one has:

$$\dot{\psi} = \dot{e} - \dot{e}_{us}$$

(3-37)

where $\dot{e}$ and $\dot{e}_{us}$ show the increments of the void ratio of the soil and ultimate state line. respectively. Considering compressive stresses and strains as positive. one can write:

$$\dot{e} = -\dot{\varepsilon}_v (1 + e_{in})$$

(3-38)

in which e_{in} and $\dot{\varepsilon}_v$ are the initial void ratio and increment of volumetric strain. respectively. Combining equations (3-36) to (3-38) with some manipulations. one will have:

$$\dot{m}_{ud} = k\left[(\frac{\dot{p}}{B} - 3\lambda R'')(1 + e_{in}) + \dot{e}_{in}\right] < -\frac{\psi}{|\psi|} >$$
(3-39)

where $\dot{p}$ is the increment of mean effective stress.

Using equations (3-39) and (3-35). one can determine the plastic modulus for the last yield surface. remembering that $\dot{m}_{ud}$ is $\dot{m}_v$ for the dense side.

Although by using isotropic-kinematic hardening. one can also capture the strain softening response of dense sands in drained conditions. in most practical problems. using pure kinematic hardening is acceptable (see chapter 4).

A comparison of model predictions with pure kinematic and isotropic-kinematic hardening rules under drained conditions has been shown in Figures (3-6).(3-7) and(3-8). In these figures. model predictions for a set of conventional drained triaxial tests have been presented. It was assumed that the samples have been consolidated isotropically and initial mean effective stress is 1 MPa for all of them. For covering a complete set of initial states. the initial void ratio of the samples has been taken from 0.6 to 0.95.

As can be seen. for the samples initially loose of the ultimate state. the predictions of the model with both kinematic and isotropic-kinematic hardening are the same. This is not surprising. because in this condition. state parameter is positive and based on equation (3-34). the size of yield surfaces does not change. But with decreasing void ratio. the difference between the two hardening rules appears. Using the isotropic-kinematic hardening. during shearing. the mean effective stress and deviatoric stress increase. After reaching a maximum value which is higher than the ultimate state value. however. they start to decrease and come back to the ultimate state condition. The values

of maximum mean effective stress and deviatoric stress depend on the state parameter of the soil. However. for kinematic hardening. stresses increase continuously up to the ultimate state value. In this condition. the stress paths never pass the ultimate state line. As can be observed. for the loose and medium dense sands. the difference between the application of the two hardening rules is not significant and even using the kinematic hardening rule is acceptable. For the stress-strain and volumetric strain-axial strain curves. the same trends can be observed. For isotropic-kinematic hardening. different degrees of softening based on soil state occur. The maximum stress ratio during shearing depends on the initial state parameter. In Figure (3.9). the variation of η_{max} with initial state parameter. ψ_i. for both hardening rules has been shown. For the kinematic hardening rule. as expected. the η_{max} is constant and equal to η_u. For isotropic-kinematic hardening. however. η_{max} change with ψ_i. This variation for samples denser than ultimate state corresponds with what has been reported by Been and Jefferies (1985) for the variation of the angle of shearing resistance with state parameter (see Figure 2.3).

The same comparisons but in undrained conditions have been presented in Figures (3.10). (3.11) and (3.12). The void ratio for all the samples has been 0.78. With decreasing mean effective stress. the state of the samples changes from looser than ultimate state to denser. Similar to drained conditions. for loose and medium dense samples. the difference between predictions of the model with two different hardening rules is negligible. However. for dense samples this difference is more apparent.

Considering Figures (3.6) to (3.8) and (3.10) to (3.12). one can see that the difference caused by two hardening rules depends on the state parameter. For problems in which the soil is loose or medium dense. the use of the pure kinematic hardening is acceptable. However. if the soil is very dense. using isotropic-kinematic hardening rule is an essential condition to predict soil response. especially at small strains. In any case. the proposed model contains both options.

3.9. Elastic moduli

In the elastic region, the material is assumed to be isotropic. Therefore. two elastic parameters such as shear modulus and bulk modulus or shear modulus and Poisson's ratio are required for introducing the model response in this region. Shear and bulk modulus generally increase with mean effective stress and decrease with the increase of void ratio (Richart et al., 1970). In this model the variation of shear modulus is defined as:

$$G = G_0(\frac{p}{p_0})^{0.5}\frac{(2.17-e)^2(1+e_0)}{(2.17-e_0)^2(1+e)} \qquad (3\text{-}40)$$

where

G = Shear modulus

G_0 = Reference shear modulus at p_0 and e_0

p_0 = Reference mean effective stress

e = Current void ratio

e_0 = Reference void ratio

Bulk modulus is also defined similarly as:

$$B = B_0(\frac{p}{p_0})^{0.5}\frac{(2.17-e)^2(1+e_0)}{(2.17-e_0)^2(1+e)} \qquad (3\text{-}41)$$

in which B_0 is the reference bulk modulus at p_0 and e_0 . p_0 and e_0 are two reference values and can be fixed to any arbitrary constant values like p_{atm} and $e_0 = 1$: however. after choosing any values for them, G_0 and B_0 must be defined for those values. Comparing equations (3-40) and (3-41), one can see that the definition of equation (3-41) is equal to usage of a constant Poisson's ratio.

3.10. Plastic modulus

Plastic modulus has an important effect on the response of all elasto-plastic constitutive models. In this model the plastic modulus for each yield surface is

determined by the result of experiments. Therefore it is not necessary to have any pre-definition for variations of plastic modulus in different yield surfaces. As a result. the model will be able to show the behavior of any soil for which the model has been calibrated. It is clear that such a plastic modulus cannot be constant. but rather depends on mean effective stress and void ratio. To achieve a better performance of the model in simulation of the monotonic and cyclic behavior of sands. after testing for different soils in different void ratios and mean effective stresses. the following relationship is suggested:

$$H = H_0 (\frac{p}{p_0})^{0.5} \left[\frac{(2-e)(2+e_0)}{(2-e_0)(2+e)} \right]^{n_H} \tag{3-42}$$

in which

H_0 = Reference plastic modulus at p_0 and e_0

n_H = Material parameter

The value of H in general condition is determined by the following equation that has been suggested by Prevost (1985):

$$H = \frac{H_c + H_E}{2} + \cos 3\theta \frac{H_c - H_E}{2} \tag{3-43}$$

in which H_c and H_E are plastic modulus in triaxial compression and extension.

3.11. Calibration of the model

The model is fully calibrated by 11 parameters with kinematic hardening or by 12 parameters with isotropic-kinematic hardening. All parameters are determined from conventional laboratory tests. Considering the process of calibration. one can see that the most of the parameters are determined directly during calibration and only a few parameters must be determined by curve fitting. This allows convenience for users. In this section the calibration of the model will be described. An example of calibration of the model is presented in details in the appendix.

Shear modulus. G . can be determined by the shear wave velocity:

$$G = \rho v_s^2 \qquad (3\text{-}44)$$

where ρ and v_s are the density of soil and shear wave velocity. respectively. As was mentioned in the past. this modulus is determined for a specific mean effective stress. p . and a specific void ratio. e . Using equation (3-40). G_0 in p_0 and e_0 can be determined. In the absence of the result of shear wave velocity test. the shear modulus can be determined by the steepest slope measured at the origin of the deviator stress-shear strain curve. The empirical relationships which have been proposed by different researchers may also be used with approximation (for example. Richart et al.. 1970).

Bulk modulus. B . is determined by measuring the slope of the mean effective stress-volumetric strain curve of unloading in a hydrostatic test or with some approximation by the initial slope of mean effective stress-volumetric strain obtained in a drained triaxial test. As with the shear modulus. B is related to a specific p and e. and can be normalized (B_0) at p_0 and e_0 . using equation (3-41).

The ultimate state line in the ($p - e$) plane also must be defined to retain it as a reference in the model during the analysis. There are some discussions regarding the shape of the ultimate state line and its uniqueness for different shearing modes and drainage conditions. For keeping the versatility of the model. no specific shape for the steady state line is considered. This line must be defined for the model but can have any shape without adding any limitation to the model. In the future. if the variation of this line is defined. it can be considered in the model without any necessary change in the proposed formulation.

m_k is determined using the slope of ultimate state lines in the ($q - p$) plane for triaxial extension and compression (i.e.. η_{ulE} and η_{ulc}) and equation (3-11).

Each conical yield surface is defined in terms of m_c, representing the size of the yield surface for triaxial compression, α, representing the position of the yield surface in the stress space, H_{0c} and H_{0E}, the reference plastic moduli in compression and extension, and $\overline{\eta}_{0c}$ and $\overline{\eta}_{0E}$, the reference dilation parameters in compression and extension. These parameters can be determined from the results of one pair of drained compression and extension triaxial tests on loose sand.

In the triaxial test, the specimen is under axi-symmetric conditions, i.e.,

$$\sigma_2 = \sigma_3 \qquad : \qquad \varepsilon_2 = \varepsilon_3 \qquad\qquad (3-45)$$

$$\alpha_{ij} = 0 \quad \text{for } i \neq j \qquad : \qquad \alpha_{22} = \alpha_{33} = -\frac{1}{2}\alpha_{11} \qquad (3-46)$$

If we simplify equation (3-9) for triaxial conditions, with the assumption of $\alpha = \frac{3}{2}\alpha_{11}$, we will have:

$$f = (q - p\alpha)^2 - g^2(\theta)m_c^2 p^2 = 0 \qquad (3-47)$$

where

$$q = \sigma_1 - \sigma_3 \qquad : \qquad p = \frac{1}{3}(\sigma_1 + 2\sigma_3) \qquad (3-48)$$

The sizes of the yield surface in compression and extension are m_c and $m_k m_c$, respectively. Therefore:

$$q - p\alpha = pm_c \qquad \text{for compression} \qquad (3-49)$$

$$q - p\alpha = -pm_k m_c \qquad \text{for extension} \qquad (3-50)$$

Thus each yield surface in $(q - p)$ plane consists of two lines which pass through the origin. Volumetric and shear strains in this condition are defined as:

$$\varepsilon_v = \varepsilon_1 + 2\varepsilon_3 \qquad : \qquad \varepsilon_d = \varepsilon_1 - \varepsilon_3 \qquad (3-51)$$

Using these definitions and equations (3-5), (3-8) and (3-16), after some manipulations we will have:

$$\frac{\dot{\varepsilon}_d}{\dot{q}} = \frac{1}{2G} + \frac{1}{H} \frac{1 - \eta \frac{\dot{p}}{\dot{q}}}{1 + \frac{2}{9}\eta^2} \qquad (3\text{-}52)$$

$$\frac{\dot{\varepsilon}_v}{\dot{p}} = \frac{1}{B} \pm \frac{1}{H} \frac{2}{\sqrt{6}} \frac{1 - (\frac{\eta}{\overline{\eta}})^2}{1 + (\frac{\eta}{\overline{\eta}})^2} \frac{\frac{\dot{q}}{\dot{p}} - \eta}{(1 + \frac{2}{9}\eta^2)^{0.5}} \qquad (3\text{-}53)$$

In the latter equation. the positive sign is related to compression and the negative sign is for extension. Stress ratio. $\eta = \dfrac{q}{p}$. and plastic modulus. H. in the above equations can be shown as η_c and H_c for compression and as η_l and H_l for extension.

To determine the parameters of the model. $(q - \varepsilon_d)$. $(p - \varepsilon_v)$. $(q - p)$ and $(p - e)$ curves which have been obtained by the conventional drained triaxial tests are divided into linear segments so that the slopes of $(q - \varepsilon_d)$ curves for each pair of segments in compression and extension are the same. The degree of accuracy depends on the number of these segments. Using equations (3-49) and (3-50). m and α can be determined for each yield surface. Then using equation (3-52). H_c and H_l can be determined. $\overline{\eta}_c$ and $\overline{\eta}_l$ also are determined by equation (3-53). It is clear that $\overline{\eta}_c$ and $\overline{\eta}_l$ are related to specific ψ_c and ψ_l and also related to specific position α_{ij}^p. which are determined during the calibration process for each yield surface. As described in the appendix. plastic moduli and dilation parameters can finally be defined for a unique mean effective stress. void ratio and state parameter.

The parameter n_H. which shows the rate of variation of plastic modulus with void ratio. must be determined by trial and error for obtaining the best fit to the results of undrained triaxial tests.

The parameter k_α can be determined by using the results of the undrained cyclic triaxial test or monotonic triaxial test on an anisotropically consolidated sample. The parameter k_α must be chosen so that the stress path. in the changing of load direction. matches the observed behavior.

To use isotropic-kinematic hardening. the parameter k must be also determined. This parameter. which controls the maximum stress ratio in dense side of ultimate state. is determined by trial and error for best fitting to the drained or undrained test performed on dense samples.

The model parameters and the necessary tests for determination of them have been shown in Table (3.1). Furthermore. an example of calibration of the model can be found in the appendix.

3.12. Calibration of the model in the lack of complete data

In this section. a method for calibration of the model. in the absence of complete data. will be presented. The result of the drained triaxial compression test is often available. However. in the literature. sometimes the result of the drained triaxial extension test cannot be found. In the following. it is assumed that the slope of the ultimate state line in ($q - p$) plane for triaxial extension ($\eta_{u,l}$) has been defined. but the result of the drained extension test is not available.

Equation (3-49) and (3-50) can be written as:

$$\eta_c - \alpha = m_c \tag{3-54}$$

$$\eta_E - \alpha = -m_k m_c \tag{3-55}$$

Therefore one has :

$$m_c = \frac{\eta_c - \eta_l}{1 + m_k} \qquad (3\text{-}56)$$

and
$$\alpha = \eta_c - m_c \qquad (3\text{-}57)$$

As can be seen in equations (3-56) and (3-57), if η_k is known, m_c and α can be determined.

Considering equation (3-52), if one has η_l for each yield surface, H_l can be determined, because, on one hand, the ratio of $(\dot{\varepsilon}_d/\dot{q})$ in compression and extension is the same for each yield surface and, on the other hand, the ratio of $(\dot{p}/\dot{q})$ for drained triaxial extension is known (for example for $\sigma_1 = cte$ test, $\dot{p}/\dot{q} = -2/3$).

One can assume that G is equal in compression and extension for each yield surface in the calibration. Although this assumption has some approximation, considering the lack of sufficient data, this estimation would be acceptable.

Based on existing data, the ratio of (η_l/η_c) for the first yield surfaces is smaller than that in the outer yield surfaces. Therefore the value of (η_l/η_c) increases with η_c. Meanwhile, the ratio of (η_l/η_c) for the last yield surface is equal to m_c. Considering these two facts, the following equation is suggested for determination of η_l for each yield surface:

$$\eta_l = -\eta_c \left[d_0 + (m_k - d_0)(\frac{\eta_c}{\eta_{uc}})^{C_0} \right] \qquad (3\text{-}58)$$

Considering two constants (d_0 and C_0) provides enough flexibility in the equation. d_0 affects mostly the first yield surfaces. As can be seen, if $\eta_c = \eta_{uc}$ for any d_0 and C_0, $\eta_l = -m_k \eta_{uc} = \eta_{ul}$.

If the result of undrained triaxial extension test is available. $d_{()}$ and $C_{()}$ are determined by trial and error to produce the best fitting to experimental observations. If data is not available for extension. it is suggested that d_0 and $C_{()}$ be taken equal to 0 and 1.0. respectively. With this assumption. the variation of (η_{L}/η_{c}) versus η_{c} will be a straight line that passes through the origin. For Toyoura sand based on the curve fitting (see Figure A.5 in the appendix). $d_0 = 0.45$ and $C_0 = 6$.

To determine $\overline{\eta}_{E}$. there are two options as:

$$\overline{\eta}_{E} = \overline{\eta}_{c}(-\frac{\eta_{f}}{\eta_{c}})$$

(3-59)

or

$$\overline{\eta}_{E} = \overline{\eta}_{c}m_{k}$$

(3-60)

The negative sign in equation (3-59) is to produce a positive value for $\overline{\eta}_{f}$. although we have the square of $\overline{\eta}_{L}$ in equation (3-21). This change does not make any difference in the calculations. If the experimental result for curve fitting is available. any of the above equations that match better with the experiment should be used.

3.13. Methodology in developing formulation of the model

Figure 3.13 shows briefly the methodology which has been used in developing the formulation of the present constitutive model. In the first step. circular cones with an apex at the origin were chosen for yield surfaces. However. using the circular cone created a significant difference. in some zones. between the ultimate friction angle that the model showed and the observed friction angle of the soil (for example. compared with Mohr-Coulomb or Matsuoka-Nakai criteria). Therefore $g(\theta)$ was added to modify the circular section of the cones (see equation 3-9). Different functions for $g(\theta)$ were chosen. By comparison of the ultimate state surface of the model with Mohr-Coulomb. Matsuoka-Nakai (1974) and Lade-Duncan (1973) criteria on the deviatoric plane. the best $g(\theta)$ was selected (see equation 3-10).

In the flow rule. considering the observations of Lade and Duncan (1973). normality has been accepted in the deviatoric plane. Then Prevost's proposal (1985) for R'' (see equation 3-21) has been chosen. However. this function could not show the response of the soils at different states. Thus. a function for variation of $\bar{\eta}$ with state parameter (ψ) was defined. Considering observations of Been and Jefferies (1985). this function must show more contraction for the soils with higher state parameters. By trial and error. when used in the model. the final function gave better results than the other functions. In this effort. the observed behavior of different soils in the experiments under different loading and drainage conditions has been considered.

In the prediction. it was observed that at the starting of unloading or reloading. the model showed less contraction compared with the real behavior of the soil. For solving this problem. another part has been added to the proposed equation for considering the variation of $\bar{\eta}$ with respect to the position of yield surfaces (see equation 3-23).

The Mroz kinematic hardening rule was chosen for translation of yield surfaces. Using only kinematic hardening. the model was not able to show softening behavior of dense soils under drained conditions or decreasing of stress ratio under undrained conditions. For solving this problem. the size of yield surfaces was related to state parameter (see equation 3-34). This relationship is such that for soils looser than the ultimate state. the size of the yield surfaces is constant.

In both kinematic and isotropic-kinematic hardening. the consistency condition was satisfied. For inner yield surfaces. $\dot{\alpha}_{ij}$ (see equation 3-32) and for the last yield surface. plastic modulus (H) were determined (see equation 3-35) using the consistency condition.

Elastic moduli change with mean effective stress and void ratio. Equations (3-40) and (3-41) have been used to consider these variations. The section related to the variation of elastic moduli with void ratio has been adapted from Richart et al. (1970).

Plastic modulus also changes with mean effective stress and void ratio. Both an increase in mean effective stress and a decrease in void ratio can cause some increase in plastic modulus. Equation (3-42) was developed for considering these variations. This function was developed by using trial and error. For any trial function. calibration of the model was performed for different soils. and predictions of the model were compared with the observed behavior of those soils under different loading and drainage conditions. Finally. based on these comparisons. equation (3-42) has been selected.

3.14. Explicit algorithm for stress increment calculation

Ortiz and Popov (1985) mentioned that an acceptable algorithm should satisfy three basic requirements:

(a) Consistency with the constitutive relations to be integrated or first-order accuracy

(b) Numerical stability

(c) Incremental plastic consistency

A non-required but desirable feature to add to the above list is: (d) second-order accuracy.

Considering (a) and (b) are needed for attaining convergence of the numerical solution as the time step becomes vanishingly small. Condition (c) is the algorithmic counterpart of the plastic consistency condition and requires that states of stress computed from the algorithm be contained within the elastic domain.

Using an analysis of accuracy of algorithms for the integration of elastoplastic constitutive relations. Ortiz and Popov (1985) have shown that the choice of (0.5) for the algorithmic parameter results in second-order accuracy for two families of algorithms. Ortiz and Popov (1985) proposed also a methodology which allows a systematic assessment of the numerical stability properties of integration rules for elastoplastic constitutive relations. Based on this method, the minimum value of algorithmic parameter to achieve unconditional stability is (0.5).

Considering the above discussion, with explicit algorithms in which the algorithmic parameter is zero, achieving a second-order accuracy or unconditional stability is not possible. However, in multi-yield surface theory, using explicit-implicit or fully implicit algorithms results in expensive algorithms. Therefore, to have an efficient algorithm for the multi-yield surface models, one can be satisfied with first-order accuracy and conditional stability.

In this thesis, a forward different scheme has been used. This algorithm is simple but not perfect for use as an interface with a finite element code for the solution of boundary value problems. The presented algorithm is consistent, first-order accurate and only conditionally stable. For using finite element codes, the algorithm which has been suggested by Lacy (1986) can be used. This is an explicit one-step algorithm, simple and relatively inexpensive.

The problem can be defined at a step of an analysis (n), the stress tensor ($\sigma_{ij}^{(n)}$) and the position tensor of yield surfaces ($\alpha_{ij}^{(n)}$) are known. If the strain increment at step ($n+1$) is $\varepsilon_{ij}^{(n+1)}$, we want to determine $\sigma_{ij}^{(n+1)}$ and $\alpha_{ij}^{(n+1)}$ for all the yield surfaces.

In the algorithm that has been used in this study, at first with the assumption that the deformation is completely elastic, the first trial stress ($\sigma_{ij}^{tr(n+1)}$) is determined, i.e.,

$$\sigma_{ij}^{tr(n+1)} = \sigma_{ij}^{(n)} + E_{ijkl}\dot{\varepsilon}_{kl}^{(n+1)} \tag{3-61}$$

If the trial stress exceeds the yield surface, the new trial stress is determined by using following equations:

$$\dot{\varepsilon}_{ij}^{p} = \lambda R_{ij} \tag{3-62}$$

$$\sigma_{ij}^{tr(n+1)} = \sigma_{ij}^{(n)} + E_{ijkl}\left[\dot{\varepsilon}_{kl}^{(n+1)} - \dot{\varepsilon}_{kl}^{p(n+1)}\right] \tag{3-63}$$

Then yielding is checked by using this new trial stress. If trial stress still exceeds than the yield surface, equations (3-62) and (3-63) will be used again but with the parameters related to the next yield surface. This process will be repeated until the trial stress does not exceed the yield surface. As can be seen, in this method, the effect of passing several yield surfaces in one increment of strain ($\dot{\varepsilon}_{ij}^{(n-1)}$) has not been considered. However, it works for small increments of strains.

The next step is updating the stress and the position of yield surfaces. The contact point on the yield surface (s_{ij}^{*}) is determined by radial mapping, using following equations:

$$K_{ij} = s_{ij}^{(n-1)} - p^{(n-1)}\alpha_{ij} \tag{3-64}$$

$$b = \frac{(\frac{3}{2}K_{ij}K_{ij})^{0.5}}{p^{(n-1)}} \tag{3-65}$$

$$s_{ij}^{*} = p^{(n-1)}\alpha_{ij} + \frac{g(\theta)m_{\iota}}{b}K_{ij} \tag{3-66}$$

After determining the contact point, the new positions of yield surfaces are determined and the calculations for step ($n + 2$) will start.

For choosing an efficient strain increment size, two typical tests for triaxial and simple shear (conducted by hollow cylinder) conditions have been considered (Figures 3.14 and 3.15). Both of these tests have been predicted by three different strain increments (0.1, 0.01 and 0.001 percent for axial strain increments in triaxial and shear

strain increments in hollow cylinder tests). The results have been shown in Figures (3.14) and (3.15). As can be seen. using 0.1 percent in the triaxial test causes an oscillation in stress path at small strains in model prediction. This oscillation for stress-strain curve and simple shear test is not seen. For 0.01 and 0.001 percent strain increments. all the stress paths and stress-strain curves match together. Therefore. considering the shorter time for analysis using the 0.01 percent strain increment. this size has been used for loading steps in the predictions. Considering Figures (3.14) and (3.15). one can conclude that the presented predictions do not depend on the size of loading step.

3.15. Implementation

In this section. l and NYS show the yield surface number and the number of total yield surfaces. respectively.

1- Initialize yield surface number:

$$l = 0$$

2- Compute elastic trial stress:

$$\sigma_{ij}^{tr(n+1)} = \sigma_{ij}^{(n)} + E_{ijkl}\dot{\varepsilon}_{kl}^{(n+1)}$$

3- Check for yielding:

If $l = NYS$ Go to 5

If $f\left[\sigma_{ij}^{tr(n+1)}, \alpha_{ij}^{(l-1)(n)}, g(\theta)\right] \leq 0$ Go to 5

$$l = l + 1$$

4-   Compute plastic trial stress:

$$H_0 = Q_{ij}^{(l)} E_{ijkl} R_{kl}^{(l)}$$

$$\lambda = \frac{Q_{ij}^{(l)} E_{ijkl} \dot{\varepsilon}_{kl}^{(n-1)}}{H^{(l)} + H_0}$$

$$\dot{\varepsilon}_{ij}^{trp} = \lambda R_{ij}^{(l)}$$

$$\sigma_{ij}^{tr(n-1)} = \sigma_{ij}^{(n)} + E_{ijkl}\left[\dot{\varepsilon}_{kl}^{(n-1)} - \dot{\varepsilon}_{kl}^{trp}\right]$$

Go to 3

5-   Updating the stress and position of the yield surfaces:

$$\sigma_{ij}^{(n-1)} = \sigma_{ij}^{tr(n-1)}$$

If $l = 0$ Go to 7

$$K_{ij} = s_{ij}^{(n-1)} - p^{(n-1)}\alpha_{ij}^{(l)}$$

$$b = \frac{(\frac{3}{2} K_{ij} K_{ij})^{0.5}}{p^{(n-1)}}$$

$$s_{ij}^{\bullet} = p^{(n-1)}\alpha_{ij}^{(l)} + \frac{g(\theta)m_c^{(l)}}{b} K_{ij}$$

$$\mu_{ij} = \frac{m_c^{(l-1)}}{m_c^{(l)}}\left[s_{ij}^{\bullet} - p^{(n-1)}\alpha_{ij}^{(l)}\right] - \left[s_{ij}^{\bullet} - p^{(n-1)}\alpha_{ij}^{(l-1)}\right]$$

$$\alpha_{ij}^{(l)} = \alpha_{ij}^{(l)} + \frac{\lambda H^{(l)}\left(\dfrac{\partial f}{\partial \sigma_{kl}}\dfrac{\partial f}{\partial \sigma_{kl}}\right)^{0.5} - 2g^2(\theta)m_c^{(l)} p^{(n-1)2} \dot{m}_c^{(l)}}{-\dfrac{\partial f}{\partial \alpha_{ij}}\mu_{ij}} \mu_{ij}$$

6-   Adjust inner surfaces:

For $k = 1$ to $(l - 1)$

$$\alpha_{ij}^{(k)} = \frac{\left\{ s_{ij}^{(n-1)} - \frac{m_c^{(k)}}{m_c^{(l)}} \left[s_{ij}^{(n-1)} - p^{(n-1)}\alpha_{ij}^{(l)} \right] \right\}}{p^{(n-1)}}$$

7-   Exit

3.16. Summary

This study has demonstrated that considering a reference to define the state of the soil is an essential condition for constitutive modelling of soil behavior over a wide range of stresses and void ratios. "Reference State Soil Mechanics" is a framework in which the behavior of soil depends on the state of the soil with respect to a reference state. To define the state of the soil, different parameters can be used. For a complete definition of state in general stress-void ratio space, however, at least seven parameters plus history of loading must be used. Using a reference, the behavior of loose and dense soils can be modelled in a unique framework. Since sands with any density finally at large strains reach the ultimate state condition, it was suggested to use ultimate state surface as the reference.

For modelling the behavior of sands in drained and undrained conditions under both monotonic and cyclic loading, the formulation of a constitutive model in general stress space has been presented. This formulation has been obtained by modifying the multi-yield surface theory (Prevost, 1985) to consider the effect of state on the soil behavior. The model is capable of predicting the behavior of loose and dense sands, the effect of initial cross-anisotropy and induced anisotropy during the loading using a unique calibration and set of parameters. Calibration of the model is done completely by conventional laboratory tests. Most of the model parameters are determined directly

during the calibration procedure and the user does not have to spend a lot of time for curve fitting. Using different parameters for compression and extension, the model is capable of representing the effect of fabric in soil response. A method also has been suggested, in the absence of complete data in extension, to use for calibration.

The ultimate state line in the ($p-e$) plane can have any shape and mathematical function. This generality gives such a flexibility to the model that whenever the exact rule of variation of the ultimate state line is proposed, it can be added to the model without any necessary change in the formulation of the model.

Two pure kinematic hardening and isotropic-kinematic hardening rules have been used. It has been shown that for modelling the response of loose and medium dense sands, using a pure kinematic hardening rule is acceptable. However, for the post peak behavior of very dense sands under drained conditions, the user must apply isotropic-kinematic hardening.

The explicit algorithm for stress increment calculation that has been used in the predictions was described. In general, this algorithm is not perfect for use in interface with finite element codes; however, for the purpose in this research it worked efficiently.

Validation of the model under monotonic and cyclic loading will be presented in Chapters 4 and 5.

Table 3.1. Test type for determination of model parameters*

Parameter	Test type for determination
G_0	Shear wave velocity or triaxial
B_0	Cyclic hydrostatic or triaxial
m_k . m_t . α	Drained triaxial compression and extension
H_{0c} . H_{0E}	
$\overline{\eta}_{0c}$. $\overline{\eta}_{0E}$	
n_H	Undrained triaxial
K_u	Undrained cyclic triaxial or undrained monotonic triaxial
k	Drained or undrained triaxial on dense sand

* The equation of ultimate state line in ($p - e$) plane must also be defined.
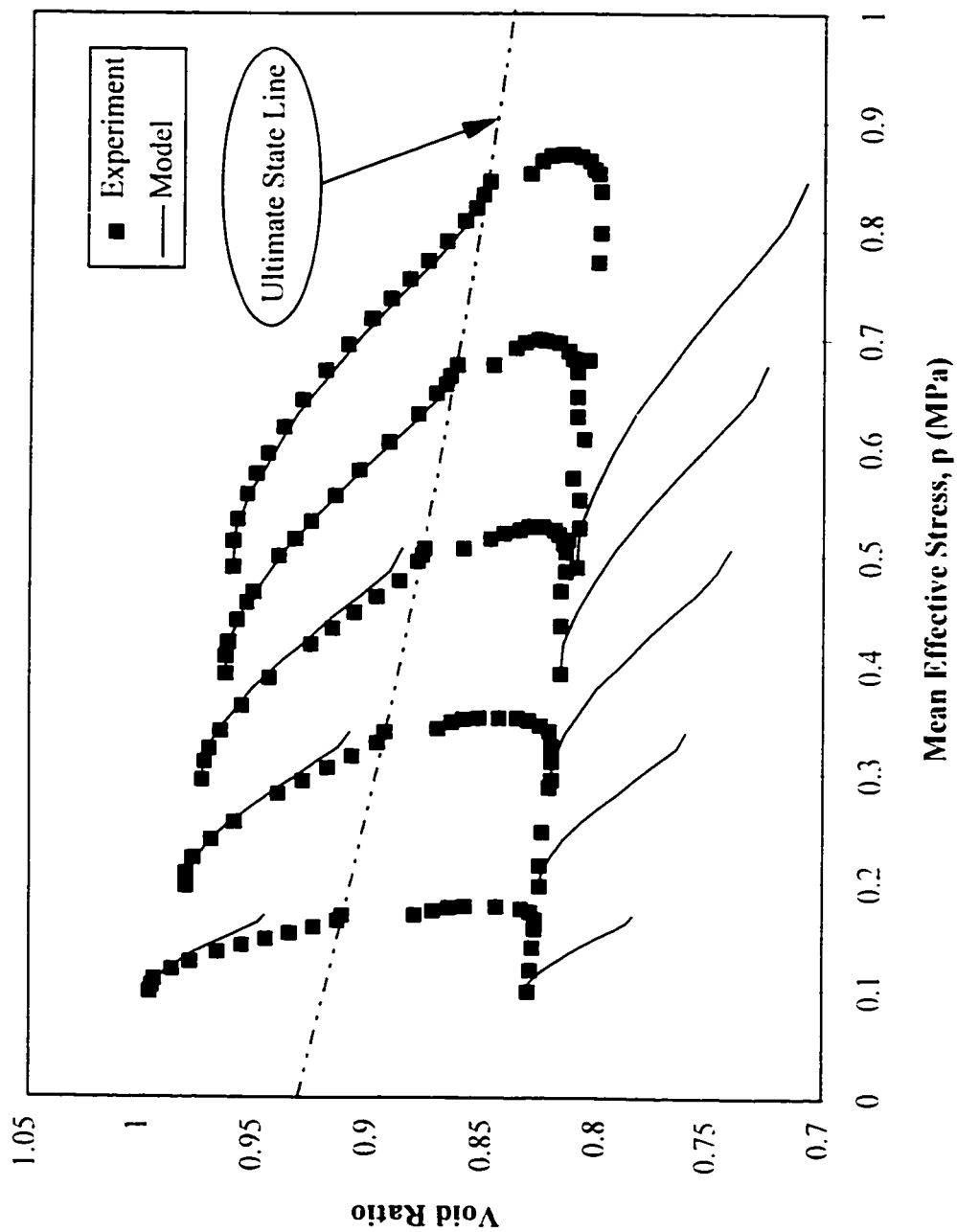
Figure 3.1. Comparison of predictions of Prevost model with experimental observations on Toyoura sand in conventional drained triaxial tests.
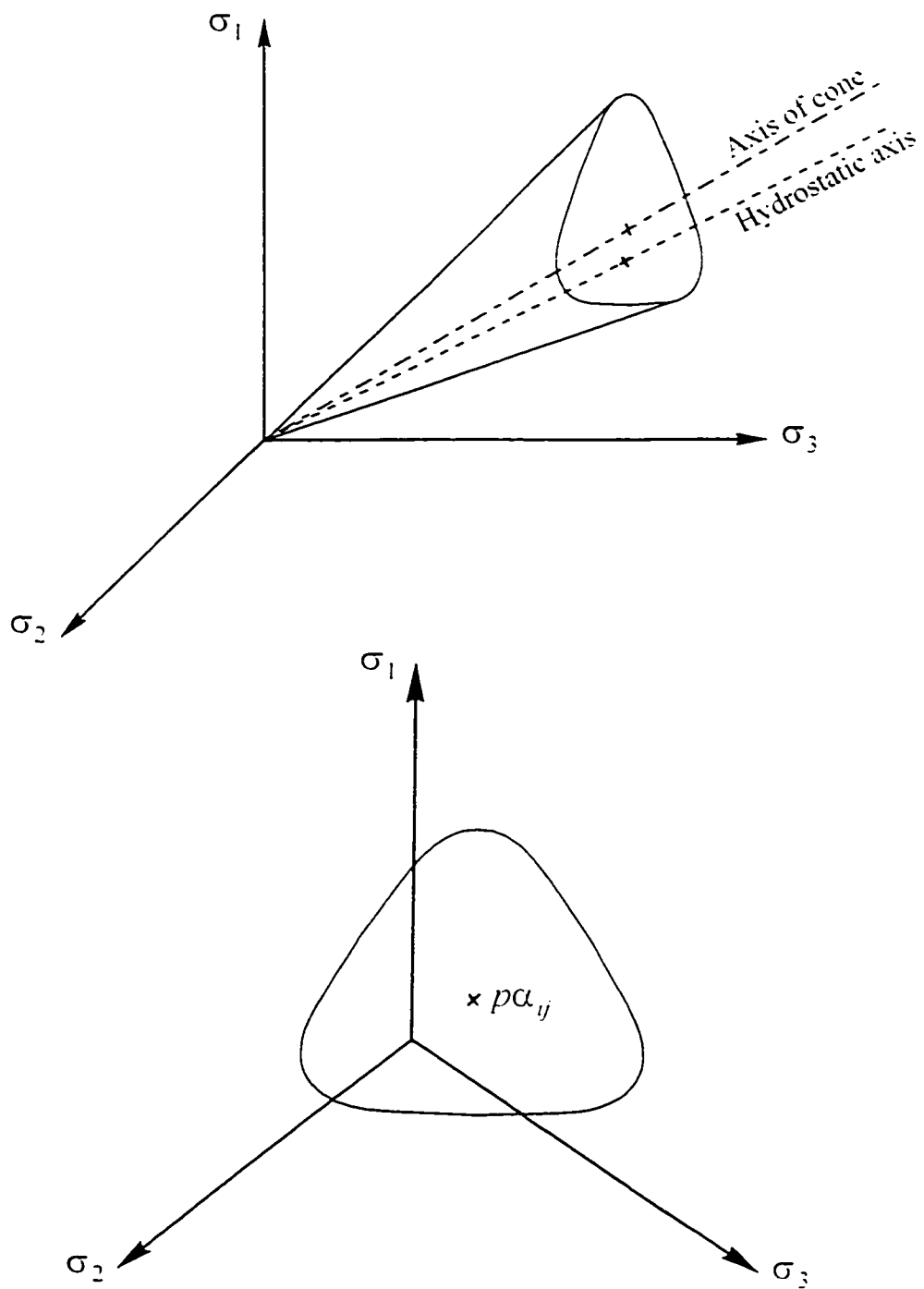
Figure 3.2. Yield surface in the stress space.
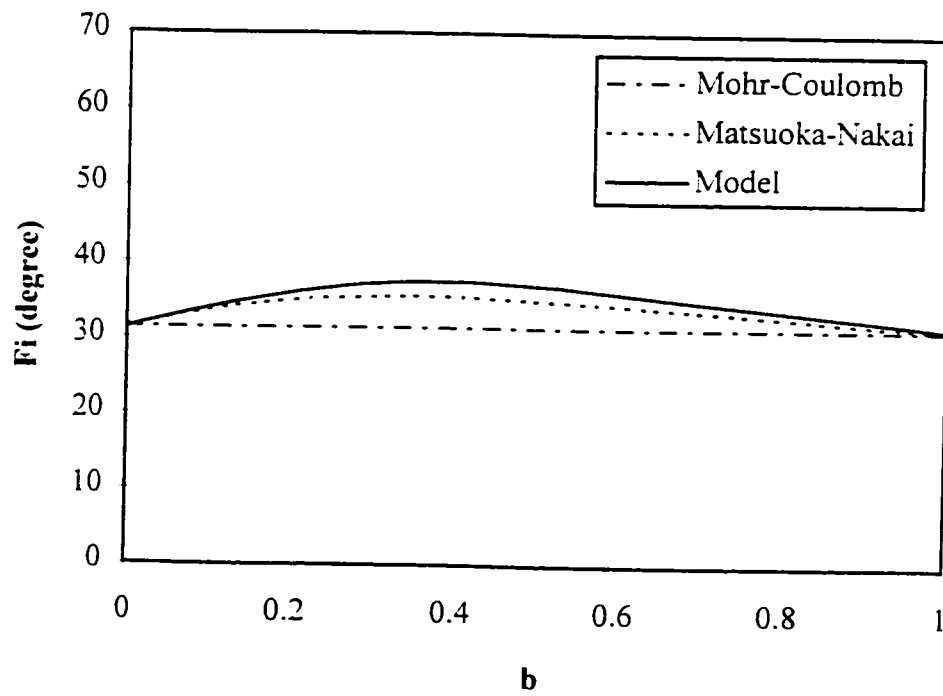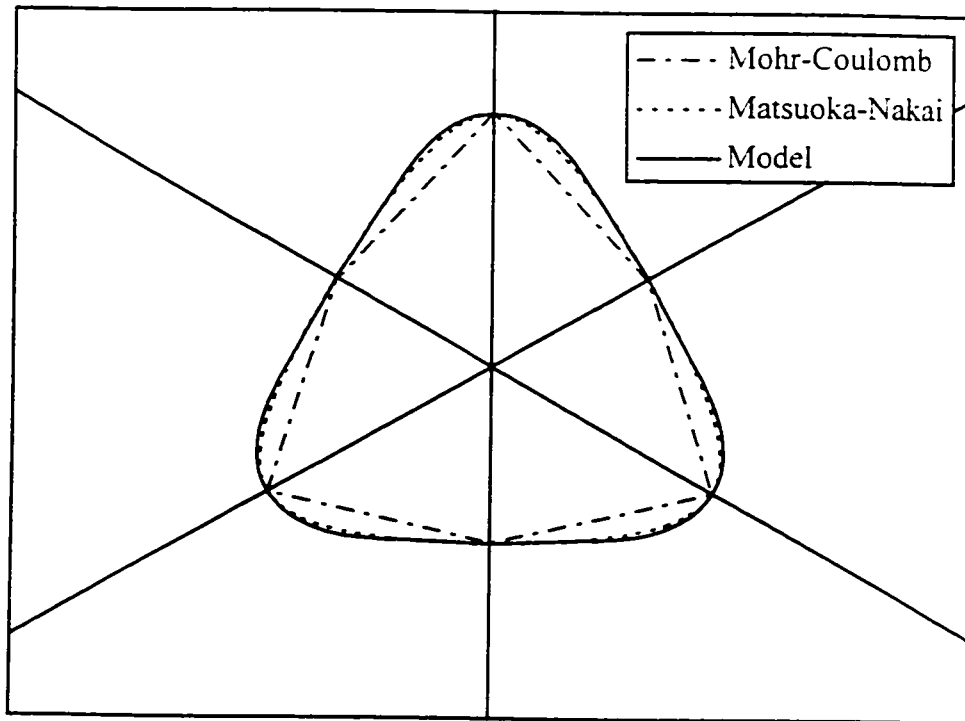
Figure 3.3. Comparison of ultimate state surface of the model with Mohr-Coulomb and Matsuoka-Nakai criteria.
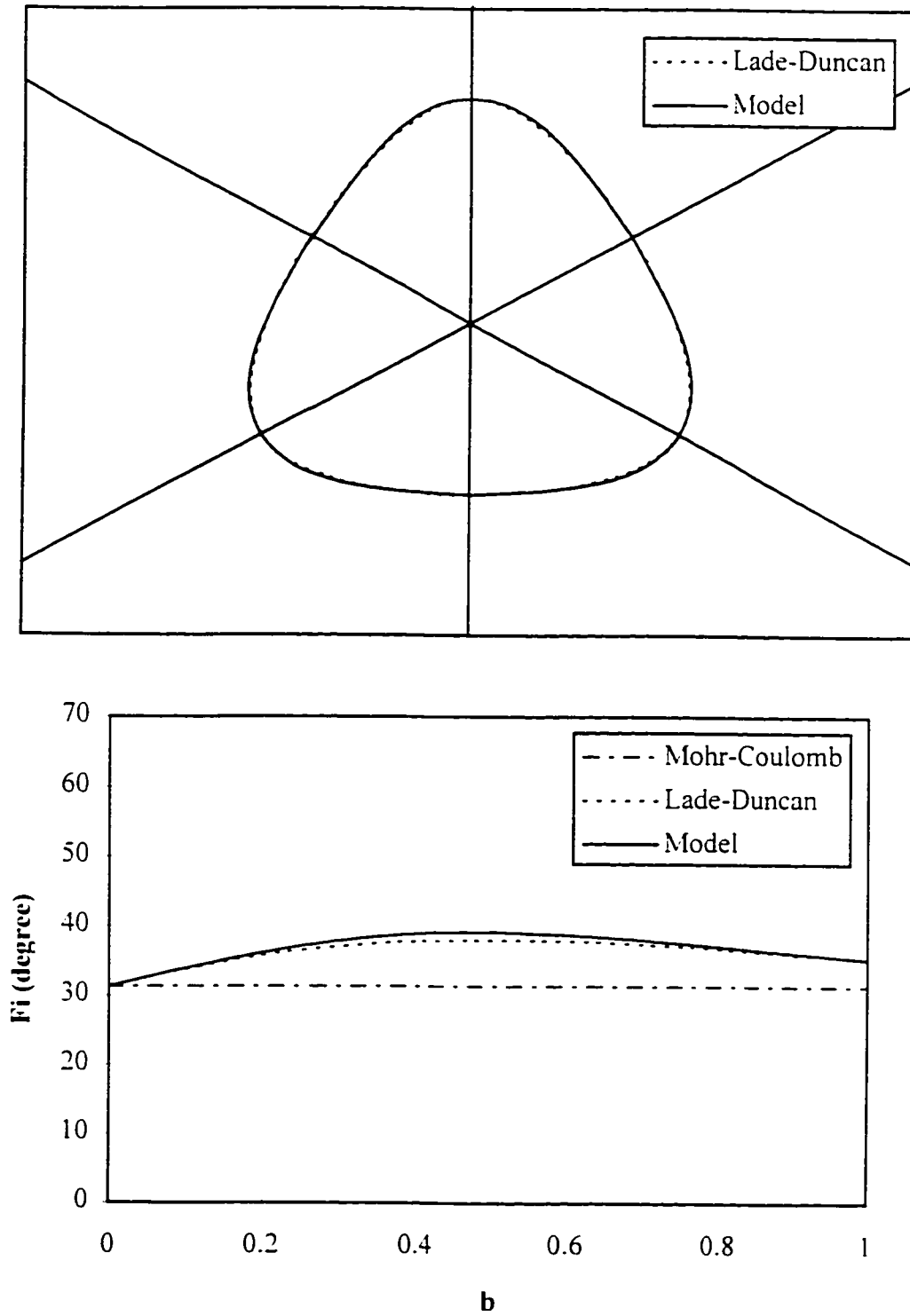
Figure 3.4. Comparison of ultimate state surface of the model with Lade-Duncan criterion.
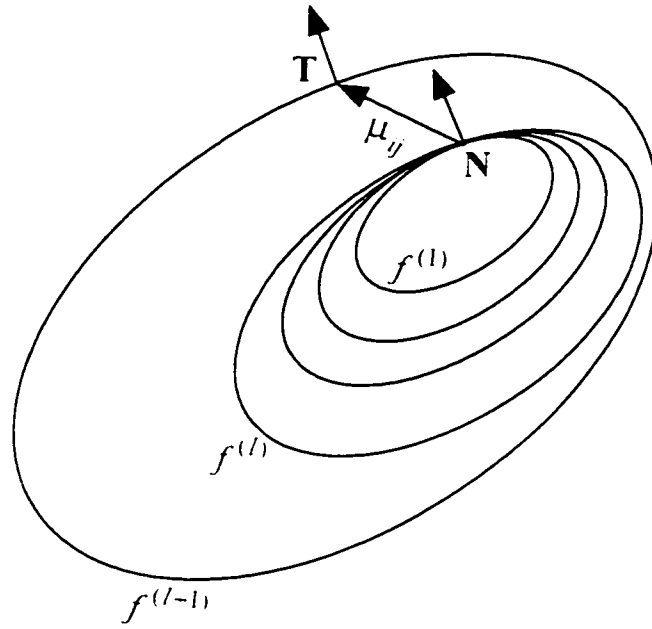
Figure 3.5. Translation of yield surfaces.
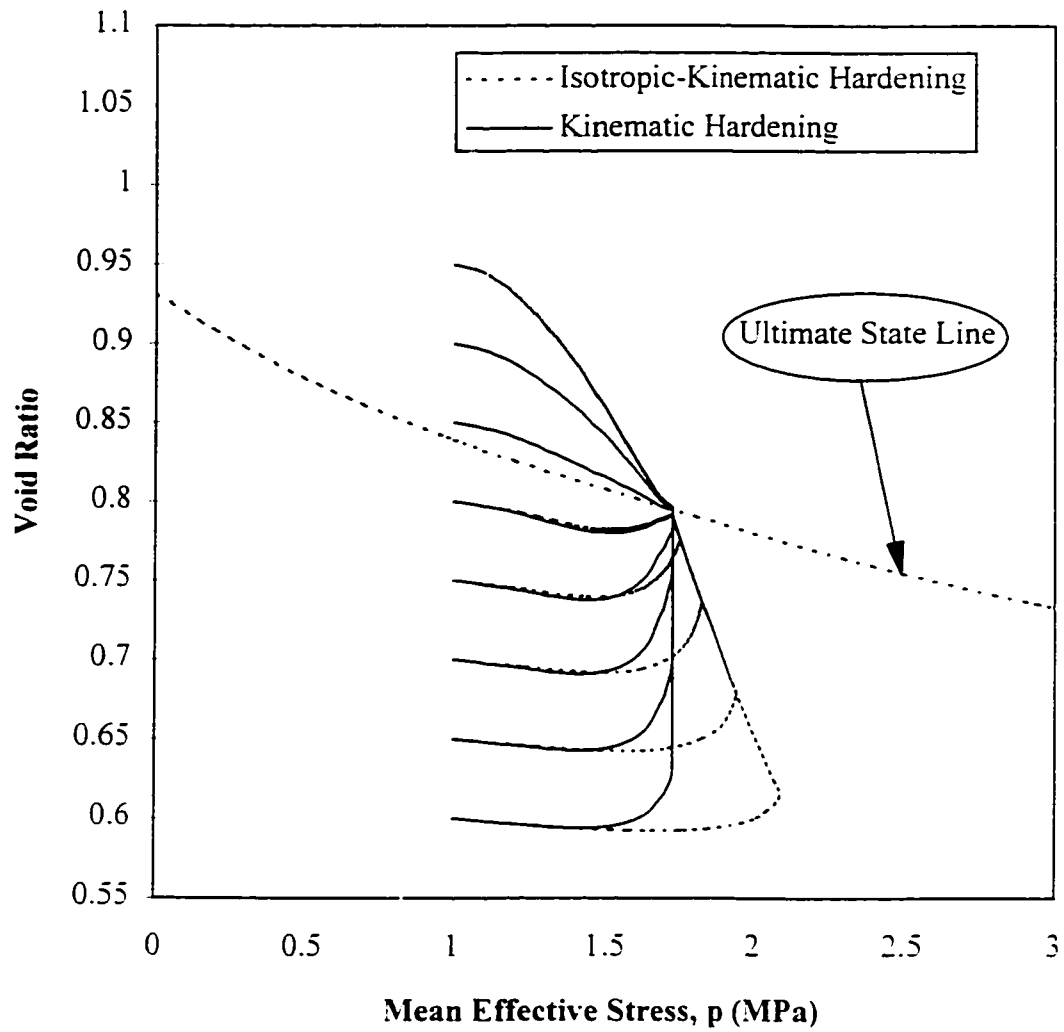
Figure 3.6. Model simulations using kinematic and isotropic-kinematic hardening in($p - e$) plane for drained triaxial tests on samples at different states.
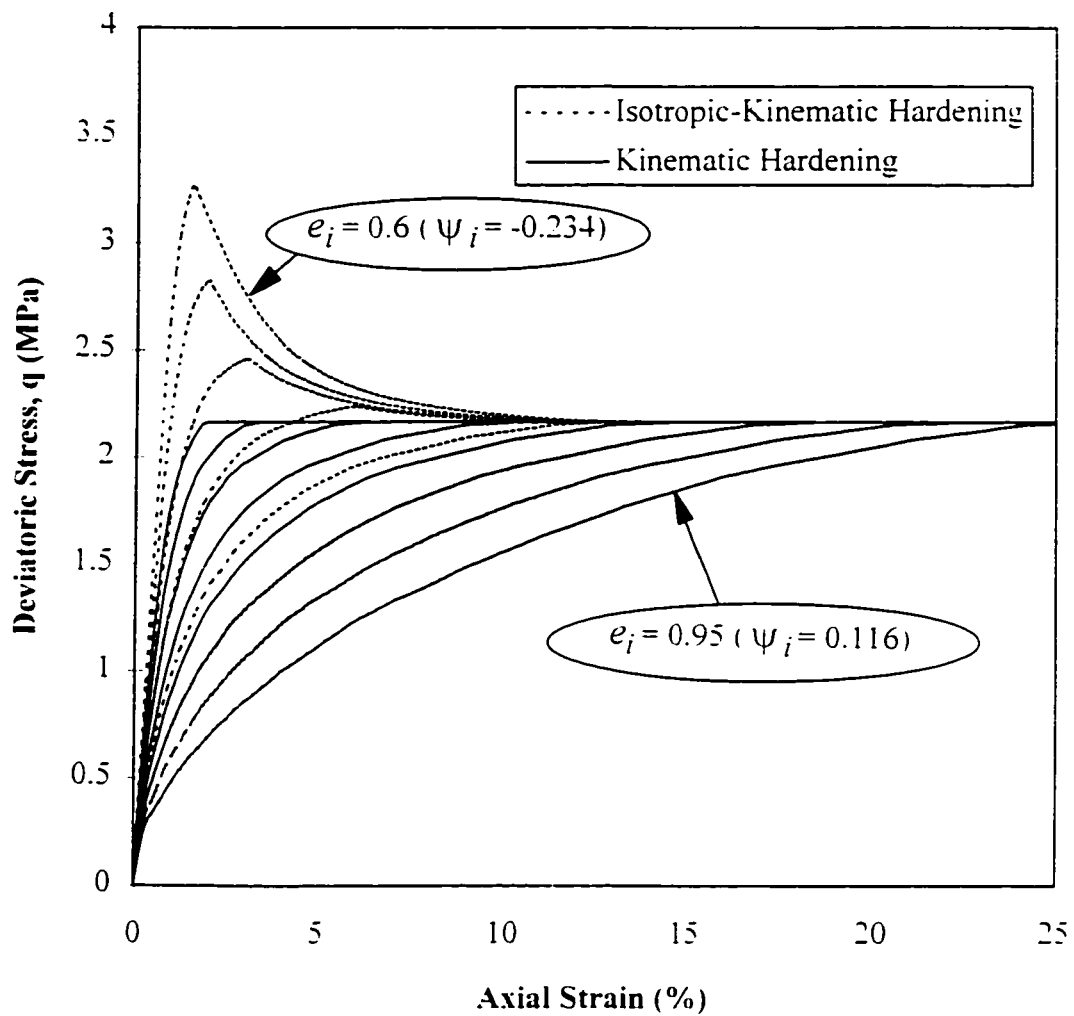
Figure 3.7. Model simulations using kinematic and isotropic-kinematic hardening rules rules in $(q - \varepsilon_a)$ plane for drained triaxial tests on samples at different states.
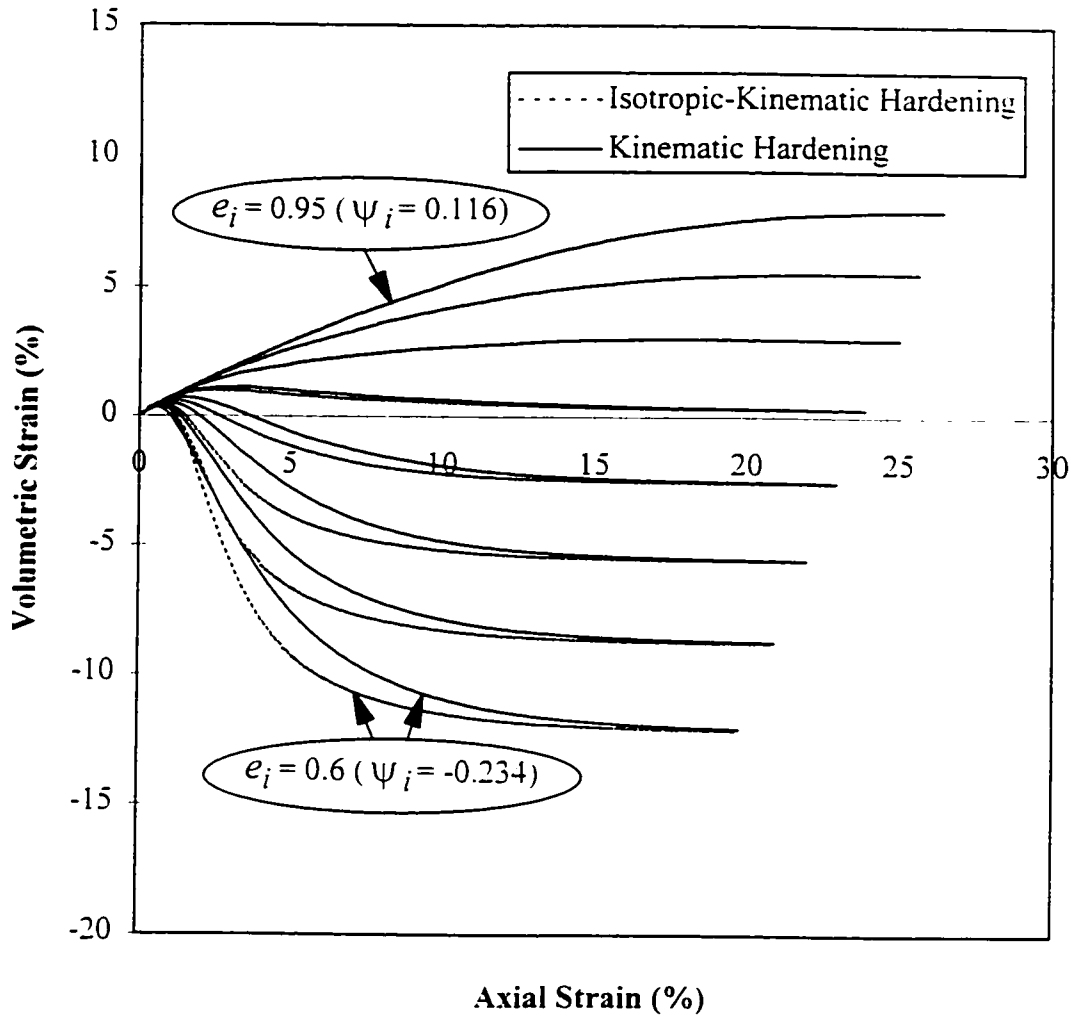
Figure 3.8. Model simulations using kinematic and isotropic-kinematic hardening rules in ($\varepsilon_v - \varepsilon_a$) plane for drained triaxial tests on samples at different states.
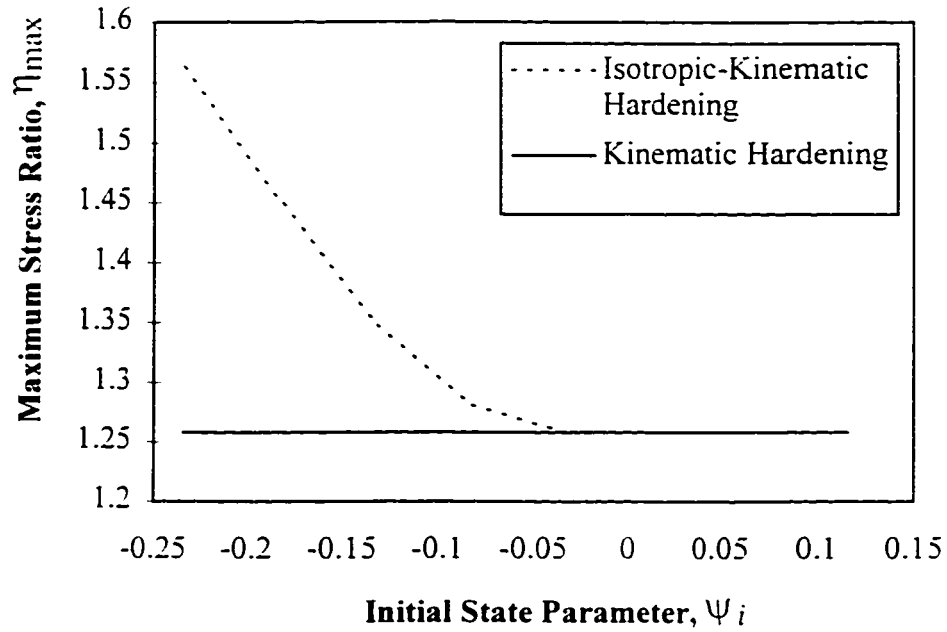
Figure 3.9. Variation of maximum stress ratio. $\eta_{\ldots}$. with initial state parameter. ψ . for drained triaxial tests in model simulations using kinematic and isotropic-kinematic hardening rules.
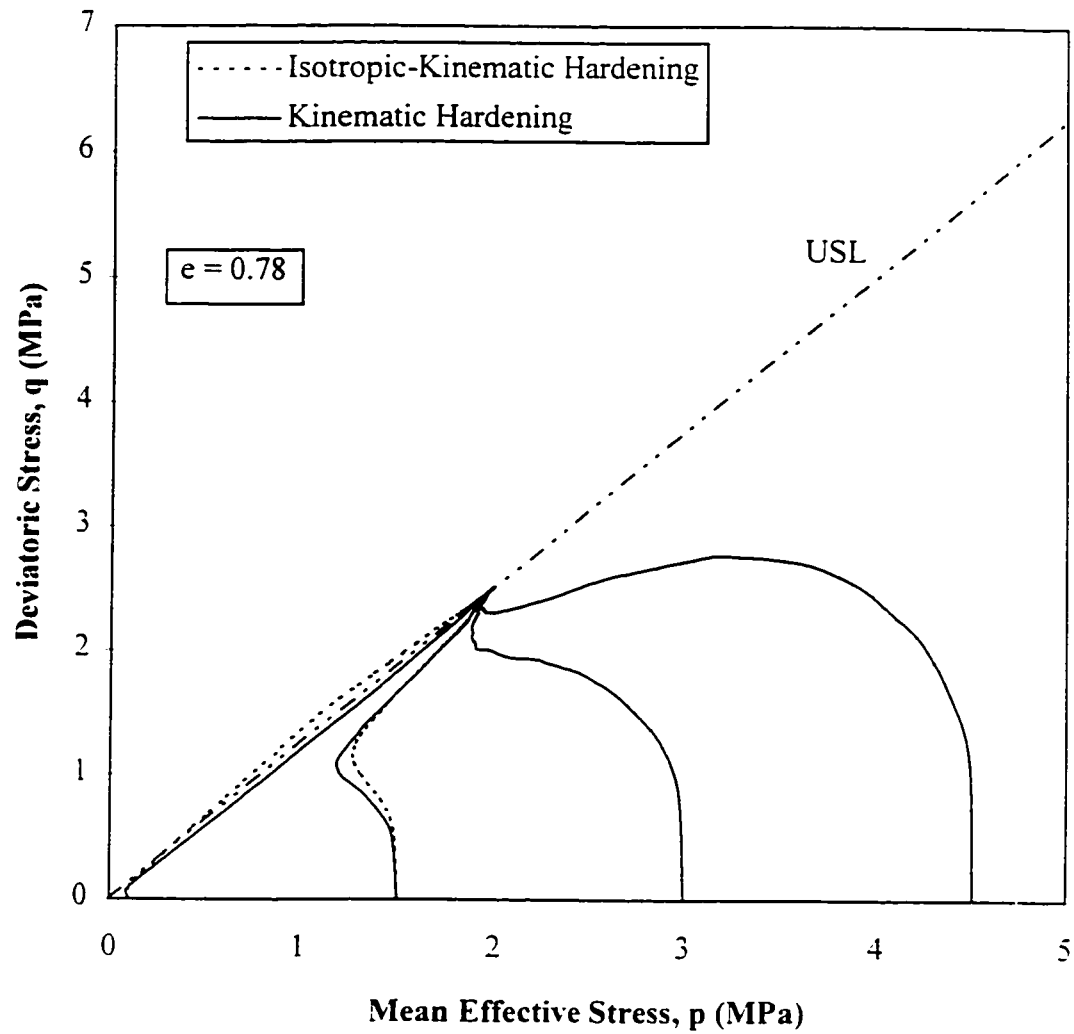
Figure 3.10. Model simulations using kinematic and isotropic-kinematic hardening rules in ($p - q$) plane for undrained triaxial tests on samples at different states.
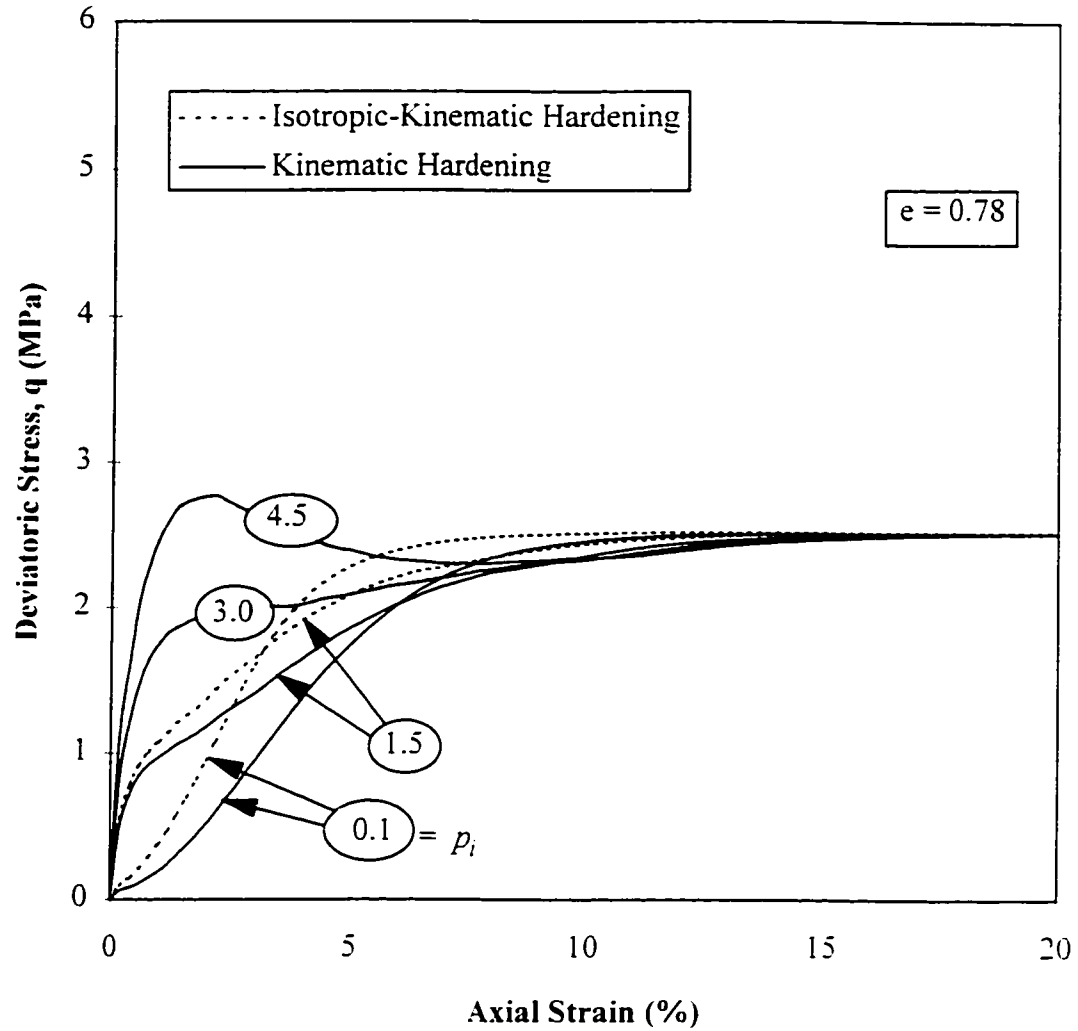
Figure 3.11. Model simulations using kinematic and isotropic-kinematic hardening rules in ($q - \varepsilon_a$) plane for undrained triaxial tests on samples at different states.
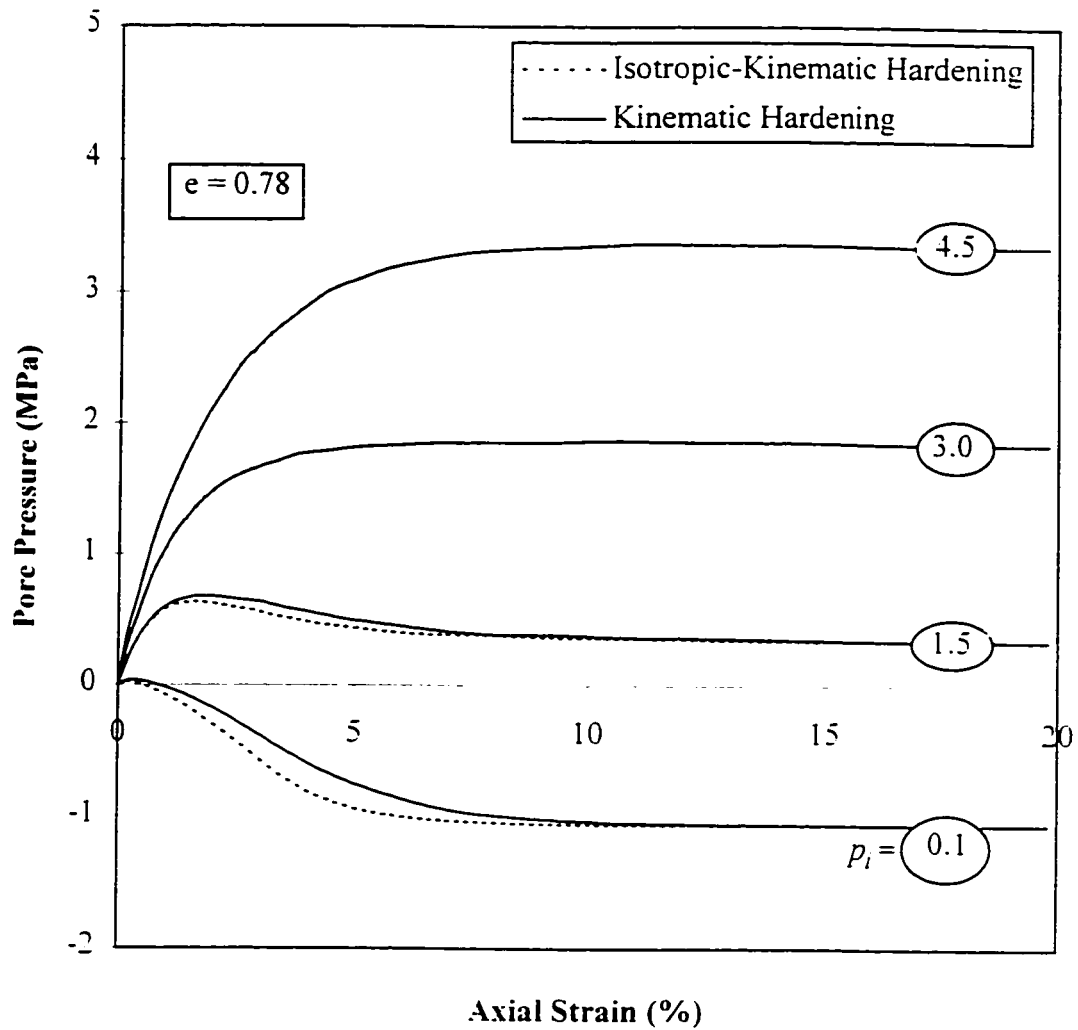
Figure 3.12. Model simulations using kinematic and isotropic-kinematic hardening rules in ($u - \varepsilon_a$) plane for undrained triaxial tests on samples at different states.

a) Defining circular cones for yield surfaces.

b) Choosing $g(\theta)$ to have a good fit to recognized criteria.

a) Considering observations of Lade and Duncan (1973).

b) Choosing Prevost's proposal for R''.

c) Defining a function for variation of $\overline{\eta}$ with ψ.

d) Adding a part to the function. which was developed in previous section. for variation of $\overline{\eta}$ with α_{ij}.

a) Using Mroz kinematic hardening rule.

b) Defining the variation of size of yield surfaces with ψ.

c) Satisfying the consistency condition.

a) Defining variation of elastic moduli with p and e.

b) Defining variation of plastic modulus with p and e.

Figure 3.13. Methodology in developing formulation of the model
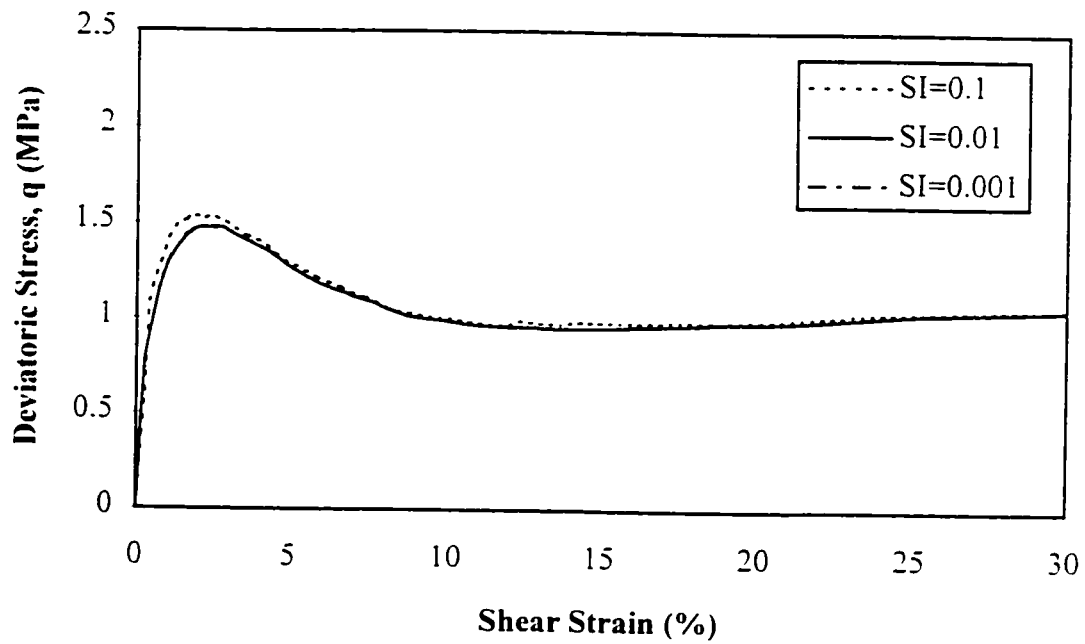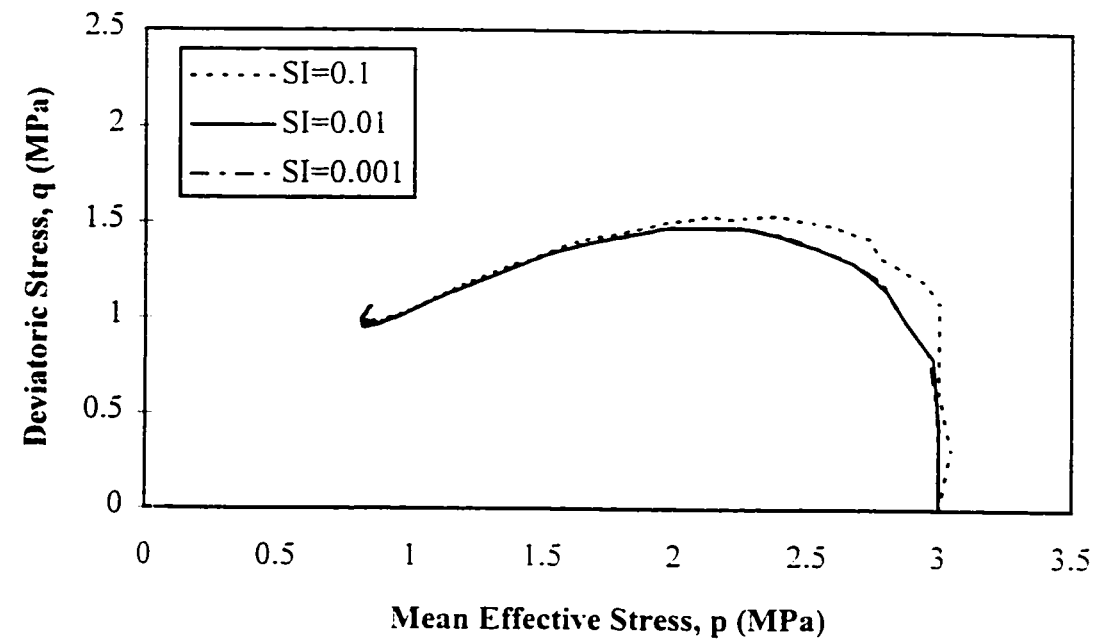
Figure 3.14. The effect of size of strain increment on the algorithm in triaxial tests.
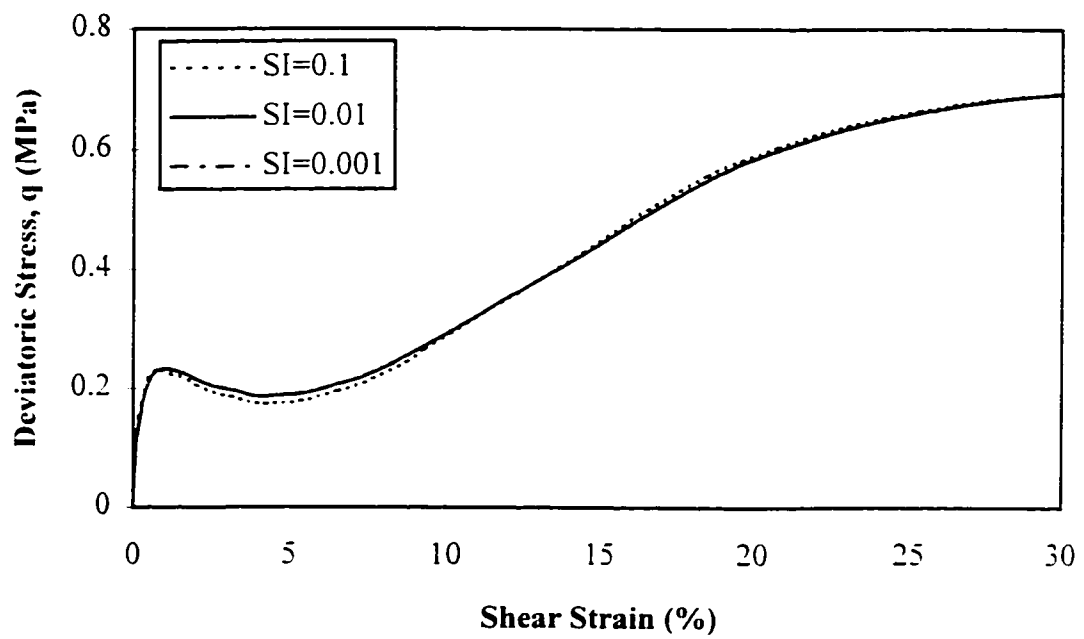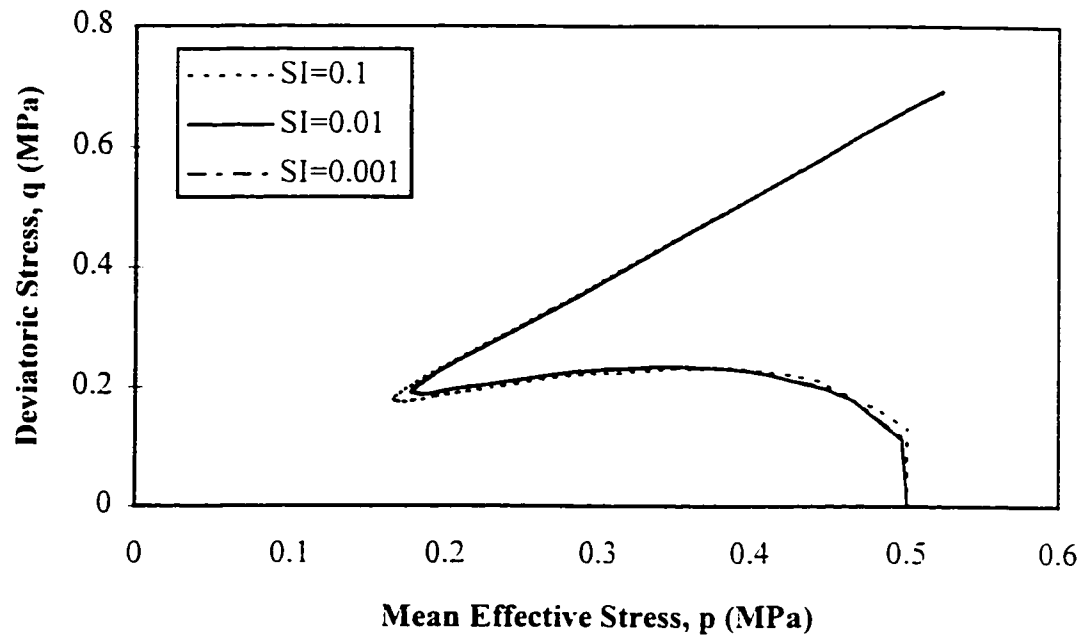
Figure 3.15. The effect of size of strain increment on the algorithm in simple shear tests.

Chapter 4

VALIDATION OF THE MODEL FOR MONOTONIC LOADING

4.1. Introduction

In this chapter the performance of the proposed model will be validated for monotonic loading in different conditions. Laboratory tests conducted by different researchers on different soils are used. Calibration of the model will be explained in detail for Toyoura sand, then an extensive comparison with measured data under undrained and drained conditions for isotropically and anisotropically consolidated samples of different soils will be presented. The results show that the model yields very good predictions of transition from contractive to dilative shear response with either decreasing mean effective normal stress or increasing relative density. The inherent existing state boundary in the model makes it capable of representing collapse in both undrained and drained conditions. The model is able to show the ultimate state conditions at large strains. Its performance in the prediction of the response of the samples at different states shows that it can accurately represent the behavior of soil in different conditions with unique calibration.

4.2. Characteristics of soils

In order to evaluate the model, tests conducted on five different soils, i.e., Toyoura sand (Ishihara, 1993; Verdugo and Ishihara, 1996; Verdugo, 1992; Yoshimine, 1996); Ottawa sand (Sasitharan et al., 1994; Skopek et al., 1994); Fraser River sand (Chillarige, 1995; Ayoubian and Robertson, 1996); Banding sand (Castro, 1969) and Fuji River sand (Tatsuoka and Ishihara, 1974) have been used. This variety of soils was chosen partly because of the lack of existing data in the literature for different stress paths and drainage conditions for a unique soil and partly to have a complete evaluation of the model for different sands with different physical properties. The general physical properties of these sands will be described in the following paragraphs.

Ishihara (1993), Verdugo and Ishihara (1996), Verdugo (1992) and Yoshimine (1996) have reported the results of a number of triaxial and simple shear tests which have been performed on Toyoura sand over a wide range of mean effective stress, 0.05 MPa$\leq p \leq 3.0$ MPa , and formation void ratios, $0.660 \leq e \leq 0.933$. Toyoura sand is a standard sand that is often used in Japan for geotechnical studies. It consists of sub-angular particles with a mean diameter $D_{50} = 0.17$ mm and a uniformity coefficient of $U_c = 1.7$ as can be seen in its grain size distribution curve (see Figure 4.1). This sand is composed of 75% quartz, 22% feldspar and 3% magnetite. The maximum and minimum void ratio of this sand, determined by the JSSMFE method, are 0.977 and 0.597, respectively, with a specific gravity of 2.65. Using the moist tamping method, its maximum void ratio can be increased to 1.04.

Ottawa (C109) sand is a uniform, medium sand comprised primarily of round to subrounded quartz grains with a specific gravity of 2.67. The mean grain size (D_{50}) of this sand is 0.34 mm. The maximum and minimum void ratio of the sand determined using ASTM method D2049 are 0.82 and 0.5, respectively. However, using the moist tamping technique, samples with higher void ratio can be obtained.

Fraser River sand is a natural sand which has been obtained from the Fraser River Delta in British Columbia. The mean grain size of this sand is 0.25 mm with a uniformity coefficient of 1.7. The mineral composition of it is 40% quartz. 11% feldspar. 45°o unaltered rock fragments and 4% other minerals. Maximum and minimum void ratios in accordance with ASTM D2049 are 1.0 and 0.6. respectively. The specific gravity of this sand is 2.75 and its silty material is non-plastic.

Banding sand. which has been used by Castro (1969) in most of his tests. is a uniform. clean. fine quartz sand with subrounded to subangular grains. The specific gravity of the grains is 2.65. Its D_{10} size is 0.097 mm and its coefficient of uniformity is 1.8. The maximum and minimum void ratios are 0.84 and 0.50. respectively.

Fuji River sand is a natural sand from the Fuji River bed near Tokyo. The specific gravity. D_{10} and U_c of this soil are 2.68. 0.22 mm and 2.21. respectively. Its maximum and minimum void ratios are 1.08 and 0.53. respectively.

The characteristics of soils have been shown in Table 4.1.

4.3. Determination of model parameters

Calibration of the model is conducted entirely by using conventional triaxial tests. Most of the model parameters are determined using one pair of conventional drained compression and extension triaxial test. This is one of the advantages of the model that reduces the number of tests necessary for its complete calibration. In the following paragraphs. determination of model parameters for Toyoura sand and the effect of variation of parameters on the model performance will be discussed. The same process has been followed for the other sands.

It is clear that for all constitutive models in the "Reference State Soil Mechanics" framework, the ultimate state line must be defined. Different modelers, based on the experimental observations or for simplicity, have assumed different shapes for this important line. However, there is still discussion among researchers regarding the real shape of the ultimate state line or its uniqueness in different modes of shearing or drainage conditions. In order to maintain the versatility of the model for using the different shapes of the ultimate state line, no particular shape has been assumed for this line in the present model. This line can have any shape with any mathematical equation. Any assumption regarding the ultimate state line will not alter the formulation of the model. The advantage of this versatility is that if, in the future, one finds the general rule of variation of the ultimate state line with shearing mode, one can add it to the model, using appropriate mathematical function, without affecting the formulation of the model.

In this study, based on existing data for each soil, the line best fitted to the experimental results has been chosen for the ultimate state line. For Toyoura sand, based on Ishihara (1993), a polynomial with order 4 has been used for the ultimate state line as follows:

$$e_{us} = 0.92649 - 0.12508\ p + 0.043665\ p^2 - 0.012639\ p^3 + 0.00154040\ p^4 \qquad (4-1)$$

The comparison of this assumption with actual observations has been shown in Figure 4.2.

Reference shear modulus, G_0, and reference bulk modulus, B_0, are determined respectively by using the initial parts of deviatoric stress-shear strain and volumetric strain-mean effective normal stress curves obtained in a triaxial compression test. Although the other methods, such as the use of shear wave velocity or the loading, unloading hydrostatic test, give more accurate parameters, in practice no problem has been observed in the usage of simple method. Reference shear modulus and reference bulk modulus for Toyoura sand are 21 MPa and 14 MPa, respectively.

Because elastic moduli depend on mean effective stress and void ratio, the value of these moduli must be defined for a specific value such as $p_0 = p_{atm}$ and $e = 1$, which have been used in this thesis..

The results of one pair of conventional drained compression and extension triaxial tests on loose sand are used for the determination of other model parameters. The deviatoric stress-shear strain curves obtained by these tests are divided into some segments so that the slope of each segment is the same in compression and extension. The level of accuracy depends on the number of segments. The author's experience shows that 10 to 15 segments yield high accuracy. With these segments, and using equations (3-56), (3-57), (3-52) and (3-53), one can determine the size and position, m, and α, reference plastic moduli in compression and extension, H_{0c} and H_{0l}, and reference dilation parameters in compression and extension, $\overline{\eta}_{0c}$ and $\overline{\eta}_{0l}$, of each yield surface. It can be seen that most of the model parameters can be determined with only one compression and extension triaxial test. The values of these parameters for Toyoura sand are shown in Table 4.2. Calibration of this soil with all details has been shown as an example in appendix.

Each of the parameters just discussed is determined directly by using the experimental observations. However, some parameters also exist which must be determined by curve fitting. The following paragraphs discuss the determination of these parameters.

The parameter n_H describes the rate of variation of plastic modulus with void ratio. Higher values of n_H show higher rate of variation. The effect of variation of n_H on model prediction is shown in Figure 4.3. Three values of 5, 8 and 12 have been assumed for n_H in this comparison. As can be seen, all stress paths, stress-strain curves and pore pressure generation are affected by this parameter. For $n_H = 5$, the model shows

contractive-dilative behavior. With the increasing of n_H . the stress path moves up. and for n_H = 12. the prediction is completely contractive. n_H does not change the model prediction at large strains related to the ultimate state condition. This parameter must be determined by curve fitting to have the best compatibility with the experimental result observed during conventional undrained triaxial test. Because this parameter has a significant effect on the shape and position of the undrained stress(or in other words. starting of flow). it is suggested that the results of tests on loose samples be used for its determination. For Toyoura sand. using the test with p_i = 3 MPa in Figure 4.16. n_H was chosen equal to 9.

The parameter k shows the level of strain softening of dense sands under drained conditions. This parameter can be determined using a drained or undrained triaxial test on dense sand. In practice. if prediction is conducted for loose or medium dense sand. this parameter can be taken as zero. i.e.. using a pure kinematic hardening rule. In chapter 3. it was seen that this assumption works well except for very dense sands. Figure 4.4 shows the effect of variation of k on model performance under undrained triaxial conditions. Three values of 0. 2 and 6 have been chosen for this comparison. The value of zero represents kinematic hardening in that the size of the yield surfaces is constant and the stress path never crosses the ultimate state line in the ($q - p$) plane. With the increase of the value of k . the stress path can pass this line. but when approaching the ultimate state. the stress path comes down and attaches to the ultimate state line. The higher the value of k . the higher the position of stress path with respect to ultimate state line. With the increase of the value of k . the model shows stiffer response for dense soils. For $k = 6$. stress-strain curve is higher than those results for $k = 0$ or $k = 2$ (see Figure 4.4). However. all the curves finally go to an ultimate state. In the case of Toyoura sand. in the predictions presented here. the value of this parameter is zero. i.e.. kinematic hardening has been applied. For typical predictions in chapter 3, k was chosen equal to 2.

The parameter K_a is a parameter that changes the rate of volumetric strain with anisotropy. In the case of monotonic loading. if initial anisotropy is not too great. this parameter can be taken as zero. Figure 4.5 shows the effect of variation of K_a on model performance. To assume that $K_a = 0$ means that $\overline{\eta}_0$ for yield surfaces does not change with respect to their positions. With this assumption. the stress path at starting of unloading or reloading is more vertical (see Figure 4.5). In other words. the model shows less contraction. With the increasing of K_a. the model shows more contraction and the stress path moves faster into the lower mean effective stresses and outer yield surfaces. As a result. in this condition. larger strains develop in the soil that can be seen in Figure (4.5). For determination of K_a. one can use an undrained cyclic triaxial test or a monotonic triaxial test which has been performed on an anisotropically consolidated sample. For Toyoura sand. using the test in Figure 5.15. the value of this parameter is 0.1.

Model parameters for Toyoura sand. Ottawa sand. Fraser River sand. Banding sand and Fuji River sand have been shown in Tables 4.2 to 4.6. respectively. To determine n_H for Ottawa sand and Fraser River sand. respectively. the tests in Figures (4.11) and (4.13) were used. For the soils for which the results of the drained triaxial extension test were not available. the parameters related to the extension side have been generated. using the method described in section 3.12.

4.4. Undrained behavior of sands

In chapter 3. the comparison of model predictions. using kinematic and isotropic-kinematic hardening rules. was discussed. To show that in most cases the use of kinematic hardening is enough. the pure kinematic hardening rule has been used in all predictions in this chapter. As will be seen. kinematic hardening is enough for capturing most observed behavior.

This section evaluates the predictions of the model for undrained tests. In the first part, the general predictions of the model for different confining pressures and void ratios will be presented. Then, model predictions will be compared with several tests performed over a wide range of confining pressures and densities on different sands. Both initially isotropic and anisotropic samples have been considered.

Figure 4.6 shows the effect of initial mean effective stress on model performance for p_i = 0.5, 2, 3, 4, 5, 6 MPa in triaxial compression and extension. The void ratio for all samples has been considered 0.82. The results show that at a given void ratio, all the specimens exhibit the same undrained strength at the ultimate state. This is consistent with observations that ultimate state conditions are only a function of void ratio. The model predicts a transition from dilative behavior at low stresses with negative pore pressure generation (see Figure 4.6) to fully contractive behavior for high stresses. For samples consolidated at small stresses, the stress-strain curve shows continuous strain hardening with peak and ultimate state conditions occurring simultaneously at large strains (ε_a > 20%). However, for samples consolidated at high stresses, the stress-strain curve shows a maximum at small strains and then a decrease of deviatoric stress leading to the ultimate state.

Figure 4.7 shows the predicted effect of void ratio on the model performance in triaxial compression and extension for samples with the same initial mean effective stress (p_i = 2 MPa). The values of 0.93, 0.90, 0.85, 0.80 and 0.75 have been considered for void ratio. As can be seen, void ratio has a significant effect on stress path, stress-strain curve and pore pressure generation. The results show that at high void ratios, the samples show a peak shear resistance which is mobilized at small strains, after which the specimens collapse to residual strength. This residual strength depends on void ratio which is consistent with observations reported by different researchers.

As the void ratio decreases ($e = 0.85$). the specimen shows a peak shear stress followed by strain softening with positive pore water pressure generation achieving a minimal strength (quasi-steady state condition). and then strain hardening reaching the ultimate state condition at large strains. For lower void ratios. the model shows continuous strain hardening. Peak strength and ultimate state conditions are achieved simultaneously at large strains.

Figures 4.8. 4.9 and 4.10 compare model predictions with CIUC tests (undrained triaxial compression test on isotropically consolidated sample) on a series of very loose to loose specimens of Toyoura sand ($e = 0.933 - 0.899$) at different mean effective stresses. The model accurately predicts the undrained stress paths. For the case of $p_i = 2$ MPa and $e = 0.908$. the model shows a small over-prediction in stress-strain curve with respect to observed behavior. However. with increasing strain. this difference reduces and for $\varepsilon_d > 15$ %. predicted and observed curves match perfectly.

To obtain a complete evaluation of the model predictions for different soils. the results of a series of CIUC tests on loose Ottawa sand (Sasitharan et al.. 1994) and Fraser River sand (Chillarige. 1995) have also been used.

Figures 4.11 and 4.12 show the comparison of model predictions with the test results on Ottawa sand for different initial mean effective stresses. As can be observed. model predictions match for both the stress path and stress-strain curves. Maximum shear stress and ultimate state are identical for both model predictions and test results.

Figures 4.13. 4.14 and 4.15 compare the predicted and measured undrained effective stress paths and stress-strain behavior of very loose and loose specimens ($e = 1.12$. 1.0. 1.02) of Fraser River sand. The test in Figure 4.13 has been used in calibration. A good agreement exists between model simulations and test results. The model predicts the undrained stress paths and. as a result. pore pressure development. Stress-strain curves predicted by the model also accord with the measurements of the

tests. For two tests. however. there is a difference between model predictions and the test results at large strains or the ultimate state condition. This difference is due to the fact that there is no unique ultimate state line based on test results for Fraser River sand. There is a significant discrepancy in the test results for the ultimate state conditions for this sand. To solve this problem. the best line passing through these points has been chosen and used in the model predictions. It is clear that all models in the "Reference State Soil Mechanics" framework finally show the ultimate state which has been defined for that. Therefore. the present model converged to the best line which has passed through experimental results. The existing difference is actually the difference between this best line and the experimental results. This problem will apply to all constitutive models as long as no adequate definition of the ultimate state line exists.

Figure 4.16 compares the predicted and measured behavior for a series of CIUC tests for medium dense Toyoura sand (e = 0.833). The model accurately predicted the transition from contractive behavior for the specimen consolidated at 3 MPa to strongly dilative behavior developed for the specimen consolidated at low stress (p_i = 0.1 MPa). In the case of a test at high confinement. the behavior is contractive with maximum shear mobilized at small strains and a post peak reduction of shear stress. decreasing to ultimate state at large strains. However. for tests at low confinement . the model predicts a substantial increase in the mean effective stress. or in other words. negative shear induced pore pressures with continuous strain hardening and maximum undrained strength at shear strains around 25 %. Figure 4.17 also shows a series of tests on medium dense samples of Toyoura sand with different void ratios and mean effective stresses. As can be seen. both stress paths and stress-strain curves obtained by model predictions and test results match nicely. The results in Figures 4.16 and 4.17 show that the model is able to accurately predict the effective stress paths and stress-strain behavior of medium dense sands over the full range of mean effective stresses.

Figure 4.18 compares the predicted and measured undrained effective stress paths and stress-strain behavior of dense specimens (e = 0.735) of Toyoura sand at 4 different

initial mean effective stresses (p_i =0.1, 1, 2, 3 MPa). Good agreement exists in undrained stress paths. The model describes the transition from strongly dilative behavior developed for specimen consolidated at low stress (p_i = 0.1 MPa) to moderate dilative behavior at high stresses (p_i=2, 3 MPa). Shear stress-strain curves predicted by the model qualitatively accord well with the measurements of tests. However, in the range of 5% to 15% shear strain, the model shows 10% over prediction for deviatoric stress for the test with p_i=0.1 MPa.

4.4.1 Effect of consolidation stress history

Figure 4.19 shows the typical model predictions of undrained triaxial compression and extension behavior of specimens consolidated with K_0=0.5, 1.0 and 1.5 at mean effective stress of 5 MPa. The void ratio of all specimens has been assumed as 0.82. The figure shows that maximum deviatoric stress increases with decreasing of K_0. However, maximum pore pressure generation in compression increases with increasing of K_0. But, in extension, maximum pore pressure generation relates to lower K_0. As can be seen, when K_0 is decreased, the brittleness of samples increases highly in compression. For sample with K_0=0.5, after a small increase of deviatoric stress in compression, collapse occurs and the sample reaches the ultimate state condition. The uniqueness of the ultimate state condition for specimens with the same void ratio is observed. In these predictions, K_u has been taken as 0.1. By increasing the value of this parameter, the model will initially show less stiffness, and the stress path will not be vertical to the same degree. The same typical model predictions for dense samples (e=0.78, p_i=0.5 MPa) have been shown in Figure 4.20. In this case, pore pressure is positive at small strains; when deformation is increased, however, it becomes negative.

Figures 4.21 and 4.22 show the comparison of model predictions with experimental results obtained from triaxial tests on anisotropically consolidated samples

of loose Toyoura sand. As can be observed. the model is able to show the effect of initial anisotropy.

Figure 4.23 also compares the model predictions with results of two tests conducted on anisotropically consolidated samples of Fraser River sand. Both compression and extension shearing modes have been used for this comparison (Ayoubian and Robertson. 1996). For both compression and extension. in small strains. the model shows slightly smaller deviatoric stress: however. this difference quickly decreases. A small difference between model predictions and the experimental results for the ultimate state condition can be attributed to the lack of unique ultimate state line for Fraser River sand (as discussed in the previous section). This ability to show the behavior of anisotropic samples is very important both for modelling the response of elements which are close to the edge of earth dams and for the modelling of all elements under cyclic loading. In the next chapter. it will be shown that the model is not only capable of representing the effect of initial anisotropy in the soil. but can also show the effect of induced anisotropy during loading.

4.5. Drained behavior of sands

This section illustrates model predictions of drained tests on sands for a wide range of mean effective stresses and densities.

Figure 4.24 shows the effect of the initial void ratio on model predictions for drained triaxial compression tests. The initial mean effective stress (p_i) has been assumed 1.5 MPa for all predictions (typically performed on Toyoura sand). However. the initial void ratios are different (e_i =0.95. 0.90. 0.85. 0.80. 0.75. 0.70). As can be seen. when initial void ratio is decreased. the behavior of samples changes from contractive to dilative. At large strains. the model shows the same ultimate state condition for all samples consistent with reported experimental results. The variation of volumetric strain

with axial strain has also been shown in Figure 4.24. For all samples at small strains. the model shows contraction. For very loose samples. the volume decreases continuously until ultimate state. However. for dense samples. behavior quickly changes from contractive to dilative in small strains. Because all samples reach a unique ultimate state condition. ultimate deviatoric stresses are the same for all of them. This uniqueness can be observed in Figure 4.24. For loose samples. the rate of increasing of deviatoric stress is lower than that in dense samples. As can be seen. the sample with e_i =0.95 has reached ultimate state after 23% axial strain. But. for the specimen with e_i =0.70. the model attains the ultimate state condition at only 8% axial strain. The lack of strain softening for the dense soils response in the predictions was due to the use of the pure kinematic hardening rule in the model. This topic was discussed in detail in chapter 3.

Figure 4.25 shows the typical model predictions for imaginary samples with the same initial void ratio (e_i =0.82) but different initial mean effective stresses (p_i =0.1. 0.5. 1.0. 1.5. 2.0 MPa). As can be observed. for the specimen with p_i =0.1 MPa. predicted behavior is highly dilative. However. when the initial effective stress is increased. the behavior changes to contractive. At large strains. all samples have reached the ultimate state condition. At small strains. volumetric strain of all samples is positive. But based on the initial level of stress. this contractive behavior may change to dilative. For example. for the sample with p_i =0.1 MPa. after a small volume increase. the volume of the sample has decreased and finally the specimen has reached ultimate state condition. The rate of change of the behavior from contractive to dilative depends highly on initial mean effective stress, or in other words. the initial state of the soil. The variation of deviatoric stress versus axial strain can also be seen in Figure 4.25. This figure shows that samples with higher initial mean effective stress reach ultimate state later than the samples with smaller p_i and the same e_i . Based on Figures 4.24 and 4.25. one can conclude that the model is able to show typically the effect of initial void ratio and initial mean effective stress on the soil performance.

To compare the model predictions with experimental observations in drained conditions. the results of ten conventional drained triaxial tests conducted on Toyoura sand have been used (Verdugo and Ishihara. 1996: Verdugo. 1992). These tests were performed on both initially loose and dense samples. The initial mean effective stresses of each pair of these tests are the same but the initial void ratios are different. Samples in the lab have reached a unique ultimate state zone. However. this zone has a width and is not a line (see Figure 4.26). The comparison of variation of void ratios with mean effective stresses is shown in Figure 4.26. As can be observed. the model could predict the behavior of all samples. For the model. the ultimate state condition has been defined as a curve: both loose and dense samples have finally reached a unique ultimate state. Figure 4.26 compares the stress-strain curves for loose and dense samples separately. As can be seen. predicted deviatoric stress-axial strain curves match with experimental results. especially in the case for loose samples. For dense samples in some cases. the model shows 10% less deviatoric stress than the observed behavior. Such a difference is acceptable and does not cause problems in practice. Using the isotropic-kinematic hardening rule. this difference will be reduced.

Figure 4.27 shows the evaluation of the model for a p-constant triaxial test. This test has been conducted by Sasitharan et al. (1994) on Ottawa sand. As can be seen in all figures. i.e.. axial strain-deviatoric stress. void ratio-deviatoric stress and axial strain-volumetric strain curves. the model predictions are consistent with experimental results.

4.6. Shearing mode

In general conditions. when a soil structure undergoes loading. different soil elements may be under different shearing modes. Therefore. constitutive models must be capable of predicting the response of the soil under different shearing modes with a unique set of parameters. Figure 4.28 and 4.29 show typical comparison of model predictions for two samples of loose and dense soils under different shearing modes. In this comparison. plane strain. triaxial compression and triaxial extension have been

considered. Overall. the model predictions show similar features in all modes of shearing. neglecting the more clear quasi-steady state for the loose sample under triaxial extension. Contractive behavior (flow deformation) for loose samples and dilative behavior for dense samples have been observed. Plane strain exhibits higher undrained strength and mobilized friction angle. In these predictions. based on Ishihara (1993) and Yoshimine (1996). the friction angles in triaxial compression and extension are almost the same. Therefore. based on the discussion in chapter 3. the ultimate friction angle is very close to the Matsuoka-Nakai criterion. The difference between the ultimate friction angle in plane strain and triaxial compression is around 4 degrees based on model predictions.

To validate the proposed model in general conditions. a set of extension triaxial tests and simple shear tests on Toyoura sand have been used (Yoshimine. 1996). The ultimate state line in triaxial extension and simple shear based on Yoshimine (1996) is not the same as what has been reported by Ishihara (1993) in triaxial compression for Toyoura sand. Therefore. in the prediction of these tests. a new ultimate state line based on limited available data has been considered. For triaxial extension and simple shear. it has been assumed that the ultimate state lines are parallel with that in triaxial compression but with 0.08 and 0.025 shifting down. respectively. A comparison of model predictions with observed behavior on four triaxial extension tests performed on isotropically consolidated samples. with different void ratios and mean effective stresses. has been shown in Figure (4.30).

In Figures (4.31) and (4.32) eight comparisons of model predictions with observed behavior of Toyoura sand in simple shear that have been conducted by hollow cylinder tests. have been presented. Eight samples with different initial mean effective stresses and void ratios have been considered in these comparisons. As can be seen. although the model has been calibrated using triaxial tests. it can also show the behavior of soil under other shearing modes. The lack of a unique ultimate state line in the experiments has caused differences between model predictions and experimental observations at large strains in some cases.

Figures (4.33) and (4.34) show four comparisons of model predictions with experiment on a deviatoric plane for simple shear conducted by hollow cylinder tests. As can be seen, model predictions are consistent with experimental observations. During the tests, the parameter of b decreases at small strains. However, with increasing strain, b increases and reaches a constant value.

4.7. Collapse

Modelling the behavior of cohesionless soils is not complete without considering collapse. The collapse surface can affect the response of loose cohesionless soils significantly. In undrained conditions when the stress path contacts with this state boundary, the soil element quickly reaches the ultimate state and as a result a significant decrease in the strength of the soil occurs. In drained conditions, because the volume of the specimen can change, the effect of collapse is manifested in a discontinuity of volume change or void ratio. By comparing the model predictions with experimental results obtained from tests conducted on loose Toyoura sand, Ottawa sand and Fraser River sand, the model shows that it was capable of predicting the role of the collapse surface in undrained conditions.

To evaluate the capability of the model to predict the effect of collapse in drained conditions, the results of two tests which have been performed by Skopek et al. (1994) on very loose dry Ottawa sand have been used. The initial void ratios of these two samples were 0.831 and 0.841. These tests have been conducted on isotropically consolidated samples. In the first step of loading, the deviatoric stress has been increased, but after some increase, the deviatoric stress has been kept almost constant. In this kind of loading, which has been called the deviatoric stress constant test, when the stress path contacts the collapse surface, a significant decrease in void ratio appears.

Figures (4.35) and (4.36) show the comparison of model predictions with Skopek et al.'s tests. In both figures, the stress path, which has been applied during the test, has

been shown and then the variation of void ratio with mean effective stress has been plotted. As can be seen, model predictions match with observed behavior. Considering the model performance in prediction of undrained and drained behavior of loose cohesionless soils, one can conclude that the model is able to show flow liquefaction during monotonic loading.

4.8. Discussion on model parameters for different sands

The parameters of the model for five different sands have been shown in Tables (4.2) to (4.6). In general, the determination of elastic moduli is independent of formulation of elasto-plastic models. Using some tests like shear wave velocity and hydrostatic cyclic tests, these parameters are determined. In this work, because the results of these tests were not available, usually the first part of deviatoric stress-shear strain and mean effective stress-volumetric strain curves in drained triaxial tests were used to determine these moduli. Considering the plastic deformation of sands from initial steps of loading, the elastic moduli which are determined by using this method often are less than real values. G_0 and B_0 are normalized values for shear modulus and bulk modulus at $p_0 = p_{atm}$ and $e_0 = 1$.

For Ottawa sand and Fuji River sand, elastic moduli that were determined by using stress-strain curves, were small. As a result, the model could not show real contractions which have been observed during the tests. For solving this problem, the values of elastic moduli were increased (by trial and error) to have acceptable prediction for these soils. Using these increased values, the plastic parameters for the first segment were determined. Then, the size of the elastic zone has been taken as zero: i.e., no pure elastic zone for these soils. Because of that, m_t for the first yield surface in Tables (4.3) and (4.6) are zero.

m_k for Toyoura sand. Fraser River sand and Fuji River sand are determined by using existing data in the literature. However. since for Ottawa sand and Banding sand data for the extension side were not available. m_k for those soils has been assumed equal to 1.

The parameters m_c, α, H_{0c}, H_{0E}, $\bar{\eta}_{0c}$ and $\bar{\eta}_{0E}$ are determined directly by using experiments. Therefore. the response of the soil under drained conditions appears in these parameters. If there is a difference between these parameters for different soils in Tables (4.2) to (4.6). it has come from the different behavior of the soils in the tests. Using normalization. H_{0c}, H_{0E}, $\bar{\eta}_{0c}$ and $\bar{\eta}_{0E}$ for all the soils have been determined at the same references ($p_0 = p_{atm}$, $e_0 = 1$, $\psi_{ref} = 0$ and $\alpha = 0$).

Observing Tables (4.2) to (4.5). one can see that. in some cases. a significant difference exists between the values of reference plastic moduli (H_{0c} or H_{0E}) for different soils. This difference has been developed by normalization. In normalization. the same values of $e_0 = 1$ and $p_0 = p_{atm}$ have been used for all the soils. In some cases (for example Ottawa sand). $e_0 = 1$ is much higher than the maximum void ratio of the soil. Therefore. after normalization. a small value has been obtained for H_{0c} (or H_{0E}).

The parameter n_H. which shows the variation of plastic moduli with void ratio. has been determined by curve fitting. For Ottawa sand. the available data (Sasitharan et al.. 1994; Skopek et al.. 1994) were in a small range of void ratios. For the best fit to the test results. n_H has been taken as 30. It seems this high value can not be realistic. However. because the best fit was obtained with this value. it was taken for n_H. For the other soils. n_H changes between 4 and 13.

The parameter K_u for Toyoura sand was obtained by curve fitting, using stress path in the test in Figure (5.15). Based on this curve fitting, K_u is equal to 0.1. For the other soils, using the same value, predictions were acceptable. The effect of K_u on model response has been shown in Figure (4.5). In general, for considering the variation of dilation parameters with respect to the position of yield surfaces, it is suggested to assume at least 0.1 for K_α.

In all predictions for Toyoura sand, Ottawa sand, Fraser River sand and Banding sand only kinematic hardening has been used. Therefore, k has been taken as zero for all of these soils. As can be seen in the predictions, this assumption was acceptable. However, for Fuji River sand, using pure kinematic hardening, a large volumetric strain was developed. For solving this problem, the isotropic-kinematic hardening with $k = 10$ was applied. This difference is due to the higher relative density of samples of Fuji River sand in the tests compared with that in the other soils.

4.9. Summary

This chapter validated the performance of the proposed model under monotonic loading. Both drained and undrained conditions and isotropically and anisotropically consolidated samples have been used in the validation. Different stress paths and shearing modes have been applied. It was shown that the model is capable of showing the effect of void ratio and mean effective stress, or in other words, the state of the soil, on soil response under both undrained and drained conditions. The consideration of the effect of state is neglected in most existing constitutive models for cohesionless soils. This has been solved in the present model. The ultimate state, which is important in large strains, can be captured by the model. Considering the state of the soil element with respect to the ultimate state, the model was able to predict the performance of both loose and dense sands with a unique calibration. It was shown that the model is able to show the effect of consolidation history in both compression and extension modes of shearing. The model is

also capable of showing the collapse. or in other words. flow liquefaction. in both drained and undrained conditions.

Table 4.1. Characteristics of soils

Soil	D_{50} (mm)	U_c	e_{max}	e_{min}	G_s	Mineral composition
Toyoura sand	0.17	1.7	0.977[1]	0.597[1]	2.65	quartz, feldspar, magnetite
Ottawa (C109) sand	0.34	-	0.82	0.50	2.65	quartz
Fraser River sand	0.25	1.7	1.00	0.60	2.75	quartz, feldspar, unaltered rock fragments
Banding sand	0.097[2]	1.8	0.84	0.50	2.65	quartz
Fuji River sand	0.22[2]	2.21	1.08	0.53	2.68	-

[1] e_{max} and e_{min} for all sands have been determined by using ASTM D2049 method, except for Toyoura sand that has been determined by using JSSMFE method.

[2] The values reported for Banding sand and Fuji River sand are for D_{10}.

Table 4.2. Model parameters for Toyoura sand

$G_0 = 21$ MPa $\qquad\qquad B_0 = 14$ MPa $\qquad m_t = 0.714$

$n_H = 9.0$ $\qquad\qquad K_a = 0.1$ $\qquad\qquad k = 0$

YS	m_c	α	H_{0c} (MPa)	H_{0E} (MPa)	$\bar{\eta}_{0c}$	$\bar{\eta}_{0E}$
1	0.129	0.024	17.848	20.713	0.395	0.283
2	0.228	0.041	3.253	4.147	0.660	0.480
3	0.363	0.066	2.614	3.480	1.085	0.794
4	0.410	0.074	1.614	2.350	1.036	0.773
5	0.503	0.090	1.187	1.758	0.940	0.710
6	0.556	0.099	0.836	1.381	1.040	0.803
7	0.639	0.11	0.529	0.915	1.037	0.814
8	0.713	0.118	0.425	0.771	1.018	0.806
9	0.757	0.120	0.288	0.553	1.071	0.851
10	0.802	0.120	0.208	0.418	1.021	0.816
11	0.875	0.117	0.153	0.316	1.052	0.839
12	0.909	0.113	0.134	0.280	1.124	0.890
13	0.950	0.106	0.097	0.219	1.071	0.842
14	0.987	0.099	0.087	0.188	1.123	0.875
15	1.028	0.089	0.062	0.148	1.121	0.866
16	1.060	0.080	0.058	0.132	1.160	0.885
17	1.101	0.066	0.038	0.091	1.160	0.877
18	1.131	0.055	0.027	0.073	1.171	0.877
19	1.163	0.043	0.028	0.070	1.202	0.892
20	1.205	0.025	0.017	0.042	1.188	0.881
21	1.233	0.013	0.017	0.035	1.204	0.891
22	1.249	0.005	0.005	0.015	1.200	0.886
23	1.256	0	1E-6	1E-6	1.193	0.881

Table 4.3. Model parameters for Ottawa sand

$G_0 = 14.9$ MPa $\qquad B_0 = 14.9$ MPa $\qquad m_k = 1.0$

$n_H = 30$ $\qquad K_\alpha = 0.1$ $\qquad k = 0$

YS	m_c	α	H_{0c} (MPa)	H_{0E} (MPa)	$\bar{\eta}_{0c}$	$\bar{\eta}_{0E}$
1	0	0.086	0.0249	0.0275	0.615	0.615
2	0.125	0.086	0.0195	0.0227	0.914	0.914
3	0.189	0.111	0.0089	0.0120	0.938	0.938
4	0.345	0.140	0.0038	0.0056	0.947	0.947
5	0.472	0.143	0.0015	0.0024	0.889	0.889
6	0.566	0.136	0.0013	0.0022	0.954	0.954
7	0.639	0.127	0.0012	0.0021	0.997	0.997
8	0.681	0.121	0.001	0.0018	1.060	1.060
9	0.770	0.104	0.0002	0.0003	1.084	1.084
10	0.906	0.072	0.0001	0.0001	1.151	1.151
11	1.035	0.036	0.00002	0.00004	1.164	1.164
12	1.099	0.016	0.00001	0.00001	1.157	1.157
13	1.147	0	1E-5	1E-5	1.142	1.142

Table 4.4. Model parameters for Fraser River sand

$G_0 = 10.4$ MPa $\qquad B_0 = 10.4$ MPa $\qquad m_k = 1.0$

$n_H = 4.0$ $\qquad K_\alpha = 0.1$ $\qquad k = 0$

YS	m_L	α	H_{0c} (MPa)	H_{0E} (MPa)	$\overline{\eta}_{0c}$	$\overline{\eta}_{0E}$
1	0.110	0.083	16.903	20.165	0.844	0.844
2	0.203	0.125	7.634	10.555	1.253	1.253
3	0.369	0.164	5.123	8.123	1.189	1.189
4	0.537	0.172	2.067	8.745	1.191	1.191
5	0.691	0.163	1.008	2.019	1.019	1.019
6	0.823	0.145	0.755	1.647	1.070	1.070
7	0.924	0.126	0.458	1.042	0.945	0.945
8	1.008	0.107	0.422	1.001	1.024	1.024
9	1.112	0.081	0.290	0.733	1.031	1.031
10	1.195	0.058	0.163	0.429	1.111	1.111
11	1.269	0.036	0.115	0.313	1.190	1.190
12	1.327	0.017	0.083	0.234	1.229	1.229
13	1.366	0.005	0.038	0.103	1.289	1.289
14	1.379	0	1E-4	1E-4	1.193	1.193

Table 4.5. Model parameters for Banding sand

$G_0 = 8.8$ MPa $B_0 = 13.1$ MPa $m_k = 1.0$

$n_H = 13$ $K_\alpha = 0.1$ $k = 0$

YS	m_c	α	H_{0c} (MPa)	H_{0E} (MPa)	$\overline{\eta}_{0c}$	$\overline{\eta}_{0E}$
1	0.142	0.096	1.9518	2.3212	0.373	0.373
2	0.218	0.124	0.8075	1.0388	0.439	0.439
3	0.297	0.142	0.2443	0.3355	0.859	0.859
4	0.379	0.152	0.0995	0.1430	0.917	0.917
5	0.432	0.155	0.0841	0.1308	1.022	1.022
6	0.527	0.154	0.0496	0.0819	1.006	1.006
7	0.601	0.148	0.0273	0.0496	0.996	0.996
8	0.734	0.131	0.0103	0.0196	1.093	1.093
9	0.799	0.119	0.0071	0.0141	1.092	1.092
10	0.874	0.104	0.0052	0.0108	1.174	1.174
11	0.943	0.087	0.0030	0.0064	1.167	1.167
12	0.981	0.078	0.0026	0.0056	1.097	1.097
13	1.028	0.065	0.0020	0.0045	1.062	1.062
14	1.061	0.056	0.0015	0.0032	1.095	1.095
15	1.084	0.049	0.0011	0.0028	1.139	1.139
16	1.110	0.041	0.0009	0.0021	1.133	1.133
17	1.130	0.035	0.0009	0.0020	1.167	1.167
18	1.148	0.030	0.0008	0.0020	1.168	1.168
19	1.171	0.022	0.0006	0.0013	1.197	1.197
20	1.190	0.016	0.0005	0.0012	1.174	1.174
21	1.220	0.006	0.0002	0.0004	1.234	1.234
22	1.228	0.004	0.0002	0.0005	1.201	1.201
23	1.237	0.0009	0.0001	0.0002	1.210	1.210
24	1.240	0	1E-4	1E-4	1.197	1.197

Table 4.6. Model parameters for Fuji River sand

$G_0 = 10.3$ MPa $\qquad\qquad B_0 = 12.3$ MPa $\qquad\qquad m_k = 0.688$

$n_H = 6$ $\qquad\qquad\qquad K_\alpha = 0.1$ $\qquad\qquad\qquad k = 10$

YS	m_c	α	H_{0c} (MPa)	H_{0E} (MPa)	$\overline{\eta}_{0c}$	$\overline{\eta}_{0F}$
1	0	0.007	2.702	1.635	2.900	0.505
2	0.300	0.007	1.189	0.603	0.806	0.842
3	0.581	-0.042	0.748	0.317	0.958	0.952
4	0.746	-0.087	0.551	0.183	1.218	1.029
5	0.895	-0.129	0.285	0.081	1.248	1.035
6	1.093	-0.141	0.181	0.045	1.181	1.160
7	1.192	-0.141	0.100	0.030	1.295	1.180
8	1.284	-0.084	0.049	0.018	1.370	1.107
9	1.352	-0.051	0.020	0.008	1.427	1.164
10	1.407	-0.022	0.013	0.006	1.454	1.104
11	1.437	-0.007	0.006	0.002	1.473	1.061
12	1.454	0	1E-6	1E-6	1.445	0.997
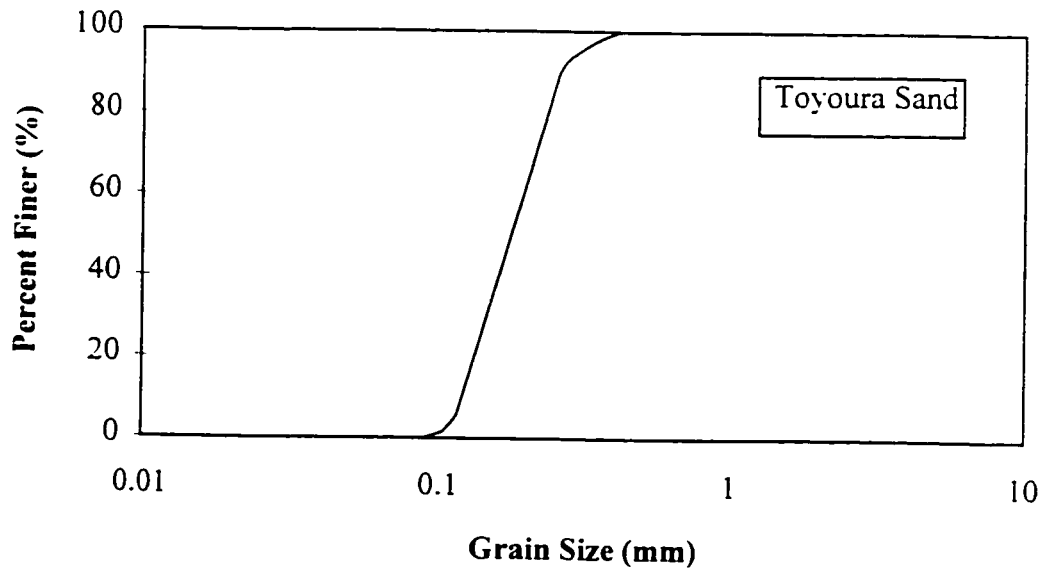
Figure 4.1. Grain size distribution of Toyoura sand.
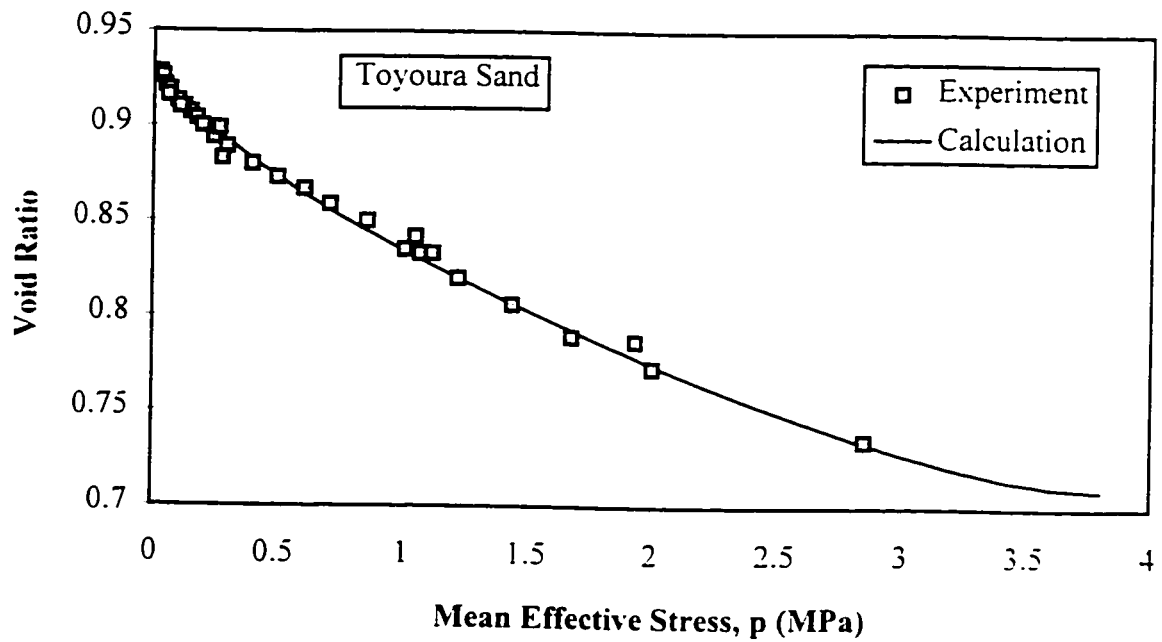
Figure 4.2. Ultimate state line of Toyoura sand.
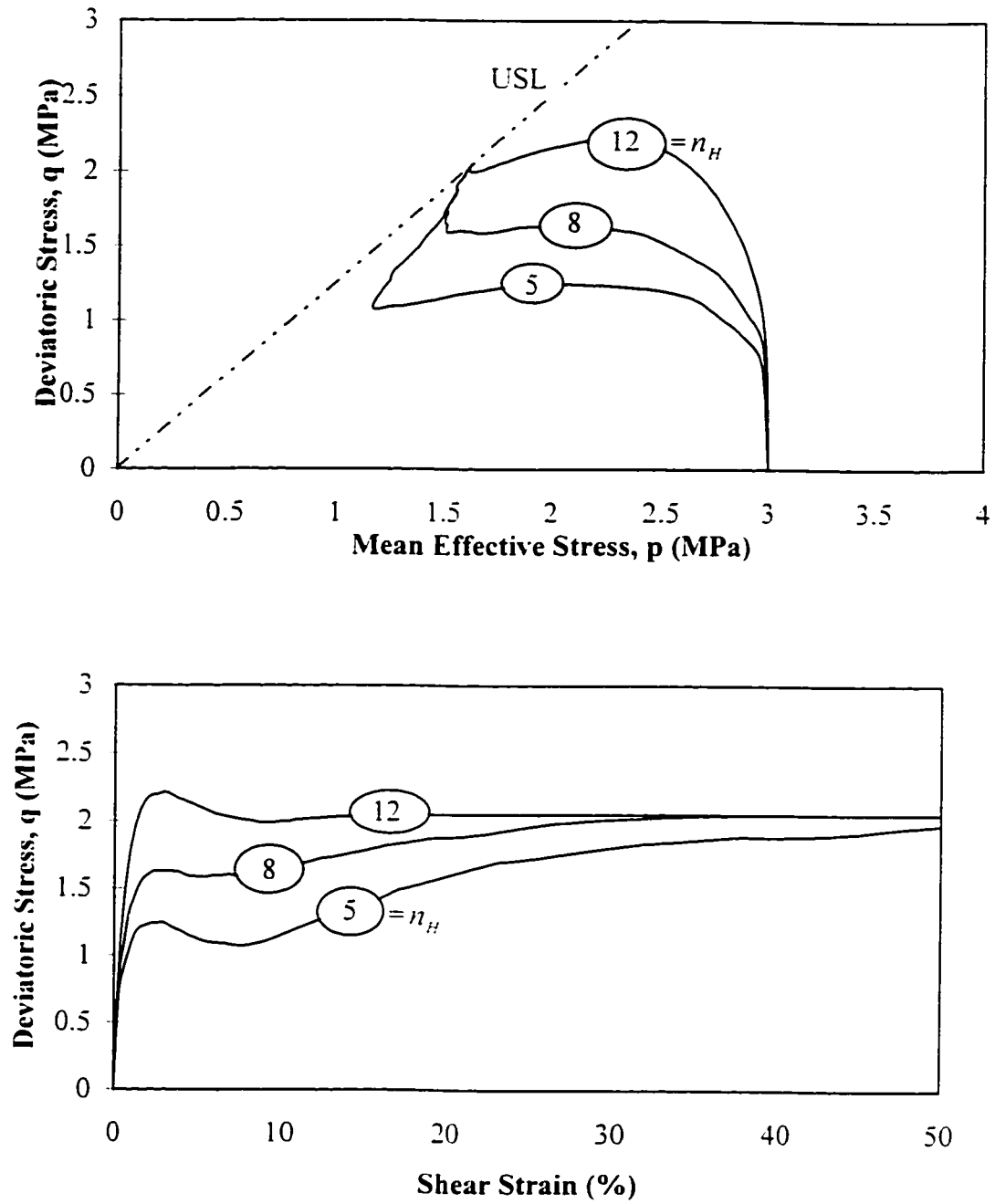
Figure 4.3. Effect of parameter n_H on model performance (Effective stress paths and stress-strain curves).
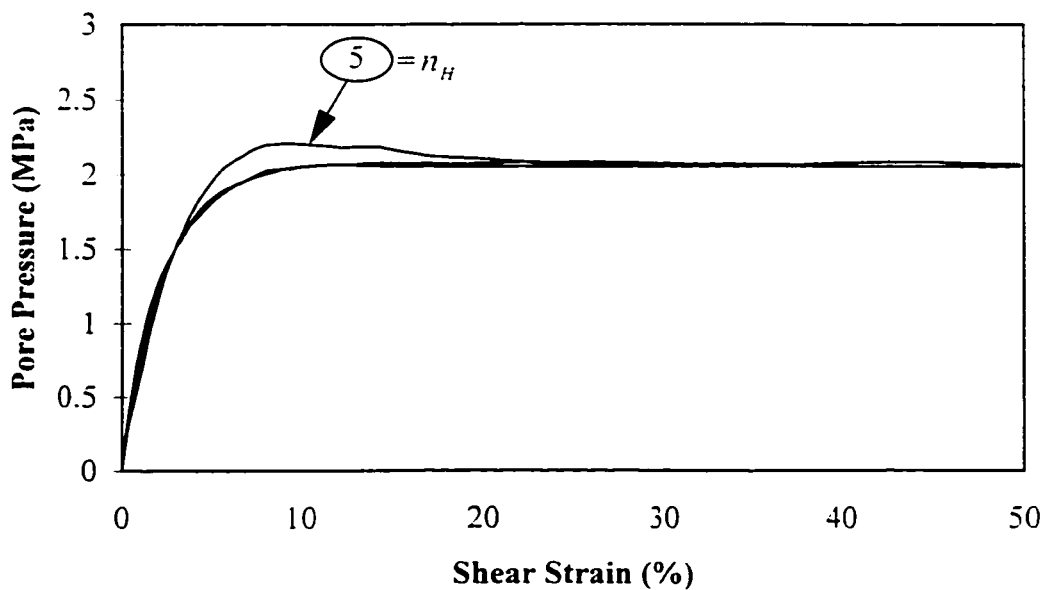
Figure 4.3. (cont.) Effect of parameter n_H on model performance (Pore pressure-strain curves).
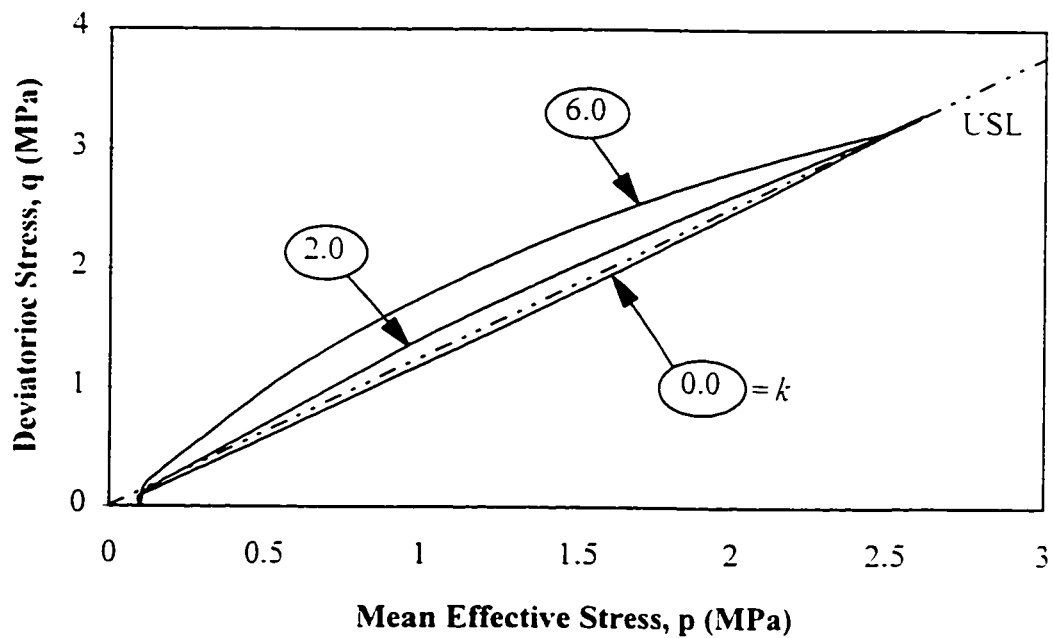
Figure 4.4. Effect of parameter k on model performance (Effective stress paths).
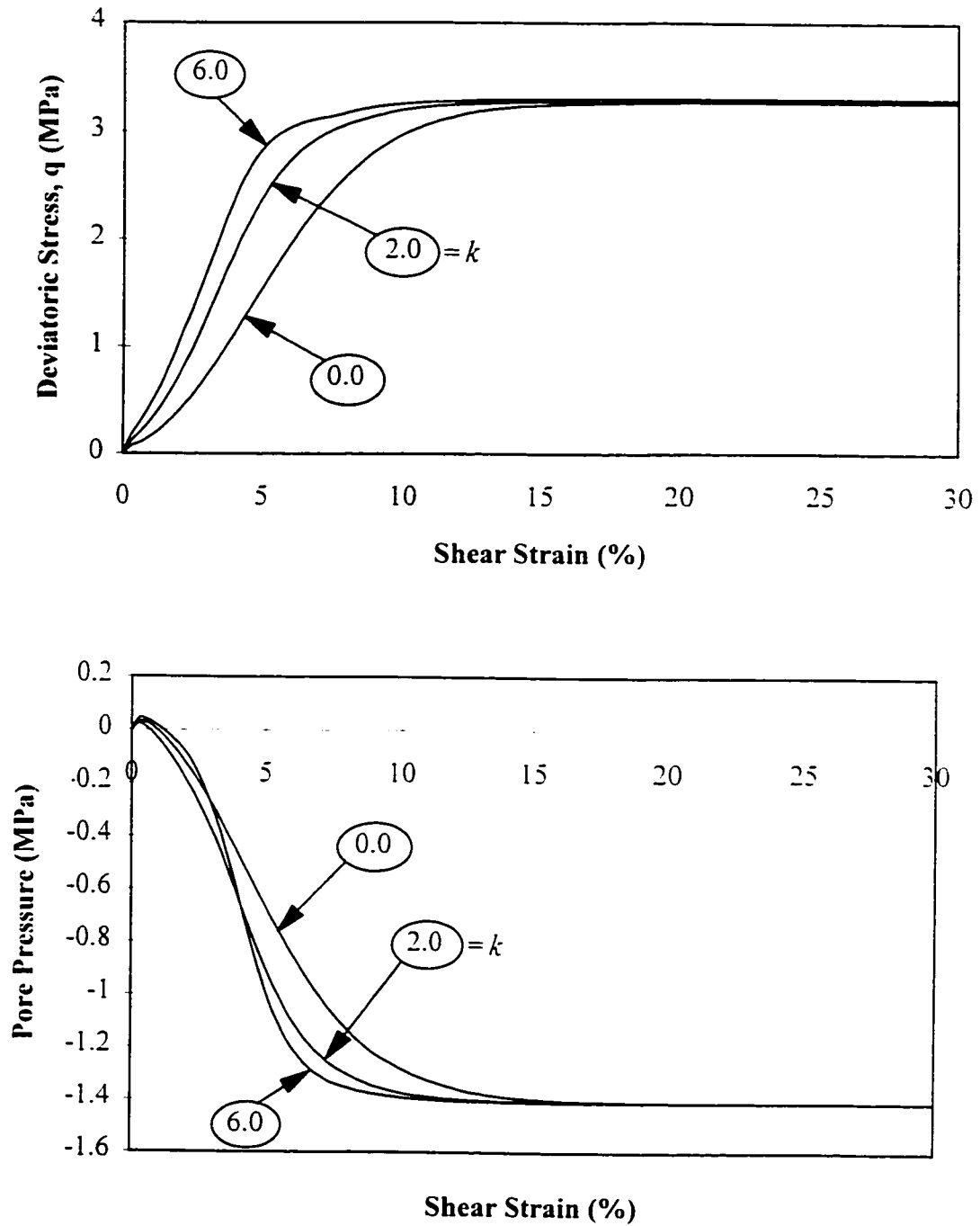
Figure 4.4. (cont.) Effect of parameter k on model performance (Stress-strain and pore pressure-strain curves).
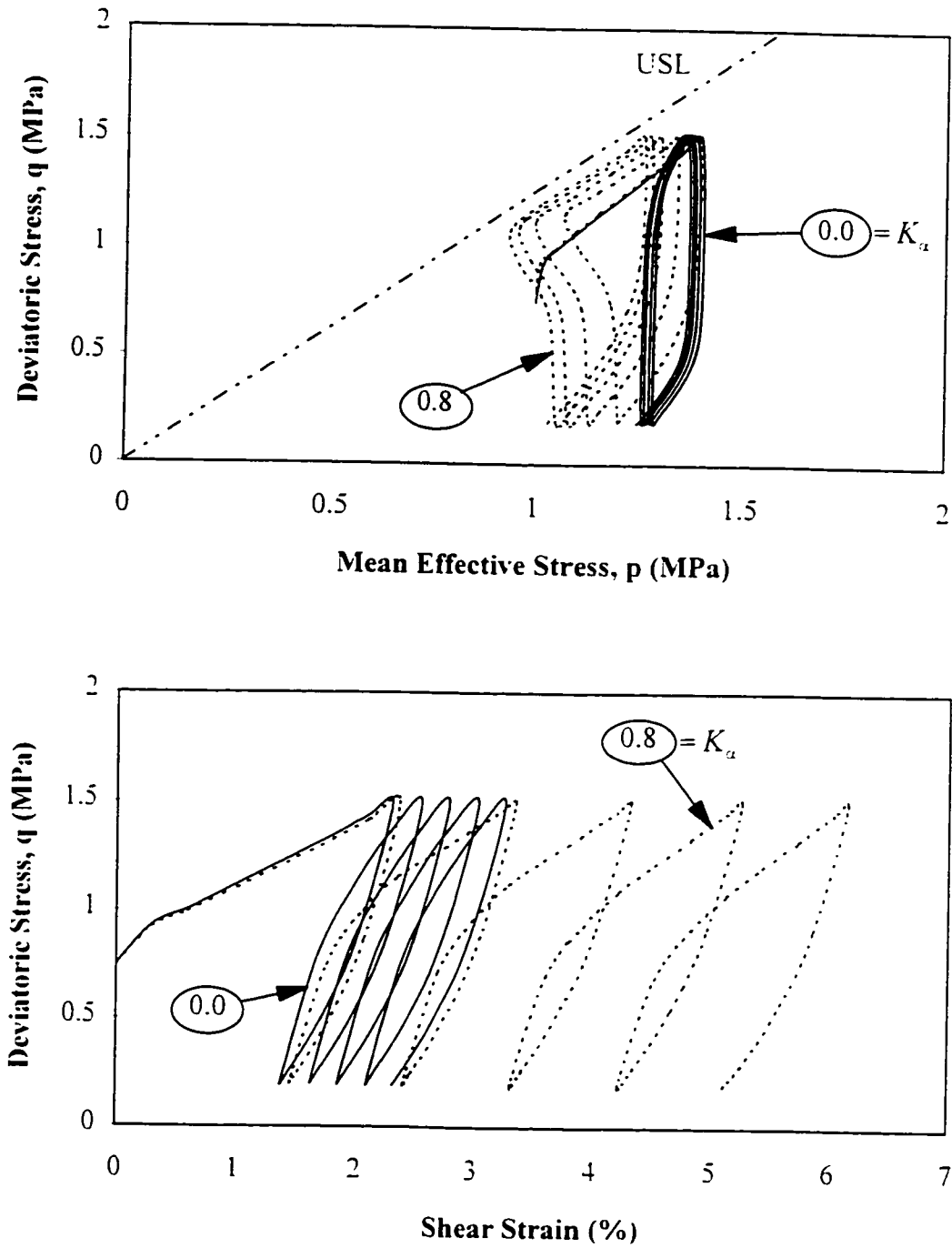
Figure 4.5. Effect of parameter K_α on model performance (Effective stress paths and stress-strain curves).
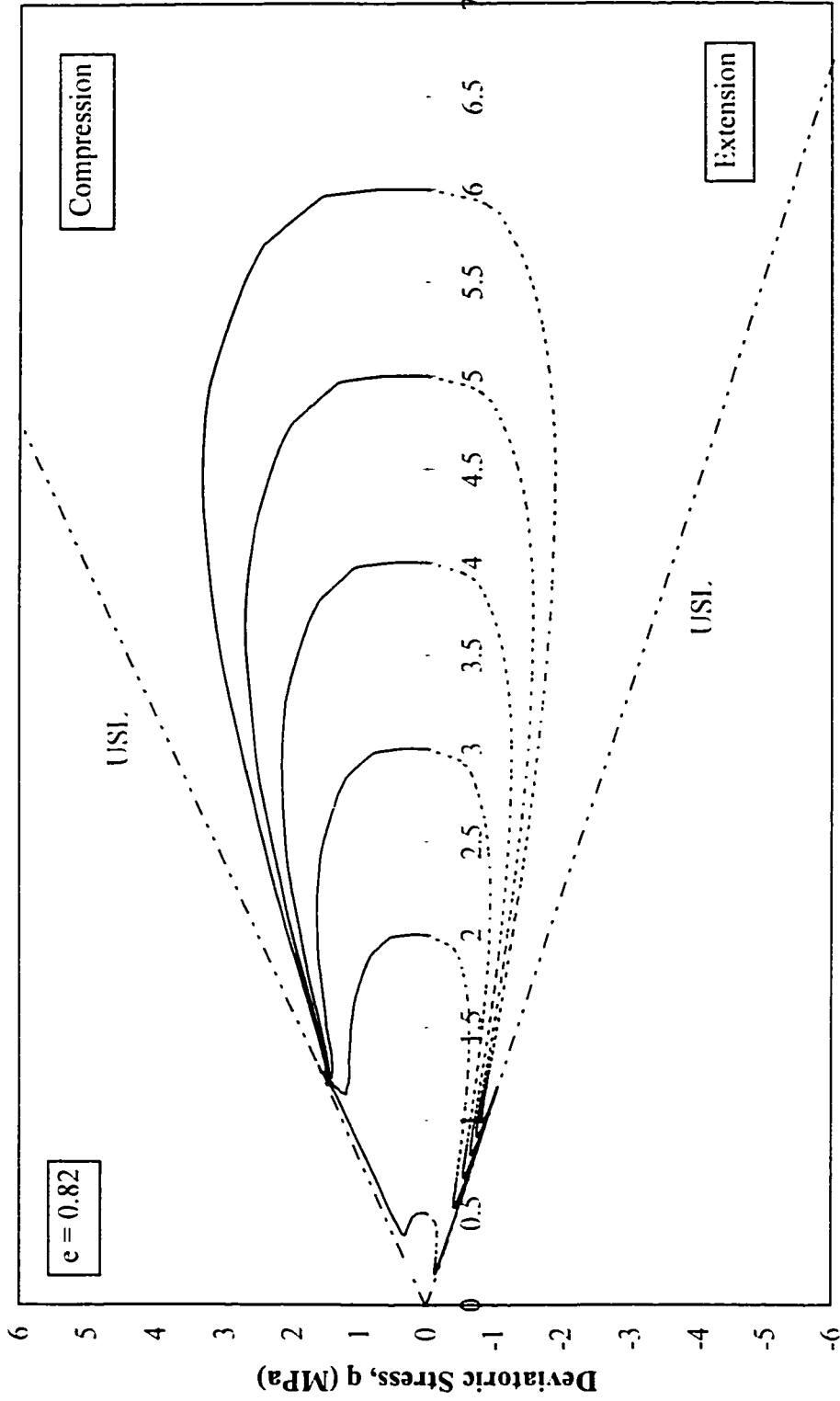
Figure 4.6. Effect of mean effective stress on model prediction for undrained behavior of sands in triaxial compression and extension (Effective stress paths).
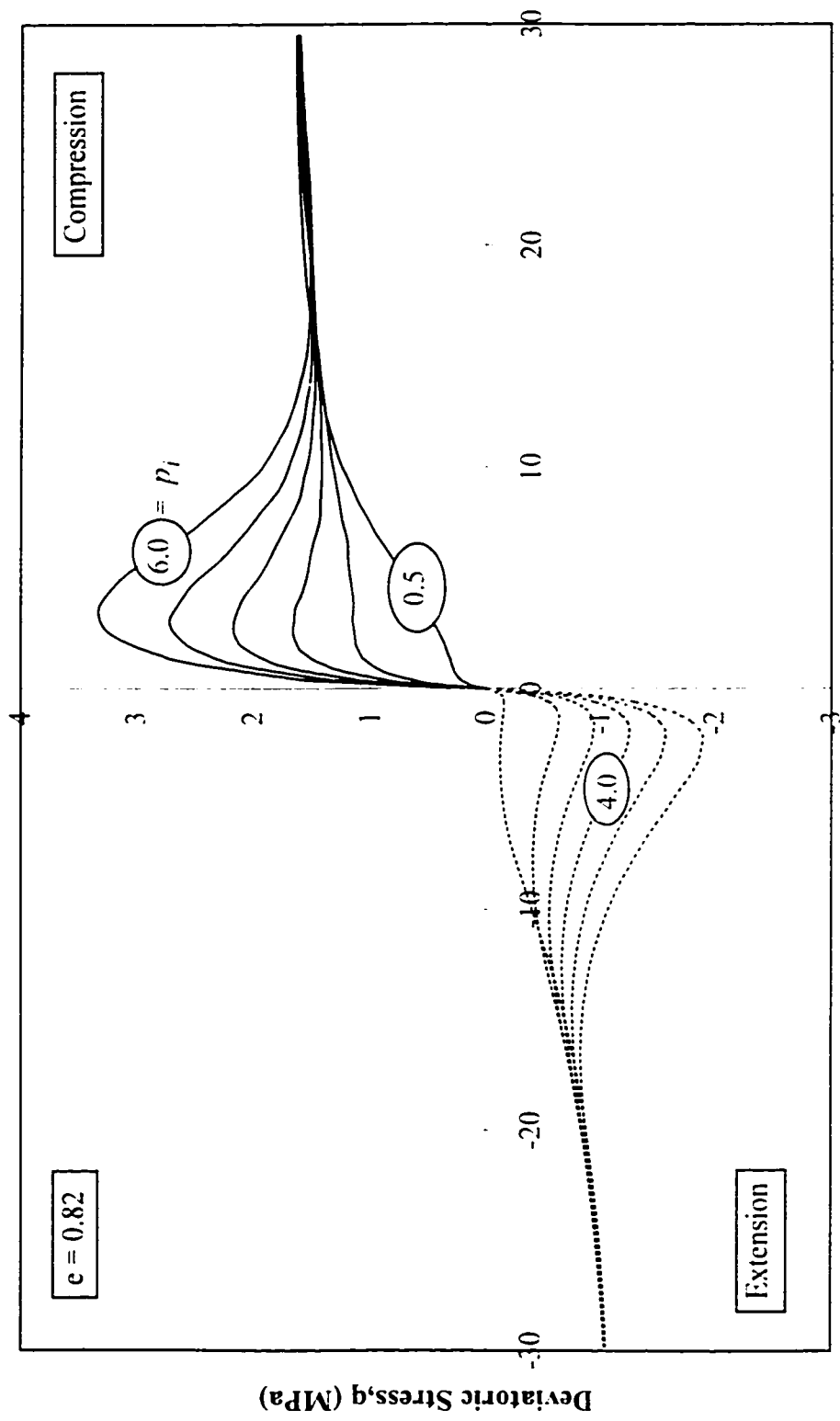
Figure 4.6. (cont.) Effect of mean effective stress on model prediction for undrained behavior of sands in triaxial compression and extension (Stress - strain curves).
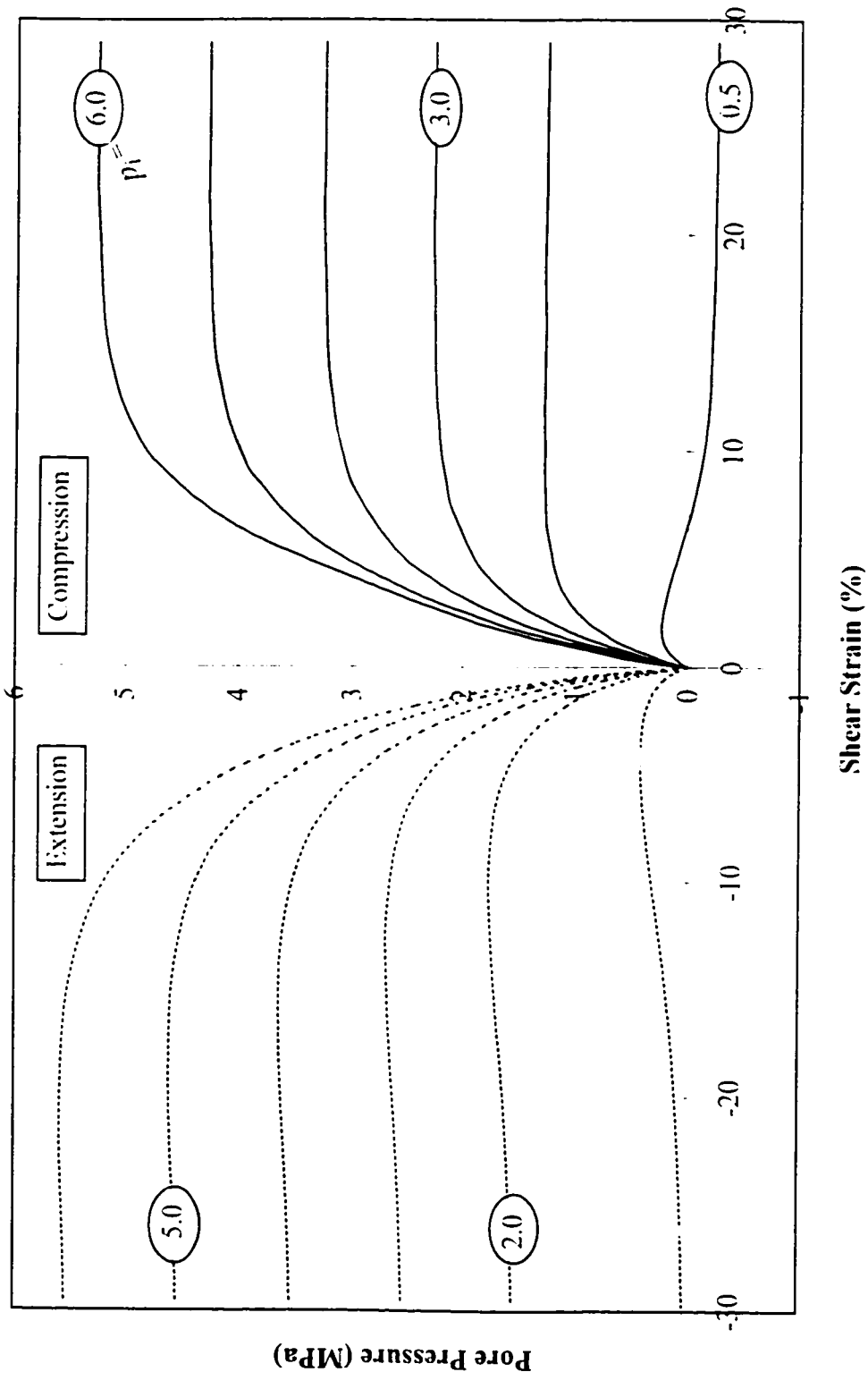
Figure 4.6. (cont.) Effect of mean effective stress on model prediction for undrained behavior of sands in triaxial compression and extension (Pore pressure-strain curves).
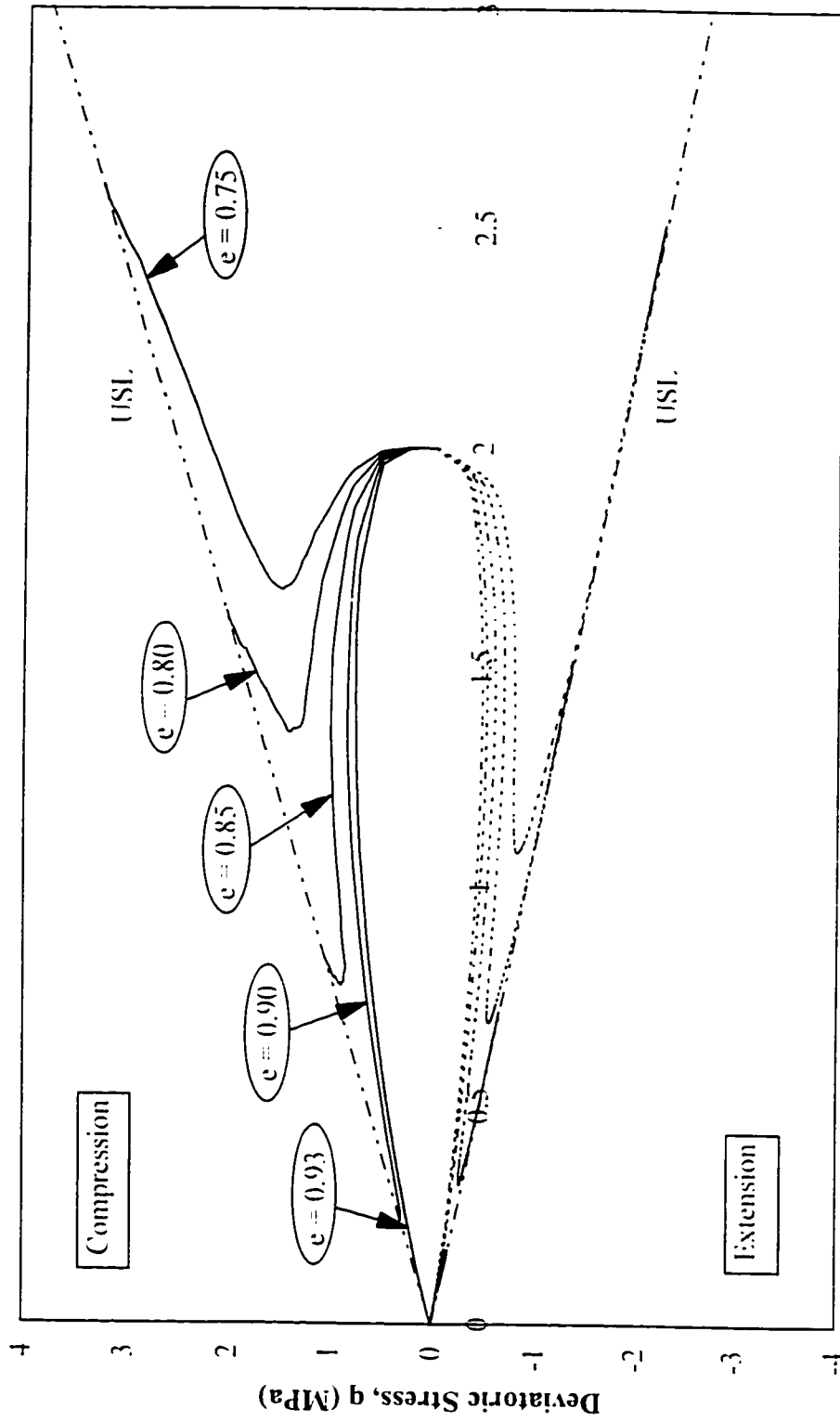
Figure 4.7. Effect of void ratio on model prediction for undrained behavior of sands in triaxial compression and extension (Effective stress paths).
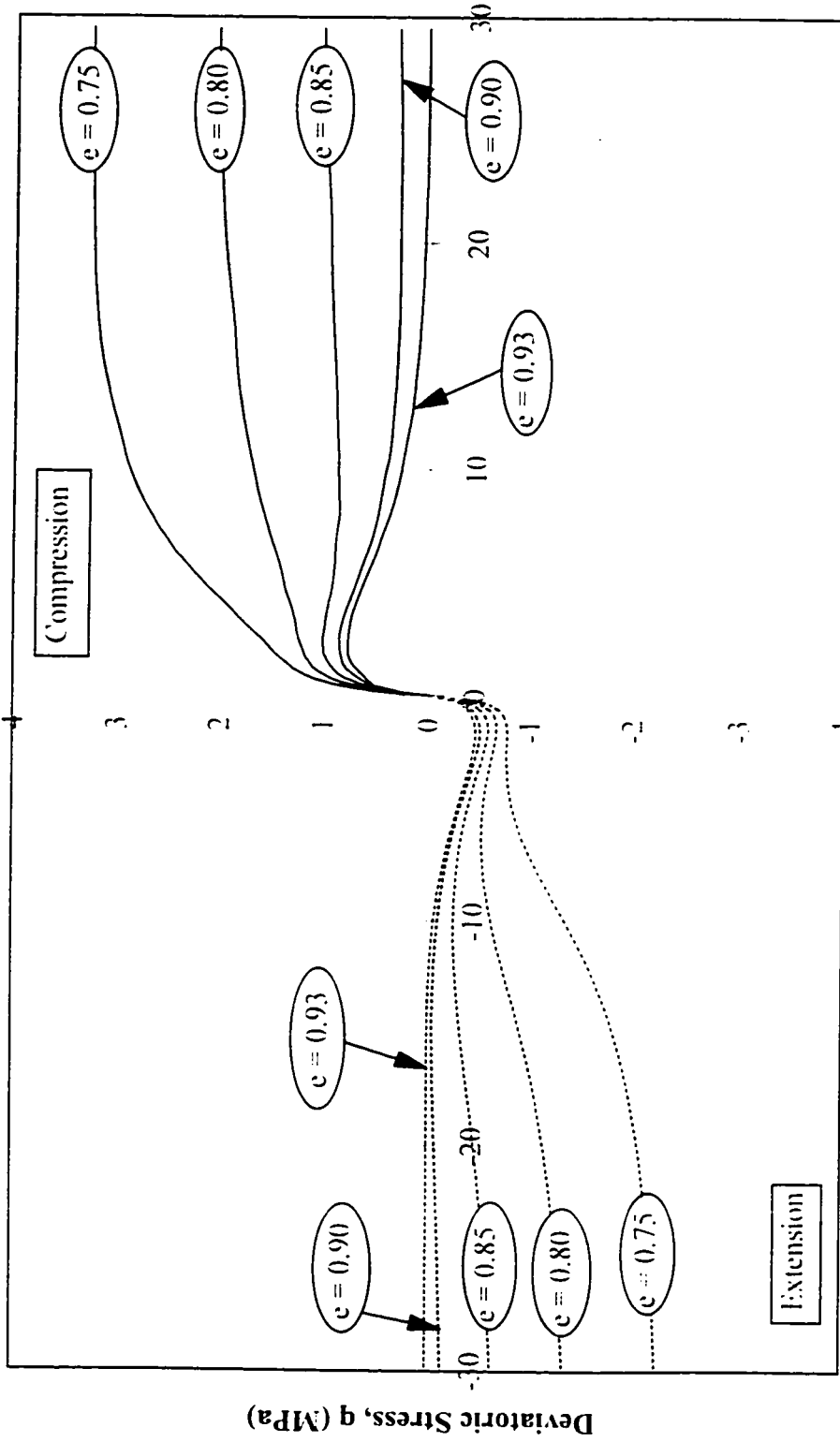
Figure 4.7. (cont.) Effect of void ratio on model prediction for undrained behavior of sands in triaxial compression and extension (Stress-strain curves).
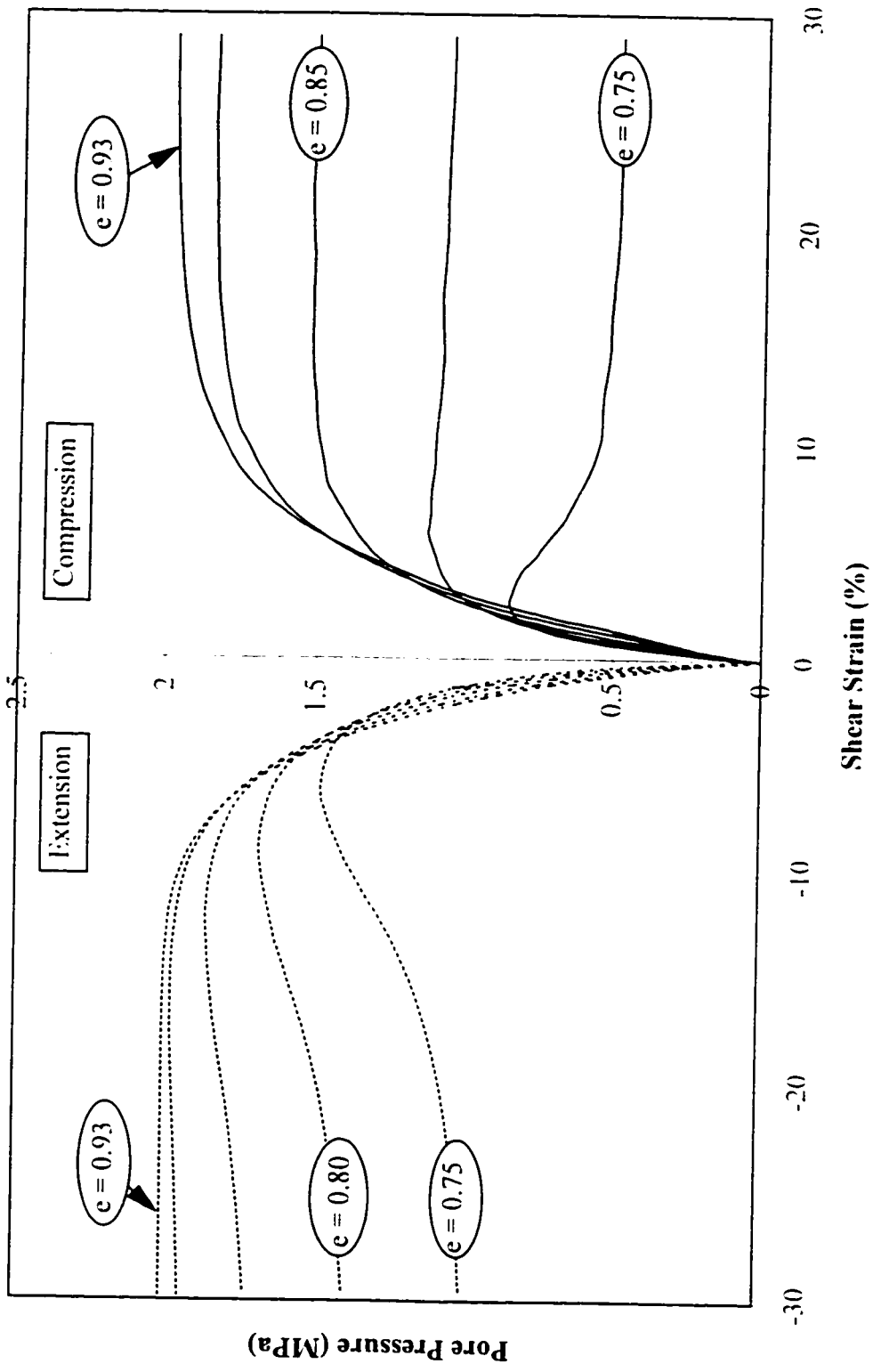
Figure 4.7. (cont.) Effect of void ratio on model prediction for undrained behavior of sands in triaxial compression and extension (Pore pressure-strain curves).
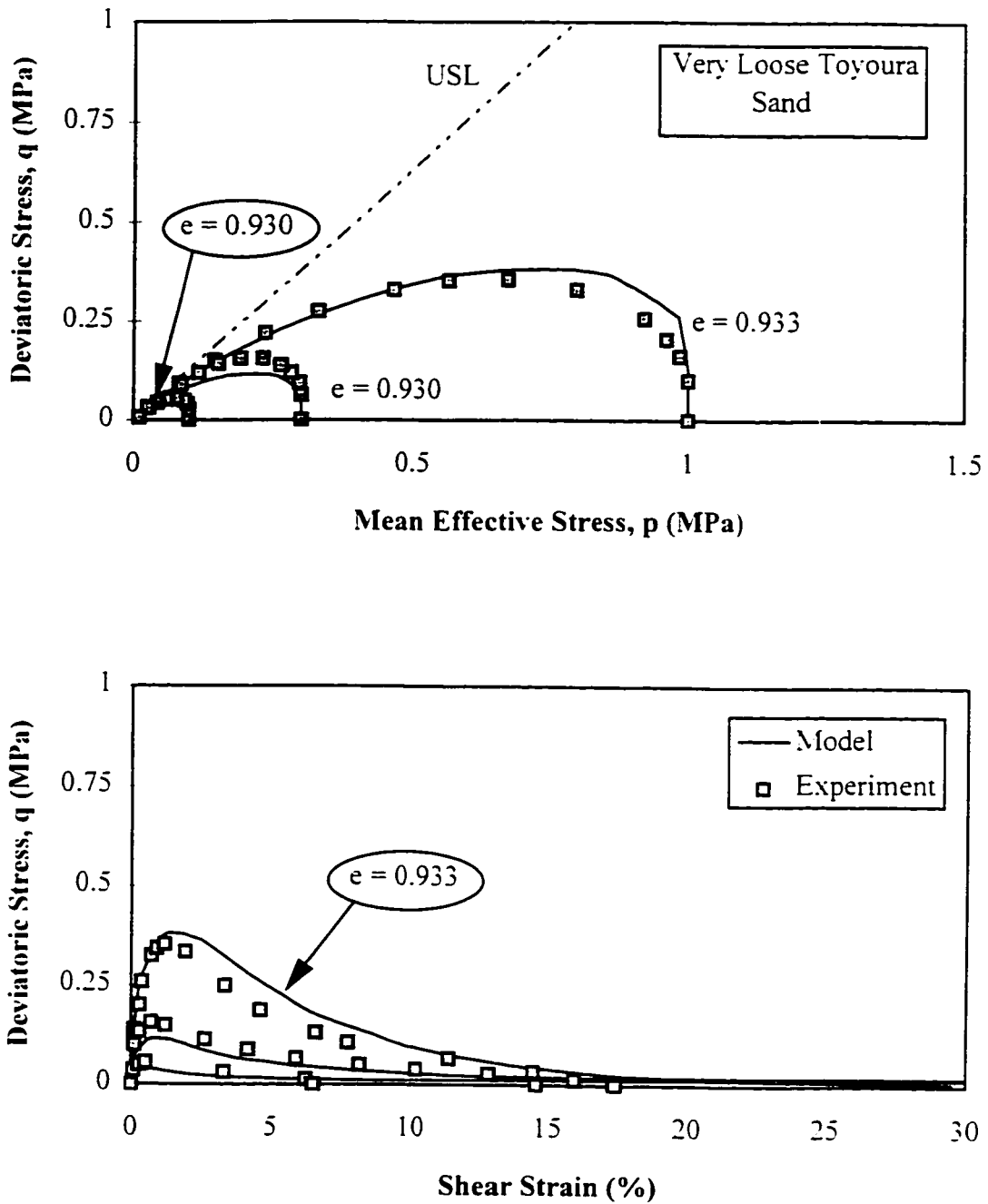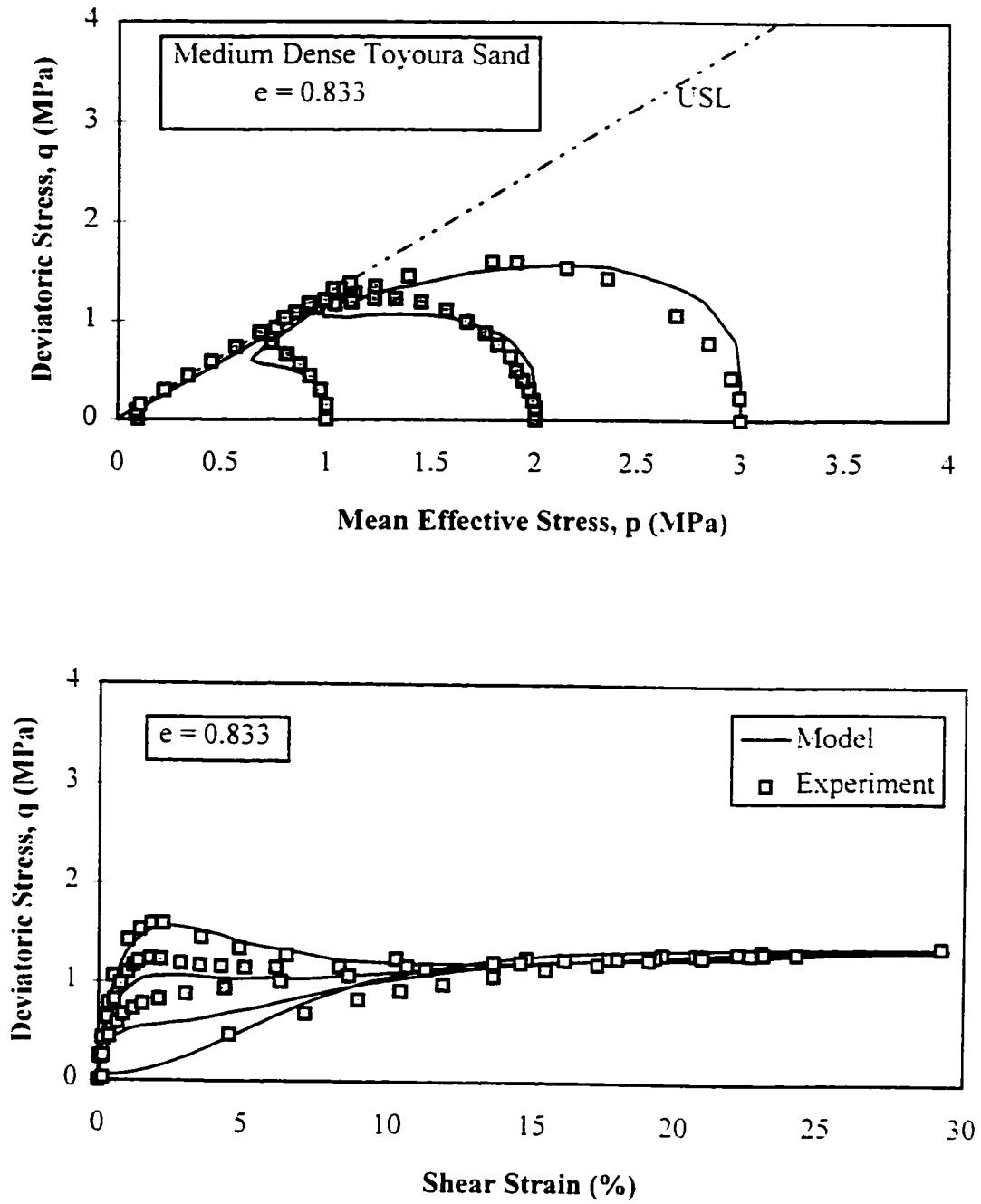
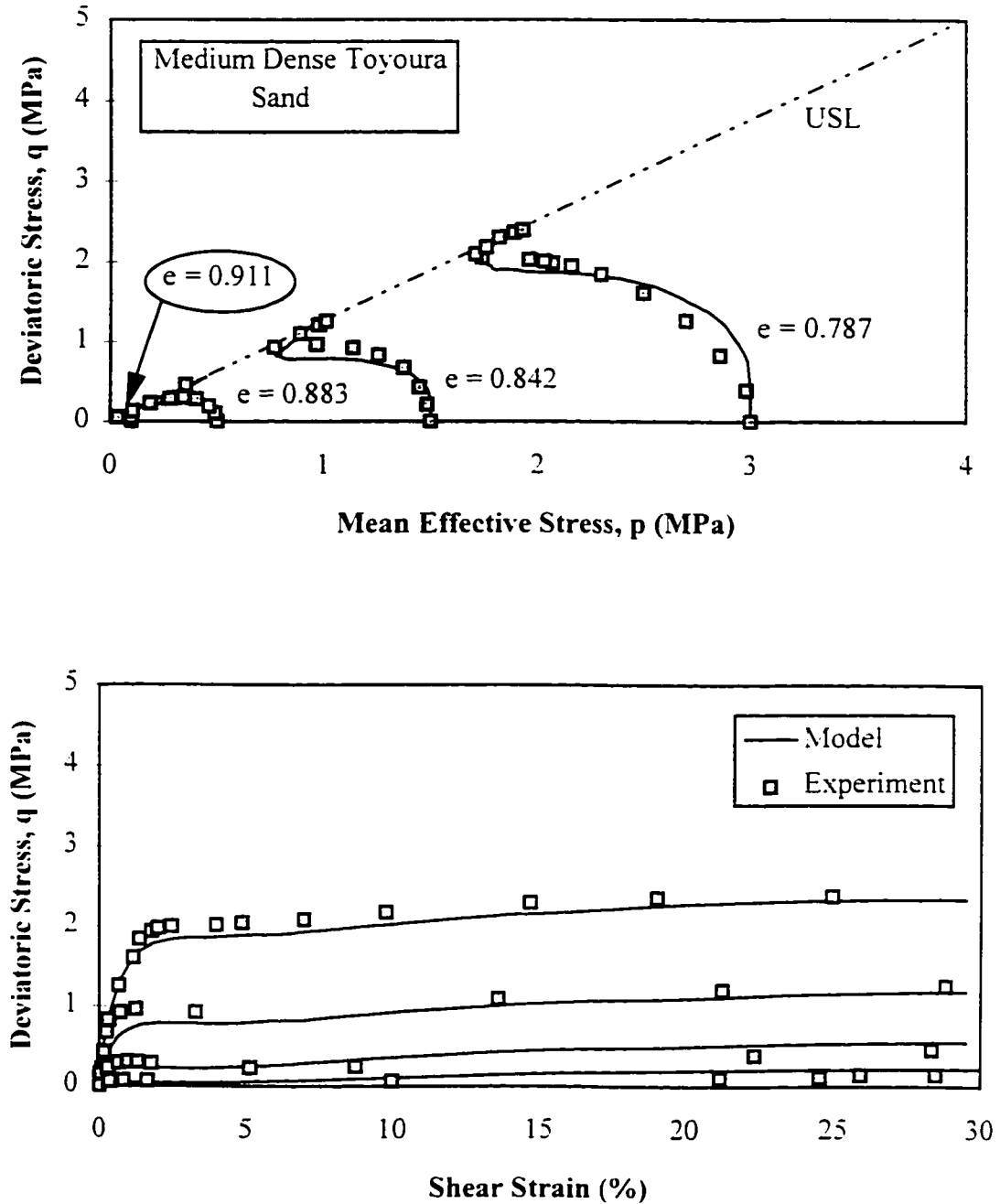**Figure 4.8.** Evaluation of model predictions for undrained triaxial compression tests on very loose specimens of Toyoura sand.
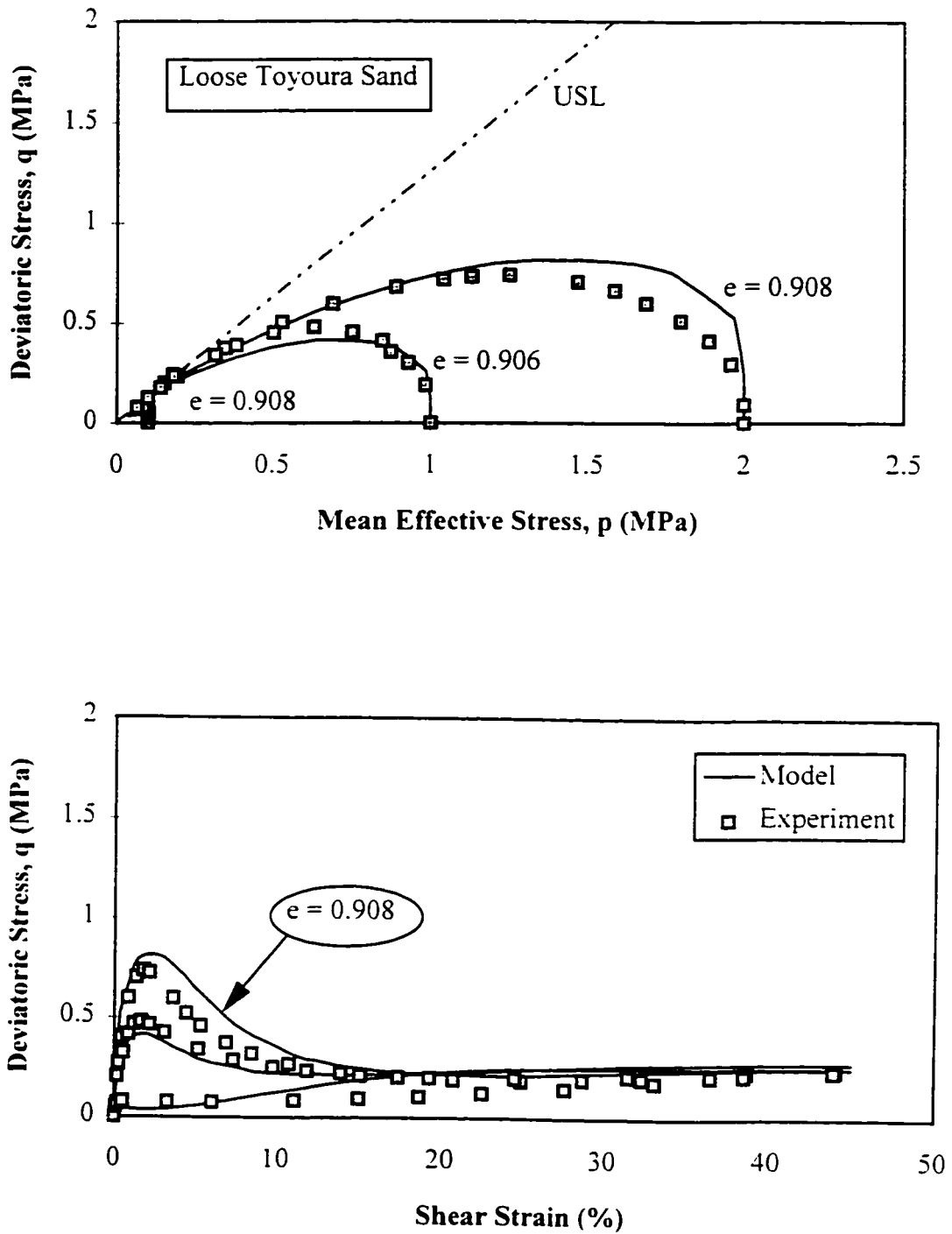
Figure 4.9. Evaluation of model prediction for undrained triaxial compression test on loose specimen of Toyoura sand (a).
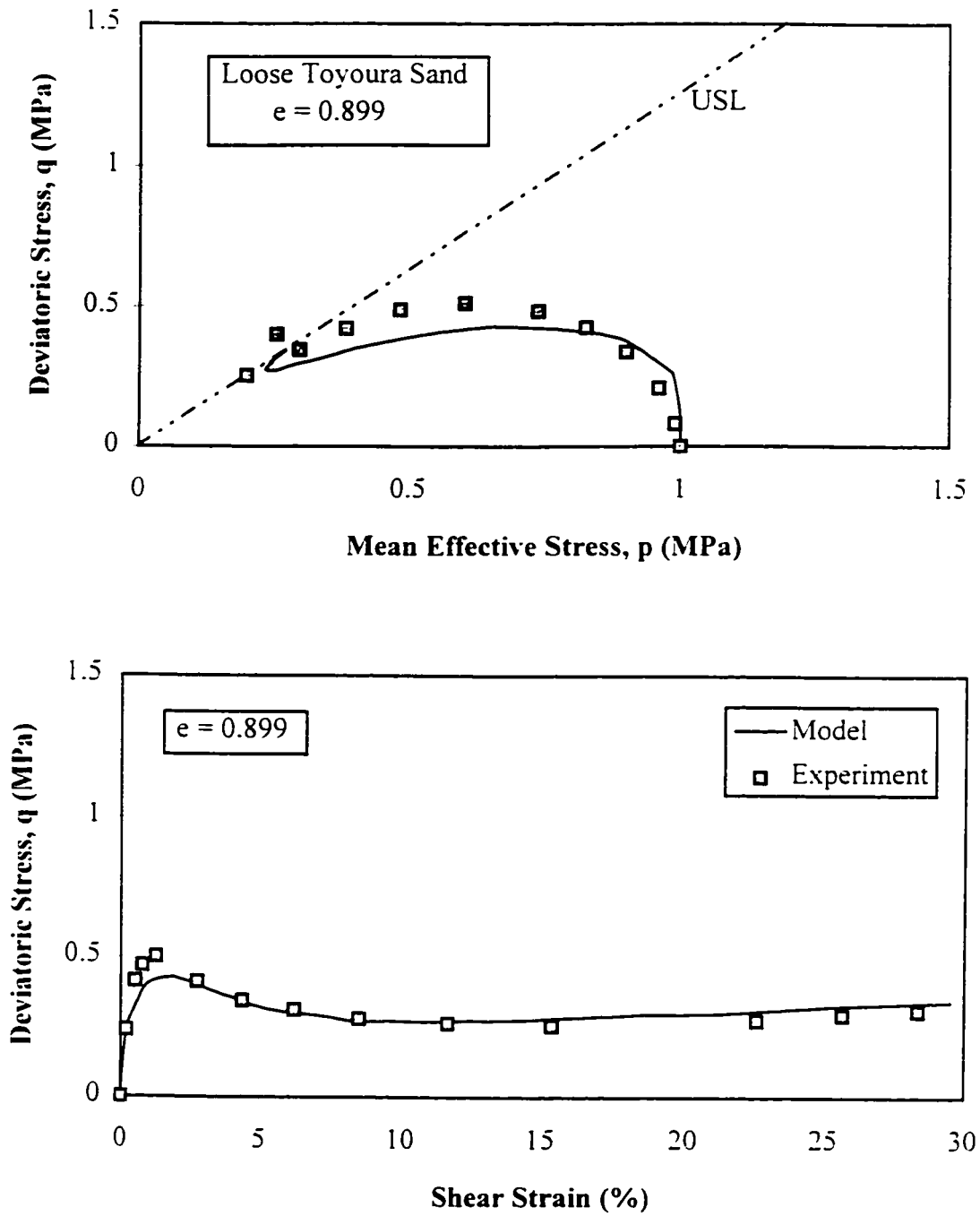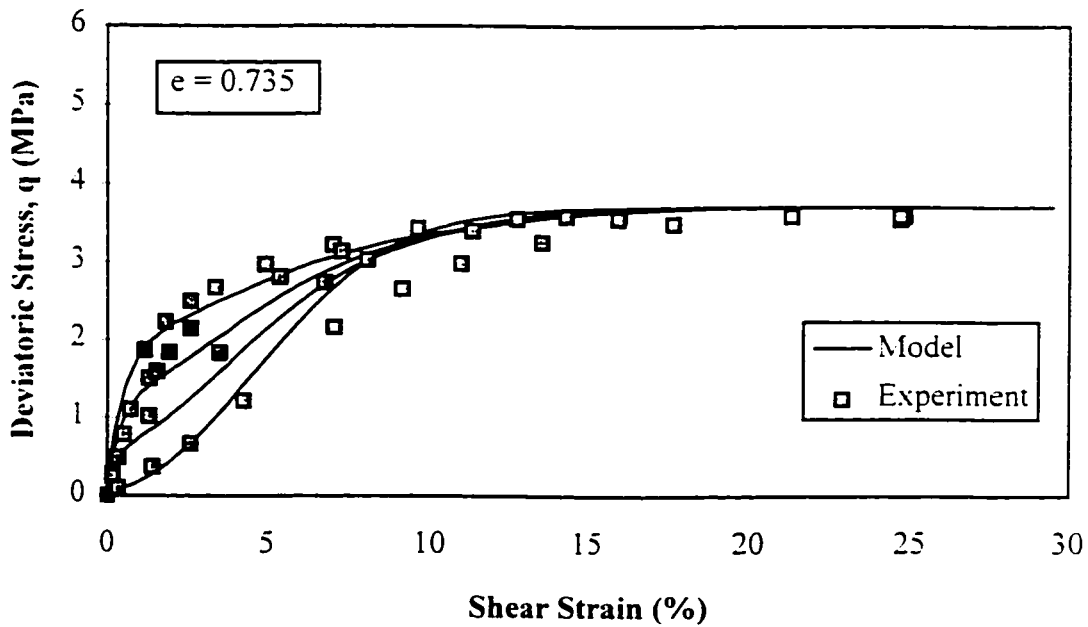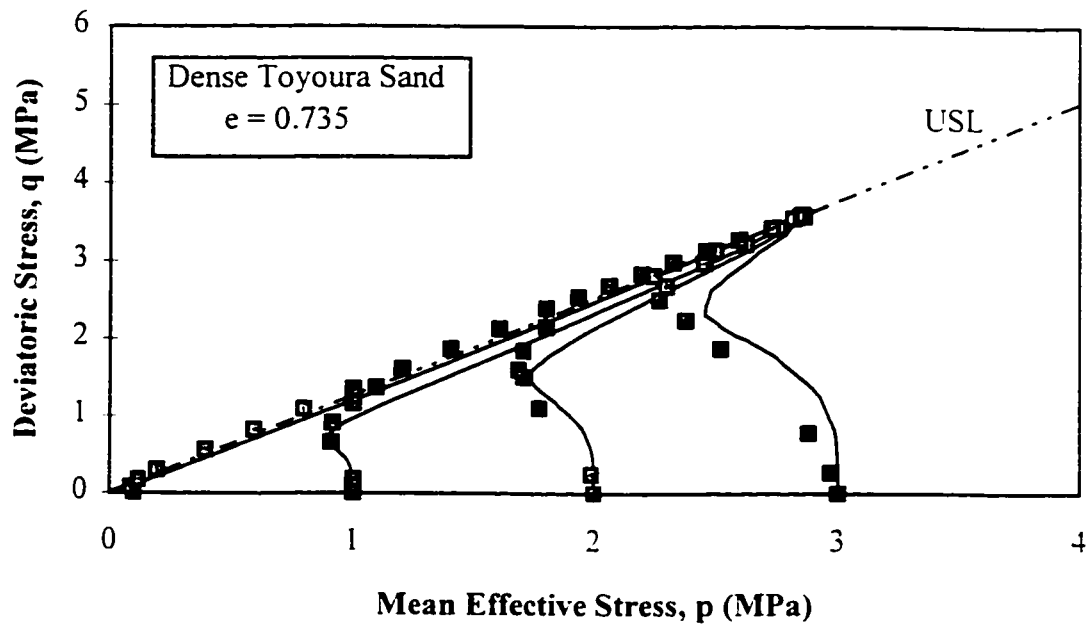
**Figure 4.10.** Evaluation of model prediction for undrained triaxial compression test on loose specimen of Toyoura sand (b).
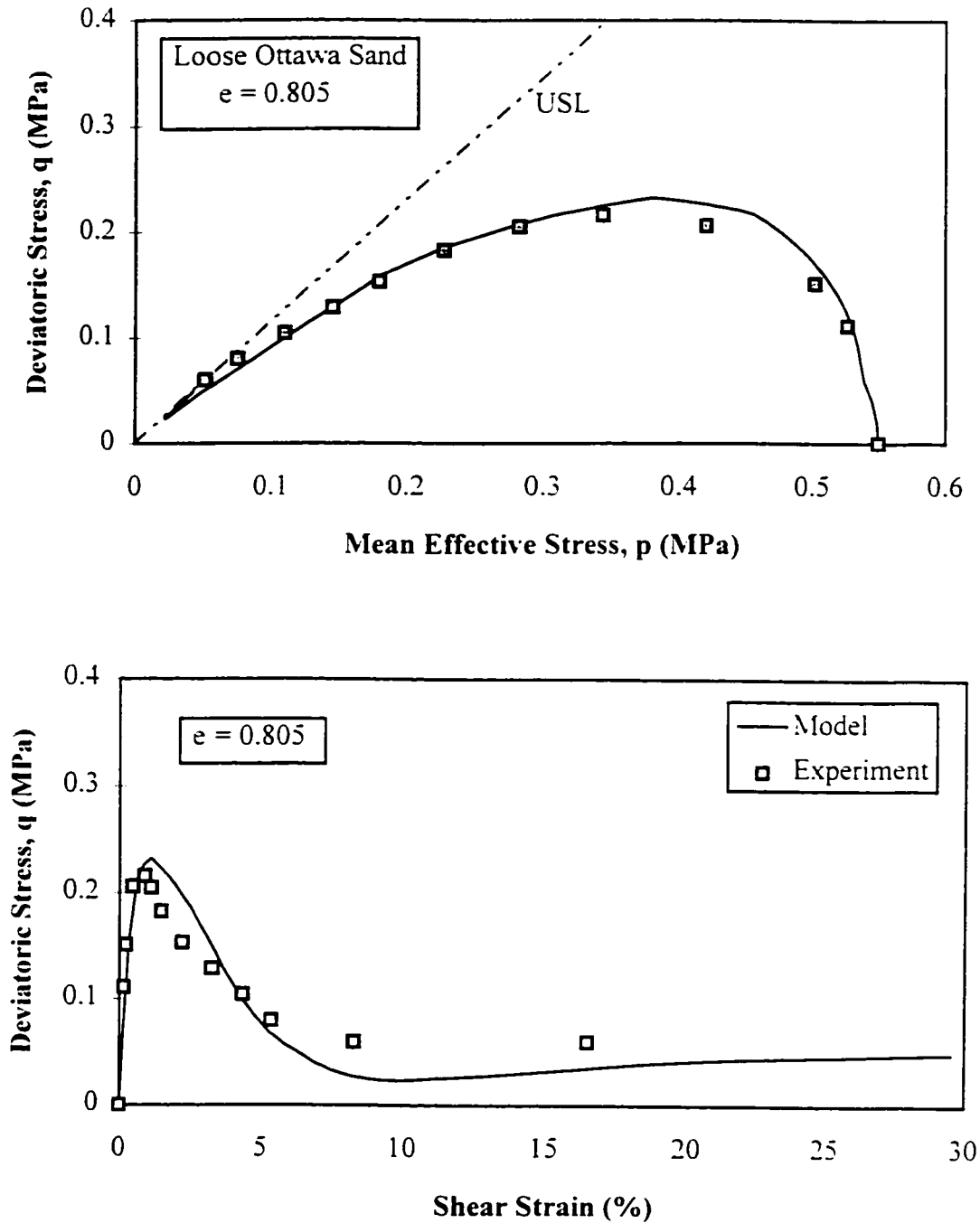
Figure 4.11. Evaluation of model prediction for undrained triaxial compression test on loose specimen of Ottawa sand (a).
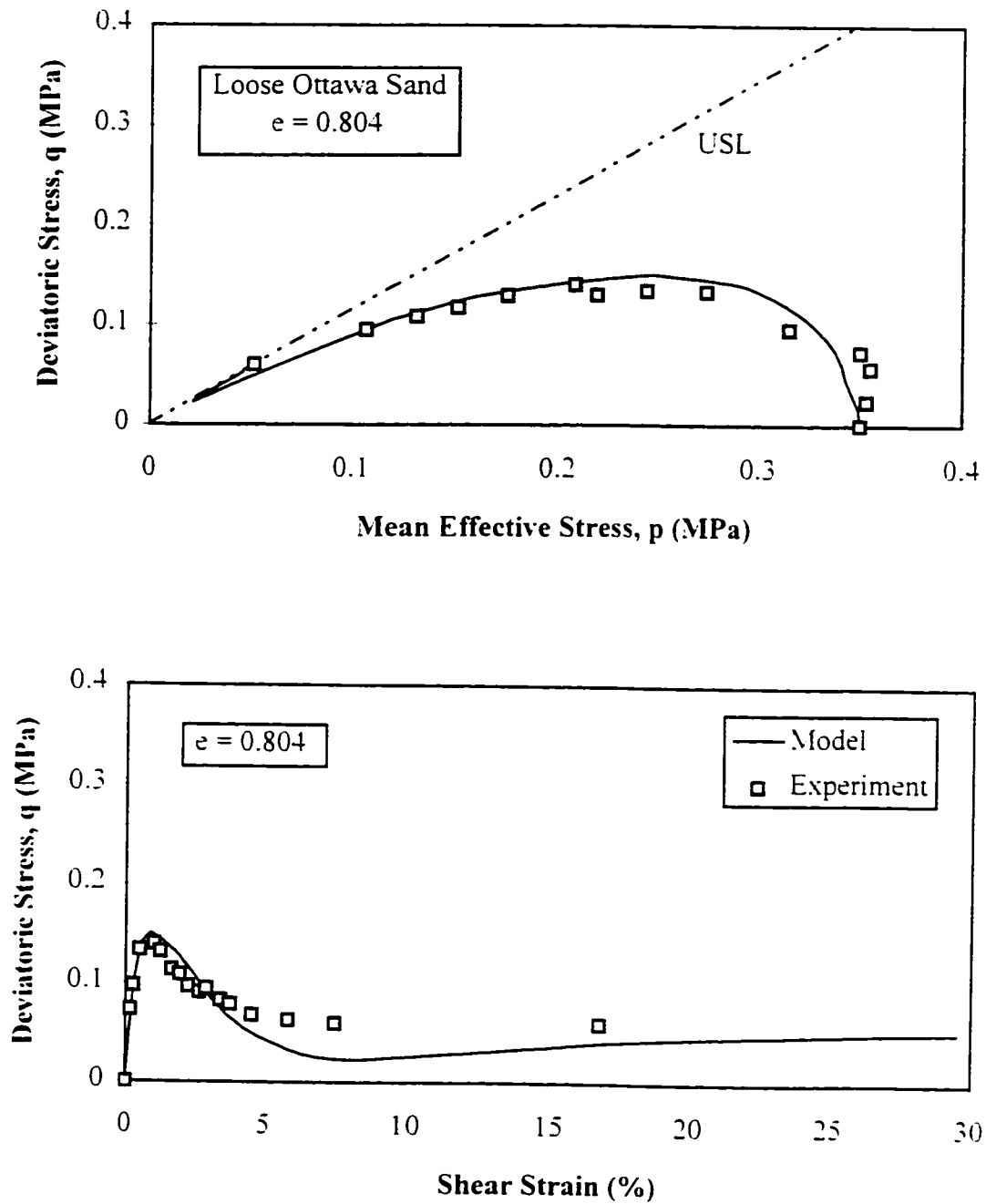
Figure 4.12. Evaluation of model prediction for undrained triaxial compression test on loose specimen of Ottawa sand (b).
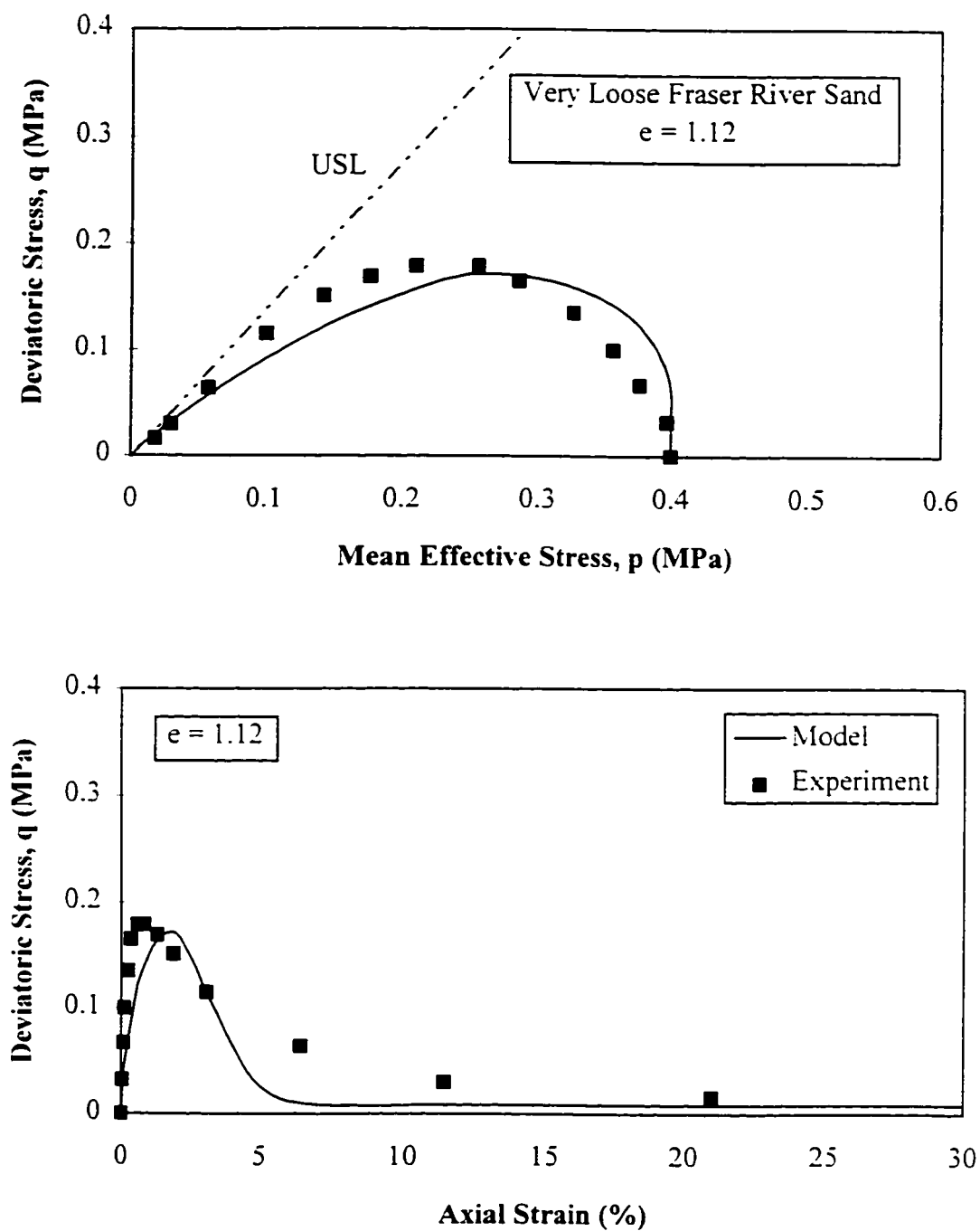
Figure 4.13. Evaluation of model prediction for undrained triaxial compression test on very loose specimen of Fraser River sand .
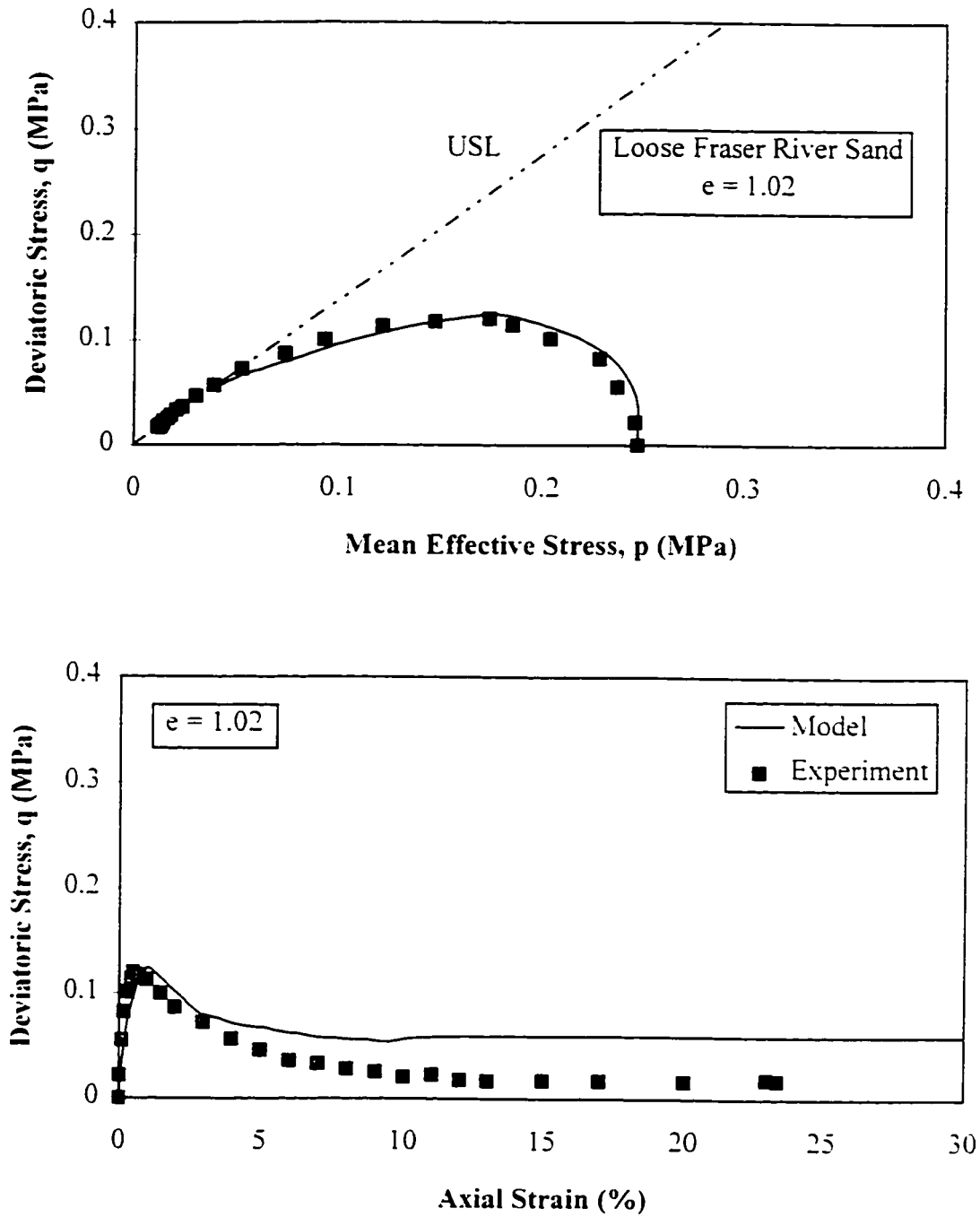
Figure 4.14. Evaluation of model prediction for undrained triaxial compression
test on loose specimen of Fraser River sand (a).
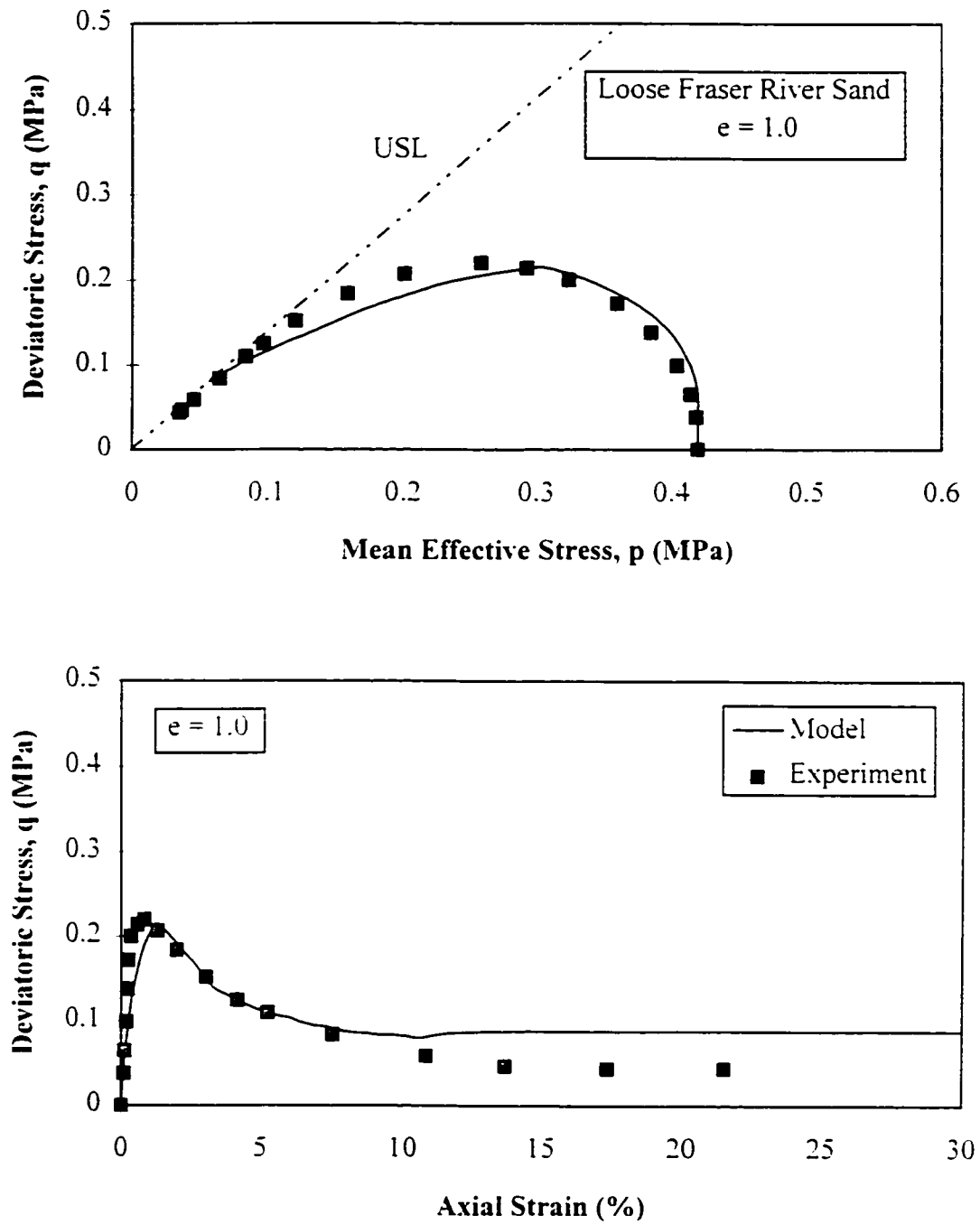
Figure 4.15. Evaluation of model prediction for undrained triaxial compression test on loose specimen of Fraser River sand (b).

Figure 4.16. Evaluation of model predictions for undrained triaxial compression tests on medium dense specimens of Toyoura sand (a).

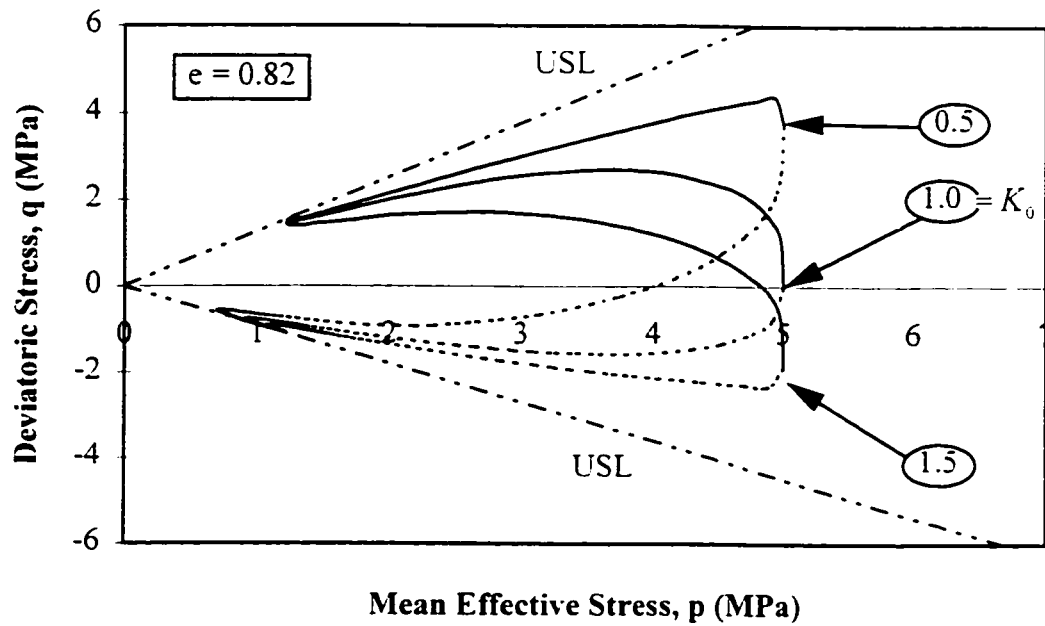**Figure 4.17.** Evaluation of model predictions for undrained triaxial compression tests on medium dense specimens of Toyoura sand (b).

Figure 4.18. Evaluation of model predictions for undrained triaxial compression tests on dense specimens of Toyoura sand.
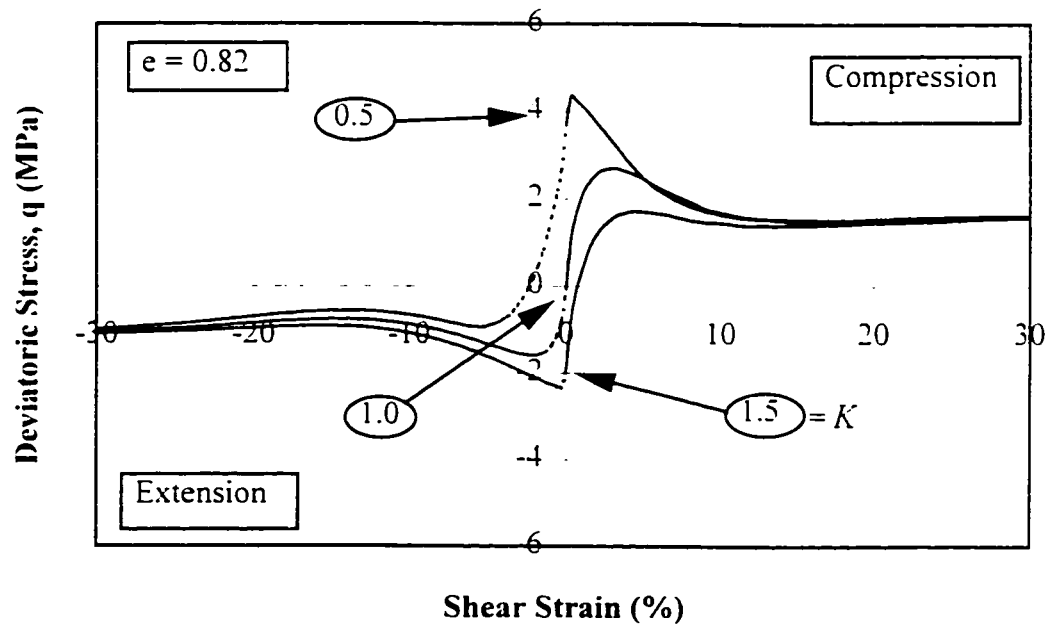
Figure 4.19. Effect of consolidation stress history on the undrained triaxial compression and extension behavior of loose sand (Effective stress paths and stress-strain curves).
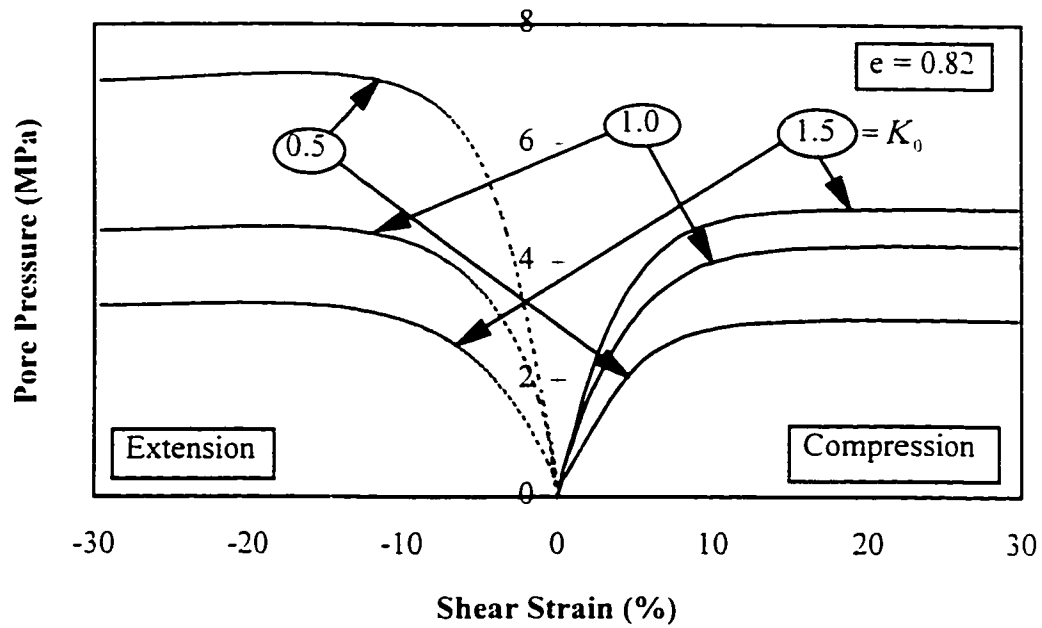
Figure 4.19. (cont.) Effect of consolidation history on the undrained triaxial compression and extension behavior of loose sand (Pore pressure-strain curves).
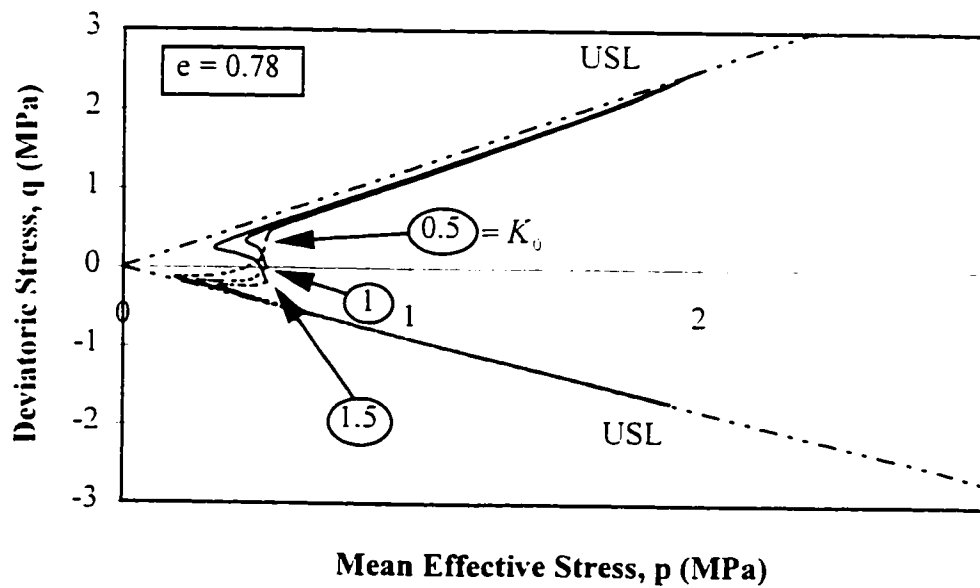

Figure 4.20. Effect of consolidation stress history on the undrained triaxial compression and extension behavior of dense sand (Effective stress paths).
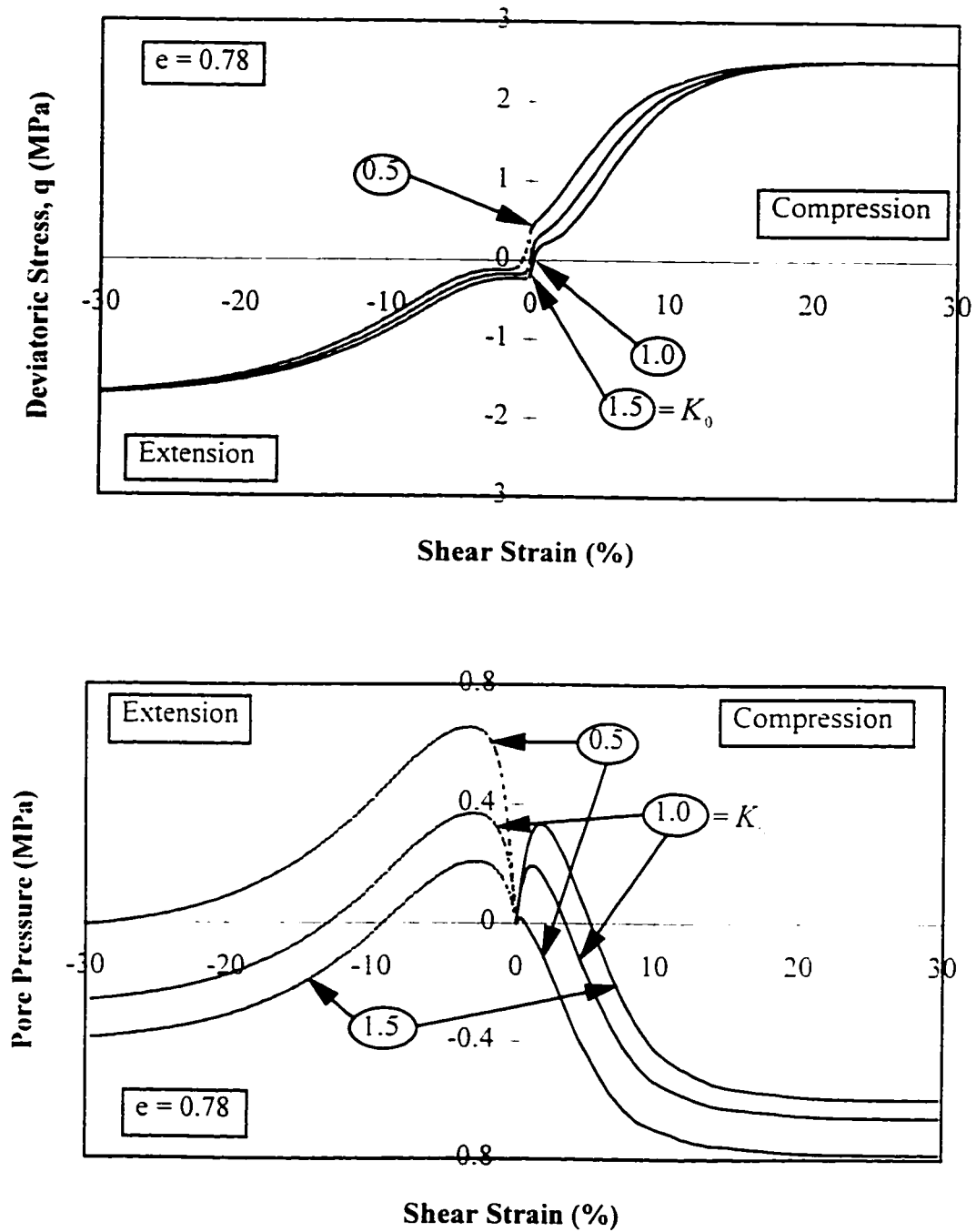
Figure 4.20. (cont.) Effect of consolidation stress history on the undrained triaxial compression and extension behavior of dense sand (Stress-strain and pore pressure-strain curves).
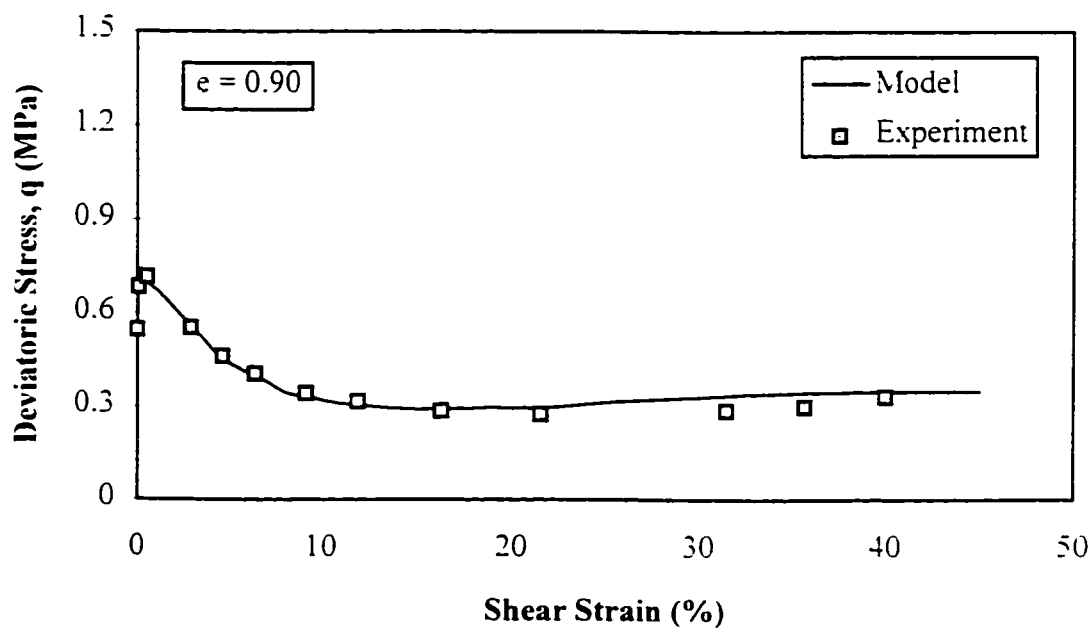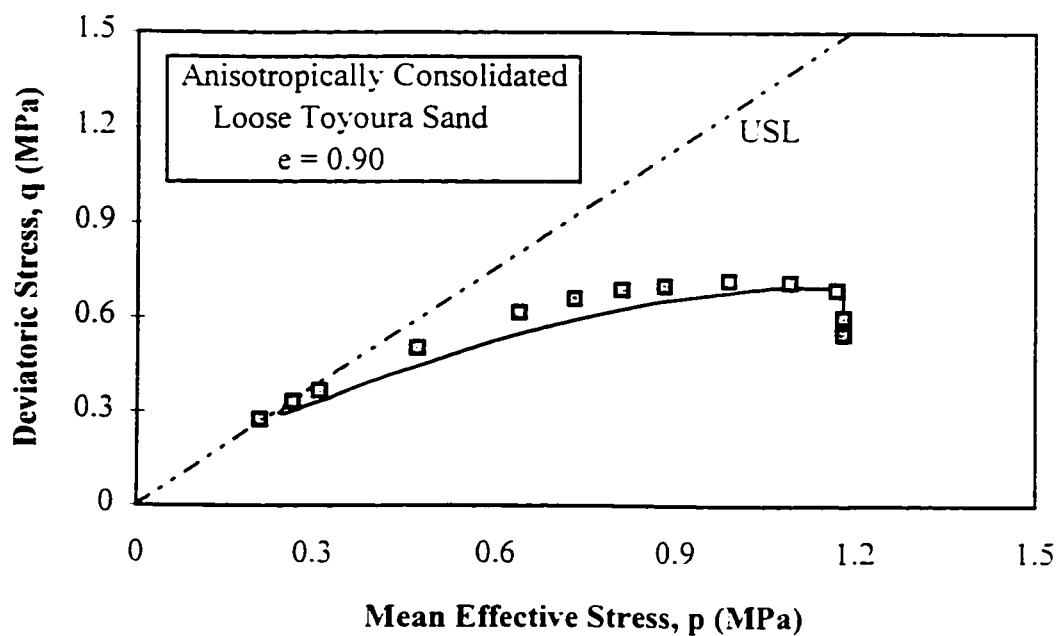
Figure 4.21. Evaluation of model prediction for anisotropically consolidated loose Toyoura sand (a).
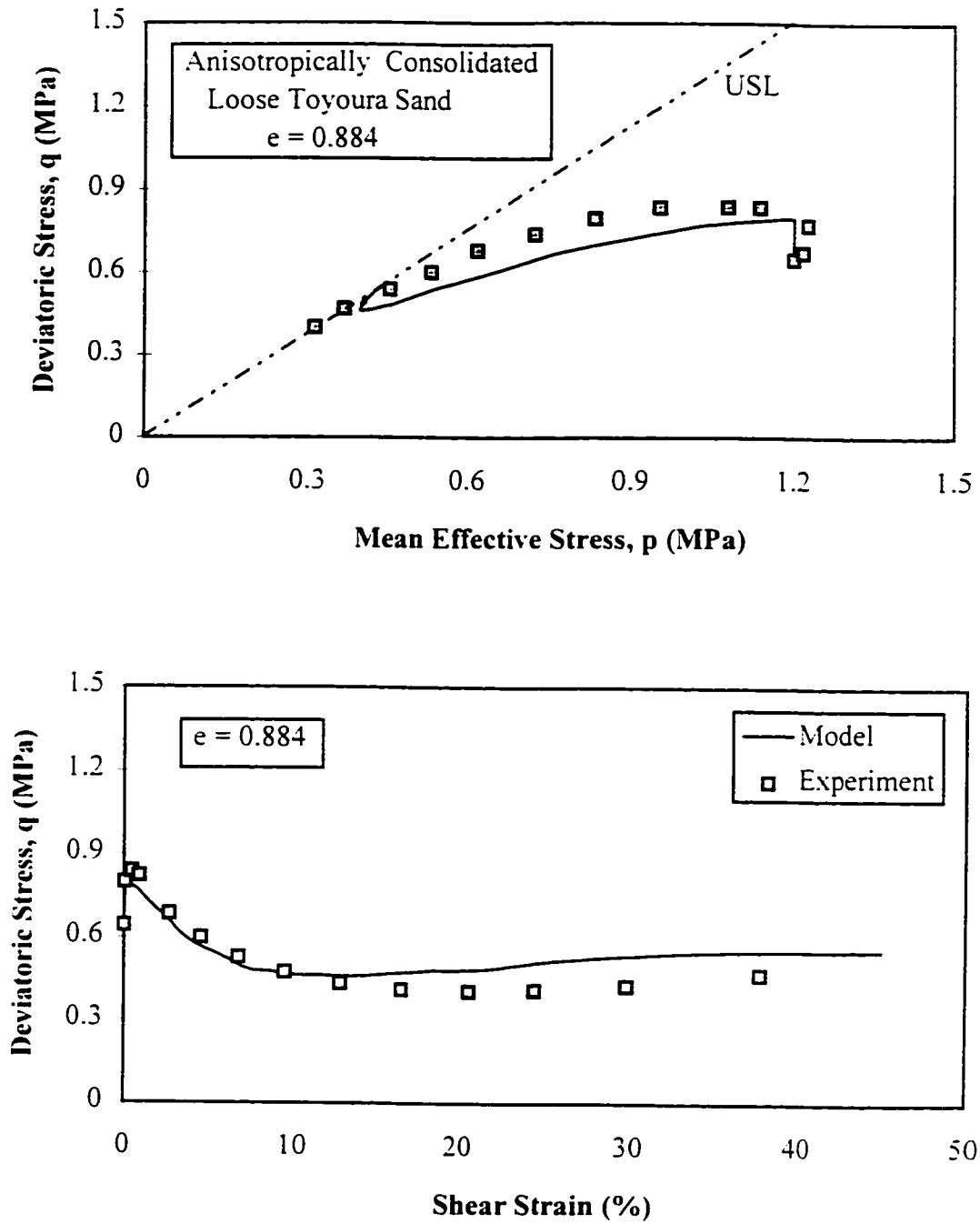
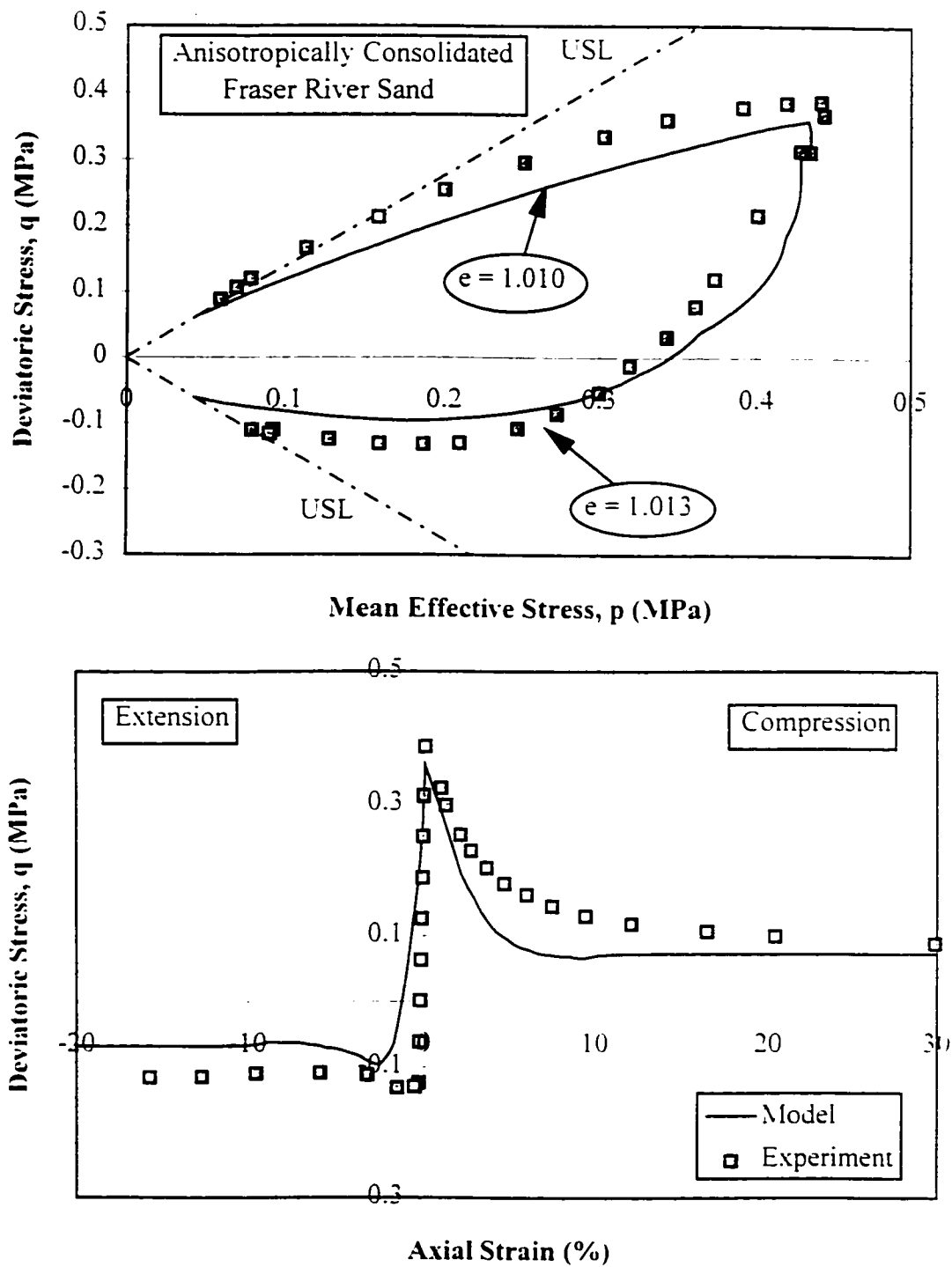**Figure 4.22.** Evaluation of model prediction for anisotropically consolidated loose Toyoura sand (b).

Figure 4.23. Evaluation of model prediction for anisotropically consolidated loose Fraser River sand in compression and extension.
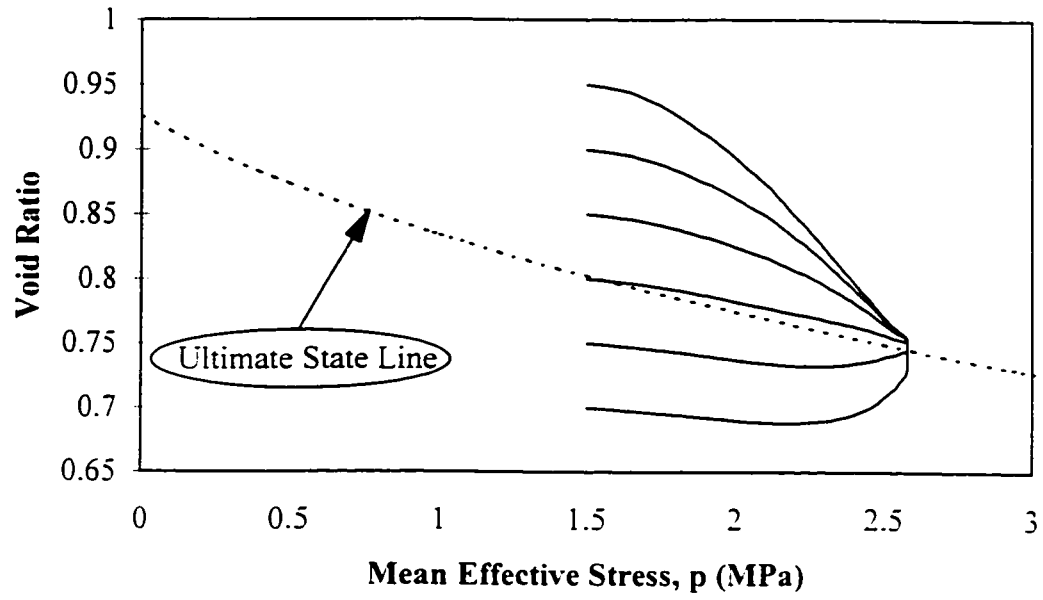
Figure 4.24. Effect of void ratio on model prediction for drained behavior of sands in triaxial compression (Mean effective stress-void ratio curves).

Figure 4.24. (cont.) Effect of void ratio on model prediction for drained behavior of sands in triaxial compression (Stress-strain curves).

Figure 4.24. (cont.) Effect of void ratio on model prediction for drained behavior of sands in triaxial compression (Volumetric strain-axial strain curves).
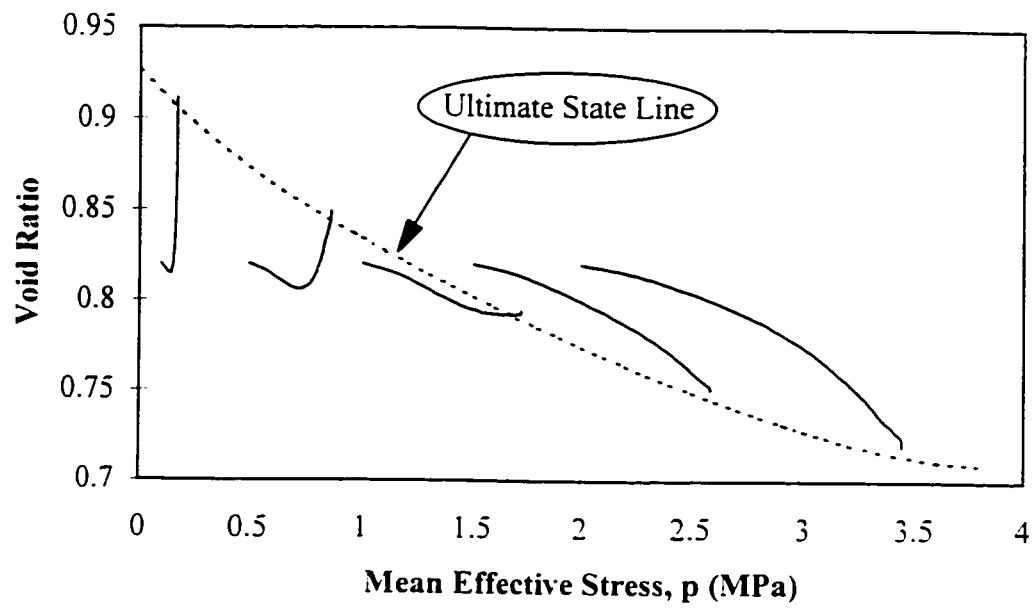
Figure 4.25. Effect of mean effective stress on model prediction for drained behavior of sands in triaxial compression (Mean Effective stress-void ratio curves).
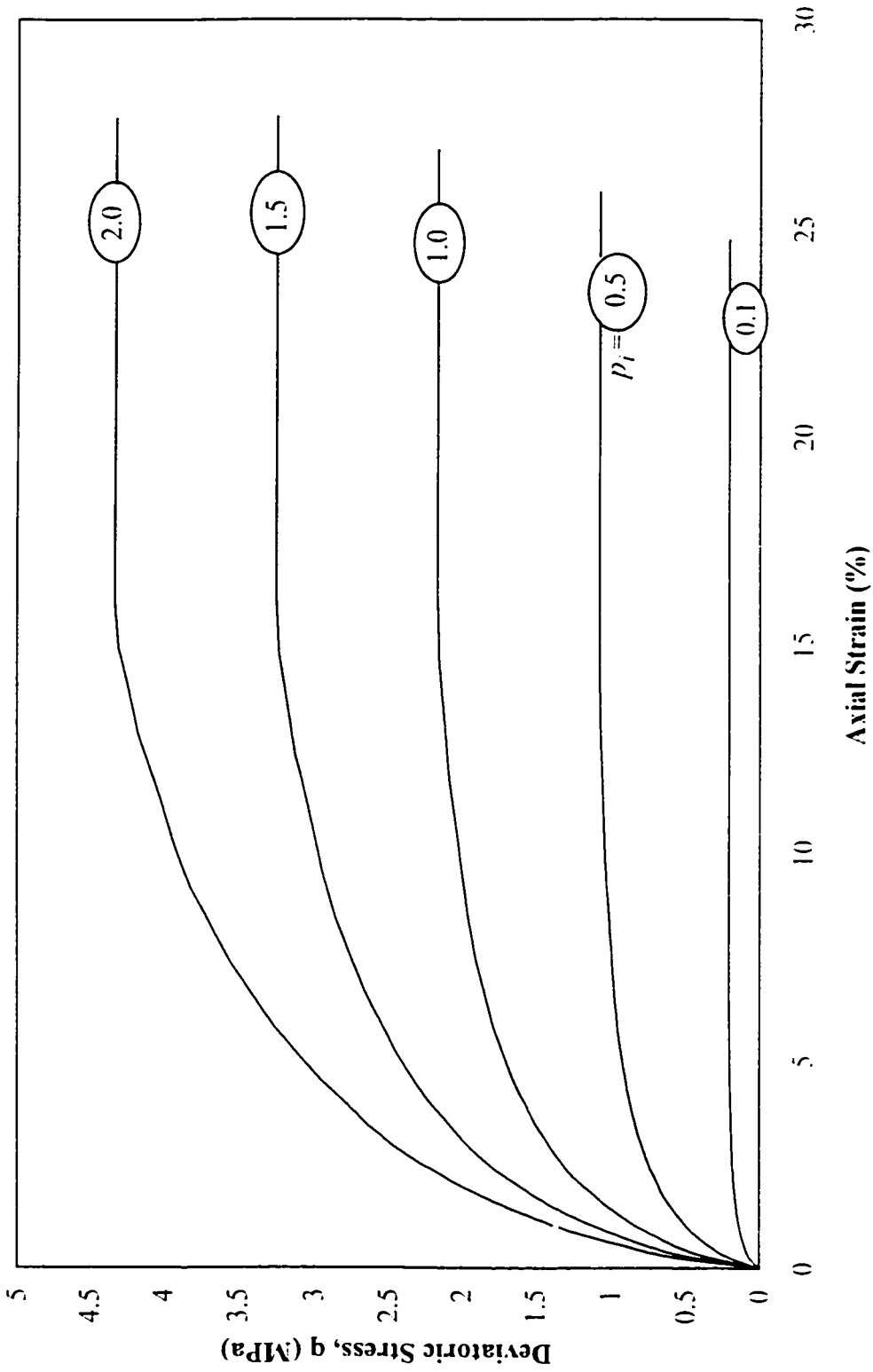
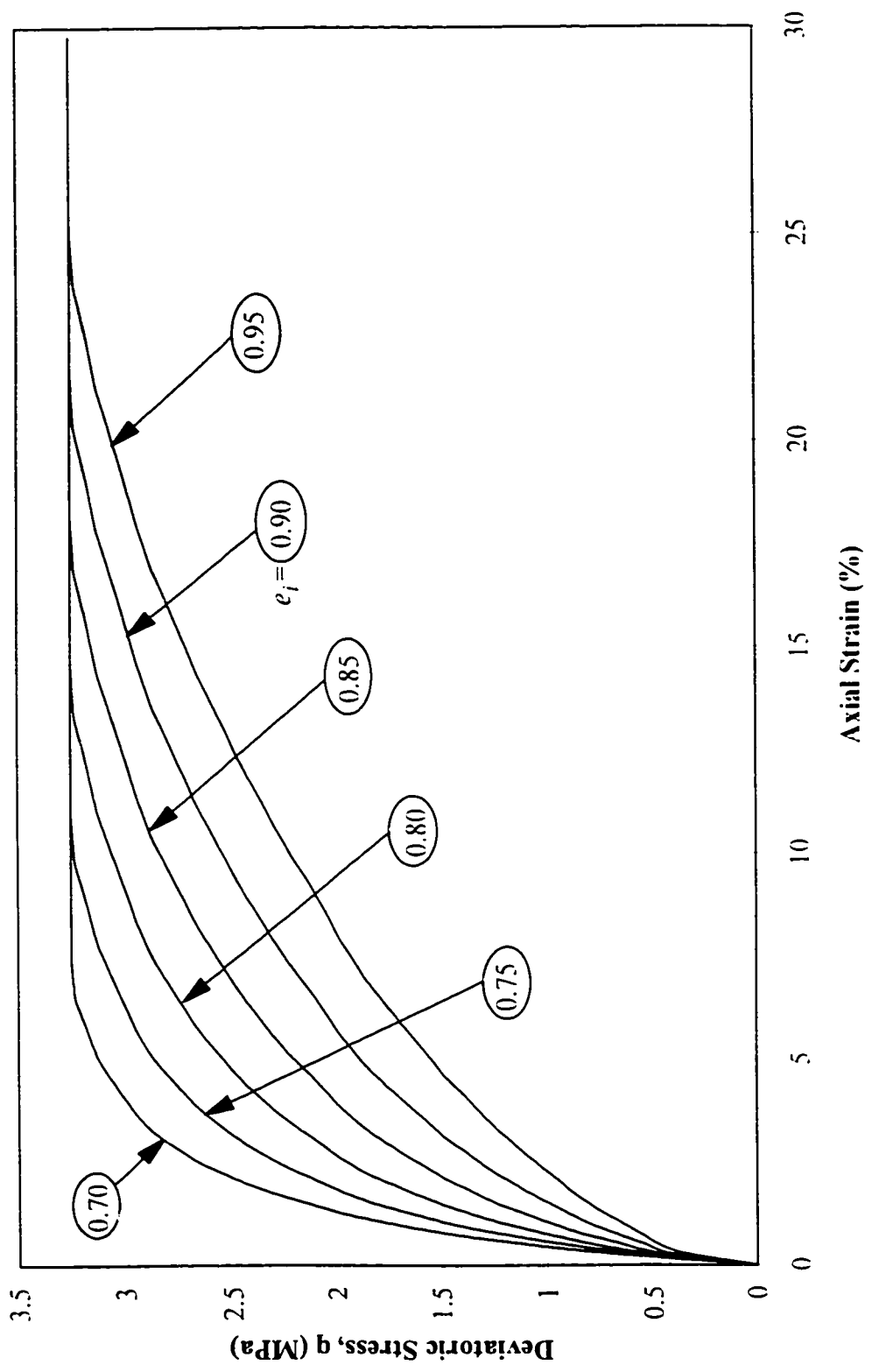**Figure 4.25.** (cont.) Effect of mean effective stress on model prediction for drained behavior of sands in triaxial compression (Stress-strain curves).
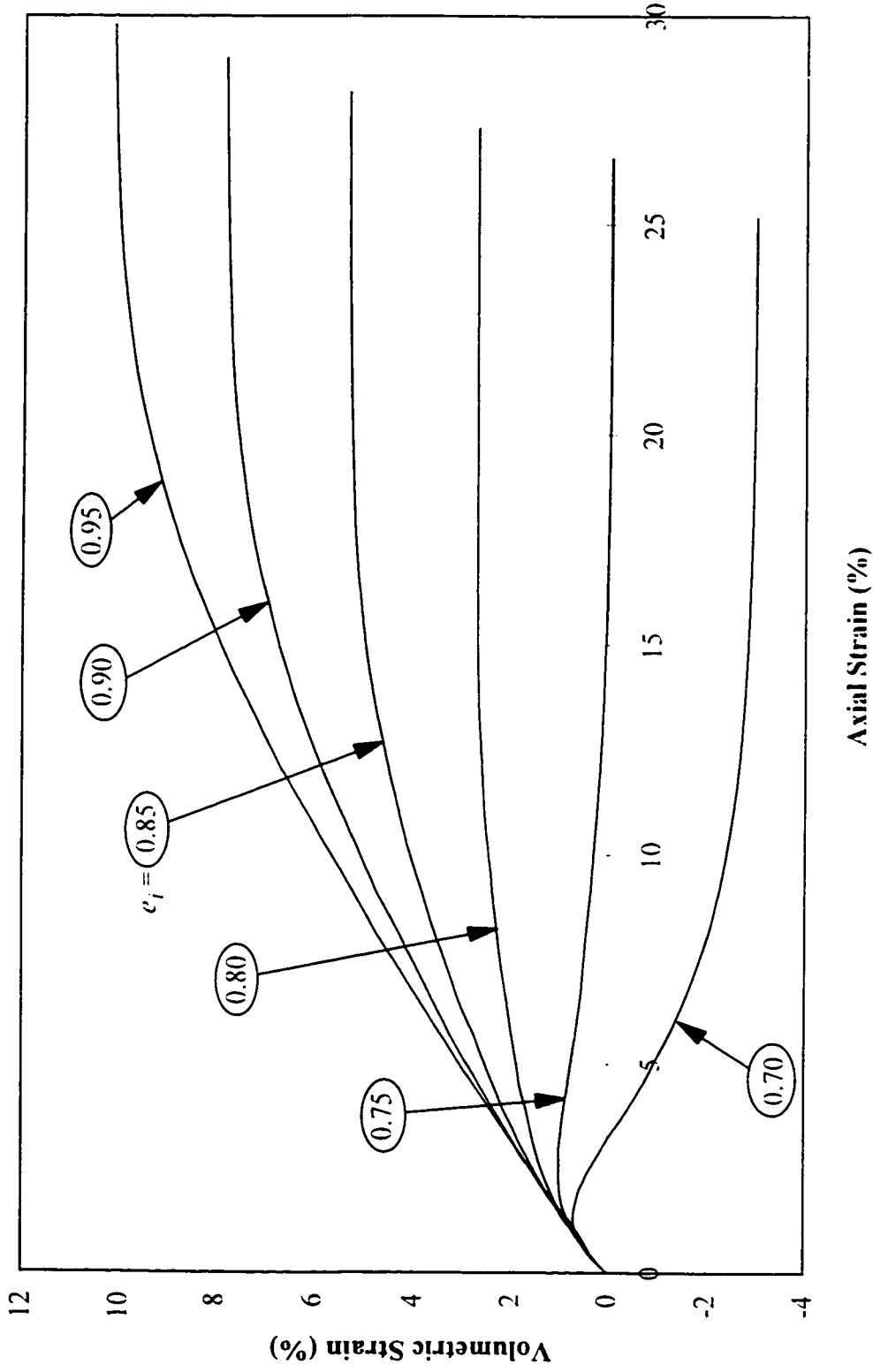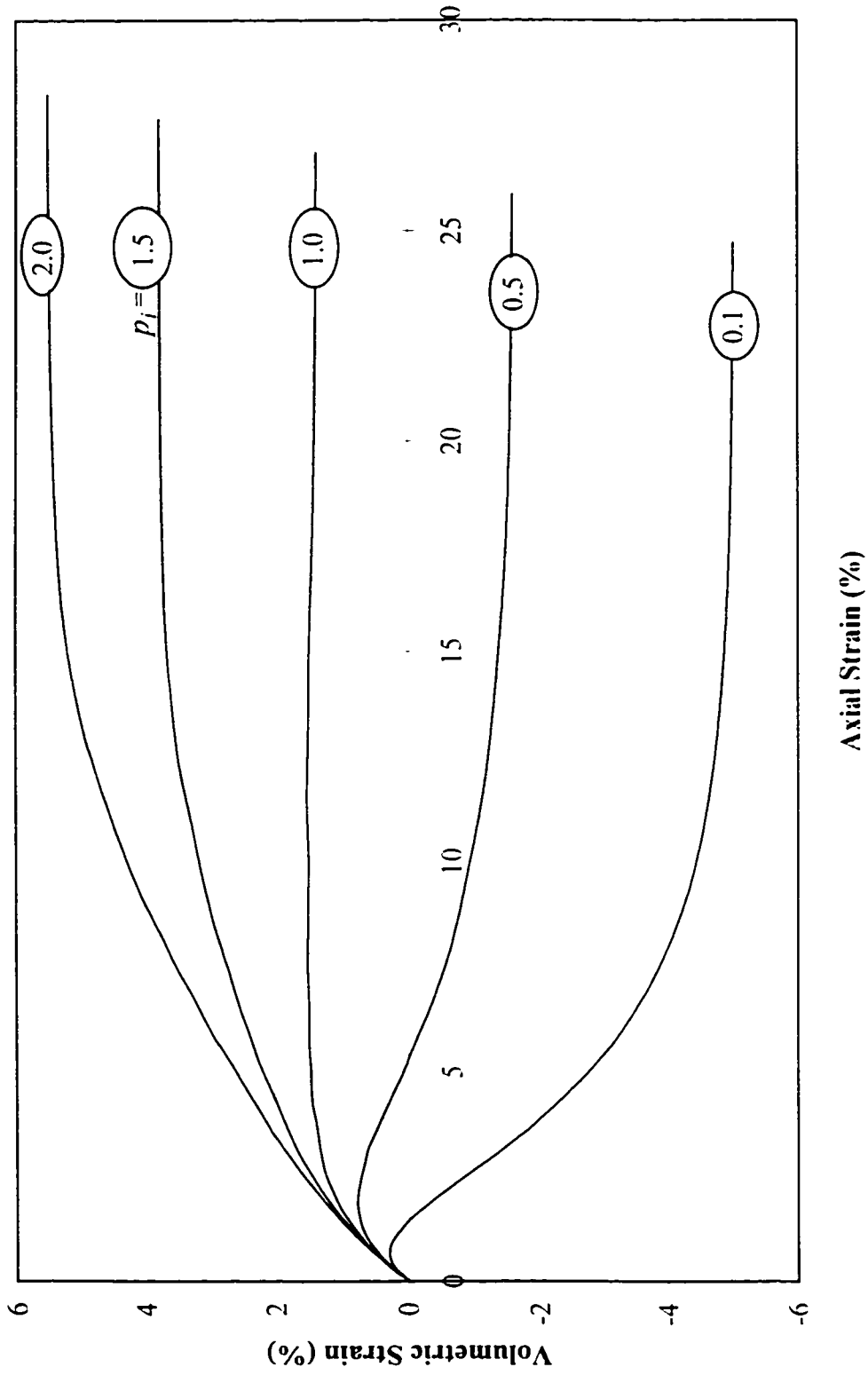
Figure 4.25. (cont.) Effect of mean effective stress on model prediction for drained behavior of sands in triaxial compression (Volumetric strain-axial strain curves).
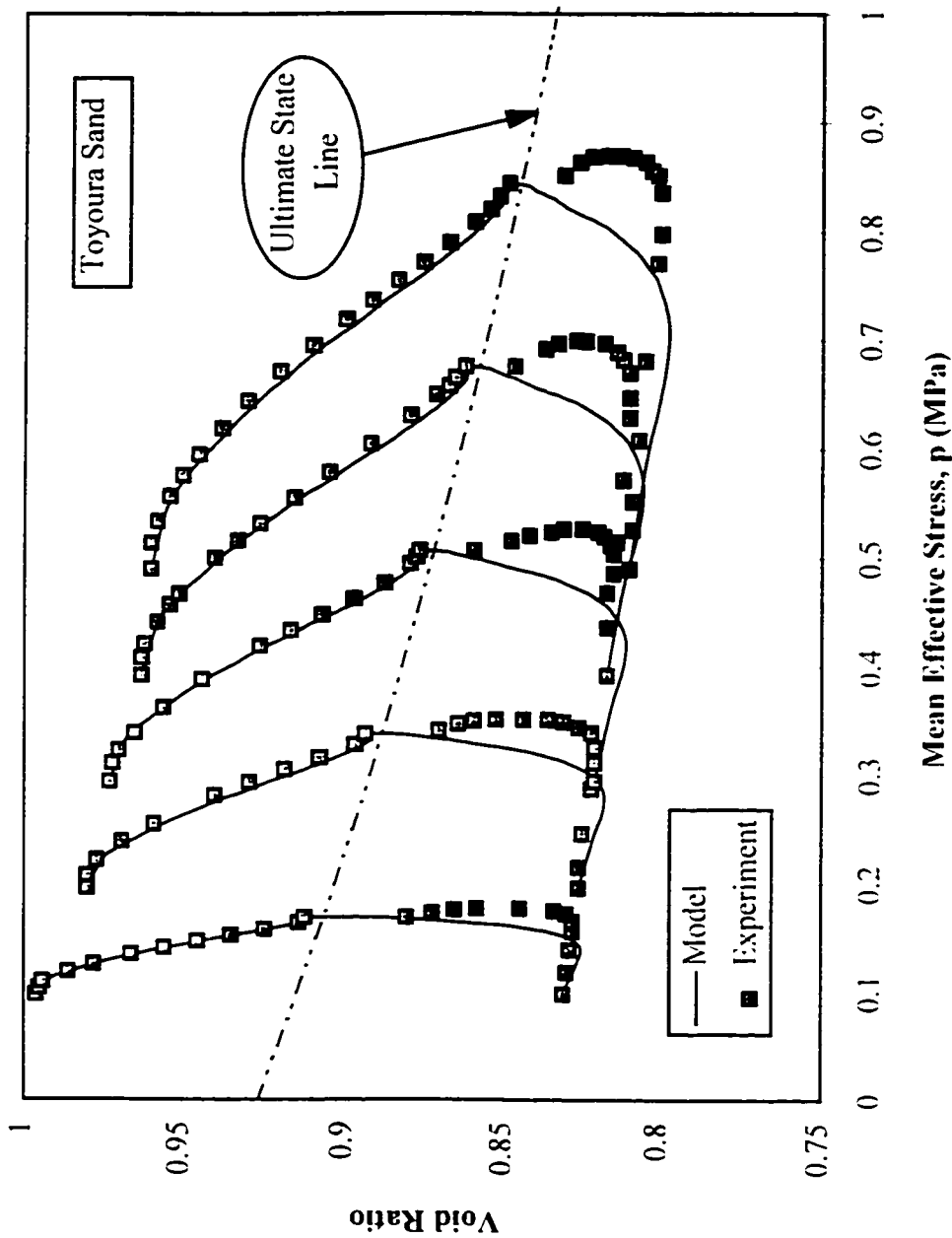
Figure 4.26. Evaluation of model predictions for conventional drained triaxial compression tests on specimens of Toyoura sand (Mean effective stress-void ratio curves).
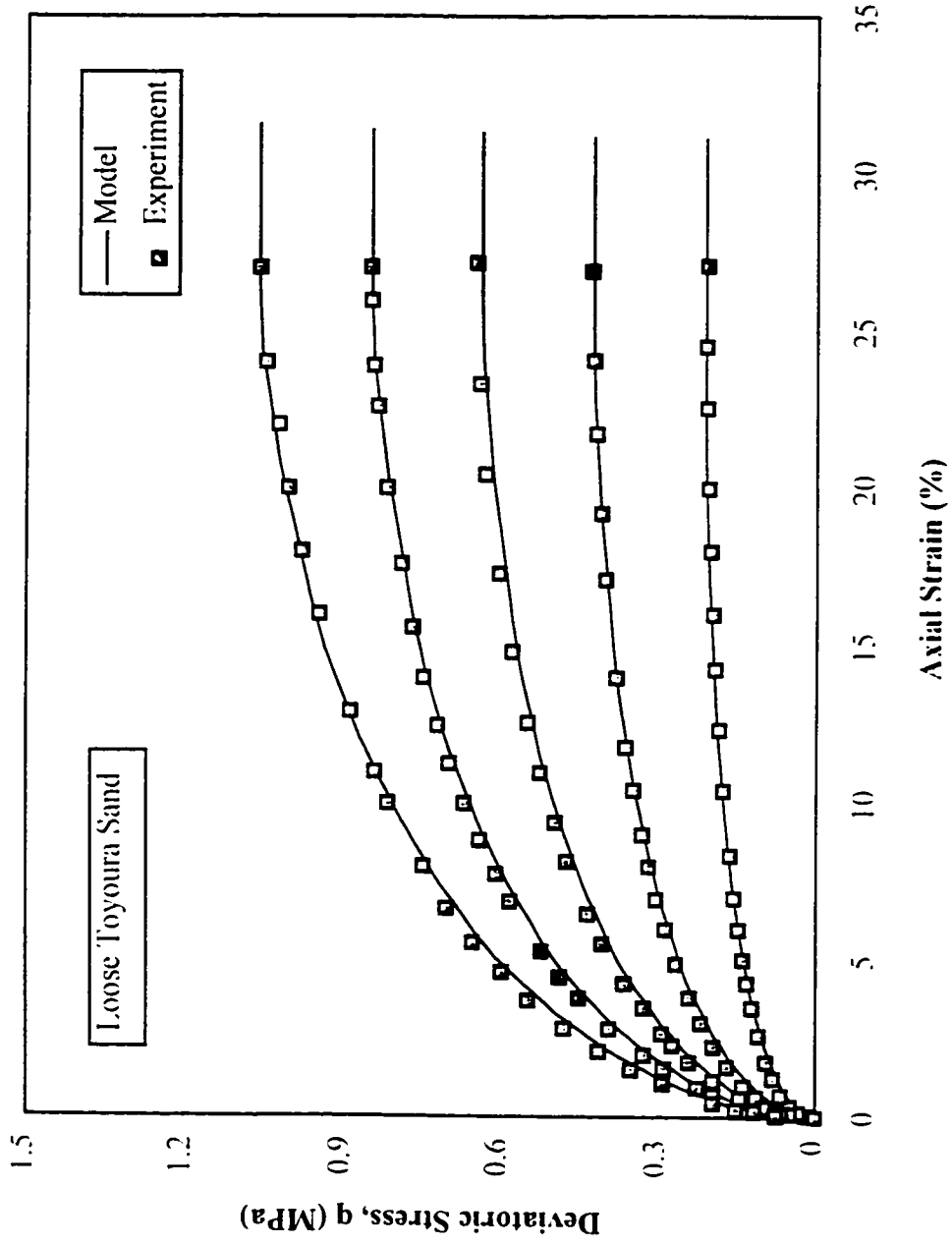
Figure 4.26. (cont.) Evaluation of model predictions for conventional drained triaxial compression tests on specimens of Toyoura sand (Stress-strain curves for loose sands).
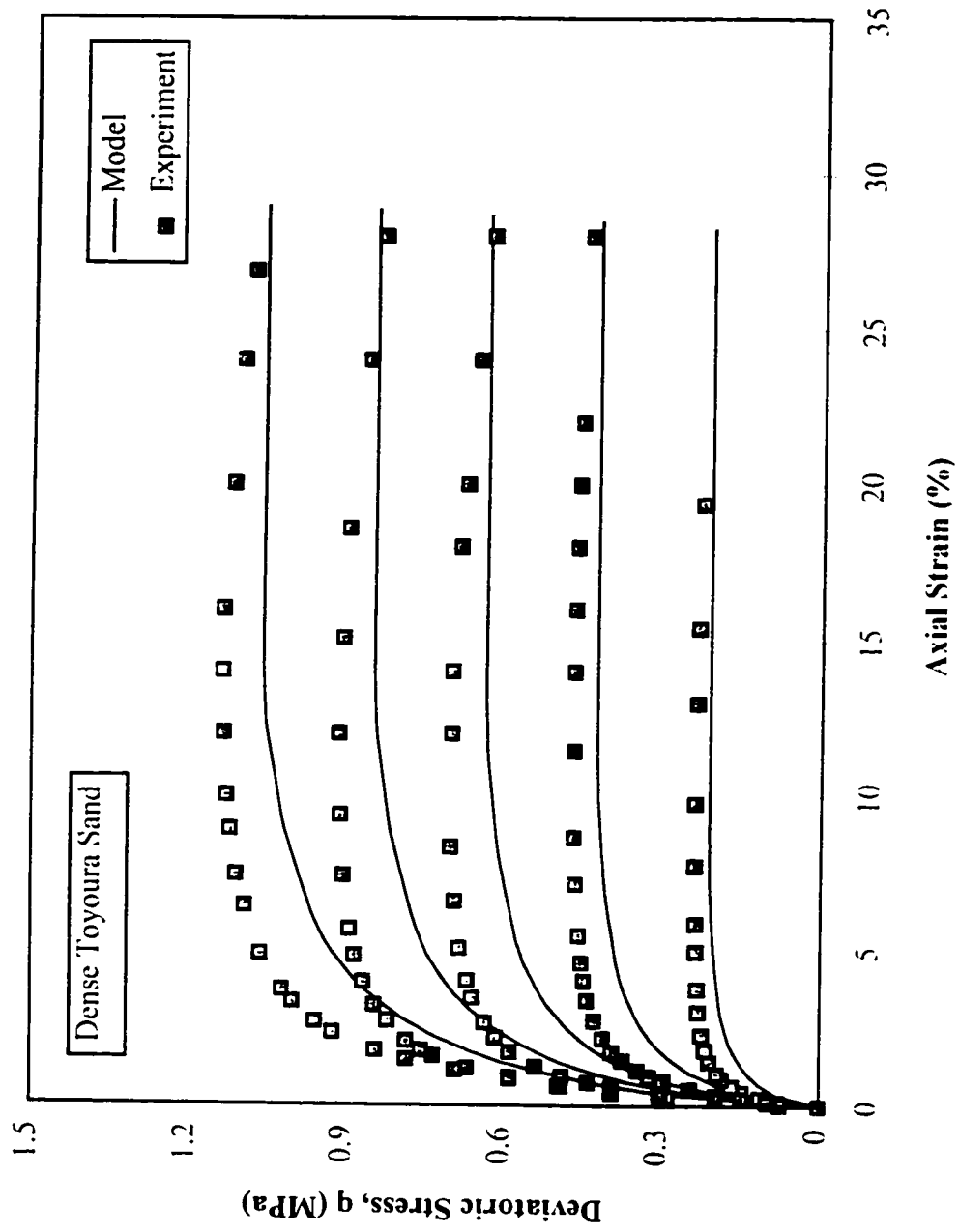
Figure 4.26. (cont.) Evaluation of model predictions for conventional drained triaxial compression tests on specimens of Toyoura sand (Stress-strain curves for dense sands).
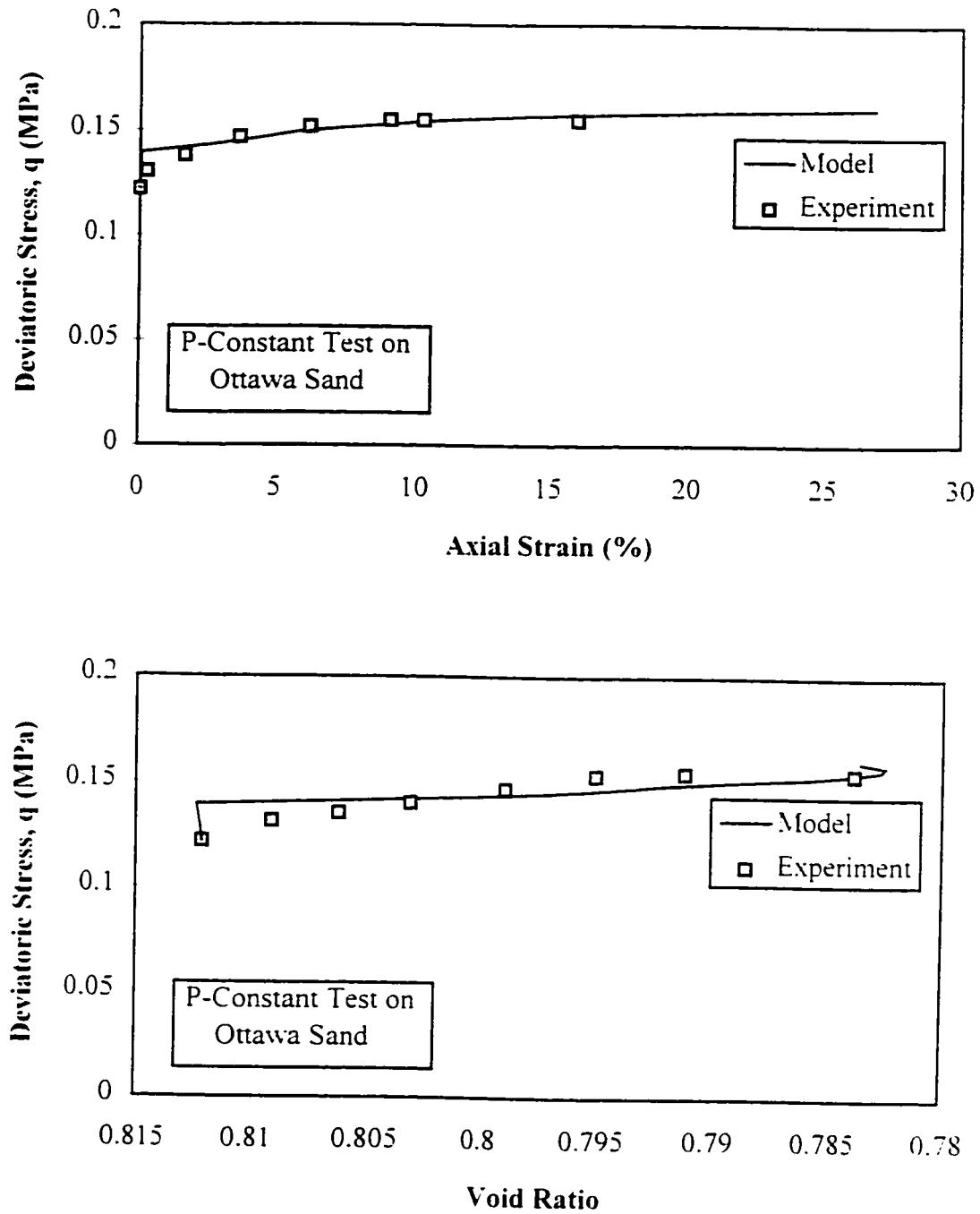
Figure 4.27. Evaluation of model prediction for p-constant test on Ottawa sand (Stress-strain and stress-void ratio curve).
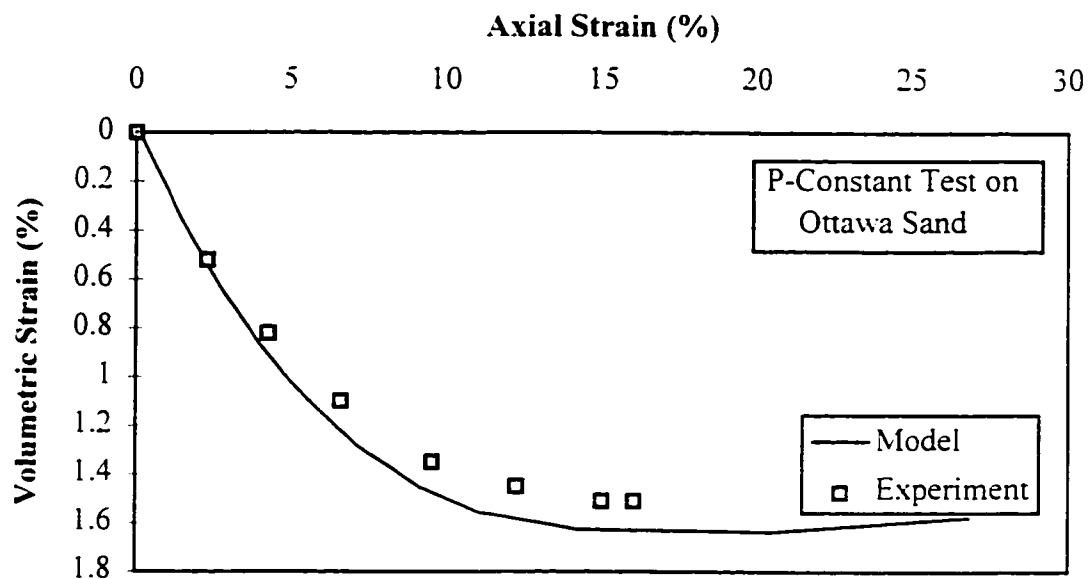
Figure 4.27. (cont.) Evaluation of model prediction for p-constant test on Ottawa sand (Volumetric strain-axial strain curve).
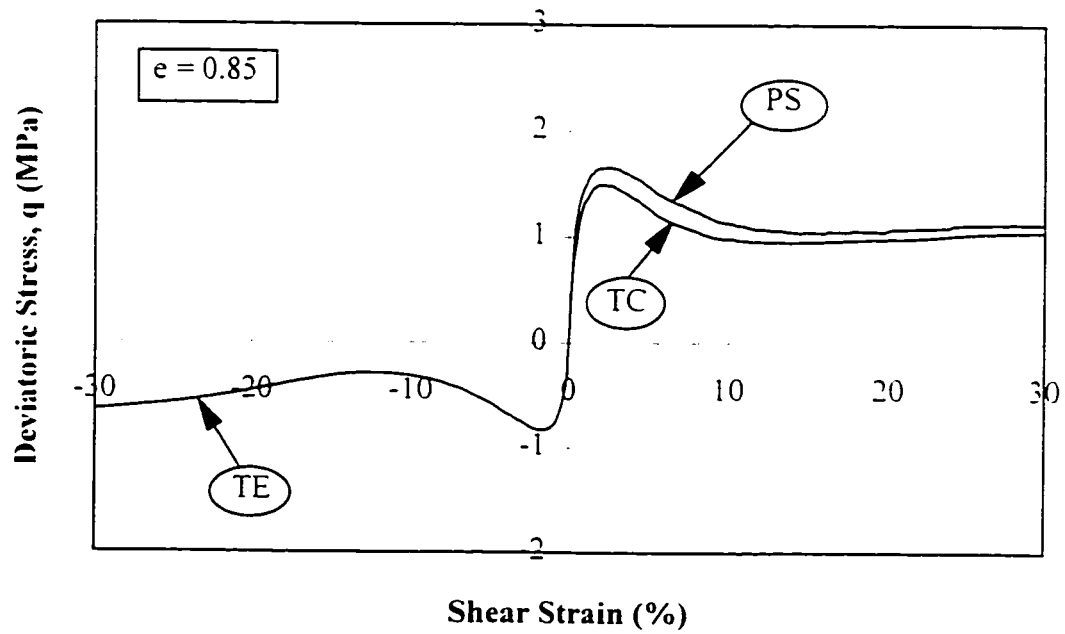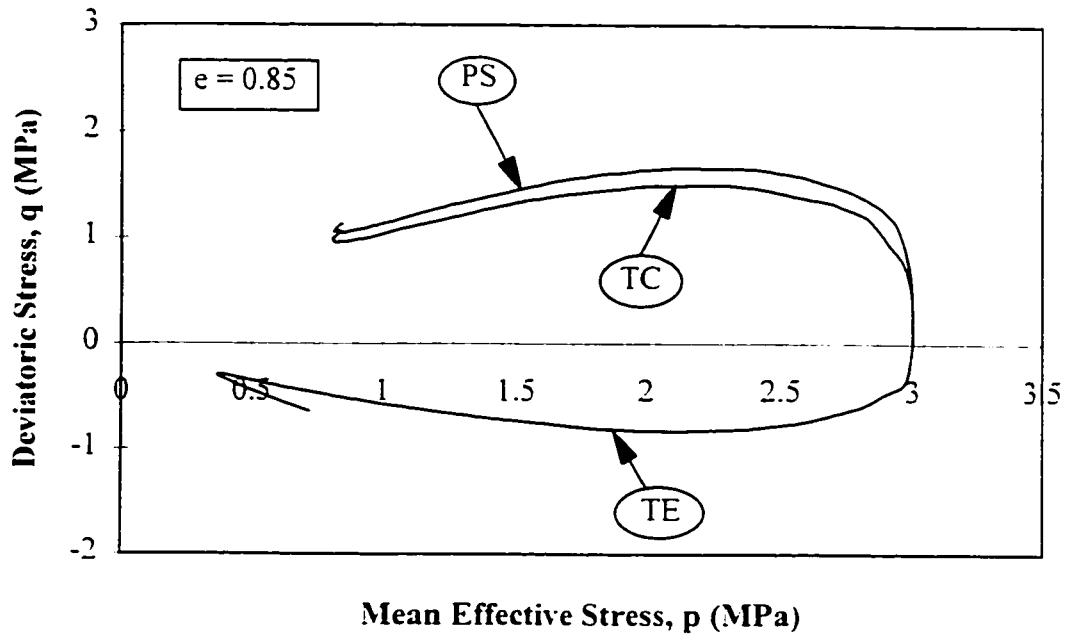
Figure 4.28. Effect of shearing mode on model predictions for loose sands.
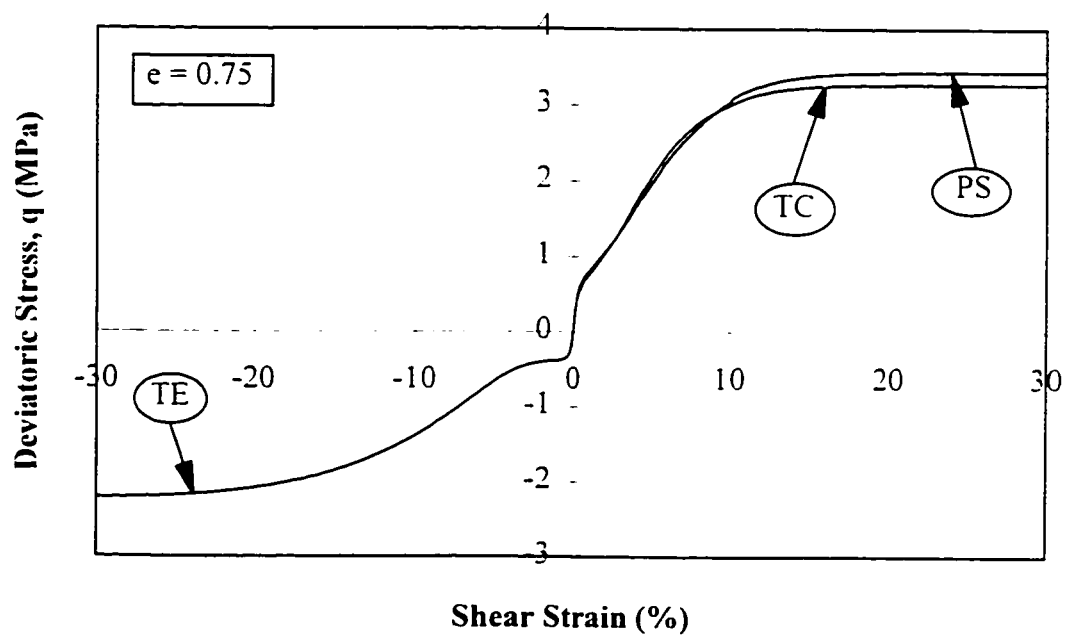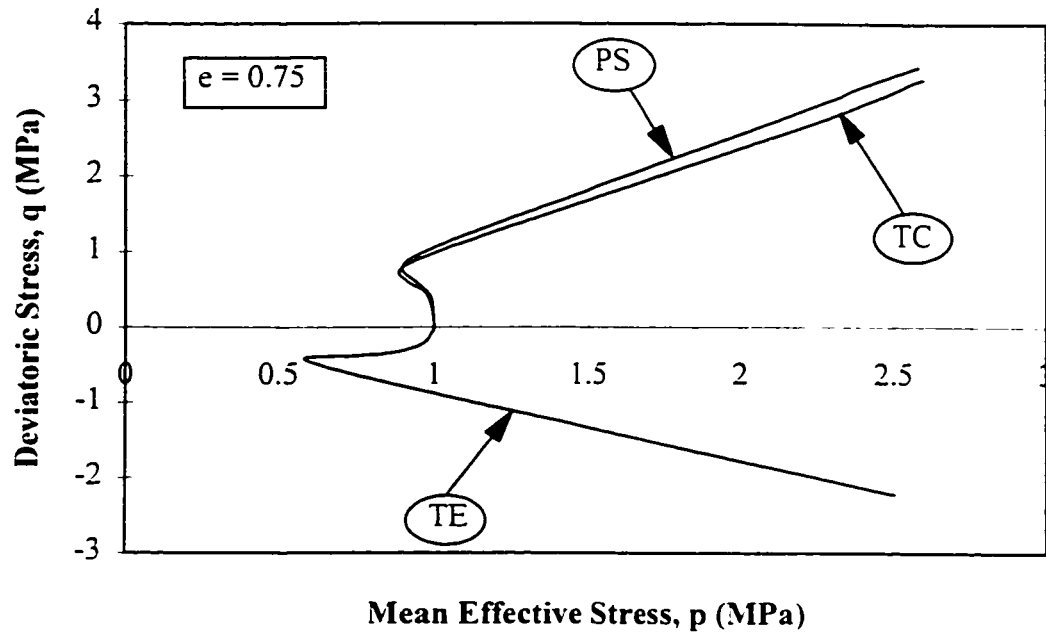
Figure 4.29. Effect of shearing mode on model predictions for dense sands.
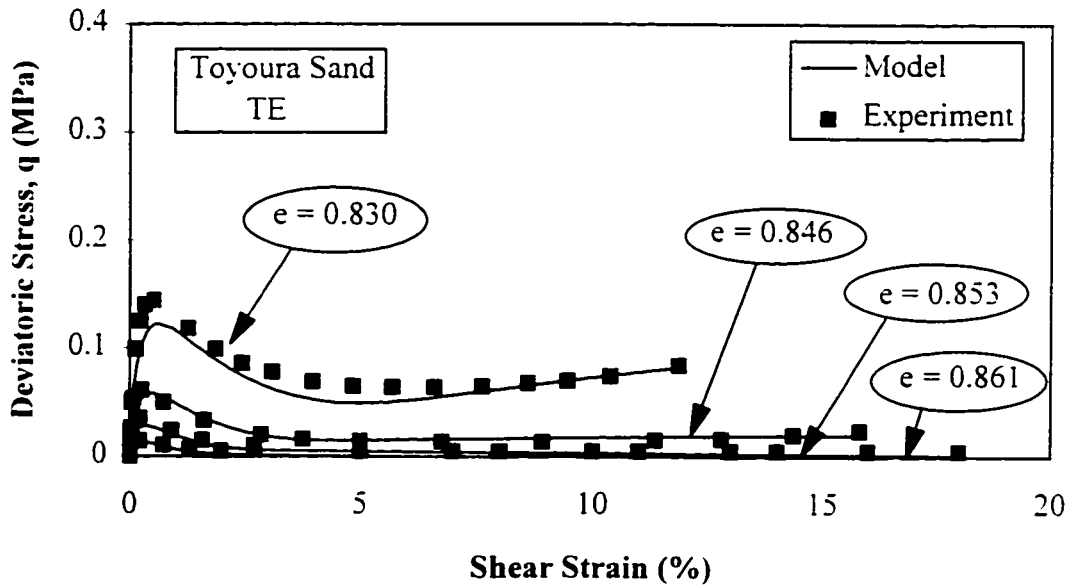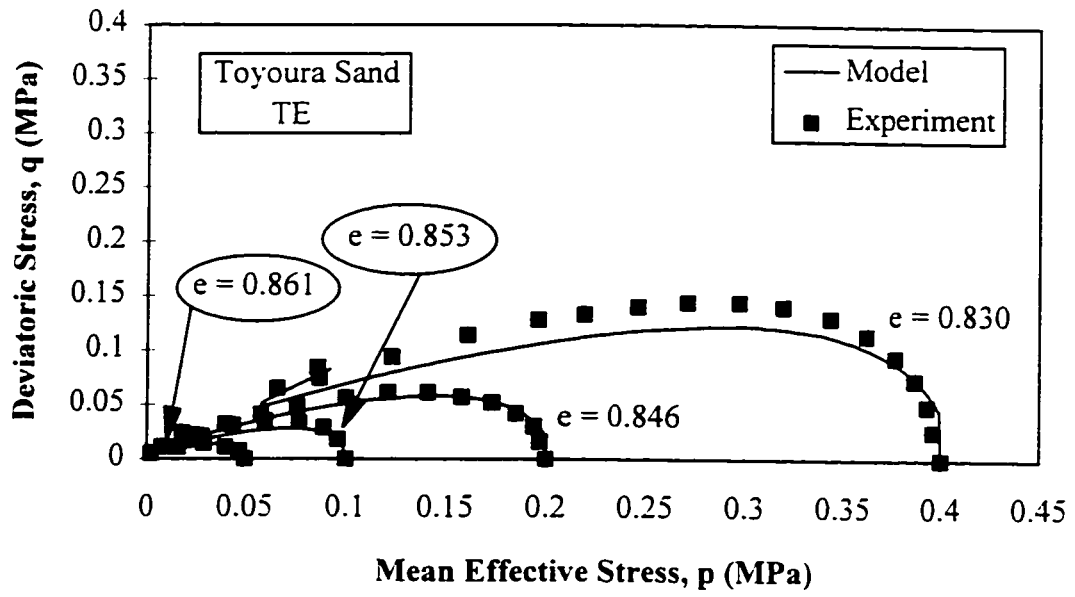
Figure 4.30. Evaluation of model predictions for undrained triaxial extension tests on Toyoura sand.
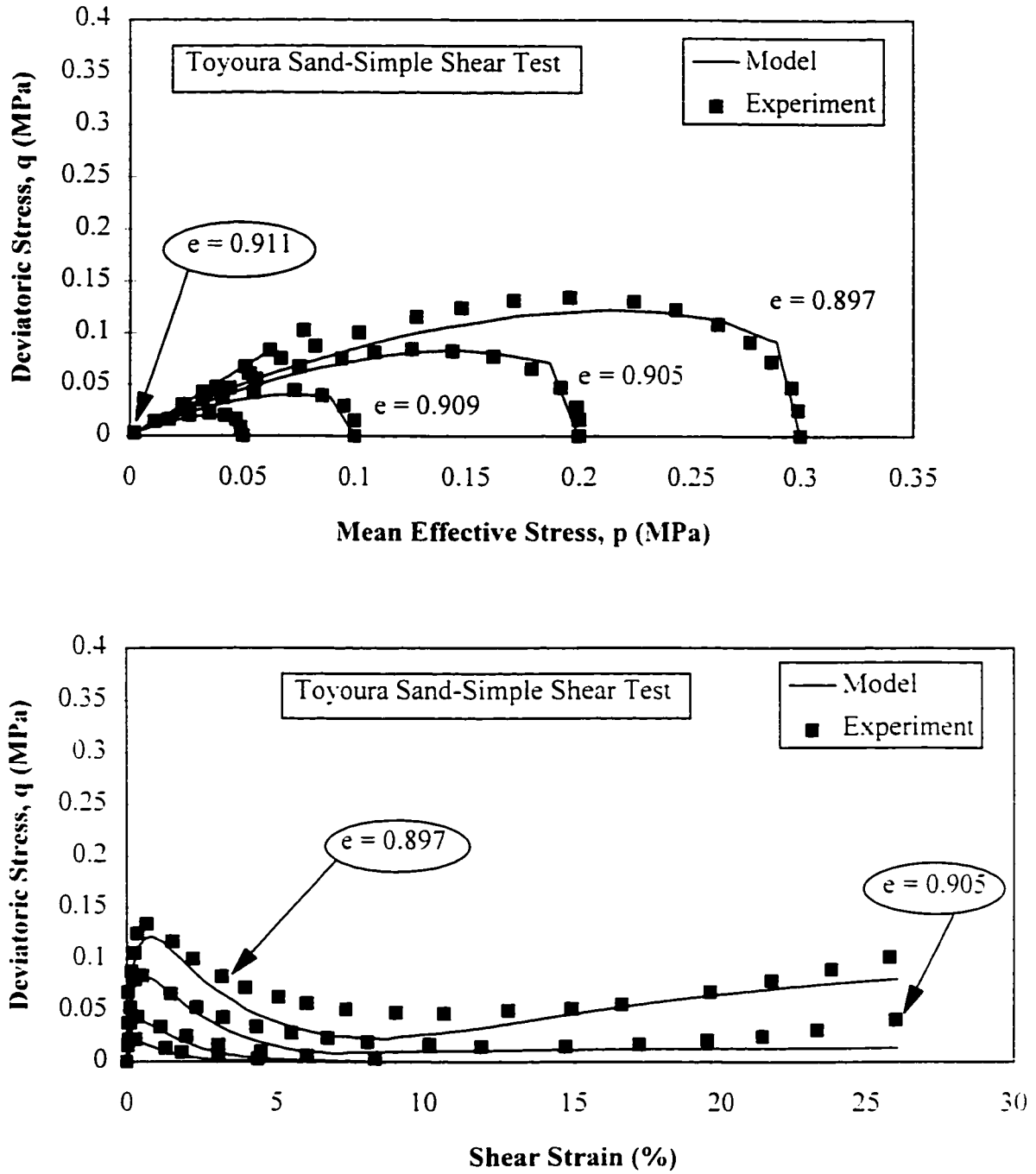
Figure 4.31. Evaluation of model predictions for simple shear tests on Toyoura sand (a).
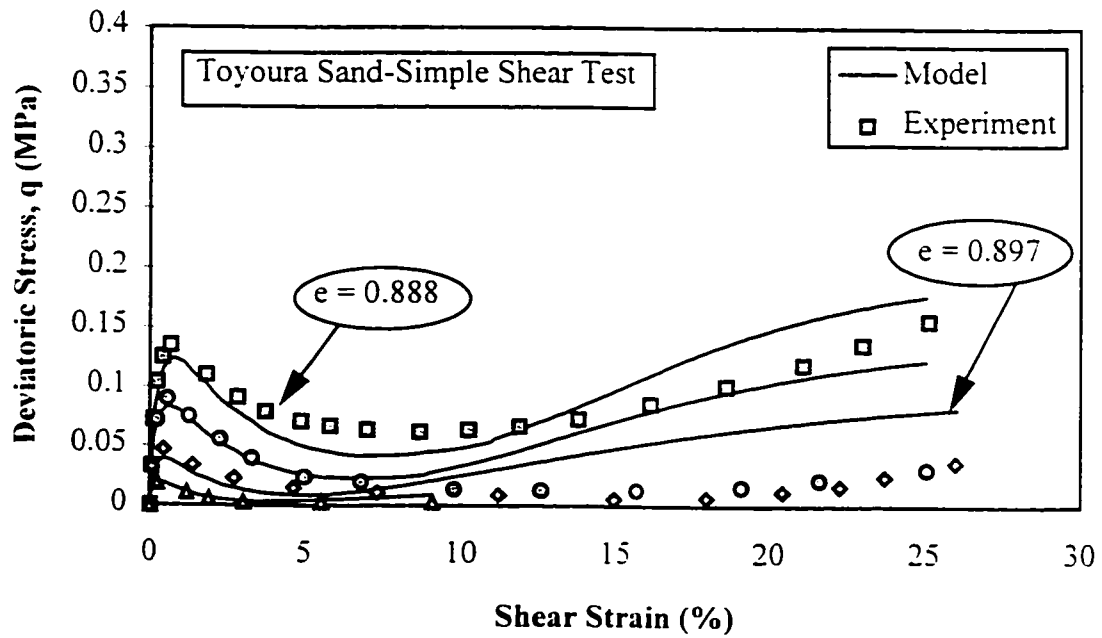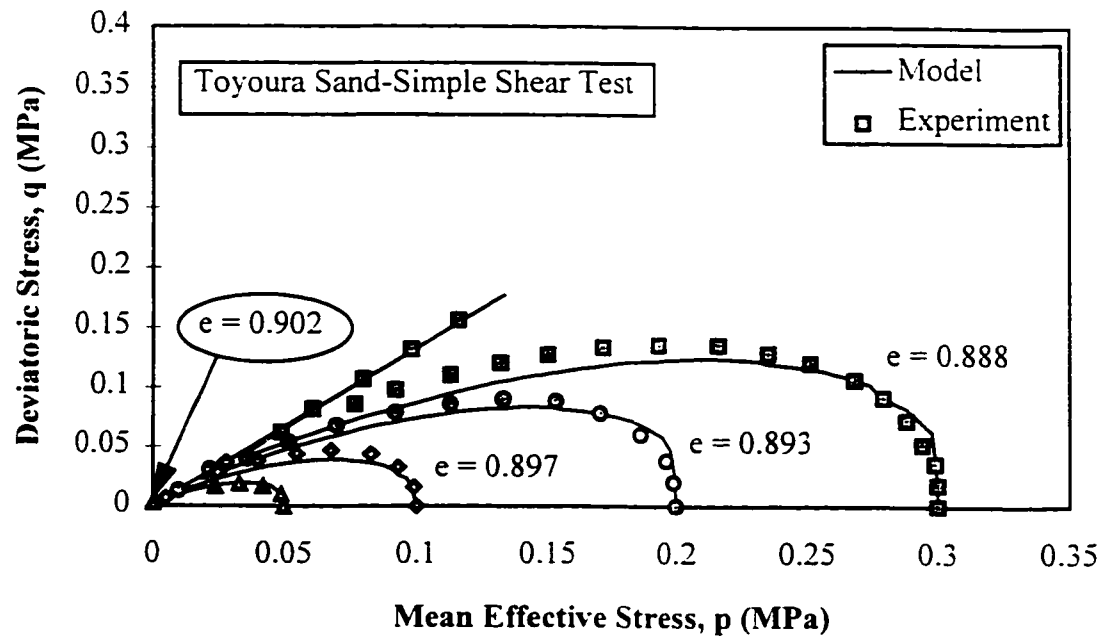
Figure 4.32. Evaluation of model predictions for simple shear tests on Toyoura sand (b).
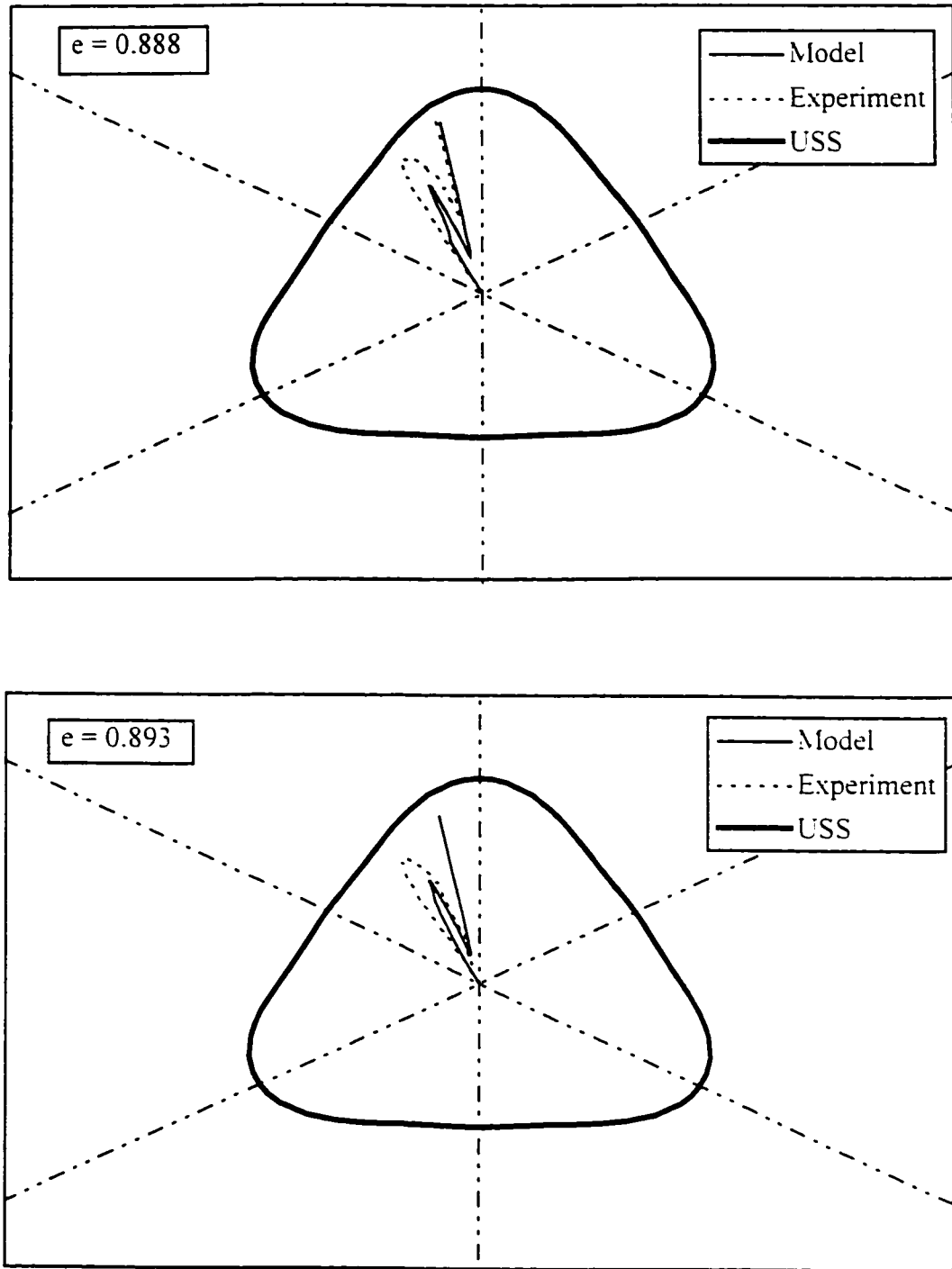
Figure 4.33. Comparison of prediction of the model with experiment on a deviatoric plane for simple shear conducted by hollow cylinder tests (a).
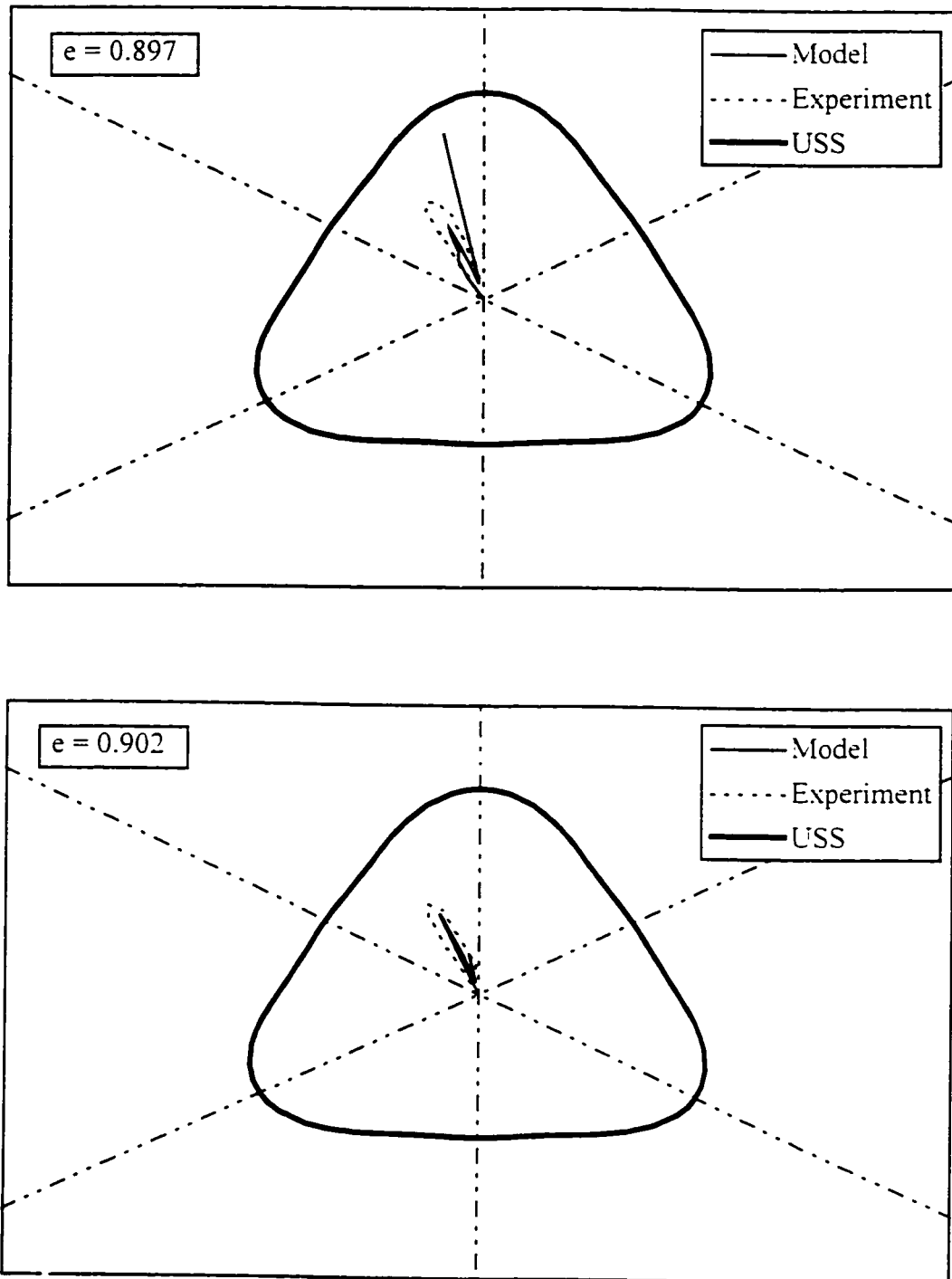
Figure 4.34. Comparison of prediction of the model with experiment on a deviatoric plane for simple shear conducted by hollow cylinder tests (b).
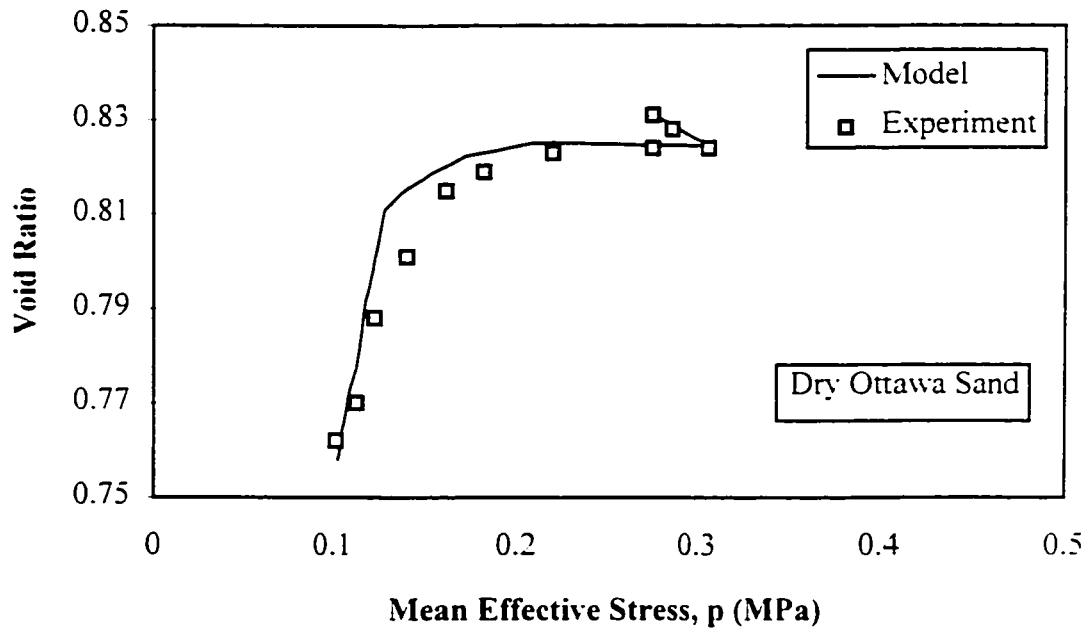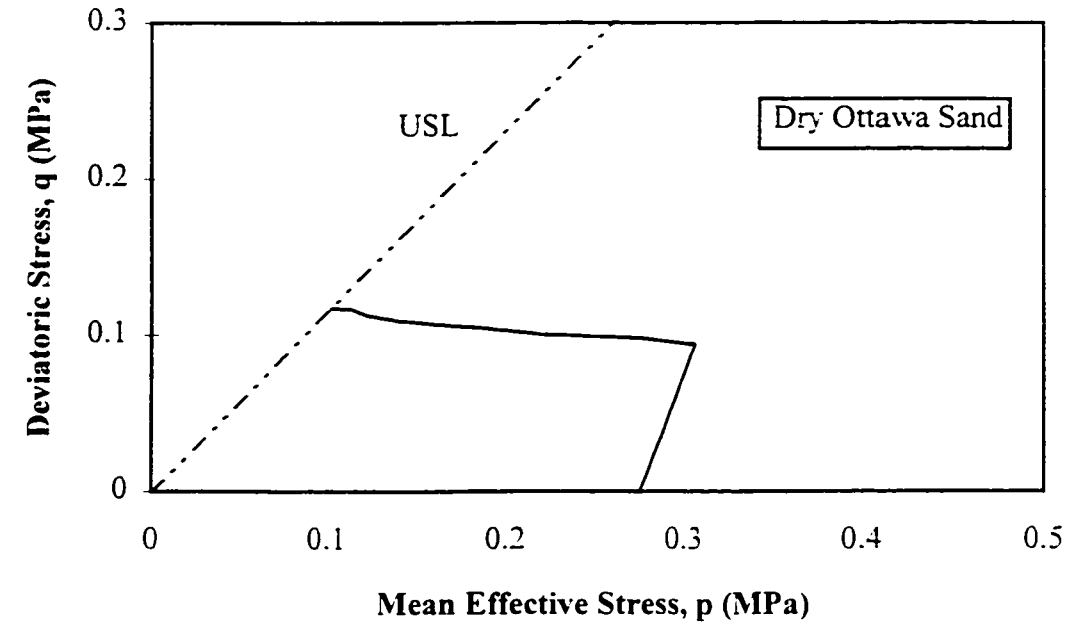
Figure 4.35. Evaluation of model prediction for deviatoric constant test on dry Ottawa sand (a).
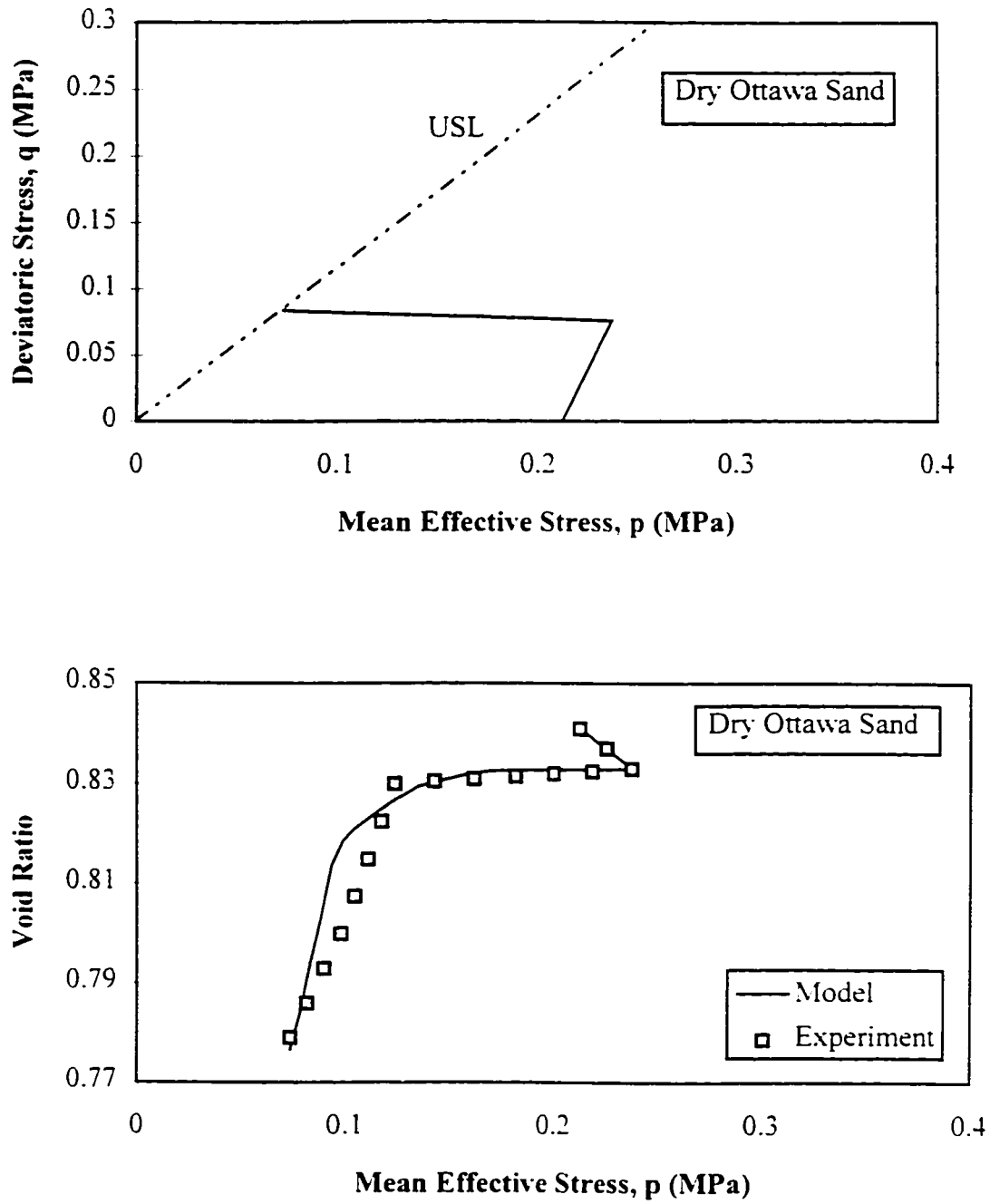
Figure 4.36. Evaluation of model prediction for deviatoric constant test on dry Ottawa sand (b).

Chapter 5

VALIDATION OF THE MODEL FOR CYCLIC LOADING

5.1. Introduction

Increasing concern in recent years regarding the likelihood of liquefaction of the ground during earthquakes has aroused the need to investigate the mechanism in which sands develop pore pressure or volume change during cyclic loading.

The behavior of cohesionless soils under cyclic loading is greatly influenced by their initial state. Using the results of triaxial tests. Ishihara et al. (1991) have shown that the stress-strain and pore pressure response of sand is governed not only by its density but also by the confining stress. A sand under small confining pressures may show dilative behavior under cyclic loading. However. with the same density. this sand at a large confining pressure may develop contractive behavior. leading to the ultimate state after applying cyclic loading.

Depending on state of the soil: initial static shear stress: amplitude of loading and number of cycles. different phenomena can be observed in cohesionless soil. In the past. because researchers worked over a limited range of possible conditions. most of them saw and reported a specific behavior for soils under cyclic loading. These different

interpretations. which were generally based on a researcher's particular observations. have caused some confusion and much discussion during the past decades. The usefulness of initial shear stress for increasing soil strength against liquefaction which has been a discussion between Casagrande and his students on one side and Seed and his coworkers on the other side. is a famous dispute in this regard. The reality. however. is that most of the results and observations which have been reported by different researchers are correct but only for the conditions in which those experiments have been performed.

From a constitutive modelling point of view. since the early years of the 1970's with the observation of the catastrophic consequences of liquefaction. modelers have felt a strong need to develop constitutive models able to capture cohesionless soil response under transient loading. From that time a lot of models with varying degrees of sophistication have been developed. The performance of these models has been evaluated in several workshops. However. there is still no agreement among modelers on a unique model. The difference observed between model predictions and experimental results are also a result of the fact that even in the experiments. with a little change in the test conditions. the response of the soils will be different.

For soils under monotonic loading. the simple constitutive models can be used to predict the deformation with sufficient accuracy. However. for more complex loading. such as earthquake or wave loading. a more advanced model must be used. Unfortunately. the efforts to model the cyclic response of a soil mostly result in the sacrifice of soil response under monotonic condition and vice versa. In practice. however. a complete model must answer both kinds of loading simultaneously.

In practice, depending on the state of the soil. amplitude of loading. initial shear stress and drainage conditions. a variety of responses such as cyclic mobility. cyclic liquefaction, flow deformation. flow and cyclic liquefaction. cyclic mobility and flow deformation. flow and cyclic mobility and etc. can be observed in the soil. All these

combinations of responses have been seen in experiments. It is believed that the prediction of all these phenomena can be undertaken only in the "Reference State Soil Mechanics" framework. The proposed model is capable of showing all these phenomena with a unique set of parameters. Flow deformation (liquefaction). cyclic mobility and cyclic liquefaction can be handled in a unique framework using this model.

5.2. Model performance

In the case of cyclic loading. the response of the soil is sensitive to different factors. Therefore. the main emphasis in model evaluation is usually placed on the qualitative demonstration of the model capabilities.

In this section the performance of the model under cyclic loading will be discussed. In the first part. typical predictions of the model for stress control and strain control analysis on specimens at different states will be presented. Next. some comparisons with real tests will be shown. In these comparisons the focus will be placed on the cases in which prediction of soil response is difficult and most existing constitutive models developed for cyclic loading show significant weaknesses. The transition from cyclic mobility to flow deformation in different range of stresses. behavior of anisotropic consolidated samples under small amplitude of loading. and prediction of volumetric strain under different ranges of stress ratios are some of these cases which will be discussed in this section.

Figures (5.1) to (5.4) show the typical performance of the model for triaxial conditions under stress control analysis. Initial mean effective and deviatoric stresses for all predictions have been chosen as equal ($p_i = 3$ MPa : $q_i = 0$). but the void ratio is different for them. As can be seen. when the number of cycles increases. the pore pressure goes up and the stress path approaches the origin. For looser samples. the number of cycles before reaching the origin is less than that for dense ones. This is consistent with experimental observations (Seed and Lee. 1966; Ishihara. 1985). For the sample with

e = 0.90. after three cycles. the soil has reached a condition where flow deformation has occurred in the soil until it reaches the ultimate state condition. This kind of behavior accords with Castro's (1969) observations. For the first cycles in all predictions. strain induced by shear is small: with repetition of loading. however. the rate of strain increment increases significantly. In unloading. when the stress path passes the phase transformation line. pore pressure increases greatly with relatively low strain increment. But when the stress path passes the phase transformation line and follows the ultimate state line. a large strain develops in the sample. This performance also corresponds with experimental observations. The banana shape of the stress-strain curve shows softening during each cycle perfectly. Considering Figures (5.1) to (5.4). one can conclude that the model is capable of representing the effect of variation of void ratio (or in better words. state) of the soil on its response under stress control cyclic tests. The transition of cyclic mobility to flow liquefaction with loosening the soil is captured by the model.

To evaluate the effect of static shear stress on the model performance. two typical predictions have been shown in Figures (5.5) and (5.6). In Figure (5.5). a dense sample with p_i = 3 MPa. q_i = 0.6 MPa and e = 0.70 has undergone a cyclic loading. The amplitude of loading. number of cycles. initial mean effective stress and void ratio in this prediction are the same as those that are in Figure (5.1). The only difference lies in the initial shear stress. As can be seen. the rate at which the stress path approaches the origin in this case is lower than that in Figure (5.1). This decreasing of the rate for the anisotropically consolidated sample is consistent with the experimental observation of Hyodo et al. (1989). Furthermore. the model in the case of an initially sheared sample shows less strain compared to that with an unsheared sample. In this case. the existence of shear stress has helped the sample maintain more strength. As with the case of Figure (5.1). the number of cycles has not been increased. But by increasing the number of cycles. it can be seen that the stress path hardly approaches the origin. This is because of the lack of shear reversal in this prediction. Considering Figure (5.5). one can see that the existence of static shear increases the strength of the dense soil against cyclic

liquefaction. This kind of behavior is similar to what has been reported by Seed and Lee (1967).

Figure (5.6) shows the effect of static shear stress on the performance of the model for loose soil. The initial mean effective stress. amplitude of loading and void ratio are the same as those in Figure (5.3): however. the static shear is different. In this case. after 2 cycles. the soil has reached a condition in which flow has started. As can be seen. however. in the case of no initial shear stress (see Figure 5.3). the model shows more strength against liquefaction. This sort of response matches with Castro's observation (1969) that an increase in static shear stress reduces the soil strength against flow liquefaction.

Figures (5.7) to (5.9) show model predictions for samples with different void ratios (e = 0.75. 0.8. 0.9) under strain control cyclic triaxial test. The maximum and minimum axial strain have been chosen as 2% and (-2%). respectively. Repetition of loading causes positive pore pressures which push the stress path to the origin. For the samples with higher void ratio. the rate of approaching the origin will be higher. For the sample with e = 0.9. the stress path has reached to the origin and cyclic liquefaction has occurred. In this case. with a very small increase of stress. a significant strain occurs in the soil.

Figures (5.10) and (5.11) show the performance of the model for stress and strain control cyclic plane strain tests. The general shape of the stress paths and stress-strain curves are similar to those in the triaxial test. However. the model shows slightly more stiffness compared with the triaxial condition that corresponds with experimental observations. Any constitutive model which is used to predict soil deformation must be capable of showing soil response under different shearing modes.

Based on initial shear stress. amplitude of loading. soil state and number of cycles. several phenomena can be seen in the soil. In Figure (5.12). an isotropically

consolidated sample has been loaded. In the first cycles of loading. strain has increased slowly in the soil: however. in one of the cycles. because of flow deformation. strain has grown significantly. Then. hardening has occurred in the soil. but again because of changing the loading direction. cyclic softening has been observed in the soil. By repetition of loading. a continuous softening occurs in the soil and maximum strain increases.

Figures (5.13) and (5.14) show the comparison of the model predictions for an undrained cyclic triaxial test on an anisotropically consolidated loose specimen of Toyoura sand. As can be seen. the specimen has undergone small amplitude cyclic loading without shear reversal. In the first steps of loading. the rate of strain increment was very low. but after a large number of cycles. flow suddenly occurred in the soil. Then the specimen has reached the ultimate state condition at large strains. The point is that. as can be observed. the monotonic stress path has been a boundary for the stress path in cyclic loading. Almost the same results have been reported by Alarcon and Leonards (1988). In the model prediction. flow has started slightly before the monotonic stress path. Although this difference is not substantial. and is on the safe side in the practice. this small difference. as will be discussed in the next section. has also been observed in Alarcon and Leonards (1988)'s works. Comparing model performance with experimental results. monotonic stress path in model prediction is lower than that in the test. As a result. the model has shown flow under cyclic loading earlier than the test did. A good simulation is observed of the stress-strain curve.

Figures (5.15) and (5.16) show a comparison of model predictions with observed behavior of a dense sample of Toyoura sand under cyclic and monotonic loading. In this test. after a number of cycles. the specimen has undergone monotonic loading and has finally reached the ultimate state at large strains. The model was able to show this behavior. In the model predictions. the variation of the stress path during loading repetition was not substantial. This is because the stress path is very close to the ultimate state line and there is not sufficient room for movement of the stress path. An almost

identical phenomenon has been observed in the experiment. In unloading, the model shows less contraction compared with the experiment. By increasing the K_u value, this difference will be reduced, but at the same time, the stress path in reloading will represent more contraction.

Figures (5.17) and (5.18) compare the model performance with observed behavior of an anisotropically consolidated loose specimen of Toyoura sand in a small range of stresses. This test is one of the very few existing reported tests on anisotropically consolidated samples in which the specimen, after loading, has shown flow deformation before reaching quasi-steady state condition when hardening began and the soil has shown higher strength under cyclic loading. As can be seen in this test, the monotonic stress path has not been a boundary (at least not a perfect boundary) for cyclic loading. Maybe in practice, such a difference actually exists between monotonic and cyclic stress path, but in high stress levels, because of the scale factor this difference can not be detected. It seems that more experimental works must be performed in order to clarify this question. This test has been performed on a sample prepared by dry deposition method. But the model was calibrated by the tests on moist tamped samples. Furthermore, the stress range is much less than what was used in Ishihara (1993) (used for calibration of the model); and the slope of ultimate state line in ($q - p$) plane is more than that in Ishihara (1993). Therefore, for simulation of this test, the ultimate state line has been shifted 0.059 down in ($p - e$) plane. Considering Figure (5.18), after starting of cyclic loading, model shows softer behavior compared with the experiment. It seems this difference is because of the higher slope of ultimate state line in ($q - p$) plane in the experiment compared with what has been defined for the model based on Ishihara (1993).

A comparison of the model predictions with experimental results on Banding sand (Castro, 1969) can be seen in Figures (5.19) to (5.22). Two isotropically consolidated samples of this sand with e = 0.692 and 0.729 have undergone cyclic triaxial test without shear reversal. The sample with lower void ratio after the 3rd cycle has shown flow deformation or flow liquefaction. Significant strain has been developed in the sample.

and, at large strain, the specimen has reached the ultimate state. The number of cycles predicted by the model is the same as that in experiment. However, unloading in the first cycles started at a higher effective normal stress than that in the experiment. The point is that the model predictions have been compared with several experimental results under monotonic loading for this sand. In all those comparisons, the model predictions corresponded with the experiments. Considering the fact that the first loading in the cyclic test is actually a monotonic loading, it shows that experimental observations for cyclic loading do not match with those for monotonic loading. In Figures (5.21) and (5.22), the number of cycles in model prediction before starting the flow is two cycles more than that in the experiment.

Figures (5.23) to (5.26) compare the model predictions with observed behavior of Fuji River sand under drained triaxial tests. In these tests, two samples with $e = 0.765$ and 0.750 have undergone stress ratio control tests. Initial stresses have been the same. In both tests, in the first cycles, the rate of volumetric strain increment was high. But after a few cycles, the variation of volumetric strain has decreased significantly. As was expected, for the sample under higher stress ratio, the volumetric strain is more than that for the sample under lower stress ratio. The performance of the model in these tests is acceptable. The variation of the stress ratio with shear strain of the samples for the first and the last cycles has been plotted in Figures (5.24) and (5.26). Compared with experiments, the model shows larger strains at the last cycles. It seems this difference is because of the softer response of the model in the extension side compared with that in the test. This is perhaps due to soft behavior of soil in the extension test which has been used in calibration.

5.3. Collapse or flow deformation

In chapter two, we saw that loose cohesionless soils have a metastable structure, and, under a specific condition, the structure of the soil may change and a discontinuity in the behavior can be seen. Alarcon and Leonards (1988) have observed this discontinuity

under torsional cyclic shear tests (see Figure 5.27). As can be seen. a specimen was sheared repeatedly. and in the 85th cycle. collapse suddenly occurred. In this case. which is the same as that for Toyoura sand. the monotonic stress path is a boundary for cyclic stress path. A small difference exists between the collapse point for cyclic loading and the monotonic stress path.

In chapter 4. the capability of the model for predicting collapse under both undrained and drained monotonic triaxial tests has been validated. In Figures (5.13). (5.14) and (5.19) to (5.22). the performance of the model in showing collapse (flow deformation) is compared with actual laboratory observations on Toyoura sand and Banding sand. Figure (5.28) also shows a typical prediction of the model for collapse under cyclic loading. In this figure. an isotropically consolidated sample underwent both monotonic and cyclic loading. It can be seen that during cyclic loading soil started to flow. This is the same as what occurs in monotonic loading. The monotonic stress path is a boundary for the cyclic stress path. A small difference exists between the collapse point in the model prediction and monotonic stress path. This corresponds to the reported results of Alarcon and Leonards (1988).

Therefore. the proposed model is capable of showing the collapse (or instability or flow deformation) under both monotonic and cyclic loading. Considering the capability of the model for showing cyclic mobility and cyclic liquefaction. one can conclude that all cyclic liquefaction. cyclic mobility and flow liquefaction (collapse) can be handled in a unique framework using this model.

5.4. Summary

In this chapter the performance of the model for cyclic loading has been validated. It was shown that the model is capable of showing the effect of soil state on its behavior. With loosening the soil. the model showed the transition of cyclic mobility to flow liquefaction. The positive or negative effect of static shear stress on occurring

liquefaction depends on which kind of liquefaction occurs. The model is capable of showing that for dense sand. the existence of static shear increases the strength of the soil: however. for loose sands this initial shear stress increases the probability of flow liquefaction. Typical predictions of the model for different shearing modes have been presented. Model predictions were compared with real observations on different sands. In this comparison. the focus was on the prediction of particularly cases that most existing models have shown weaknesses for such predictions.

It was seen that the model could show the response of the soil under cyclic mobility. cyclic liquefaction and flow liquefaction. Considering the uniqueness of calibration and the power of the model to handle both monotonic and cyclic loading. it can be used for solving boundary value problem in a variety of possible loading conditions. degree of anisotropy. drainage conditions and shearing modes.
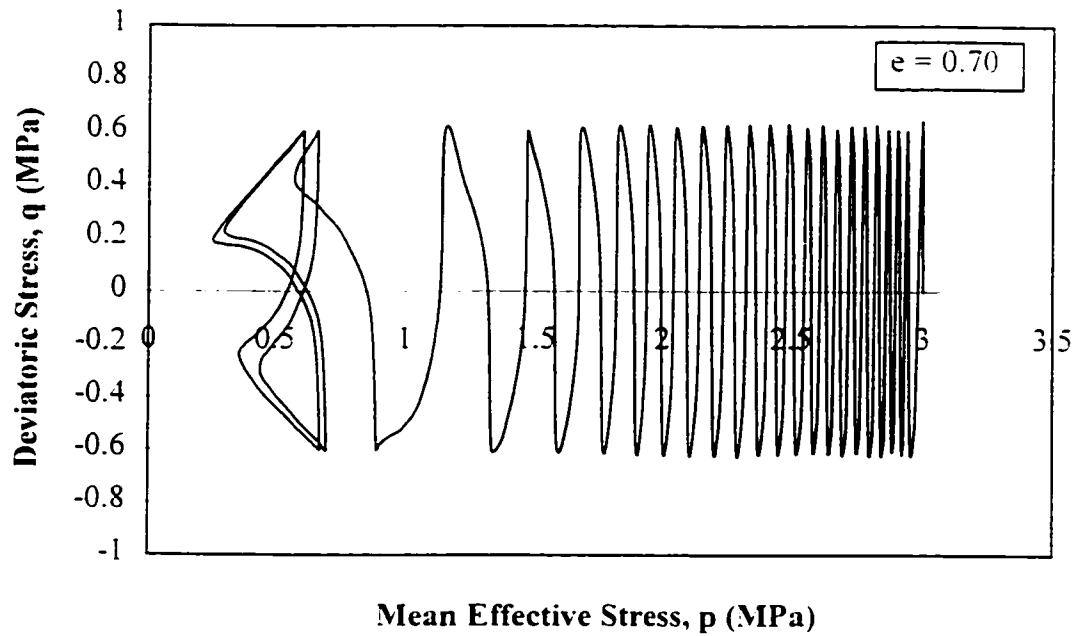
Figure 5.1. Predicted stress path and stress-strain curve during stress control undrained triaxial test at $e = 0.70$.
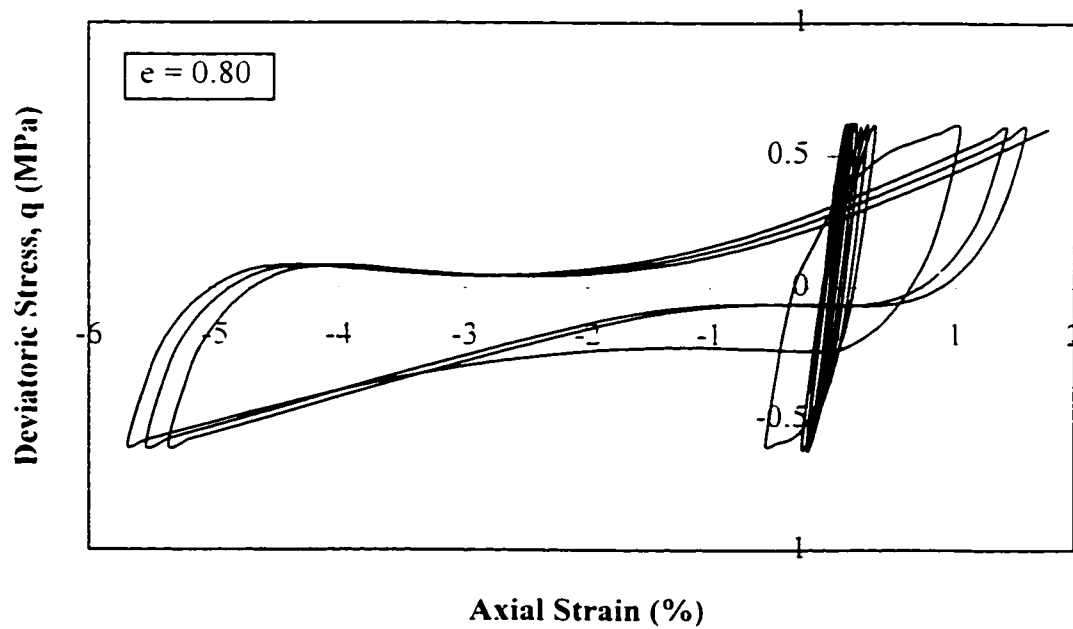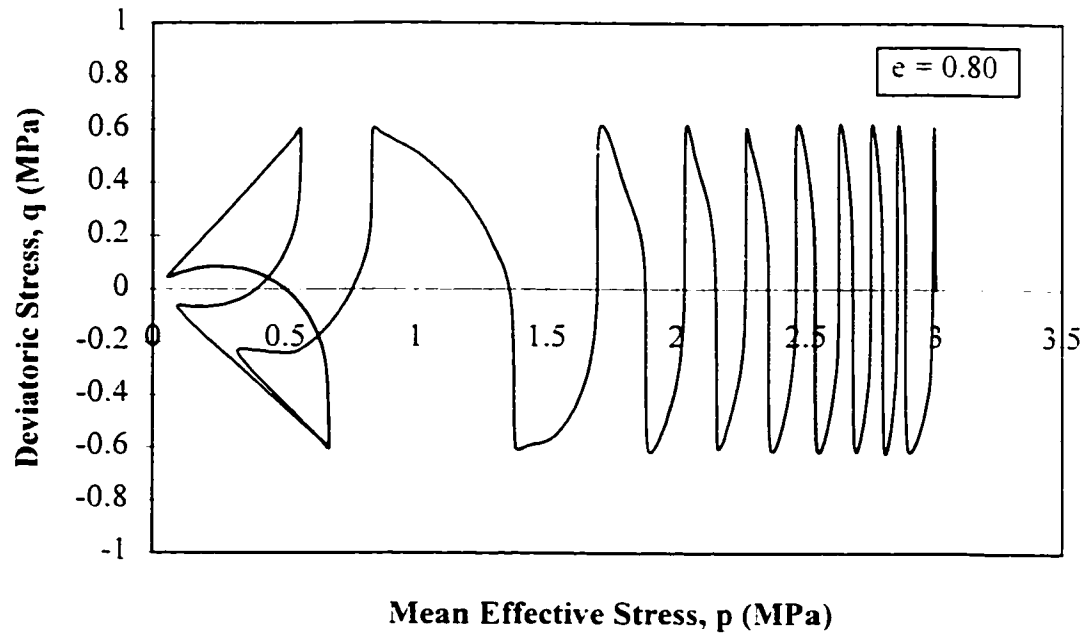
Figure 5.2. Predicted stress path and stress-strain curve during stress control undrained triaxial test at $e = 0.80$.
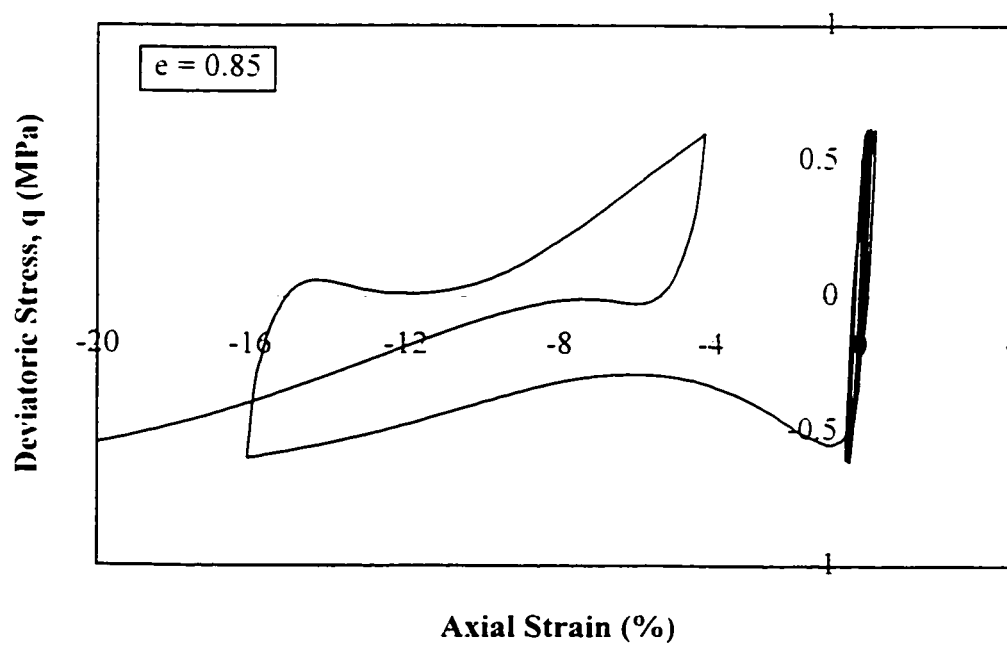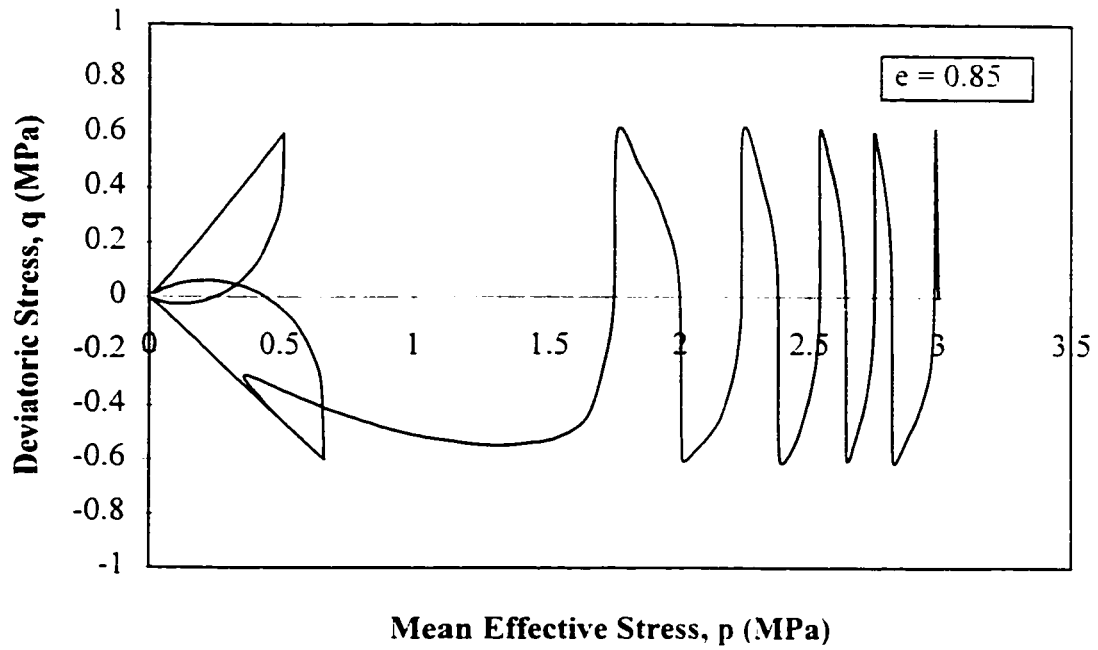
Figure 5.3. Predicted stress path and stress-strain curve during stress control undrained triaxial test at $e = 0.85$.
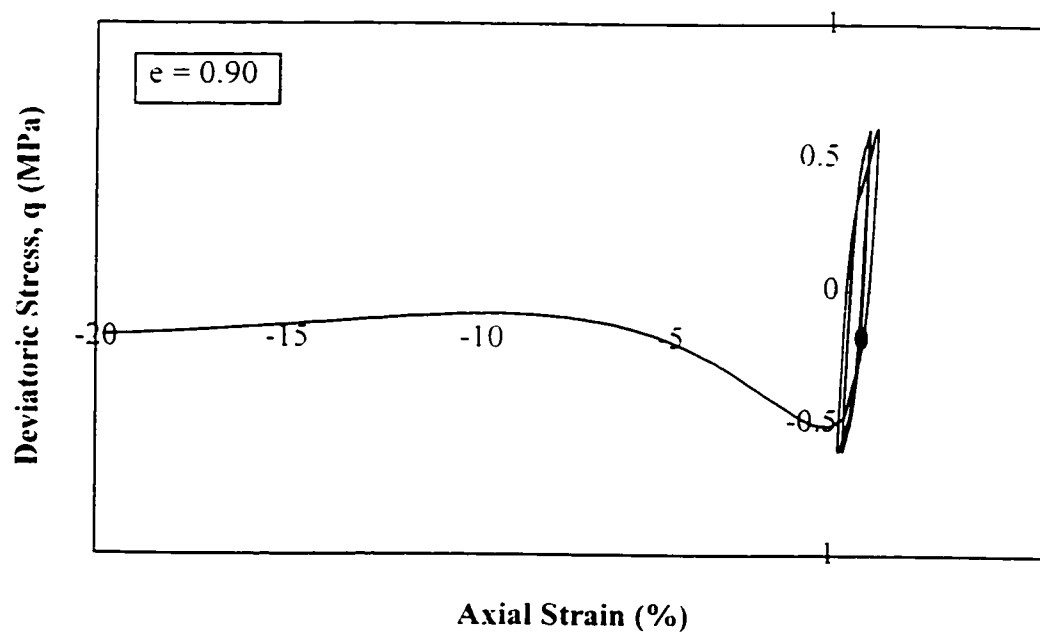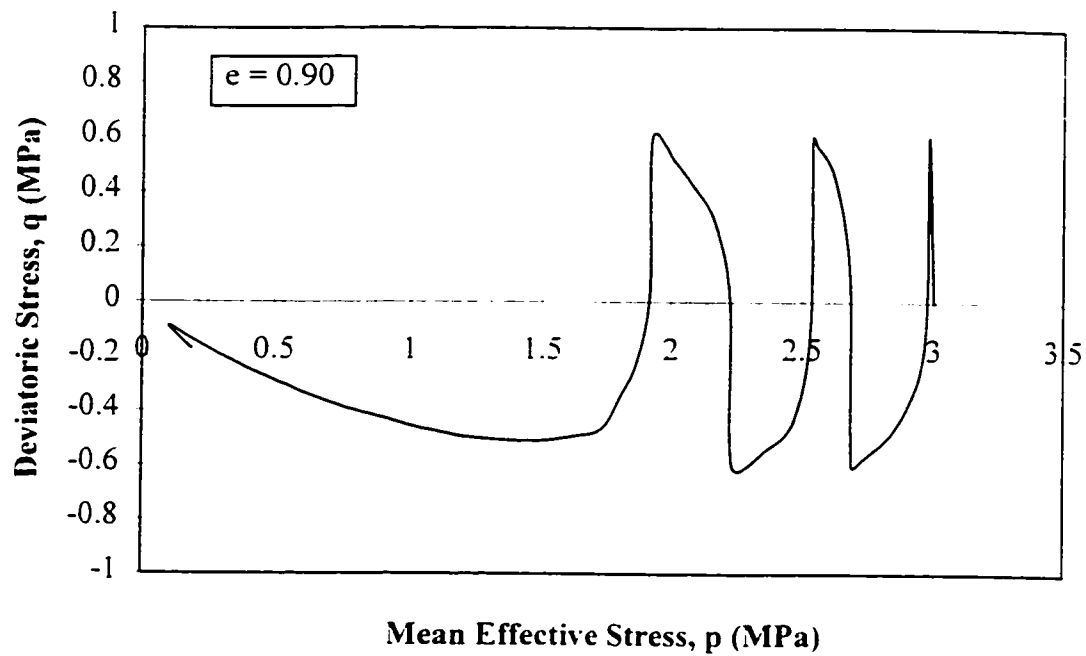
Figure 5.4. Predicted stress path and stress-strain curve during stress control undrained triaxial test at $e = 0.90$.
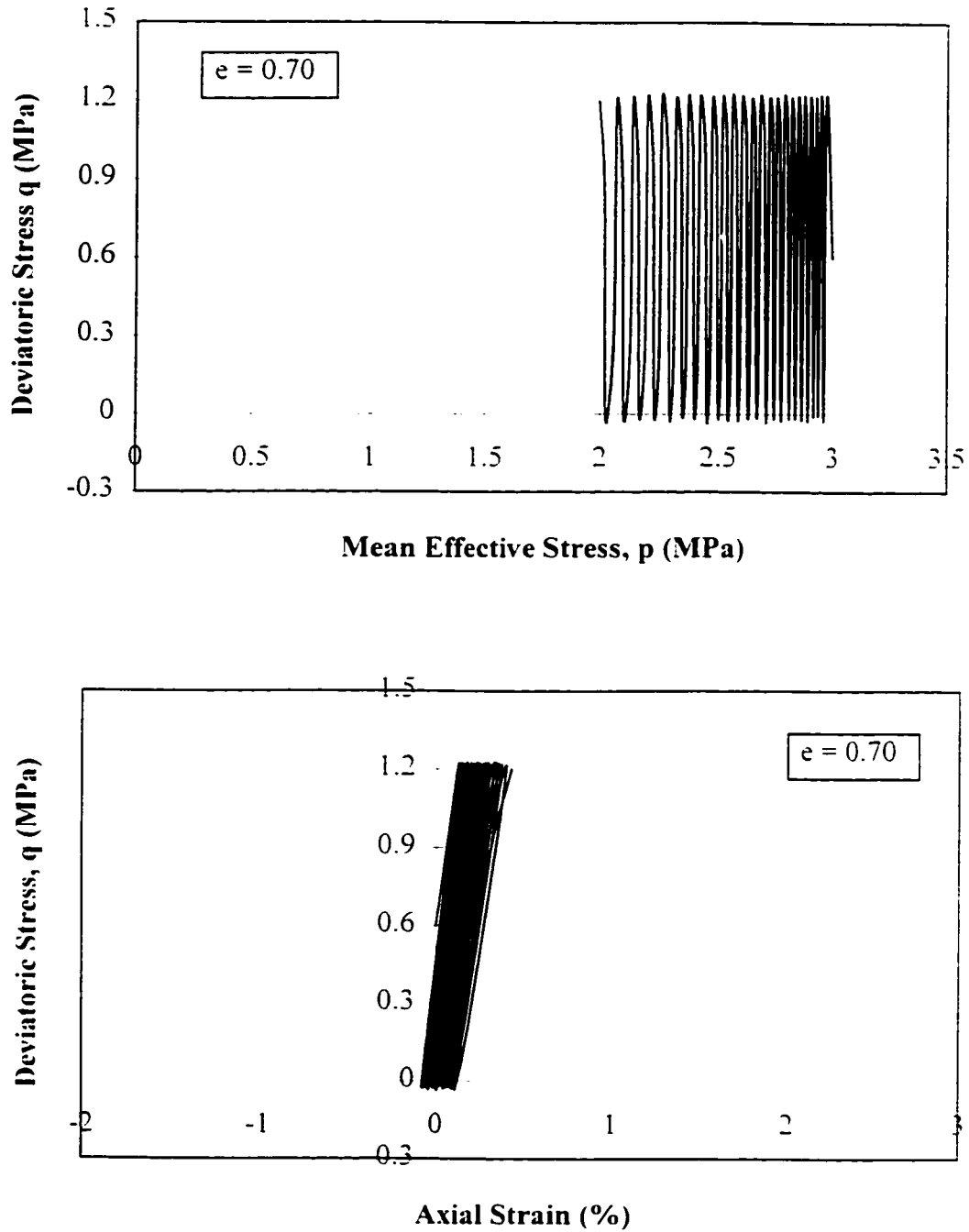
Figure 5.5. Predicted stress path and stress-strain curve during stress control undrained triaxial test on anisotropically consolidated sample at e = 0.70.
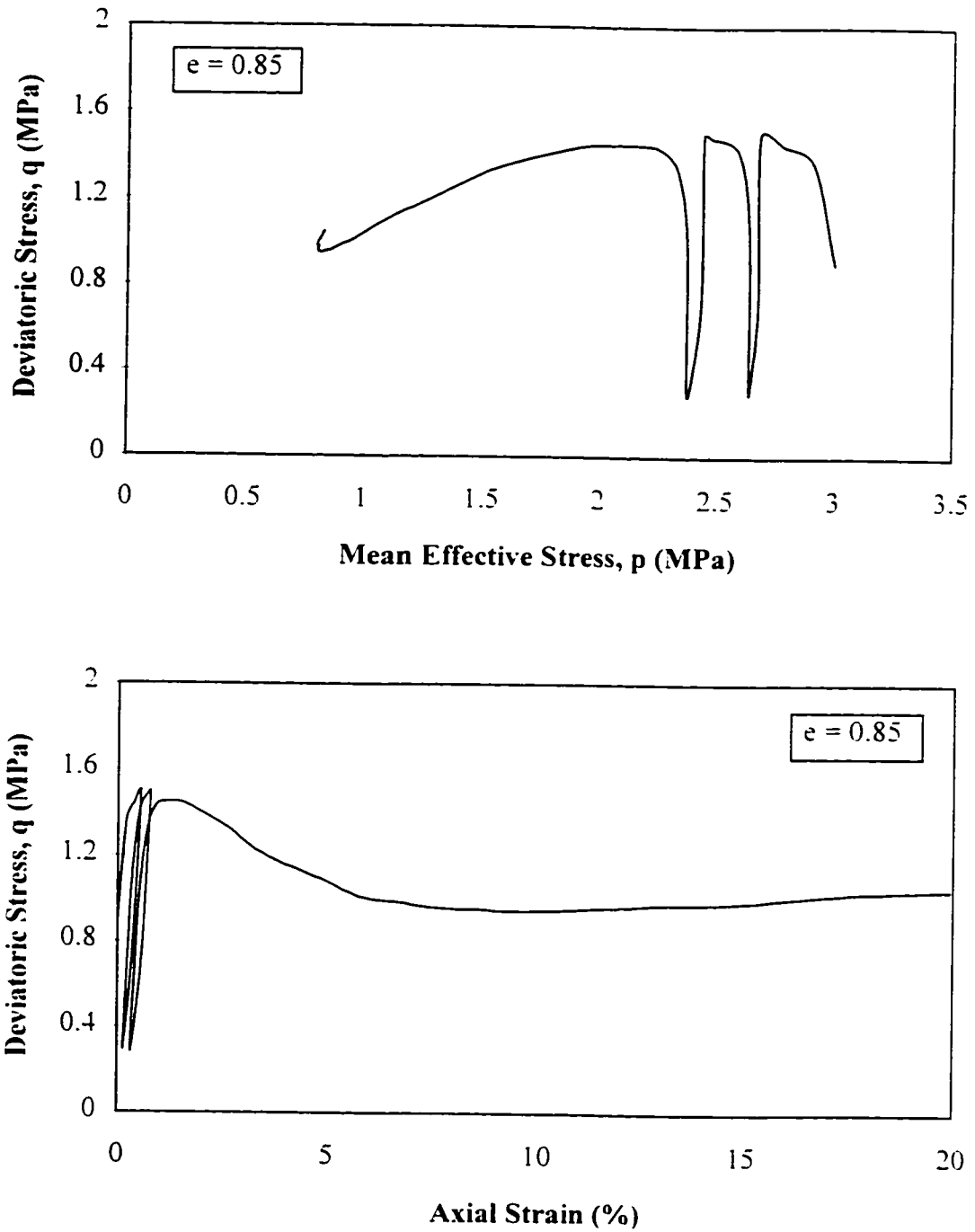
Figure 5.6. Predicted stress path and stress-strain curve during stress control undrained triaxial test on anisotropically consolidated sample at $e = 0.85$.
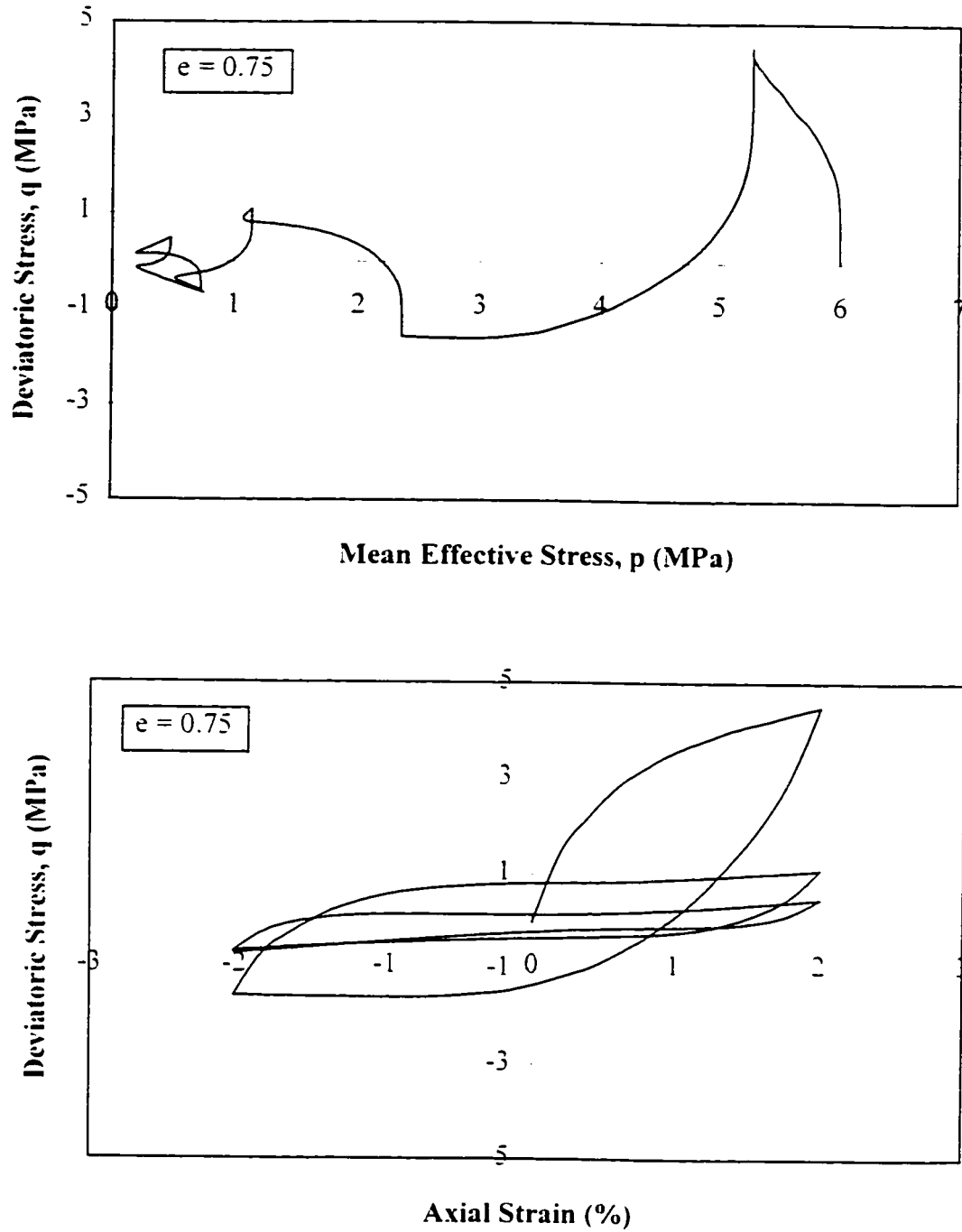
Figure 5.7. Predicted stress path and stress-strain curve during strain control undrained triaxial test at $e = 0.75$.
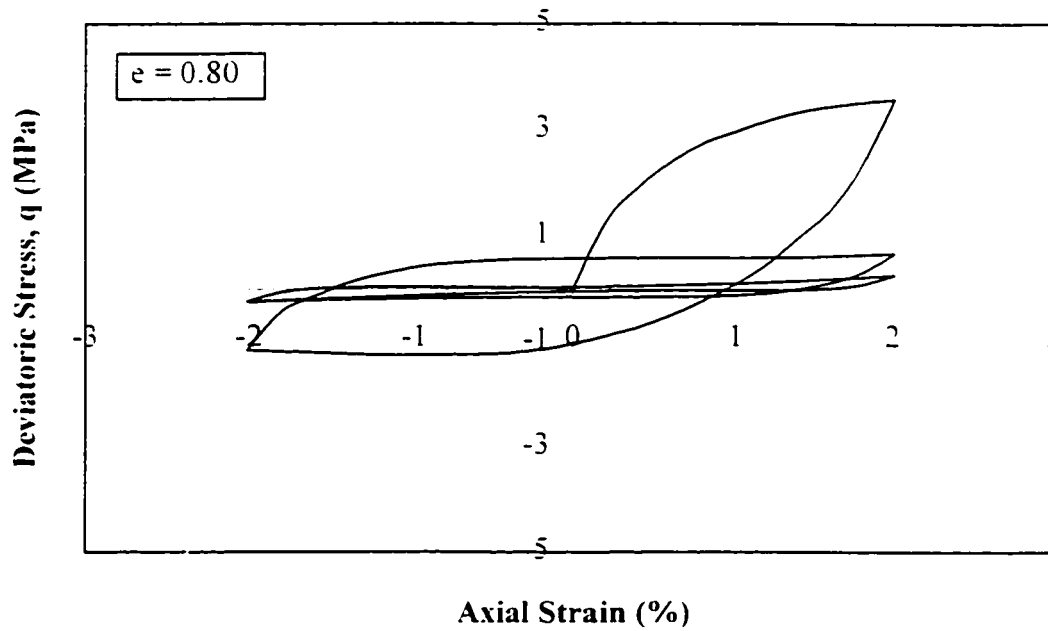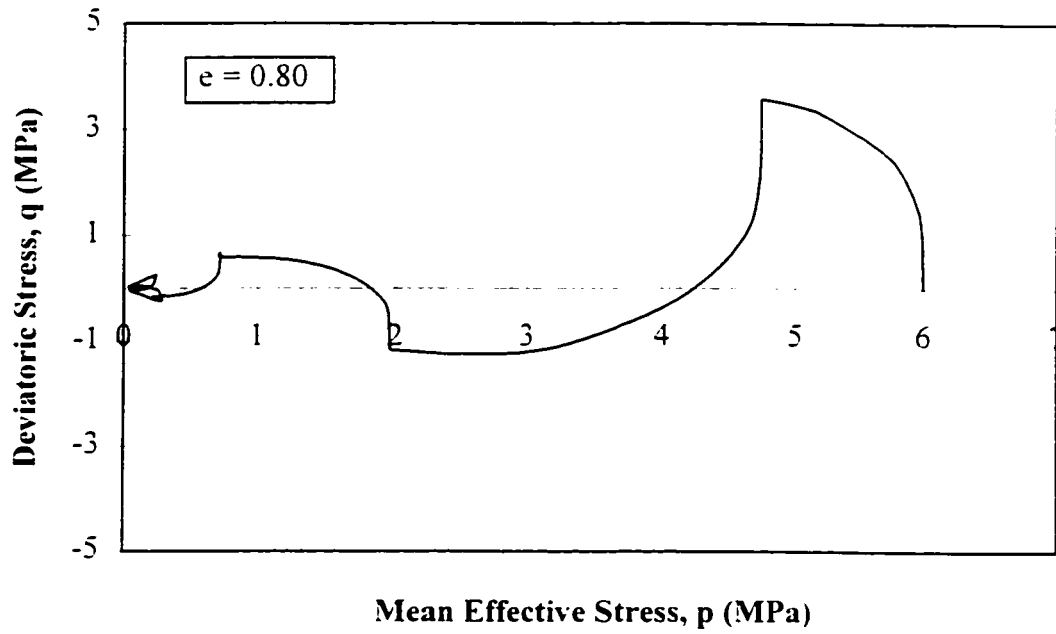
Figure 5.8. Predicted stress path and stress-strain curve during strain control undrained triaxial test at *e* = 0.80.
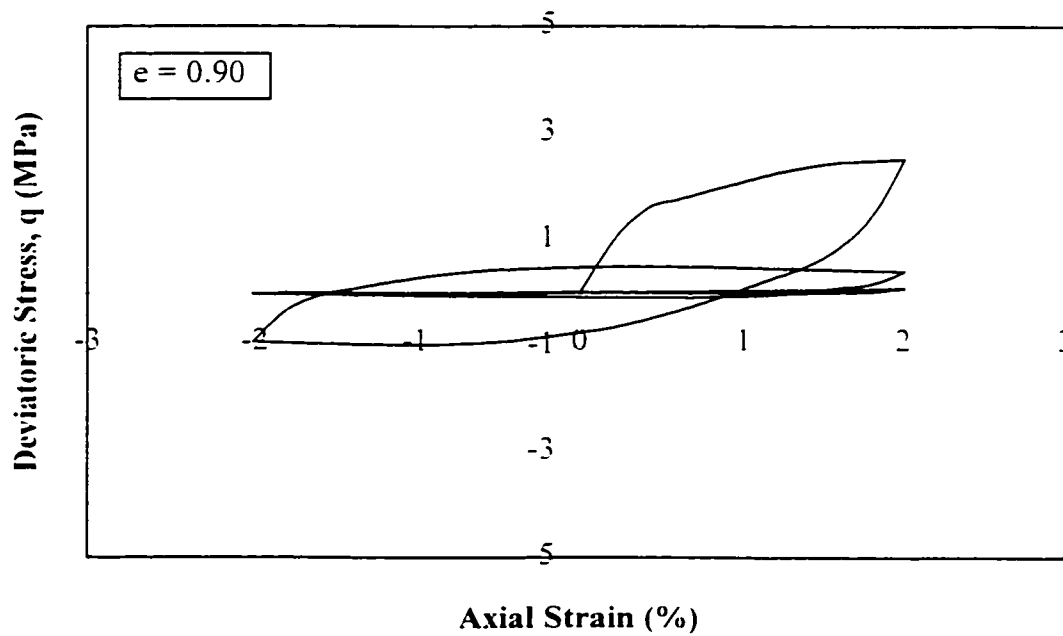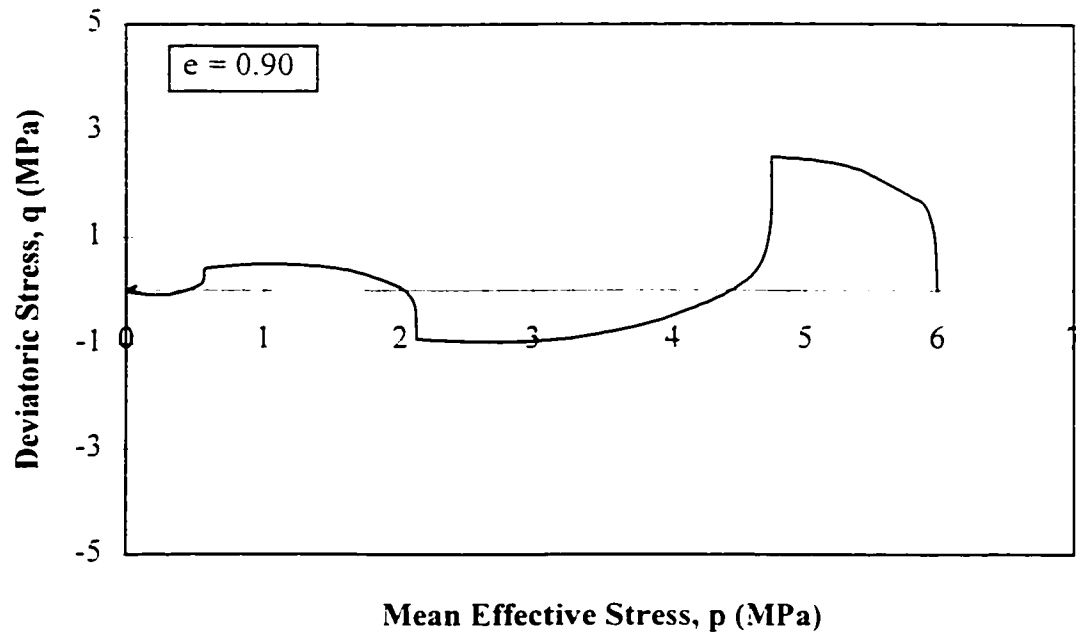
Figure 5.9. Predicted stress path and stress-strain curve during strain control undrained triaxial test at $e = 0.90$.
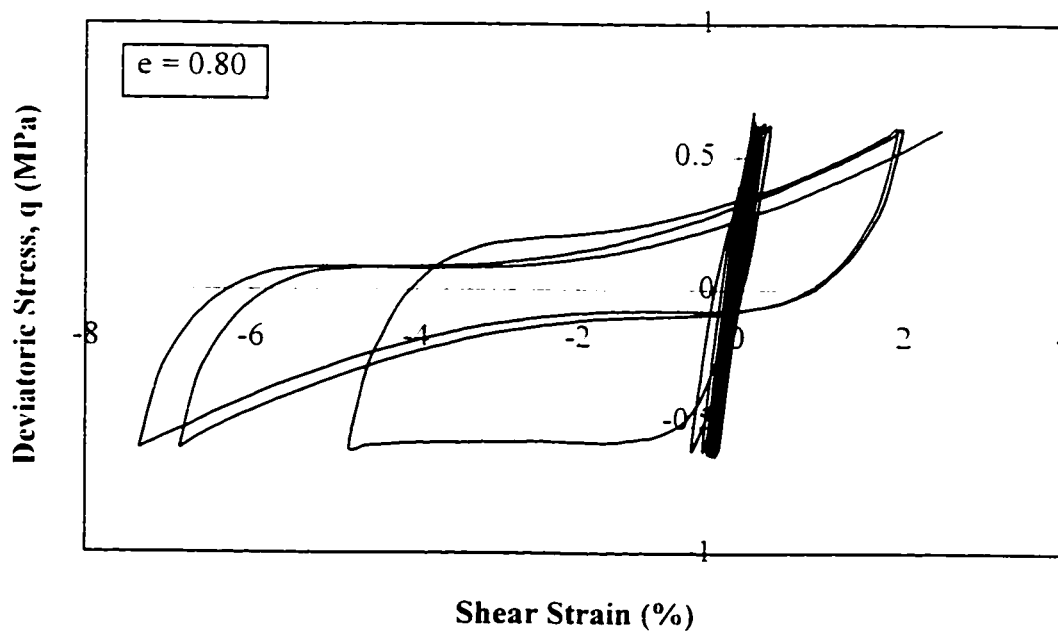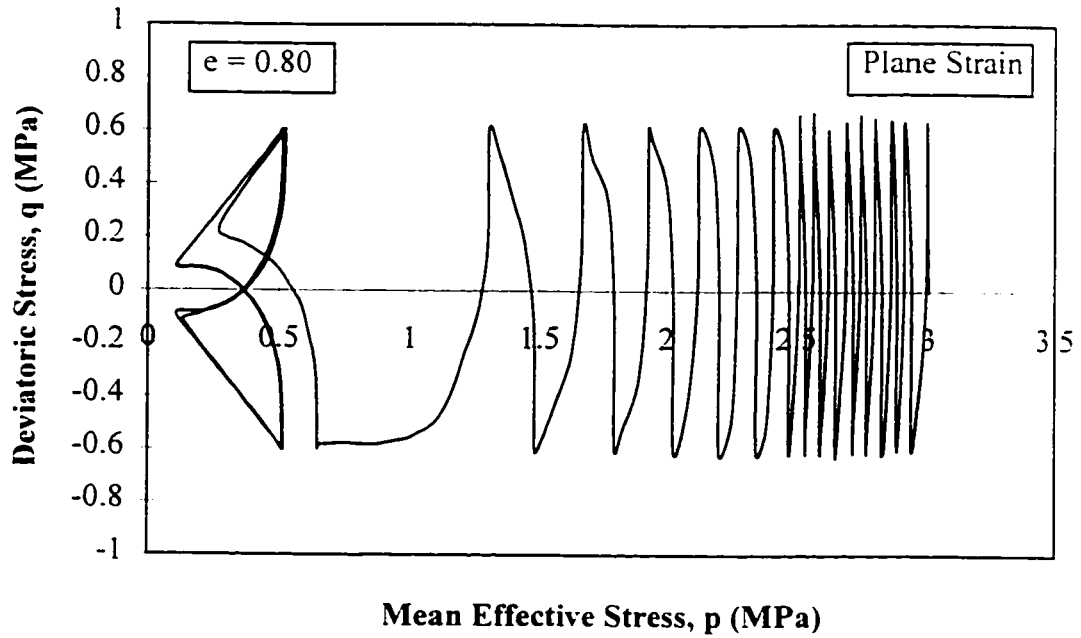
Figure 5.10. Predicted stress path and stress-strain curve during stress control undrained plane strain test at $e = 0.80$.

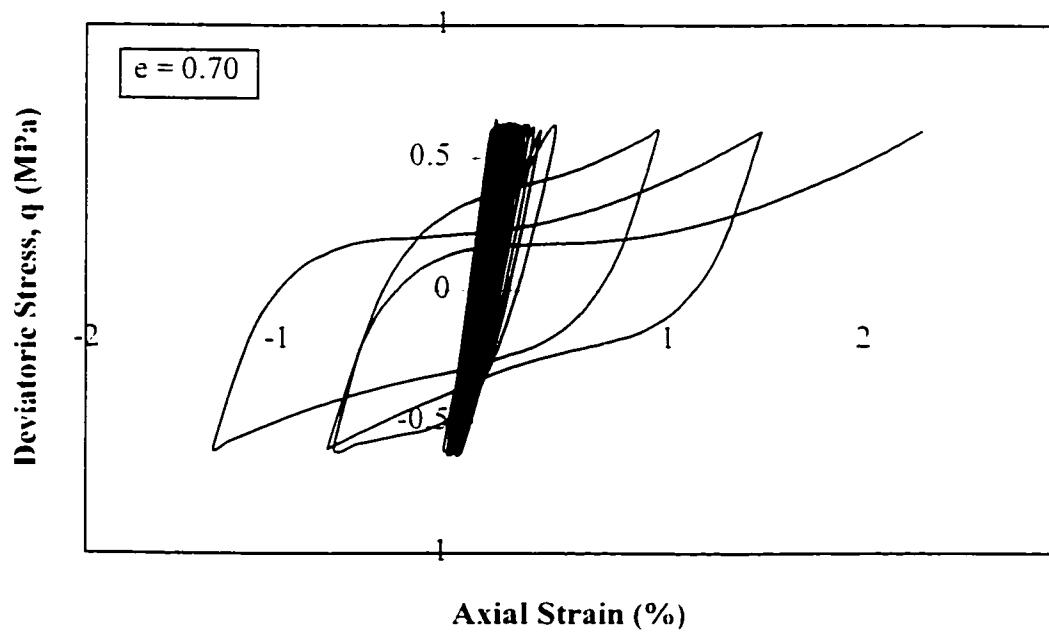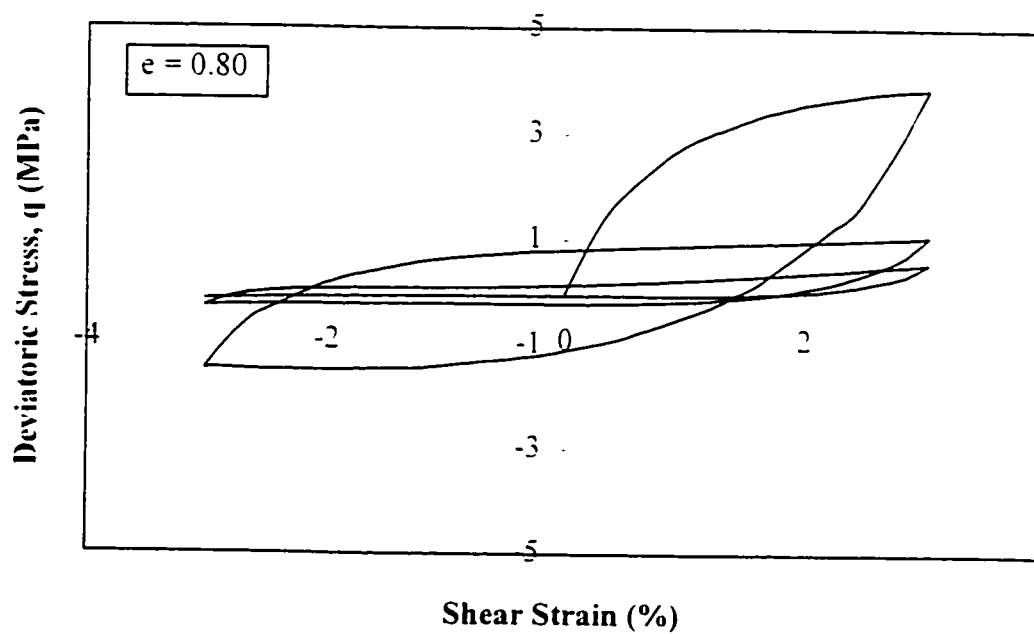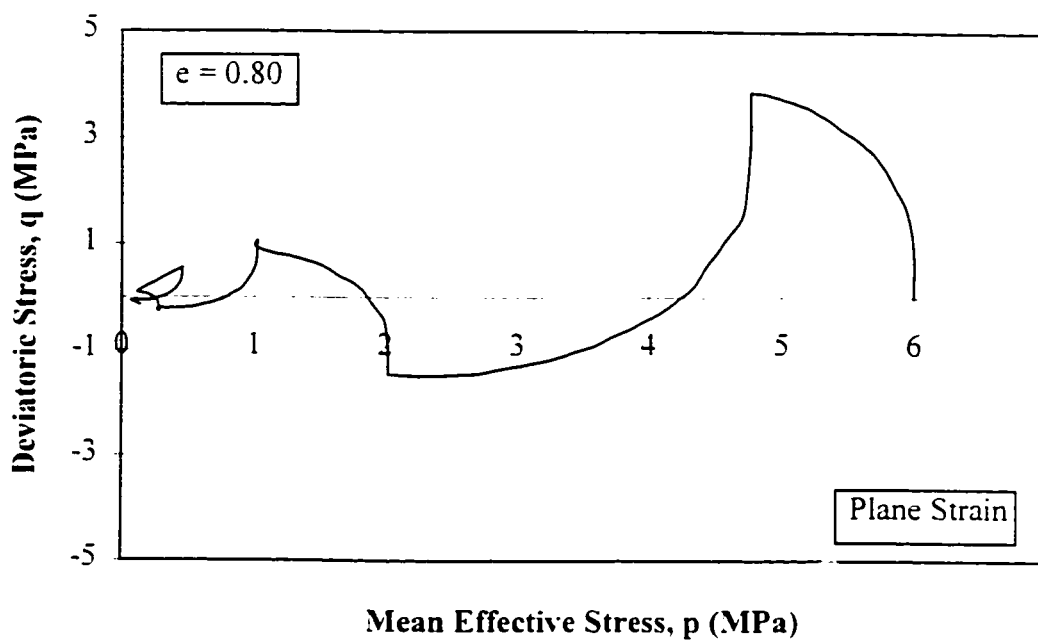**Figure 5.11.** Predicted stress path and stress-strain curve during strain control undrained plane strain test at $e = 0.80$.
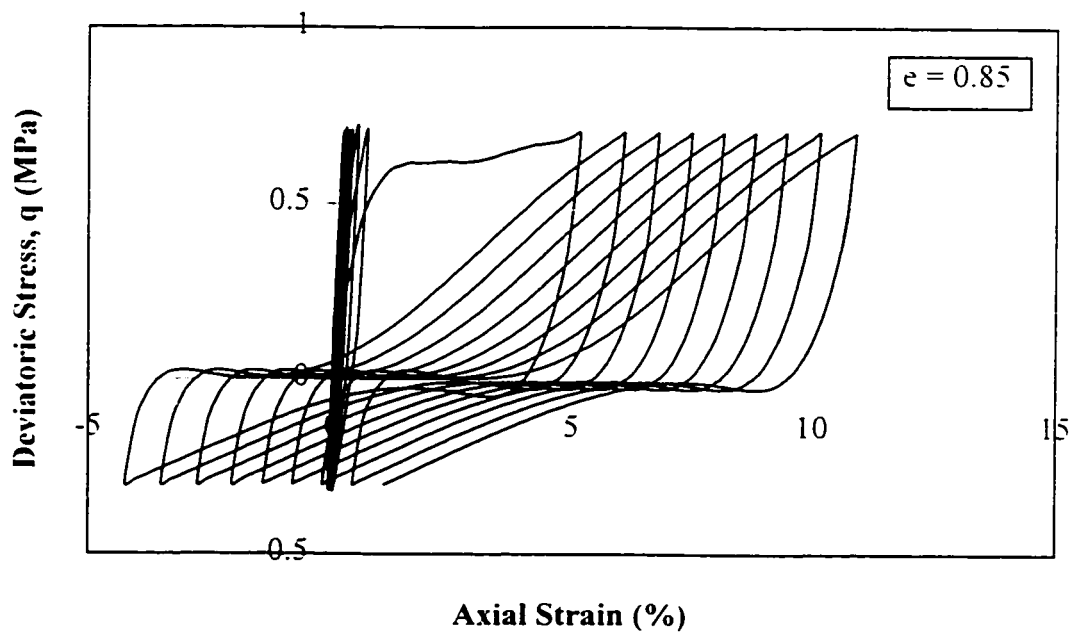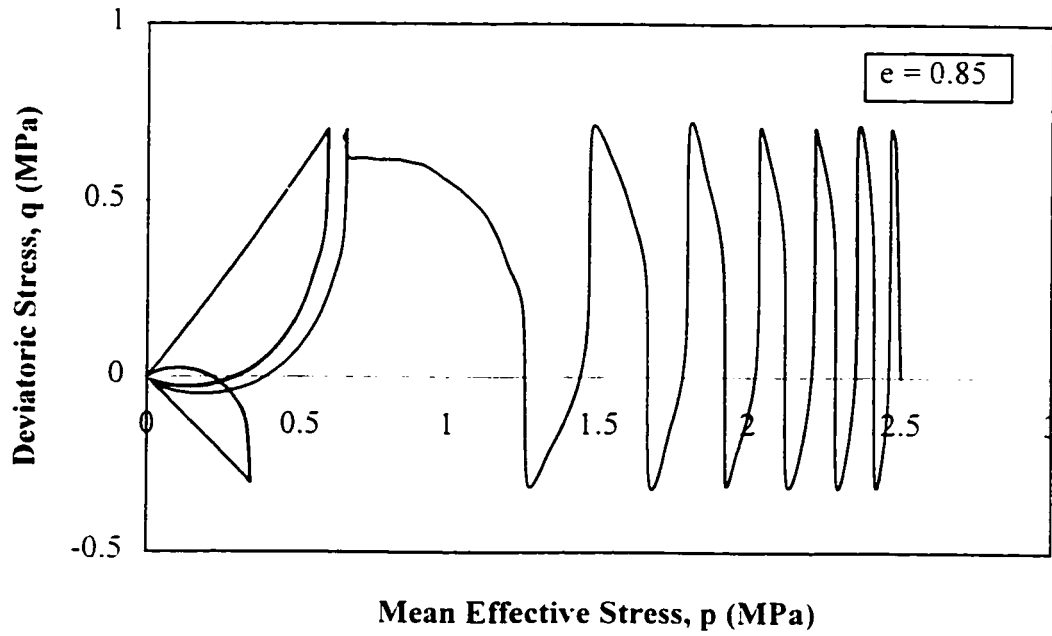
Figure 5.12. Predicted stress path and stress-strain curve during stress control undrained triaxial test in which flow deformation and cyclic mobility have been occured.
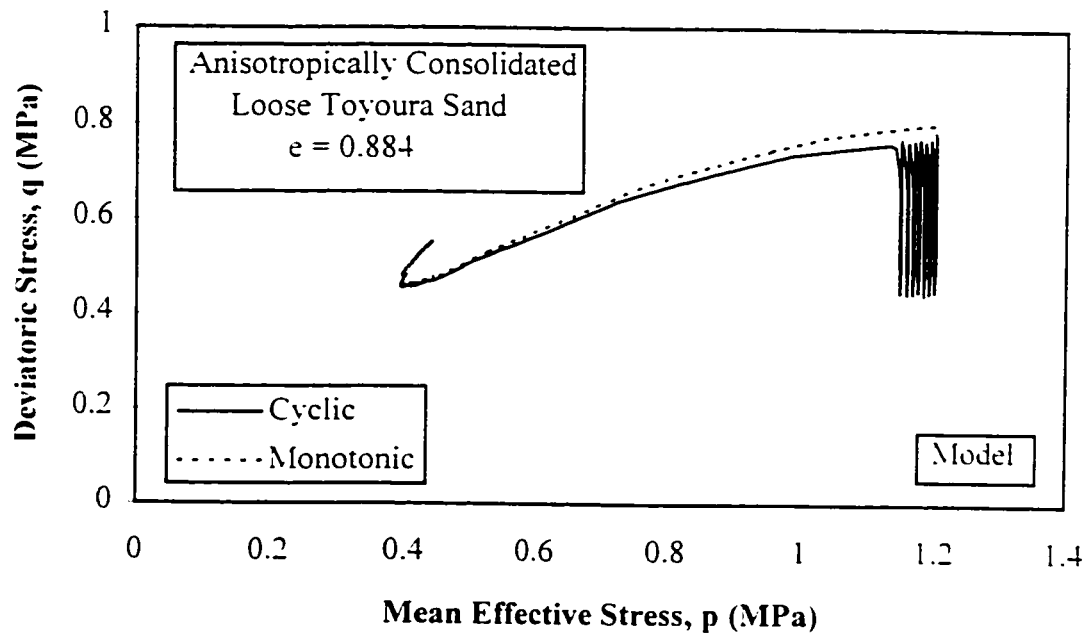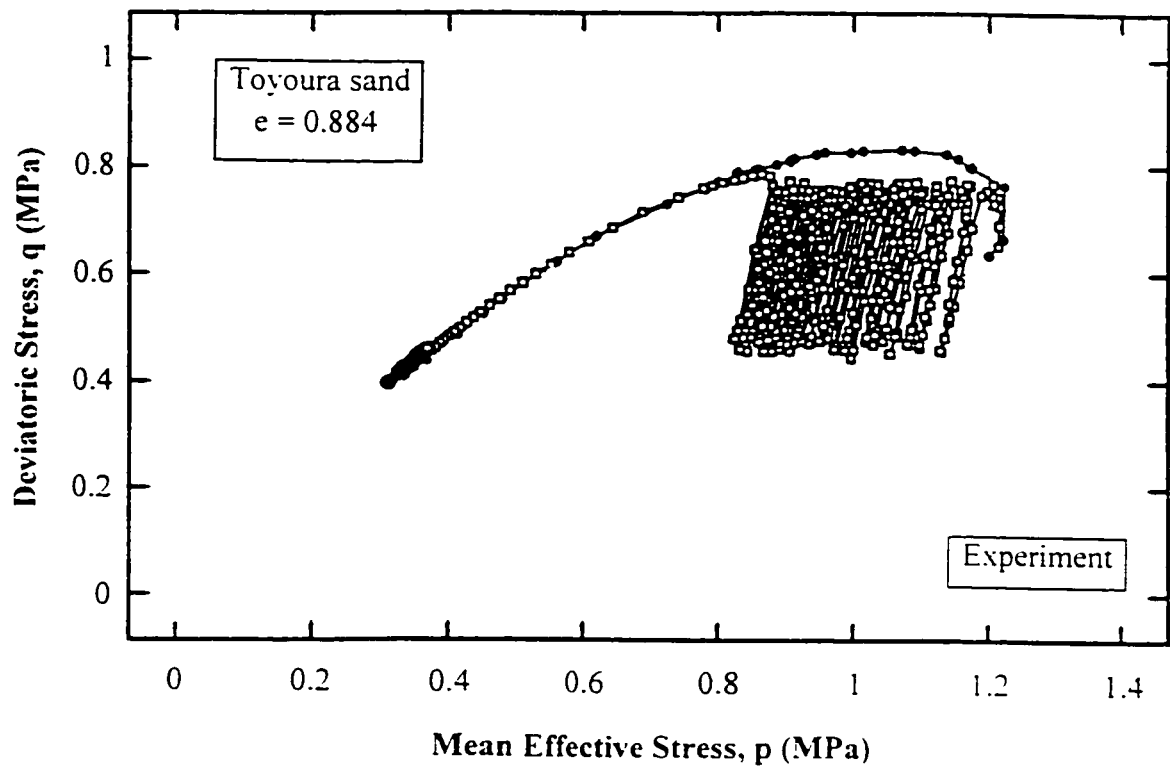
Figure 5.13. Comparison of model predictions with experimental observations on anisotropically consolidated loose samples of Toyoura sand during undrained triaxial tests (stress path).
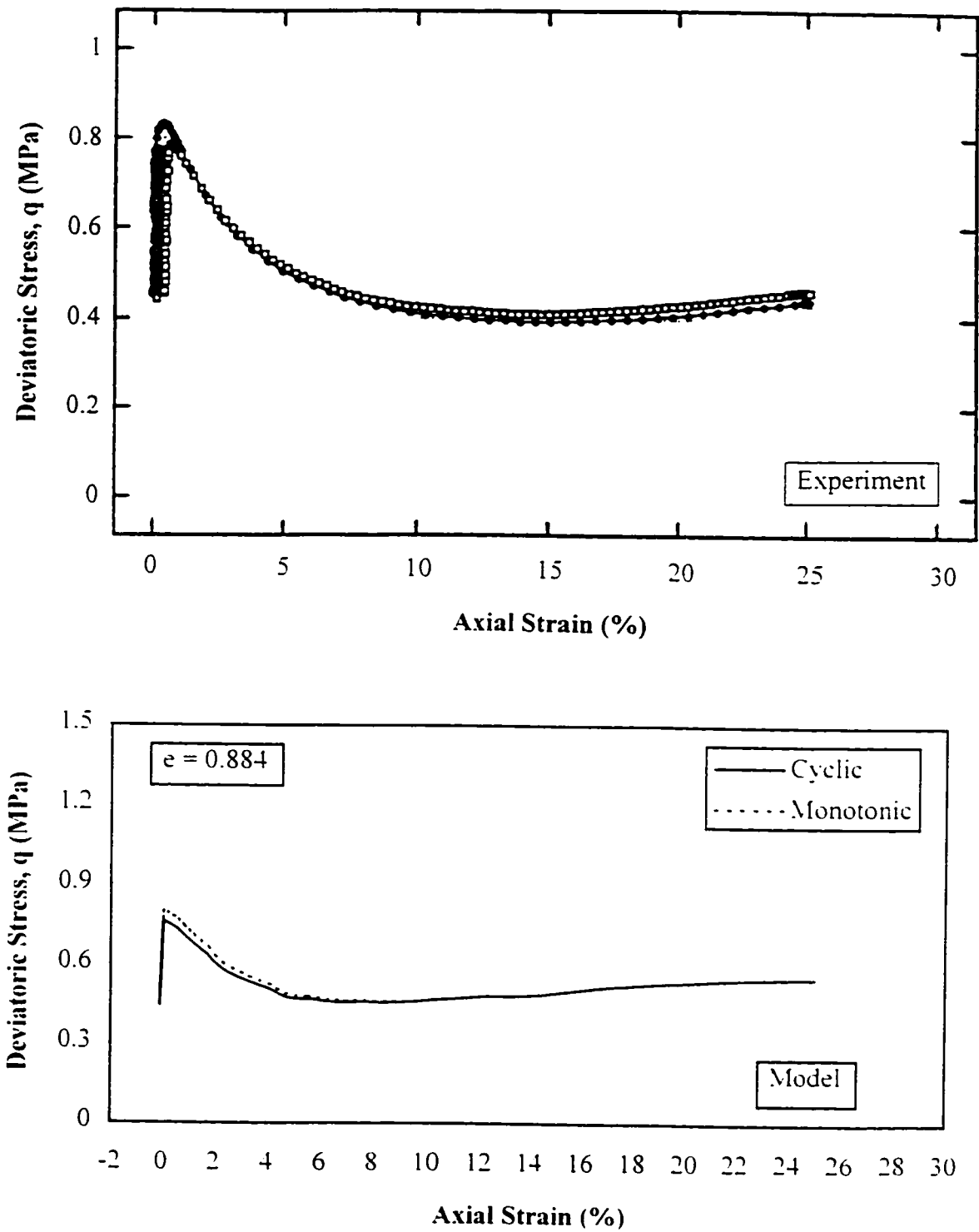
Figure 5.14. Comparison of model predictions with experimental observations on anisotropically consolidated loose samples of Toyoura sand during undrained triaxial tests (stress-strain curve).
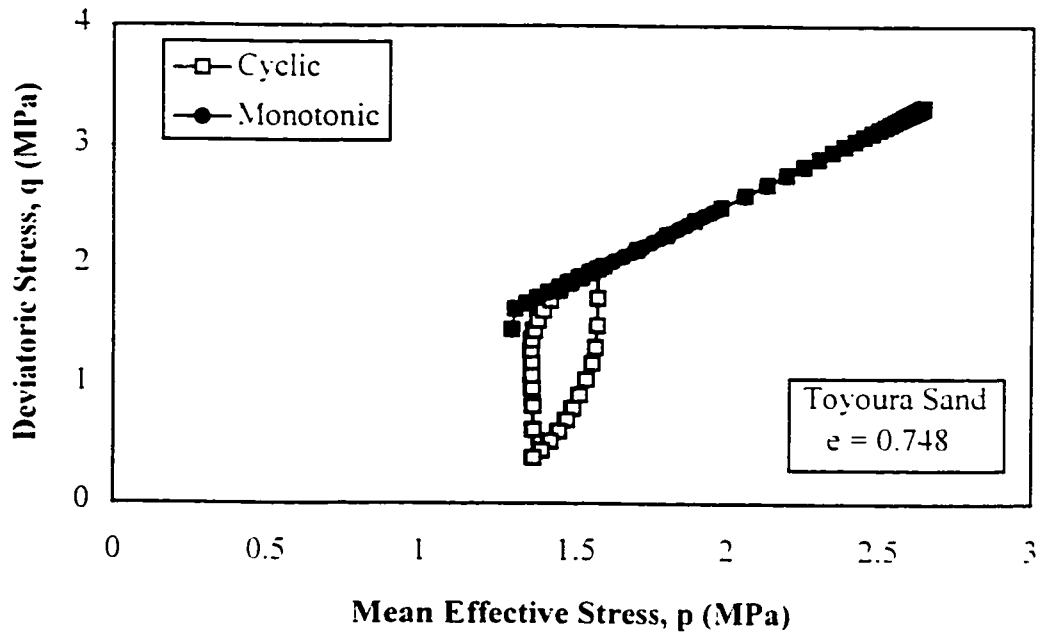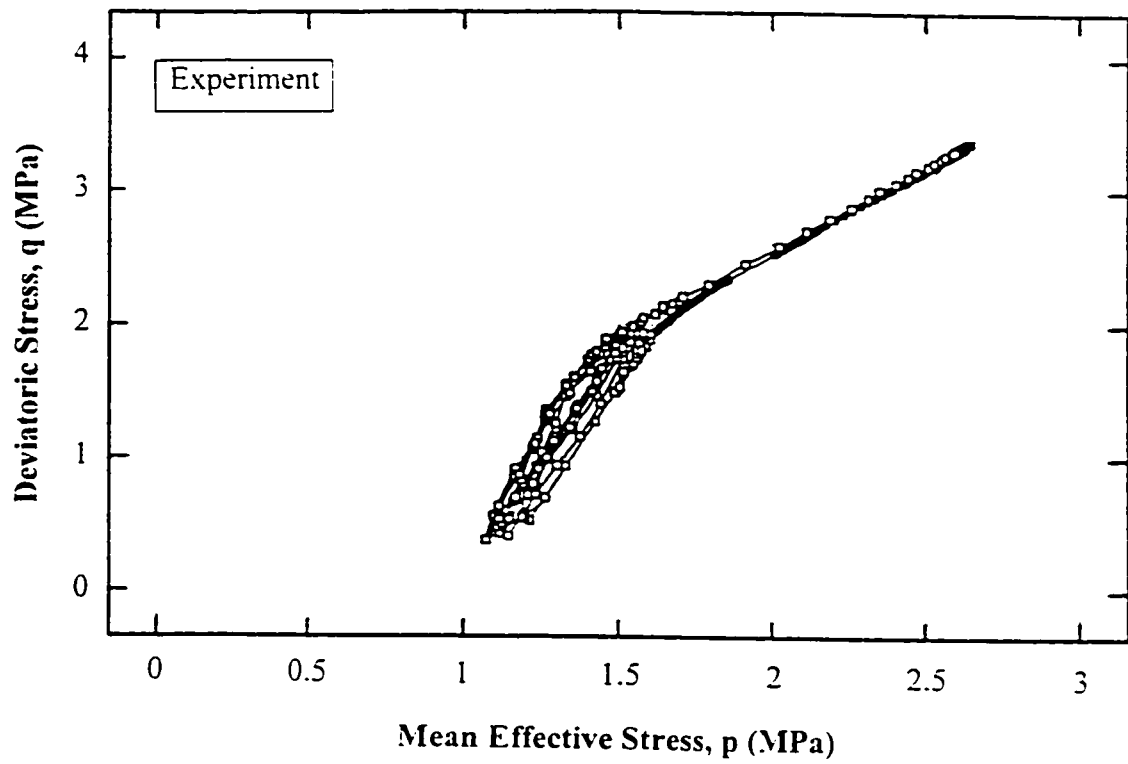
Figure 5.15. Comparison of model predictions with experimental observations on anisotropically consolidated dense samples of Toyoura sand during undrained triaxial tests (stress path).
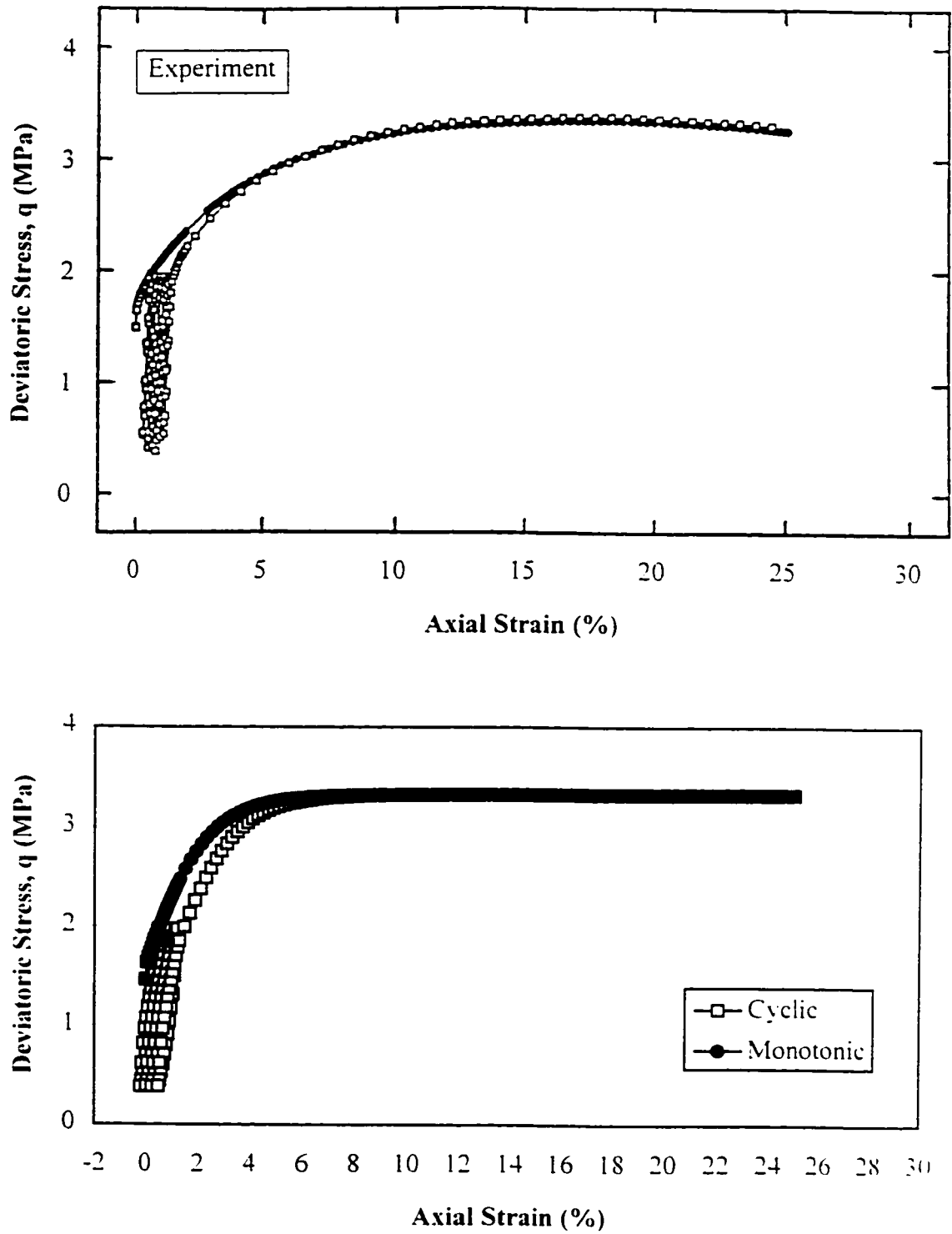
Figure 5.16. Comparison of model predictions with experimental observations on anisotropically consolidated dense samples of Toyoura sand during undrained triaxial tests (stress-strain curve).
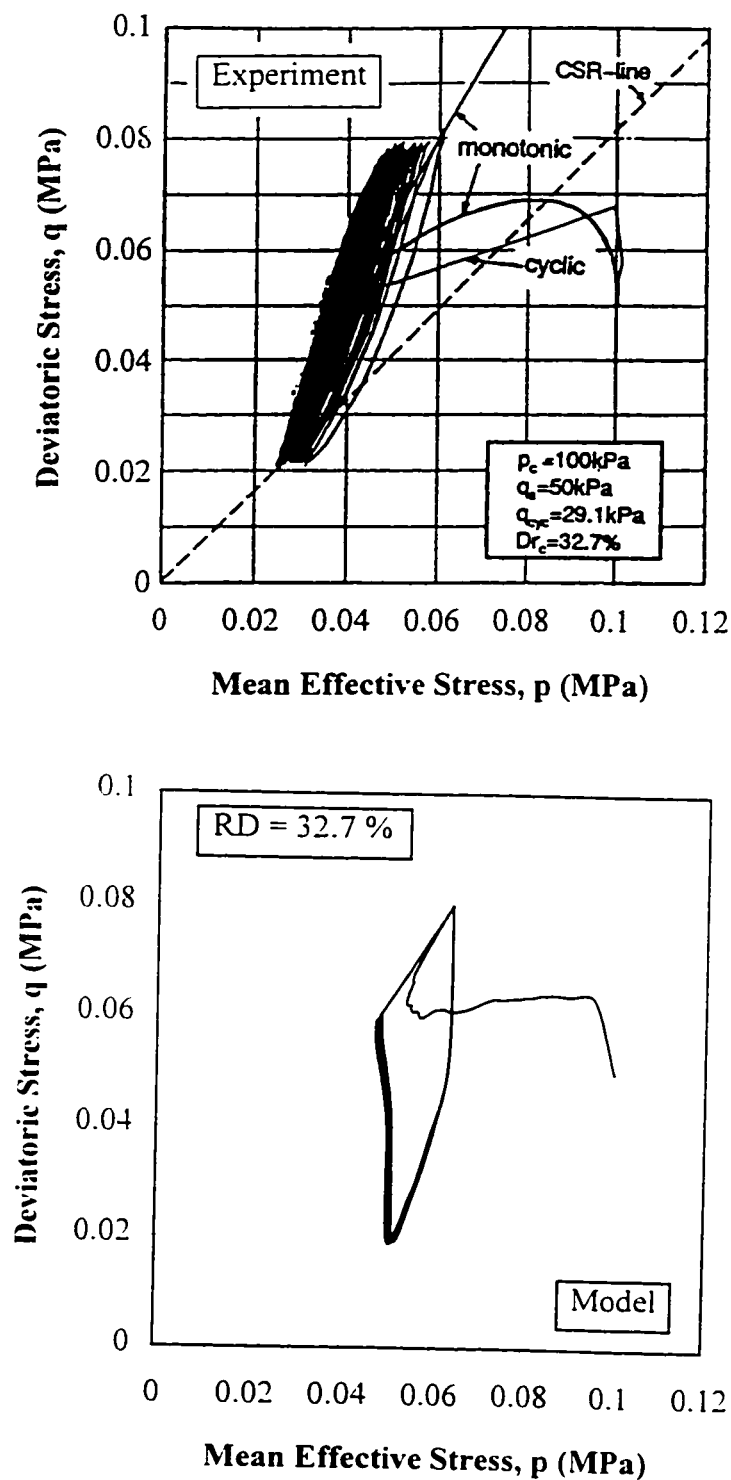
Figure 5.17. Comparison of model predictions with experimental observations on anisotropically consolidated loose samples of Toyoura sand during undrained triaxial tests in which flow deformation and cyclic mobility have occured consequently (stress path).
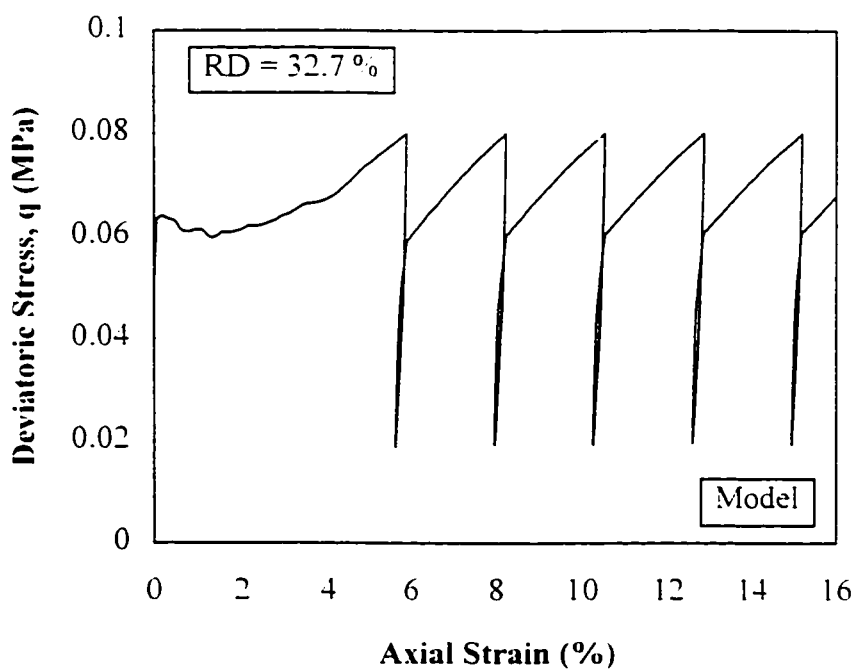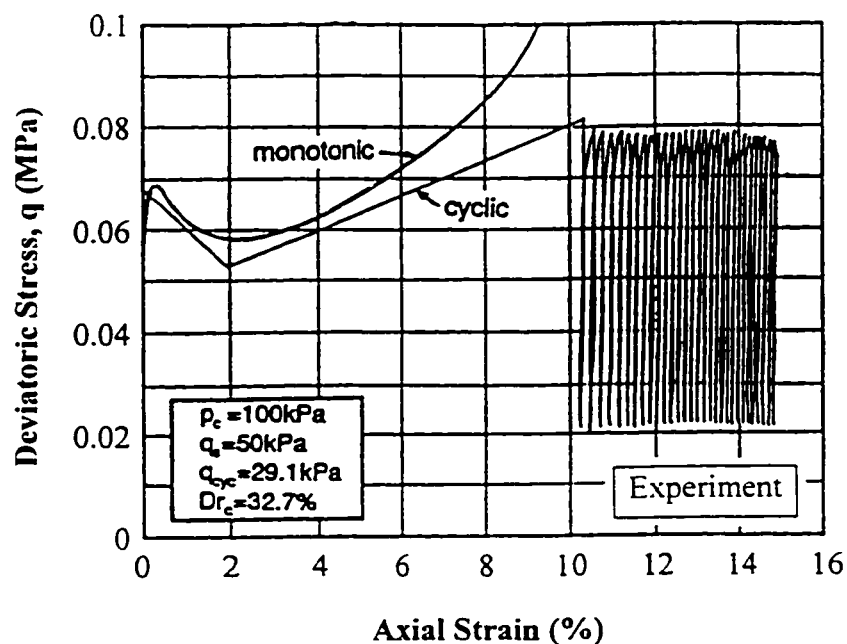
Figure 5.18. Comparison of model predictions with experimental observations on anisotropically consolidated loose samples of Toyoura sand during undrained triaxial tests in which flow deformation and cyclic mobility have occured consequently (stress-strain curve).
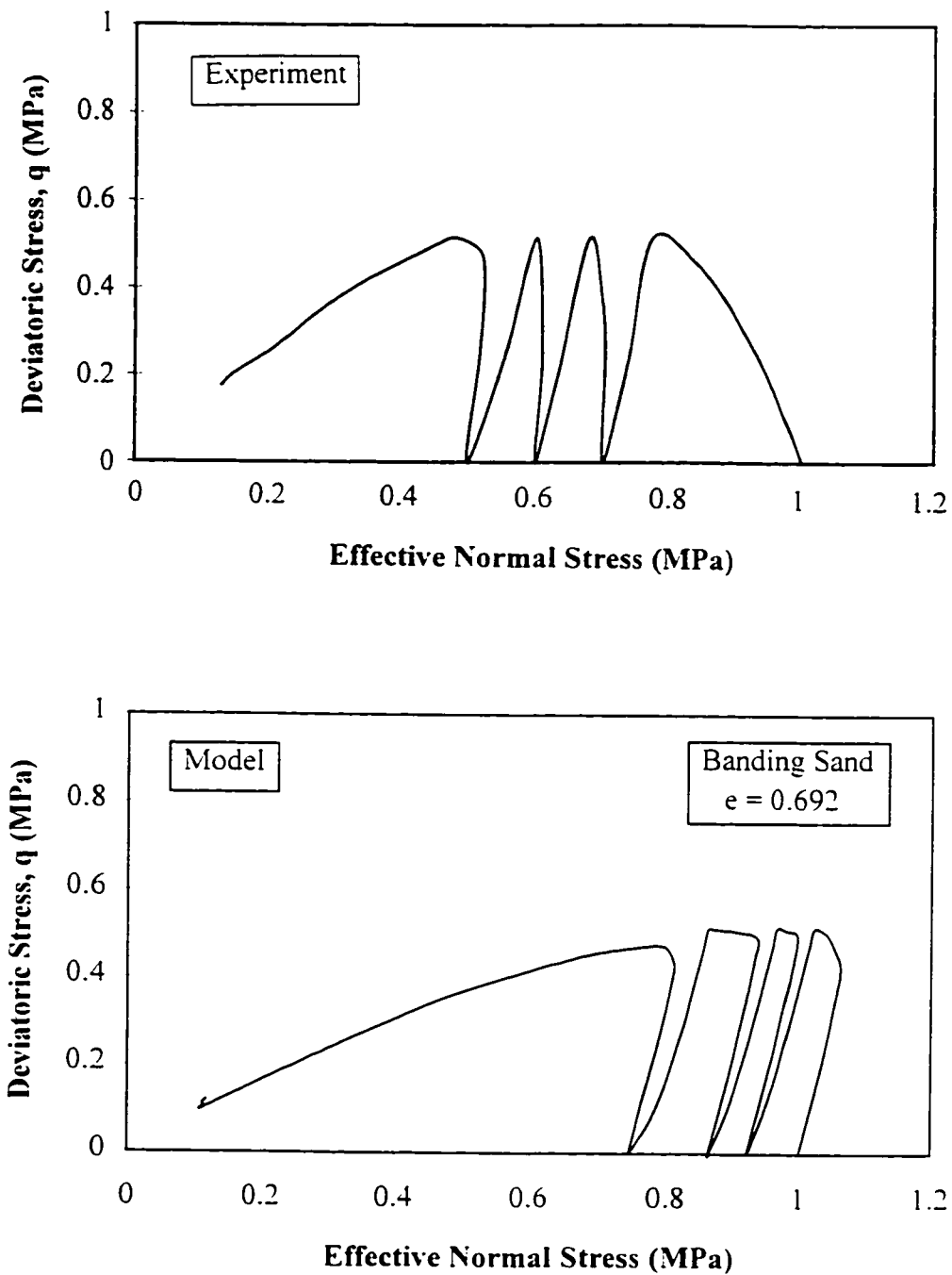
Figure 5.19. Comparison of model prediction with experimental observations on Banding sand during undrained triaxial test at $e = 0.692$ (stress path).
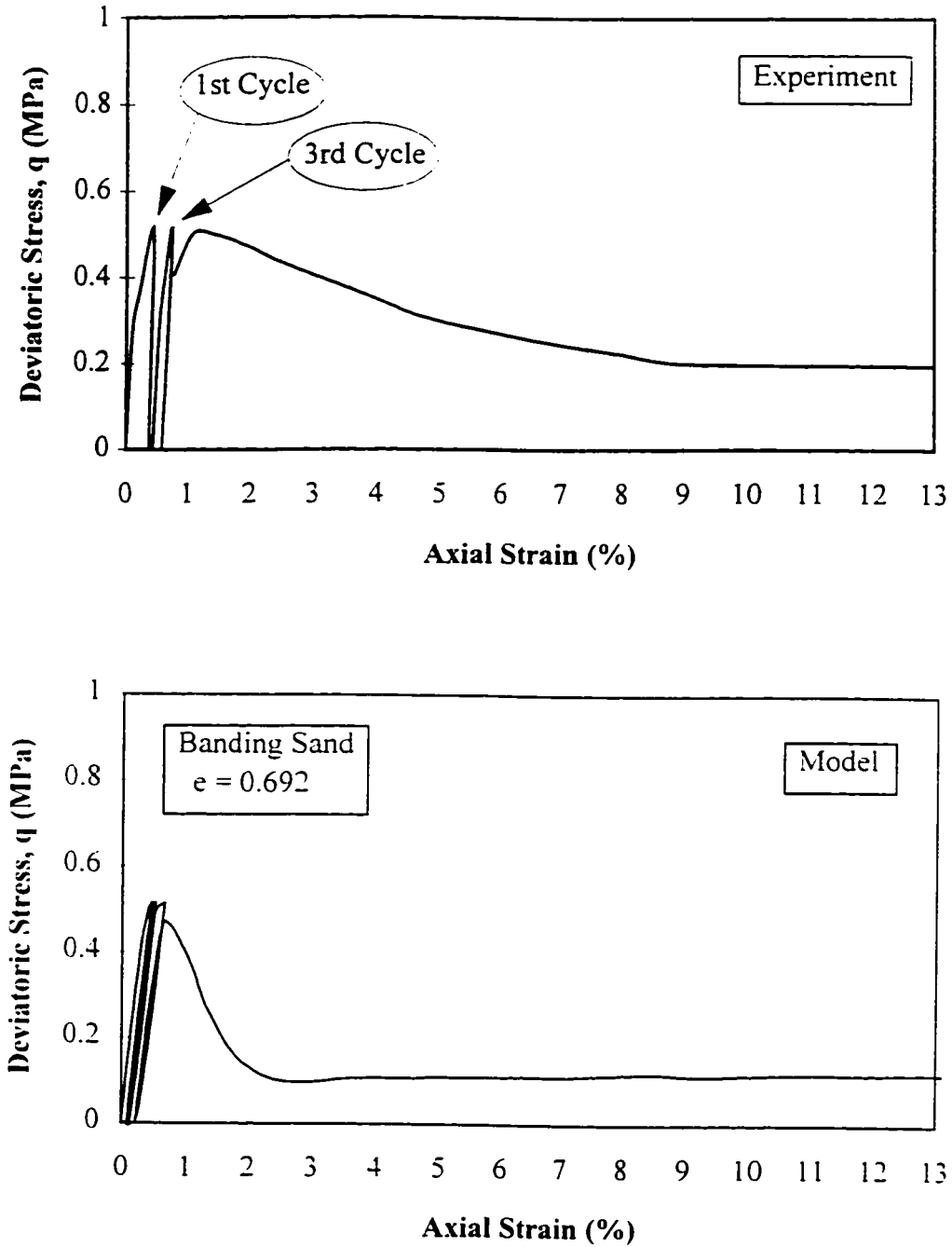
Figure 5.20. Comparison of model predictions with experimental observation on Banding sand during undrained triaxial test at $e = 0.692$ (stress-strain curve).
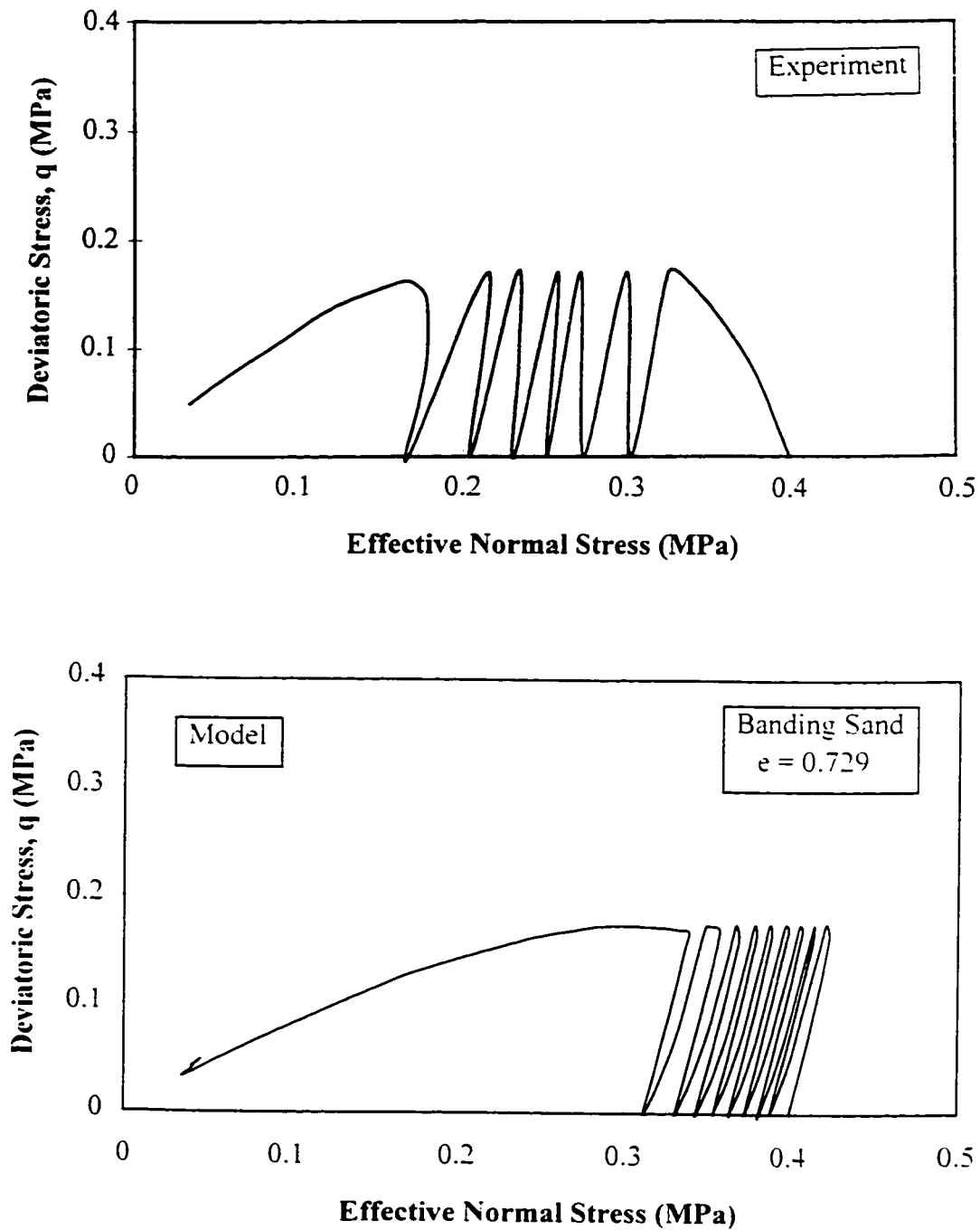
Figure 5.21. Comparison of model prediction with experimental observations on Banding sand during undrained triaxial test at $e = 0.729$ (stress path).
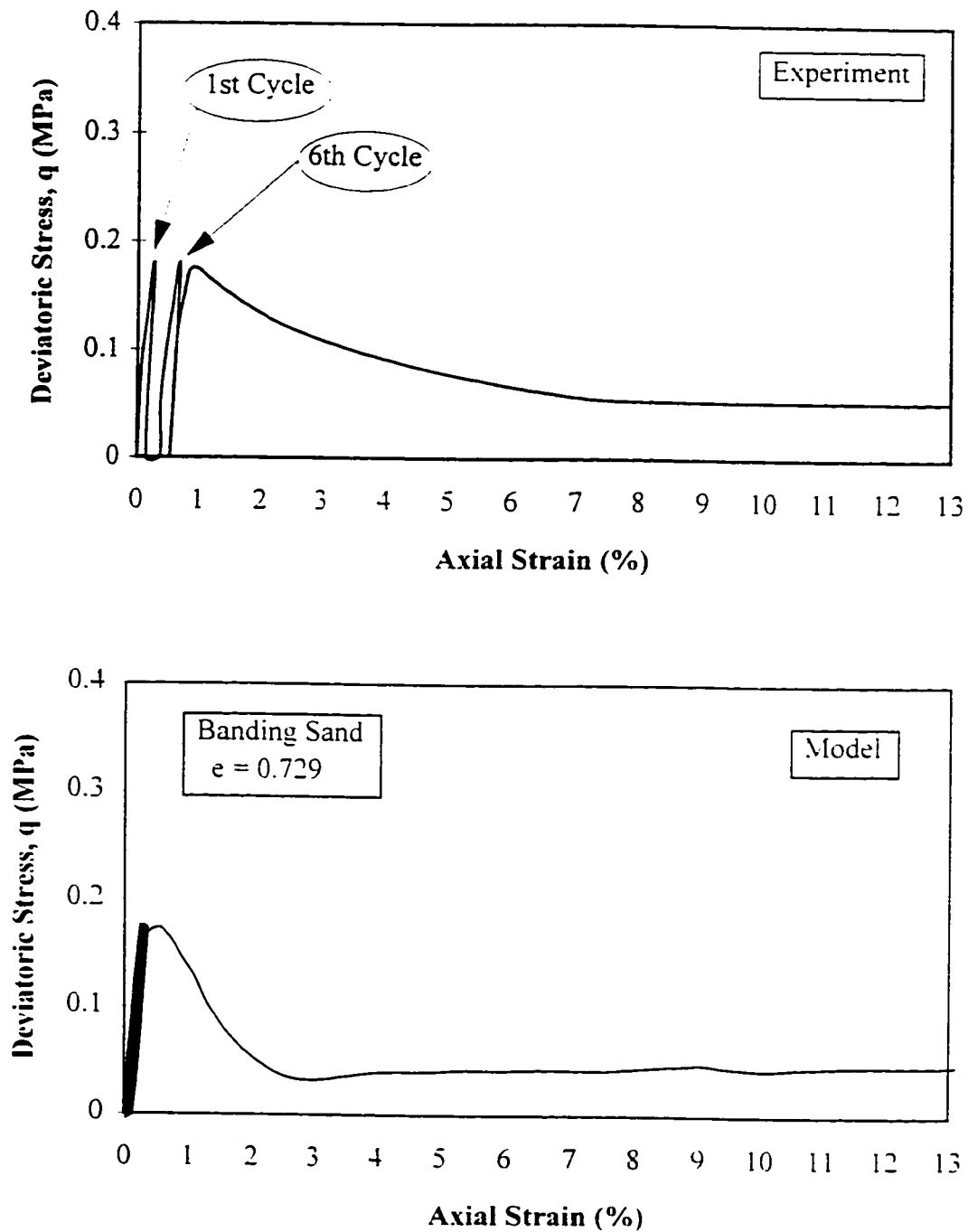
Figure 5.22. Comparison of model predictions with experimental observation on Banding sand during undrained triaxial test at $e = 0.729$ (stress-strain curve).
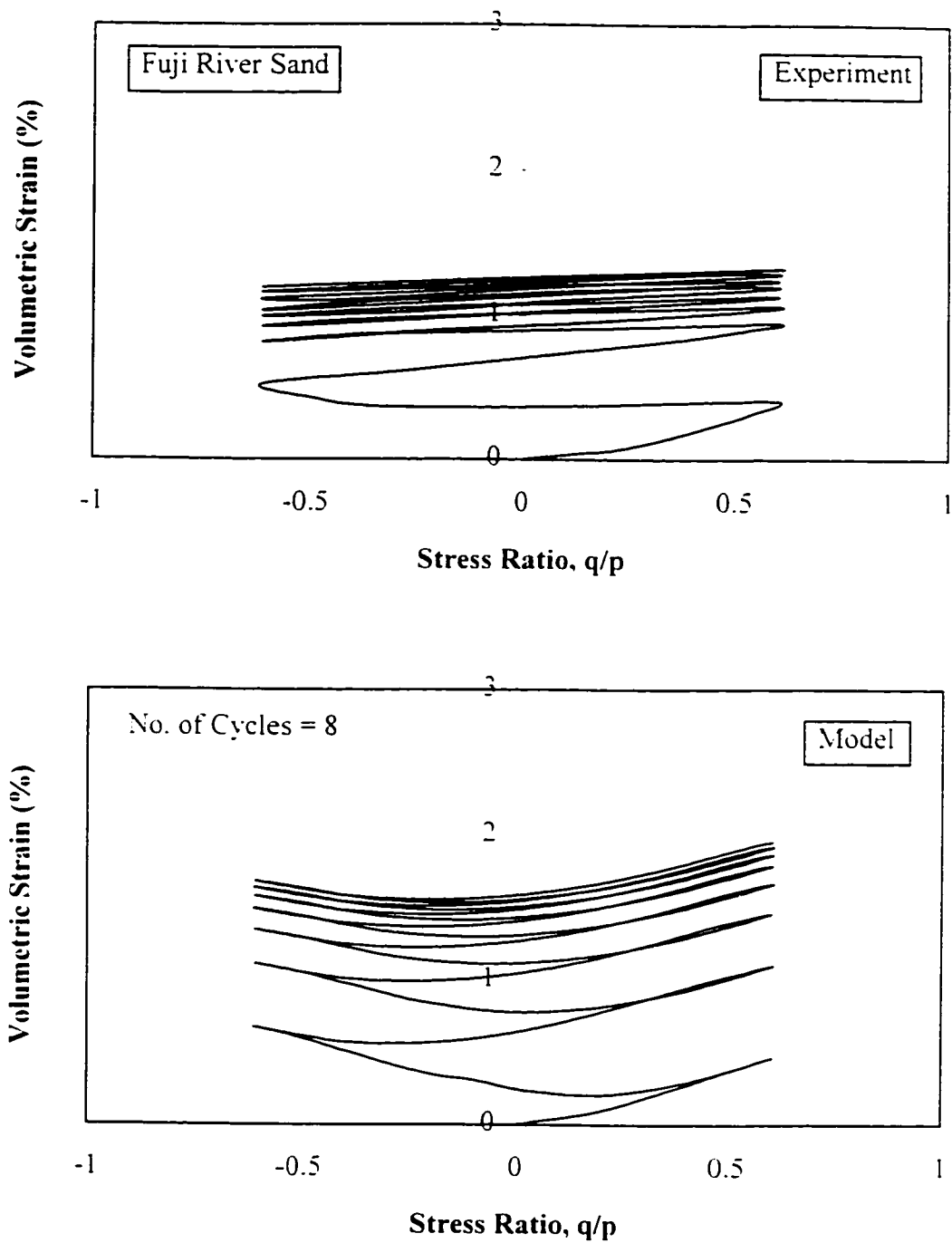
Figure 5.23. Comparison of model prediction with experimental observation on Fuji River sand during drained triaxial test with small amplitude of stress ratio (Volumetric strain-stress ratio).
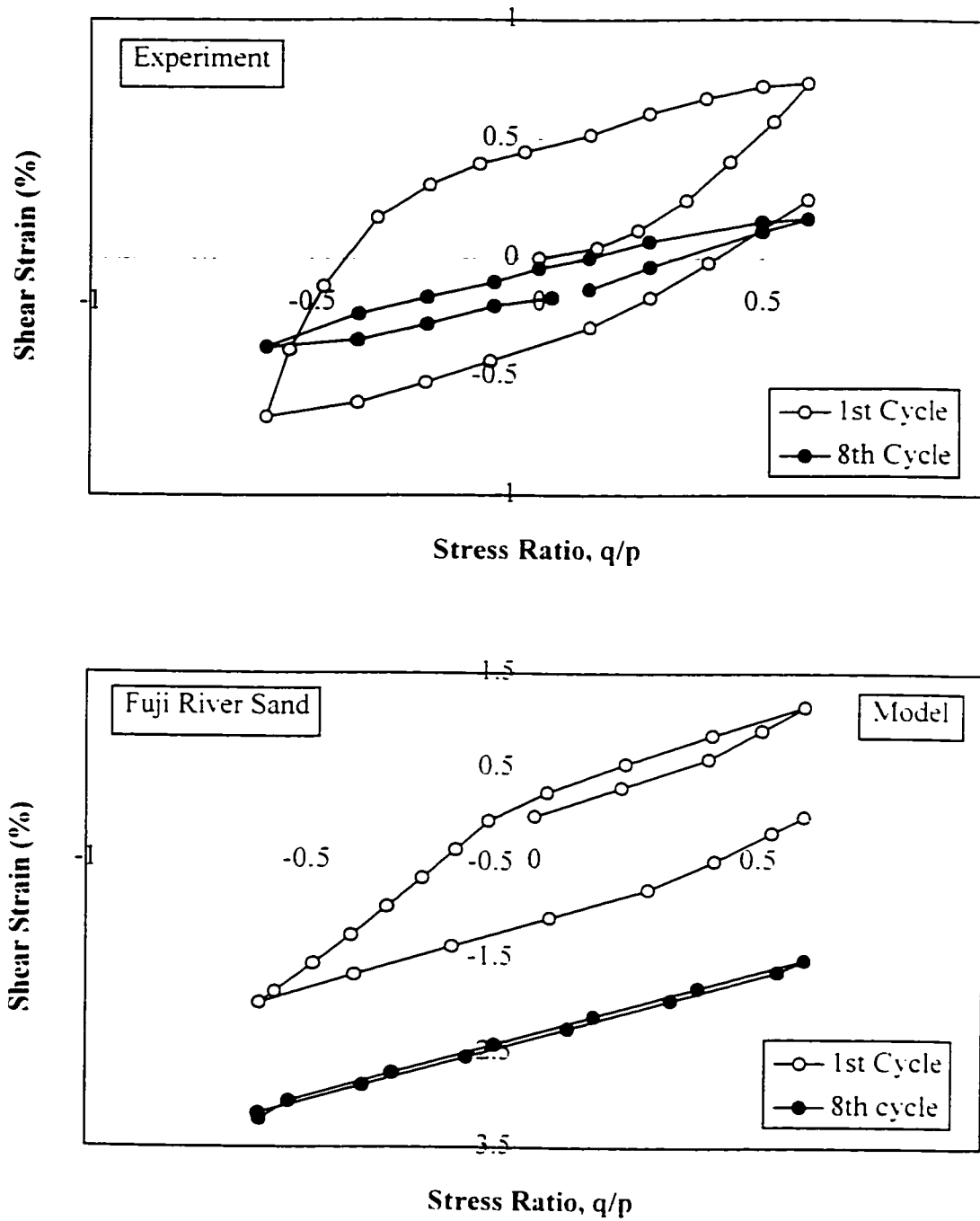
Figure 5.24. Comparison of model prediction with experimental observation on Fuji River sand during drained triaxial test with small amplitude of stress ratio (Shear strain-stress ratio).
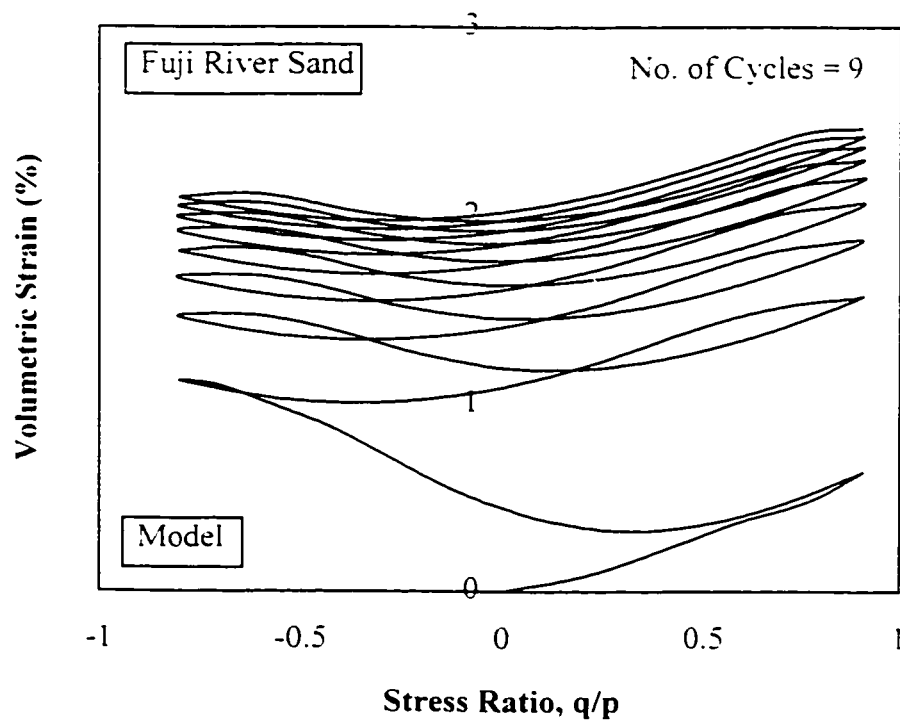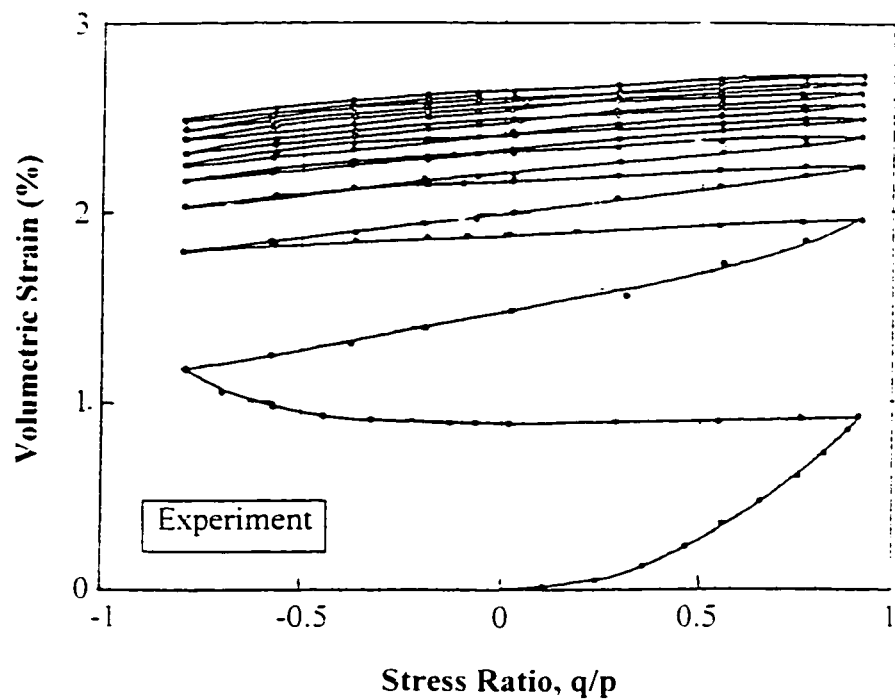
Figure 5.25. Comparison of model prediction with experimental observation on Fuji River sand during drained triaxial test with large amplitude of stress ratio (Volumetric strain-stress ratio).
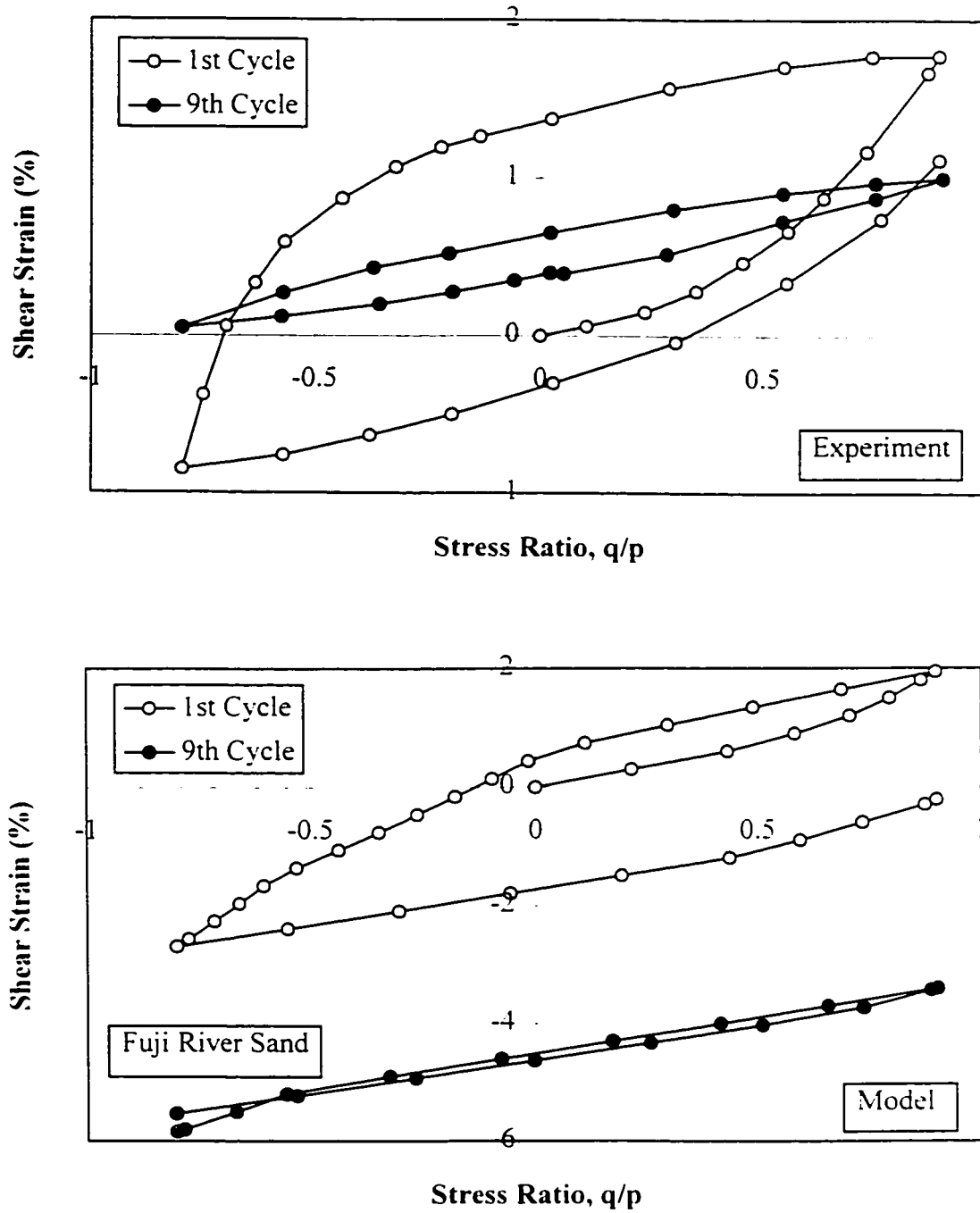
Figure 5.26. Comparison of model prediction with experimental observation on Fuji River sand during drained triaxial test with large amplitude of stress ratio (Shear strain-stress ratio).
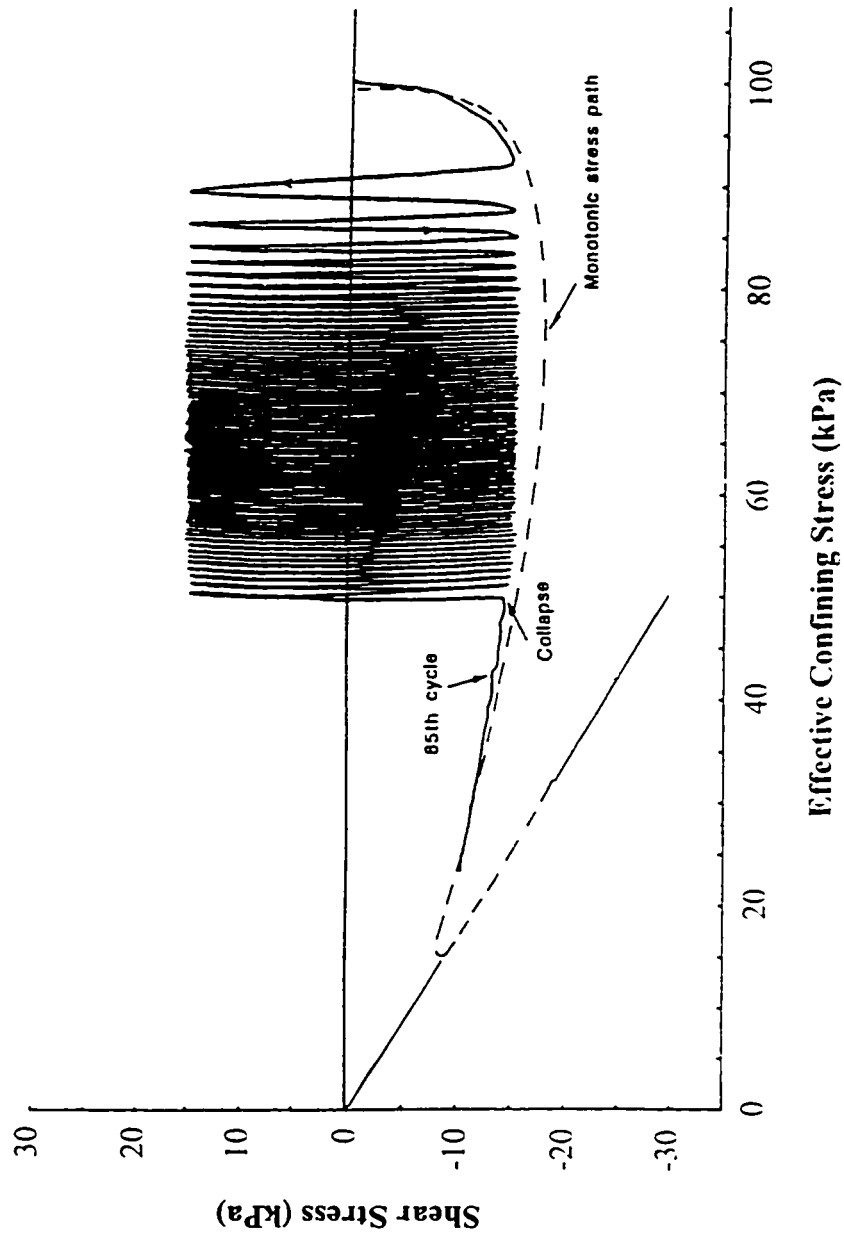
Figure 5.27. Experimental observation on collapse during monotonic and cyclic undrained torsional shear tests (after Alarcon et al., 1988).
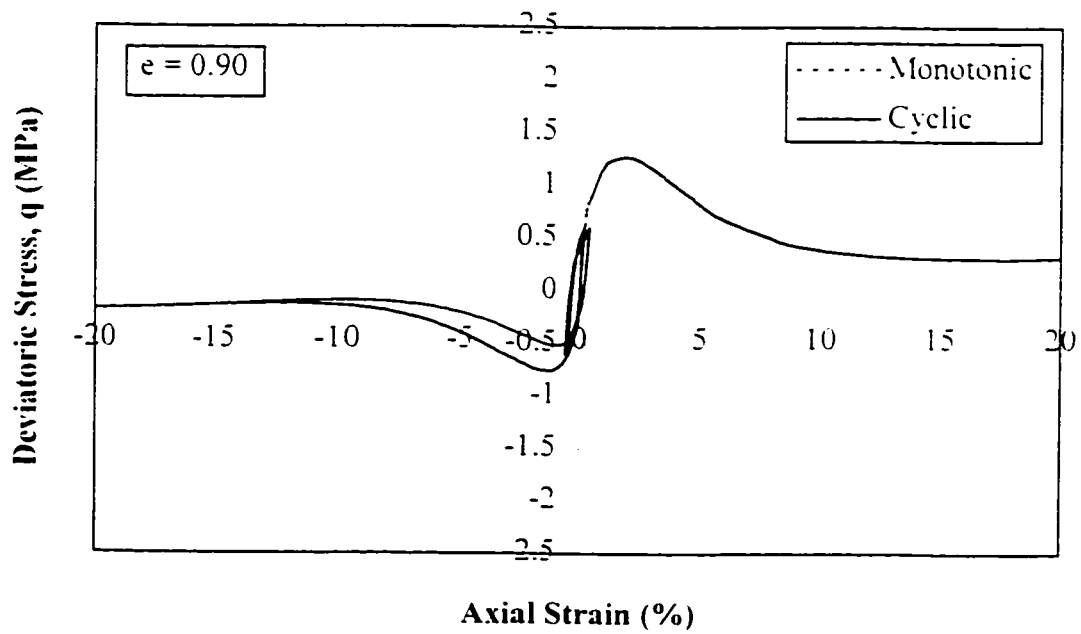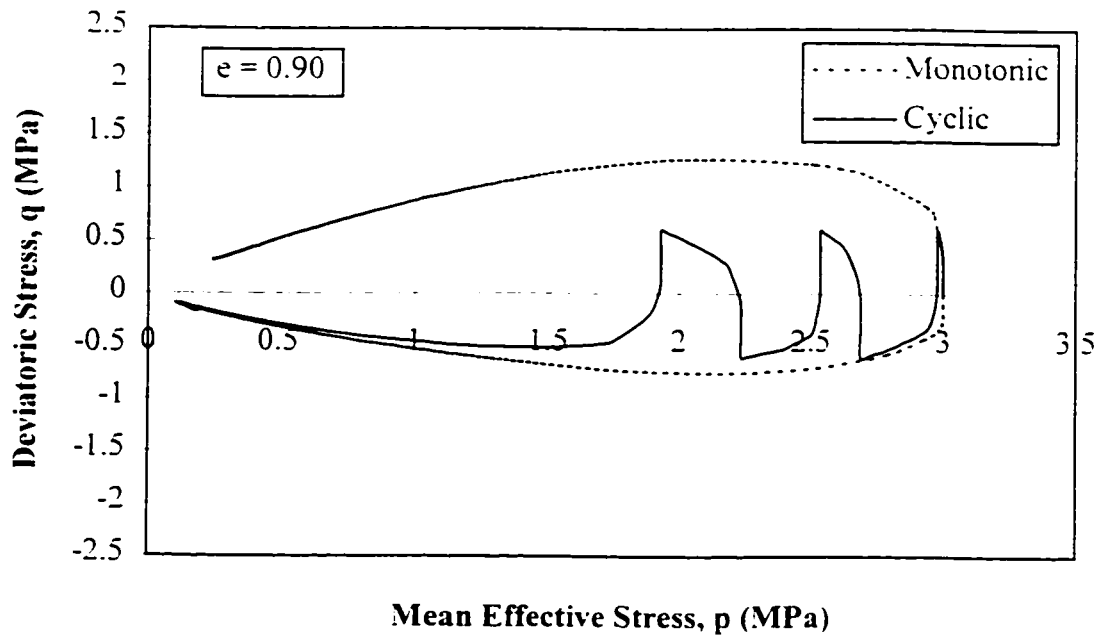
Figure 5.28. Predicted collapse during monotonic and cyclic undrained triaxial tests.

Chapter 6

CONCLUSIONS AND RECOMMENDATIONS

Liquefaction of cohesionless soils can have catastrophic consequences. Past experiences regarding this phenomenon have stimulated many researchers to try to understand the soil behavior during and after liquefaction. These attempts have been conducted in different ways. Conducting in situ tests in the areas in which liquefaction has occurred: performing laboratory tests to find the response of the soil in different conditions: and developing different methods to analyze ground response and determine permanent deformations during and after liquefaction are some of these activities.

Chapter one described how the term "liquefaction" has been used by different groups to determine soil performance under different conditions. On one side. Casagrande and his students used this term to describe the behavior of strain-softening soils. They pointed out that a trigger mechanism (static or cyclic) may cause the soil to strain-soften. This kind of liquefaction, which has been called "flow liquefaction". generally occurs in sloping ground in which the driving stresses are larger than the resulting ultimate undrained shear strength of the soil. Deformation can be catastrophic if the soil structure contains sufficient strain-softening material and if the geometry is such that a kinematically admissible mechanism can develop. On the other hand. the Berkeley group, under the leadership of the late professor Seed. has used the term "liquefaction" to

describe the cyclic softening of the soil during cyclic loading. This kind of liquefaction. which has been called ``cyclic liquefaction``. generally occurs in level to gently sloping ground in which shear stress reversal can occur. Deformation associated with cyclic liquefaction occurs only during the cyclic loading and accumulates with additional cycles of loading as a consequence of a loss in soil stiffness. Although flow liquefaction and cyclic liquefaction show two different phenomena. both of these are real.

Different methods have been developed to handle the liquefaction phenomenon. Chapter 1 illustrated that for analysis of cyclic liquefaction. three methods have been developed: empirical criteria based on field observations. the total stress approach and the effective stress approach. The first method. which has been proposed as a result of using observations and in situ measurements at locations in which liquefaction has occurred in the past. offers a rough but simple method for evaluating the probability of liquefaction based on in situ tests. The total stress approach has been developed based on a comparison of the cyclic stresses induced at different levels in the ground during shaking. with the cyclic shear stress required to cause liquefaction in the laboratory in a specified number of cycles. Due to the assumption of elastic behavior for the soil. this approach cannot represent realistic permanent deformation which is affected significantly by plastic soil behavior. The effective stress approach. which considers the effective stresses between soil grains and uses constitutive models. can solve this problem. It is believed that none of the elements in the effective stress approach is as important as the constitutive model in the determination of deformations during and after liquefaction.

Flow liquefaction or flow deformation has been observed and entered the literature earlier than cyclic liquefaction; however. the methods for its analysis are not as mature as those for cyclic liquefaction. Considering flow liquefaction as a stability problem and determining the deformation caused by it using constitutive models are two general approaches to analyze this kind of liquefaction. Although the mentioned types of liquefaction are two different phenomena. during earthquakes both of them may occur at

different times or in different zones of a soil structure. Therefore. a constitutive model must be able to show both of them in a unique framework.

In chapter 2. the behavior of cohesionless soils under different loading was discussed. Depending on the initial state. a soil can develop large volume changes under loading. Dense sands dilate: however. loose sands contract. At large strains. however. both of them reach an ultimate state. At this state. soil is continuously deforming at constant volume and constant stresses. Based on the initial state of the soil with respect to this ultimate state. soil may show fully contractive. contractive-dilative or fully dilative behavior.

The concept of critical void ratio. originally discussed by Casagrande. leads to the steady state framework. It was mentioned that there are a number of discussions regarding the uniqueness of the ultimate state. On one side. the experimental results of some researchers show that this state is only a function of the void ratio. On the other side. other researchers believe that ultimate state depends on factors such as consolidation stress. fabric or sample preparation procedure. shearing mode or even rate of deformation. It seems that comprehensive experimental work on different sands and different conditions must be conducted so as to clarify this important subject. As long as any doubt exists regarding the uniqueness of the ultimate state. all approaches in which the ultimate state is used to analyze soil structures at large strains will be incomplete.

It is believed that the state of the soil has a significant effect on its behavior. A lot of researchers have tried to define a parameter to show the state of the soil. State parameter. ψ. (Been and Jefferies. 1985). state index. I_s (Ishihara. 1993) and RSR (Robertson and Fear, 1995) are some of these parameters. But in the general case. a scalar quantity like these parameters cannot show the state of the soil completely. Experimental observations have shown that samples with the same state parameter or RSR or any other proposed parameter. but with different degrees of anisotropy. show

different responses. In general. one needs a larger number of quantities to define the state of a soil completely.

In order to apply the ultimate state in the design of soil structures. one must define the ultimate state as accurately as possible. Chapter 2 referred to some previous efforts in this regard.

The behavior of cohesionless soils under cyclic loading was discussed in chapter 2. This behavior is greatly influenced by initial state. It was pointed out that different researchers. appealing to their own observations. reported some response for the soil. In some aspects. controversial results have been reported by different groups (for example. the effect of static shear on occurring liquefaction). Recently. it has been shown that these observations are correct but only in the conditions in which experiments have been conducted. Depending on soil state. static shear stress. amplitude of loading and drainage conditions. a variety of responses can be seen. It is not resaonable that researchers extend the results of tests conducted under limited conditions to all other conditions.

Collapse or instability of the soil is an important phenomenon that must be considered when working with loose soils in practice. Recent research has shown how a loose soil may reach a state boundary in the stress-void ratio space in which the soil structure changes. As a result. a significant change in the soil behavior can be seen. Consideration of the collapse surface and other characteristic surfaces such as phase transformation and the ultimate state is essential for the modelling soil response under loading.

A number of studies have shown that the state of a soil has a significant effect on its behavior. In most existing constitutive models for cohesionless soils. this important factor has been overlooked. As a result, these models can be used only for a small range of stresses and void ratios for which the model has been calibrated. Chapter 3 discussed how the models with no reference state may incorrectly show the response of the soil.

In chapter 3, a framework, termed "Reference State Soil Mechanics," was proposed. In "Reference State Soil Mechanics", soil behavior depends on the soil state with respect to a reference state. Because both loose and dense sands at large strains reach an ultimate state, it was suggested that this state be used as a reference to model soil behavior. To define the state of the soil with respect to the ultimate state in ($p - e$) plane, the state parameter (ψ), which has been suggested by Been and Jefferies (1985), was used.

The multi-yield surface theory (Prevost, 1985) was modified to embrace the "Reference State Soil Mechanics" framework. The complete formulation of this model was presented in chapter 3. According to experimental observations, an open cone with apex at the origin was used for the yield surfaces in the model. The equation of the yield surface is such that the shape of the yield surface in the deviatoric plane is a rounded cornered hexagon. This function has the versatility to show the same or different friction angles in triaxial compression and extension based on experimental observations. In this regard, it has an advantage over the Matsuoka-Nakai (1974) and Lade-Duncan (1973) criteria.

In the flow rule, normality was manipulated in the deviatoric plane which corresponds with Lade and Duncan (1973) observations. The rate of plastic volumetric strain was linked to the state of the soil with respect to the ultimate state using the state parameter. The latter assumption corresponds with Been and Jefferies (1985) experiments. Two pure kinematic and isotropic-kinematic hardening rules were proposed. The comparison of the model predictions using these two hardening rules for different conditions was presented in chapter 3. Calibration of the model is achieved by using a few conventional laboratory tests. The procedure of calibration, which was described completely, is such that most of the model parameters are determined directly; only a few of them are determined by curve fitting. This makes things simpler for users in practice. A method was proposed for calibration of the model in the case of existing limited data.

Its ability to consider different parameters for extension and compression makes the model more capable of showing the effect of the fabric of the soil in triaxial compression and extension.

In chapter 3, the explicit algorithm that has been used to calculate stress increments was described. This algorithm is first-order accurate and conditionally stable. Furthermore, the size of load step was chosen so that the calculations are fast and accurate.

Chapter 4 validated the model performance under monotonic loading. Due to the limited amount of existing data for different stress paths, soil states, drainage conditions and degrees of anisotropy for a unique soil, as well as for having a complete validation of the model for different sands with different physical properties, five different sands were used in this validation. Extensive comparisons with measured data under undrained and drained conditions for isotropically and anisotropically consolidated samples of different soils were presented. It was shown that the model is able to show the effect of the state of the soil on the soil response under both undrained and drained conditions. The ultimate state in large strains could be captured by the model. The model could also show the effect of the consolidation history in both compression and extension modes. An important factor for a model with a general formulation is that it must be capable of showing soil response under different shearing modes with a set of parameters. The model demonstrated this capability. The effect of collapse in the model performance was evaluated for both saturated and dry soils. It was seen that the model could show this important phenomenon.

Validation of the model for cyclic loading was presented in chapter 5. It was shown that, depending on the state of the soil, static shear stress, amplitude of loading, number of cycles and drainage conditions, the model is capable of representing different combination of flow liquefaction, cyclic liquefaction and cyclic mobility. The model could predict transition of cyclic mobility to flow liquefaction with increasing void ratio

of the soil. The model was able to show that, for dense sands, an increase in static shear stress increases the strength of the soil against cyclic liquefaction. This performance is consistent with the experimental observations of Seed and Lee (1966). However, for loose soils, with an increase of static shear stress, the probability of flow liquefaction increases. The model was able to show this performance. This response is consistent with Castro's (1969) observations. In validation, both stress control and strain control cyclic tests were used. For comparison of the model predictions with real observations, both isotropically and anisotropically consolidated samples of different soils at different states were used. Both undrained and drained tests were considered in this comparison.

The advantages of the proposed model are as following:

• The model is capable of capturing the response of loose and dense sands, or in other words, sands in different states, with a single set of parameters and calibration.

• Calibration of the model is performed completely by using a few conventional triaxial tests. Most of the model parameters are determined directly and only a few of them must be determined by curve fitting. Therefore, the calibration of the model can be done easily. This is important from an application point of view.

• The model is able to show the effect of initial cross-anisotropy and induced anisotropy during loading. This capability is important for elements near to the edge of soil structures, such as dams, and in all elements under cyclic loading.

• The model can predict the response of the soil under both monotonic and cyclic loading. This is important for application of the model in practice because during shaking and after its cessation, different elements of soil structure may undergo monotonic and cyclic loading.

• Formulation of the model has been presented in the general case and can be used to predict soil responses under different shearing modes or stress paths.

• From the application point of view, the formulation of the model is straight forward and easy for implementation in numerical analysis.

- The model can show the ultimate state at large strains. This is important for analysis of soil structures with large deformations. Furthermore, as could be seen in model predictions in chapters 4 and 5, the model can show the quasi-steady state of the soil.

- The shape of the ultimate state surface in the deviatoric plane is flexible. Based on experimental observations, the model can show the same ultimate friction angle for $b=0$ and $b=1$ conditions. As a result, it can match different criteria such as Matsuoka-Nakai and Lade-Duncan, depending on experiments.

- Considering different parameters for triaxial compression and extension, the model can show the effect of fabric in soil response under compression and extension.

- The model can show flow liquefaction or collapse under both monotonic and cyclic loading.

- The model can show flow liquefaction, cyclic mobility and cyclic liquefaction in a unique framework. Therefore, it can be used to analyze different kinds of liquefaction simultaneously. This capability is significant from an application point of view to capture permanent deformations in an effective stress method of analysis in the general case.

It is believed that this variety of capabilities could be found only in a "Reference State Soil Mechanics" framework.

Future work related to this study should focus on the following aspects:

- Developing a constitutive model for predicting cohesive soil behavior in "Reference State Soil Mechanics". Furthermore, a unique constitutive model for cohesionless and cohesive soils may be developed in this framework.

- Integration of the model in a finite element analyses for applications in the solution of boundary value problems.

- As was mentioned. the response of the model under stress ratio constant loading is elastic. Based on experimental observations. up to a very high level of stresses (in which geotechnical engineers are rarely interested). the behavior of medium dense and dense sands under this kind of loading is elastic. But if one is interested in modifying the model for even these high stresses. he can add a cap to the model similar to what has been done by Vermeer (1979) or Lacy and Prevost (1987). The position and the size of this cap should be a function of volumetric strain.

- To define the state of the soil in ($p - e$) plane with respect to the ultimate state in this study. state parameter (ψ) has been used. However. different researchers have reported different parameters such as RSR or I_s . If. in the future. it was found that another parameter rather than ψ can better show the state of the soil. it can be replaced by ψ in the formulation of the model. This can be done by changing equation (3-23).

- As was discussed. there are still controversial experimental results regarding the uniqueness of ultimate state line. It seems that complete and comprehensive experiments should be conducted to solve this problem. After finding how this line changes with different parameters. it can be added to the model. This will not make any change in the formulation of the model.

- State parameters which have been defined by different researchers are not able to show soil response completely. Some research must be performed to define more sophisticated parameters to consider other factors such as shear stress at the same time.

BIBLIOGRAPHY

Alarcon-Guzman. A.. Leonards. G. A. and Chameau. J. I. (1988). "Undrained Monotonic and Cyclic Strength of Sands." Journal of Geotechnical Engineering Division. ASCE. Vol. 114. No. 10. pp. 1089-1109.

Anderson. S. A. and Riemer. M. F. (1995). "Collapse of Saturated Soil Due to Reduction in Confinement." Journal of Geotechnical Engineering. Vol. 121. No. 2. February. pp. 216-220.

Arango. I. (1996). "Magnitude Scaling Factors for Soil Liquefaction Evaluation." Proceedings. NCEER Workshop on Evaluation of Liquefaction Resistance. Salt Lake City, Utah. January 4-5.

Ayoubian. A. and Robertson. P.K. (1996). "Triaxial Testing on Anisotropically Consolidated Sands for Flow Liquefaction Analyses." Proc. of 49th Canadian Geotechnical Conference. Vol. 1, pp. 449-456.

Baziar, M.H. and Dobry, R. (1995), "Residual Strength and Large-Deformation of Loose Silty Sands." Journal of Geotechnical Engineering. ASCE. Vol. 121. No. 12. pp. 896-906.

Been. K.. Crooks. J. H.. Becker. D. E. and Jefferies. M. G. (1986). "The Cone Penetration Test in Sand: Part I. State Parameter Interpretation." Geotechnique. Vol. 36. No. 2. pp. 239-249.

Been. K. and Jefferies. M. G. (1985). "A State Parameter for Sands." Geotechnique. Vol. 35. No. 2. pp. 99-112.

Been. K.. Jefferies. M. G.. Crooks. J. H. and Rothenburg. L. (1987-a). "The Cone Penetration Test in Sands: Part II. General Inference of State." Geotechnique. Vol. 37. No. 3. pp. 285-299.

Been. K.. Jefferies. M. G. and Hachey. J. (1991). "A Critical State of Sands." Geotechnique. Vol 41. No. 3. pp. 365-381.

Been. K.. Lingnau. B. E.. Crooks. J. H. and Leach. B. (1987-b). "Cone Penetration Test Calibration for Erksak (Beaufort Sea) Sand." Canadian Geotechnical Journal. Vol. 24. pp. 601-610.

Biot. M. A. (1941). "General Theory of Three-Dimensional Consolidation." Journal of Applied Physics. Vol. 12. No. 2. pp. 155-164.

Bishop. A. W. (1966). "Strength of Soils as Engineering Materials." 6th Rankine Lecture. Geotechnique. Vol. 16. pp. 81-130.

Bishop. A. W. (1967). "Progressive Failuire With Special Reference to the Mechanism Causing it." Proc. of the Geotechnical Conference. Vol. 2. pp. 142-150. Oslo. Norway.

Bishop. A. W. (1971). "Shear Strength Parameters for Undisturbed and Remolded Soil Specimens." Proc. of the Roscoe Memorial Symposium. Cambridge University. pp. 3-58.

Bjerrum. L. (1971). "Subaqueous Slope Failures in Norwegian Fjords." Norwegian Geotechnical Institute. Publication No. 88.

Boulanger. R. W.. Seed. R. B.. Chan. C. K.. Seed. H. B. and Sousa. J. (1991). "Liquefaction Behavior of Saturated Sands Under Uni-Directional and Bi-Directional Monotonic and Cyclic Simple Shear Loading." Geotechnical engineering Report. University of California. Berkeley.

Casagrande. A. (1936). "Characteristics of Cohesionless Soils Affecting the Stability of Slopes and Earth Fills." Journal of Boston Society of Civil Engineers. Jan.. pp. 13-32.

Casagrande. A. (1965). "Role of the Calculated Risk in Earthwork and Foundation Engineering." The Terzaghi Lecture. Journal of Soil Mechanics and Foundations Division. ASCE. Vol. 91. No. SM4. July. pp. 1-40.

Casagrande. A. (1975). "Liquefaction and Cyclic Deformation of sands-A Critical Review." Harward Soil Mechanics Series. No. 88.

Casagrande. A. and Fadum. R. E. (1942). "Application of Soil Mechanics in Designing Building Foundation." ASCE Transactions. Vol. 107. pp. 383-490.

Castro. G. (1969). "Liquefaction of Sand." Ph.D. thesis. Harvard Univesrity.

Castro. G. (1975). "Liquefaction and Cyclic Mobility of Saturated Sands." Journal of Geotechnical Engineering. ASCE. Vol. 101. No. GT6. June. pp. 551-569.

Castro. G. (1987). "On the Behavior of Soils During Earthquakes-Liquefaction." Soil Dynamics and Liquefaction. A. S. Cakmak. Editor. Elsevier. pp. 169-204.

Castro. G. and Poulos. S. J. (1977). "Factors Affecting Liquefaction and Cyclic Mobility." Journal of Geotechnical Engineering. ASCE. Vol. 103. No. GT6. pp. 501-516.

Castro. G.. Poulos. S. J.. France. J. W. and Enos. J. I. (1982). "Liquefaction Induced by Cyclic Loading." Geotechnical Engineering. Inc.. Report Submitted to National Science Foundation. March.

Castro. G..Poulos. S. J. and Leathers. F. D. (1985). "Re-Examination of Slide of Lower San Fernando Dam." Journal of Geotechnical Engineering. ASCE. Vol. 111. No. 9. Sept.. pp. 1093-1107.

Chillarige. A. V. (1995). "Liquefaction and Instability in the Fraser River Delta." Ph.D. thesis. Alberta University.

Chillarige. A. R. V.. Robertson. P. K.. Mogenstern. N. R.. Christian. H. and Woeller. D. J. (1994), "Evaluation of Wave Effects on Seabed Instability in the Fraser River Delta." Proceedings of 47th Canadian Geotechnical Conference. September. Halifax. pp. 186A-186j.

Christian. J. T. and Swiger. W. F. (1975). "Statistics of Liquefaction and SPT Results." Journal of the Geotechnical Engineering Division. ASCE. Vol. 101. No. GT11. pp. 1135-1150.

Chu. J. (1992). "Discussion to Minimum Undrained Strength versus Steady-State Strength of Sands." Journal of the Geotechnical Engineering. Vol. 118. No. 2. pp. 360-361.

Cunning. J. C.. Robertson. P. K. and Sego. D. C. (1994). "Shear Wave Velocity to Evaluate In-Situ State of Cohesionless Sands." Canadian Geotechnical Journal. Vol. 32. pp. 848-858.

Dafalias. Y. F. And Popov. E. P. (1975). "A Model of Nonlinearity hardening Materials For Cyclic Loading." Acta Mechanica. Vol. 21. pp. 173-192.

Davis. A. P.. Castro. G. and Poulos. S. J. (1988). "Strength Backfigured from Liquefaction Case Histories." 2nd. International Conference on Case Histories in Geotechnical Engineering. Rolla. Missouri. Vol. 3. pp. 1693-1701.

DeGregorio. V. B. (1990), "Loading Systems. Sample Preparation. and Liquefaction." Journal of Geotechnical Engineering. Vol. 116. No. 5. pp. 805-821.

Dierichs. D. and Forster. W. (1985). "Results of Liquefaction Tests under Static Conditions." XI ICSMFE. Vol. 2. pp. 437-441. San Fransisco. USA.

Dobry. R. (1991). "Soil Properties and Earthquake Ground Response." Guest Lecture. Proceedings 10th European Conference on Soil Mechanics and Foundation Engineering. Florence. Italy. pp. 1171-1187.

Drucker. D. C. (1950). "Some Implication of Work Hardening and Ideal Plasticity." Quarterly of Applied Mathematics. Vol. 7. pp. 411-418.

Drucker. D. C. (1959). "A Definition of Stable Inelastic Material." Journal of Applied Mechanics. Vol. 26. Series E. No. 1. pp. 101-106.

Drucker. D. C.. Gibson. R. E. and Henkel. D. J. (1957). " Soil Mechanics and Work Hardening Theories of Plasticity." Transactions of ASCE. Vol. 122. pp. 338-346.

Drucker. D. C. and Prager. W. (1952). "Soil Mechanics and Plastic Analysis or Limit Design." Quarterly of Applied Mathematics. Vol. 10. pp. 157-165.

Fear. C. E. and McRoberts. E. C. (1995). "Reconsideration of Initiation of Liquefaction in Sandy Soils." Journal of Geotechnical Engineering. ASCE. Vol. 121. No. 3. pp. 249-261.

Fear. C. E. and Robertson. P. K. (1995). "Estimating the Undrained Strength of Sand. a Theoretical Framework." Canadian Geotechnical Journal. Vol. 32. No. 5. pp. 859-870.

Geuze. E. (1948). "Critical Density of Some Dutch Sands." Second ICSMFE. Vol. 3. pp. 125-130.

Gu. W. H.. Morgenstern. N. R. and Robertson. P. K. (1993-a). "Progressive Failure of the Lower San Fernando Dam." Journal of Geotechnical Engineering. ASCE. Vol. 119. No. 2. pp. 333-348.

Gu, W. H., Morgenstern, N. R. and Robertson, P. K. (1993-b). "Post Earthquake Deformation Analysis of Wild Life Site." Journal of Geotechnical Engineering, ASCE, Vol. 120, No. 2, pp. 274-285.

Hanzawa, H. (1980). "Undrained Strength and Stability Analysis for a Quick Sand." Soils and Foundations, Vol. 20, No. 2, pp. 17-29.

Hardin, B. O. and Drenevich, V. P. (1972). "Shear Modulus and Damping in Soils: Measurements and Parameter Effects." Journal of the Soil Mechanics and Foundation Engineering Division, ASCE, Vol. 98, No. SM6, Proc. Paper 8977, June, pp. 603-624.

Hazen, A. (1920). "Hydraulic-Fill Dams." ASCE Transactions, Vol. 83, pp. 1713-1745.

Highter, W. H. and Valee, R. P. (1980). "The Liquefaction of Different Mine Tailing under Stress-Control Loading." Engineering Geology, Vol. 16, pp. 147-150.

Hird, C. C. and Hassona, F. A. (1990). "Some Factors Affecting the Liquefaction and Flow of Saturated Sands in Laboratory Tests." Engineering Geology, Vol. 28, pp. 149-170.

Hyodo, M., Murata, H., Yasufuko, N. and Fujii, T. (1989). "Undrained Cyclic Shear Strength and Deformation of Sands Subjected to Initial Static Shear Stress." Soil Dynamics and Liquefaction, A.S. Cakmak and I. Herrera Editor, Elsevier, pp. 81-103.

Hyodo, M., Tanimizu, H., Yasufuko, N. and Murata, H. (1994). "Undrained Cyclic and Monotonic Triaxial Behavior of Saturated Loose Sand." Soils and Foundations, Vol. 34, No. 1, March, pp. 19-32.

Ishihara, K. (1985). "Stability of Natural Deposits During Earthquakes." Theme Lecture, Proceeding of the XI ICSMFE, Vol. 2, pp. 321-376.

Ishihara. K. (1993). "Liquefaction and Flow Failure During Earthquakes" Geotechnique. Vol. 43. No. 3. pp. 351-415.

Ishihara. K.. Tatsuoka. F.. and Yasuda. S. (1975). "Undrained Deformation and Liquefaction of Sand under Cyclic Stresses." Soils and Foundations. Vol. 15. No. 1. March. pp. 29-44.

Ishihara. K.. Verdugo. R. and Acacio. A. A. (1991). "Characterization of Cyclic Behavior of Sand and Post-Seismic Stability Analyses." Proc. 9th Asian Regional Conference on Soil Mechanics and Foundation Engineering. Bangkok. pp. 45-68.

Ishihara. K. and Yasuda. S. (1975). "Sand Liquefaction in Hollow Cylinder Torsion Under Irregular Excitation." Soils and Foundations. Vol. 15. No. 1. pp. 49-59.

Iwan. W. D. (1967). "On a Class of Models for the Yielding Behavior of Continuous and Composite Systems." Journal of Applied Mechanics. ASME. Vol. 34. pp. 612-617.

Jefferies. M. (1993). "Nor-Sand: A simple Critical State Model for Sand." Geotechnique. Vol. 43. No. 1. pp. 91-103.

Joyner. W. B. and Chen. A. T. F. (1976). "Calculation of Nonlinear Ground Response in Earthquakes." Bull. Seismol. Soc. Am.. Vol. 65. No. 5. pp. 1315-1336.

Kavazanjian. E. Jr.. Roth. R. A. and Echezuria. H. (1983). "Probabilistic Evaluation of Liquefaction Potential for Downtown San Francisco." Report No. 60. Dept. of Civil Engineering. Stanford University. 147 p.

Kirkpatrick. W. M. and Belshaw. D. J. (1968). "On the Interpretation of the Triaxial Test." Geotechnique. Vol. 18. No. 3. pp. 336-350.

Kishida. H. (1966). "Damage to Rienforced Concrete Buildings in Niigata City With Special Reference to Foundation Engineering." Soils and Foundations. Vol. 6. No. 1. pp. 71-88.

Ko. H. Y. and Scott. R. F. (1967). "Deformation of Sand in Hydrostatic Compression." Journal of the Soil Mechanics and Foundations Division. Vol. 93. No. SM3. May. pp. 137-156.

Koester. J.P. (1992). "Cyclic Strength and Pore Pressure Generation Characteristics of Fine Grained Soils." Ph.D. Thesis. University of Colorado. Boulder. Colorado.

Koizumi. Y. (1966). "Change in Density of Sand Subsoil caused by the Niigata Earthquake." Soils and Foundations. Vol. 6. No. 2. pp. 38-44.

Kovacs. W. D.. Salomone. L. A. and Yokel. F. Y. (1983). "Comparison of Energy Measurments in the Standard Penetration Test Using the Cathead and Rope Method." National Bureau of Standards Report to the US Nuclear Regulatory Commission.

Krieg. R. D. (1975). " A Practical Two Surface Plasticity Theory." Journal of Applied Mechanics. Transactions of ASME. Vol. 42. pp. 641-646.

Lacy. S. J. (1986). "Numerical Procedures for Nonlinear Transient Analysis of Two-Phase Soil Systems." Ph.D. thesis. Princeton University.

Lacy. S. J. and Prevost. J. H. (1987). "Constitutive Model for Geomaterials." Proceedings of 2nd. International Conference on Constitutive Laws for Engineering Materials. Tucson. Arizona. pp. 1-12.

Lade. P. V. (1977). "Elasto-Plastic Stress-Strain Theory for Cohesionless Soil With Curved Yield Surfaces." International Journal of Solids and Structures. Vol. 13. pp. 1019-1035.

Lade. P. V. (1992). "Static Instability and Liquefaction of Loose Fine Sandy Slopes." Journal of Geotechnical Engineering. ASCE. Vol. 118. No. 1. pp. 51-71.

Lade. P. V. (1994). "Instability and Liquefaction of Granular Materials." Computers and Geotechnics. Vol. 16. pp. 123-151.

Lade. P. V. and Duncan. J. M. (1973). "Cubical Triaxial Tests on Cohesionless Soil." Journal of Soil Mechanics and Foundations Division. Proceedings of ASCE. Vol. 99. No. SM10. Oct.. pp. 793-812.

Lee. K. L. and Seed. H. B. (1967). "Cyclic Stress Condition Causing Liquefaction of Sand." Journal of the Soil Mechanics and Foundations Engineering Division. ASCE. Vol. 93. No. SM1. Jan.. pp. 47-70.

Lee. K. L. and Seed. H. B. (1970). "Undrained Strength of Anisotropically Consolidated Sands." Journal of Soil Mechanics and Foundation Division. ASCE. Vol. 96. No. SM2. pp. 411-428.

Lindenberg. J. and Koning. H. L. (1981). "Critical Density of Sand." Geotechnique. Vol. 31. No. 2. pp. 231-245.

Luong. M. P. (1980). "Stress-Strain Aspects of Cohesionless Soils under Cyclic and Transient Loading." Proc. International Symposium on Soils under Cyclic and Transient Loading. Vol. 1. Swansea. U.K. . Jan.. pp. 315-324.

Manzari. M. T.. Dafalias. Y. F. (1997). "A Critical State Two-Surface Plasticity Model for Sands" Geotechnique. Vol. 47. No. 2. pp. 255-272.

Marcuson. W. M.. Hynes. M. E. and Franklin. A.G. (1990). "Evaluation of Use of Residual Strength in the Seismic Stability of Embankments." Earthquake Spectra. Vol. 6. No. 3. pp. 529-572.

Matsuoka. H. and Nakai. T. (1974). "Stress-Deformation and Strength Characteristics of Soil Under Three Different Principal Stresses." Proc. JSCE. No. 232. pp. 59-70.

Matsuoka. H. and Nakai. T. (1977). "Stress-Strain Relationship of Soil Based on the 'SMP'." Proc. Specialty Session 9. Constitutive Equations of Soils. 9th Int. Conf. SMFE. pp. 153-162.

Middlebrooks. T. A. (1942). "Fort Peck Slide." ASCE Transactions. Vol. 107. pp. 723-742.

Mroz. Z. (1967). "On the Description of Anisotropic Hardening." Journal of Mechanics and Physics of Solids. Vol. 15. pp. 163-175.

NCEER (1996). NCEER Workshop on Evaluation of Liquefaction Resistance. Utah. January.

Nova, R. (1991). "A Note on Sand Liquefaction and Soil Instability." Proc. 3rd Int. Conf. Constitutive Laws for Engrg. Mater.. Tucson. pp. 153-156.

Nova. R. and Wood. D. M. (1979). "A Constitutive Model for Sands in Triaxial Compression." International Journal of Numerical and Analytical Methods in Geomechanics. Vol. 3. pp. 255-278.

Ohsaki. Y. (1966). "Niigata Eartquake. 1964 Building Damage and Condition." Soils and Foundations. Vol. 6. No. 2. pp. 14-37.

Ortiz. M. and Popov. E. P. (1985). "Accuracy and Stability of Integration Algorithms for Elastoplastic Constitutive Relations." Int. J. Num. Meth. Eng.. Vol. 21. No. 9. pp. 1561-1576.

Peacock. W. H. and Seed. H. B. (1968). "Sand Liquefaction Under Cyclic Loading Simple Shear Conditions. " Journal of Soil Mechanics and Foundations Division. ASCE. Vol. 94. No. SM3. May. pp. 689-708.

Poorooshasb. H. B.. Houlbec, I. and Sherbourne. A. N. (1966). "Yielding and Flow of Sand in Triaxial Compression. Part I." Canadian Geotechnical Journal. Vol. 3. No. 4. pp. 179-190.

Poorooshasb. H. B.. Houlbec. I. and Sherbourne. A. N. (1967). "Yielding and Flow of Sand in Triaxial Compression. Part II and III," Canadian Geotechnical Journal. Vol. 4. No. 4. pp. 377-398.

Poorooshasb. H. B. (1971). "Deformation of Sand in Triaxial Compression." Proceedings of 4th. Asian Regional Conference on Soil Mechanics and Foundation Engineering. Bangkok. Vol. 1. pp. 63-66.

Poorooshasb. H. B. (1989). "Description of Flow of Sand Using State Parameters" Computers and Geotechniques. Vol. 8. pp. 195-218.

Poulos. S. J. (1971). "The Stress-Strain Curves of Soils." Geotechnical Engineers. Inc.. Winchester. Mass.

Poulos. S. J. (1981). "The Steady State of Deformation." Journal of Geotechnical Engineering Division. ASCE. Vol. 17. No. GT5. May. pp. 553-562.

Poulos. S. J. (1988). "Liquefaction and Related Phenomena." Advanced Dam Engineering for Design. Construction and Rehabilitation. Edited by R. B. Jansen. Van Nostrand Reinhold. New York. pp. 256-320.

Poulos. S. J.. Castro. G. and France. J. W. (1985). "Liquefaction Evaluation Procedure." Journal of Geotechnical Engineering Division. ASCE. Vol. 111. No. 6. pp. 772-791.

Poulos. S. J.. Castro. G. and France. J. W. (1988). Closure to "Liquefaction Evaluation Procedure." Journal of Geotechnical Engineering Division. ASCE. Vol. 114. No. 2. Feb.. pp. 251-259.

Prevost. J. H. (1977). "Mathematical Modeling of Monotonic and Cyclic Undrained Clay Behavior." International Journal of Numerical and Analytical Methods in Geomechanics. Vol 1. pp. 195-216.

Prevost. J. H. (1978). "Plasticity Theory for Soil Stress Strain Behavior." Journal of the Engineering Mechanics Division. Proceedings of ASCE. Vol. 104. No. EM5. pp. 1177-1194.

Prevost. J. H. (1985). "A simple Plasticity Model for Frictional Cohesionless Soils." Journal of Soil Dynamics and Earthquake Engineering. Vol. 4. No. 1. January. pp. 9-17.

Pyke. R. (1988). Discussion to "Liquefaction Evaluation Procedure." Journal of Geotechnical Engineering . ASCE. Vol. 114. No. 2. Feb.. pp. 246-247.

Richart. F. E.. Woods. R. D.. Hall. J. R. (1970). "Vibration of Soils and Foundations." Prentice-Hall. N.J.

Riemer. M. F. and Seed. R. B. (1997). "Factors Affecting Position of Steady State Line." Journal of Geotechnical and Geoenviromental Engineering. ASCE. Vol. 123. No. 3. March. pp. 281-288.

Reynolds. O. (1885). "The Dilating of Media Composed to Rigid Particles in Contact." Philosophical Magazine. S. 5. Vol. 20. No. 127. pp. 469-481. London.

Robertson. P. K. (1990). "Evaluation of Residual Shear Strength of Sands during Liquefaction from Penetration Tests." Proceedings of the 43rd Canadian Geotechnical Conference. Vol. 1. pp. 257-262.

Robertson. P. K. (1994). "Suggested Terminology for Liquefaction." Proceedings of the 47th Canadian Geotechnical Conference. Halifax. pp. 277-286.

Robertson. P. K.. Campanella. R. G. and Wightman. A. (1983). "SPT-CPT Correlations." Journal of Geotechnical Division. ASCE. Vol. 109. pp. 1449-1459.

Robertson. P. K. and Fear. C. E. (1995). "Liquefaction of Sands and its Evaluation." Proc. First International Conference on Earthquake Geotechnical Engineering. Vol. 3. Tokyo.

Rollins. K. and Seed. H. B. (1990). "Influence of Buildings on Potential Liquefaction Behavior." Journal of the Geotechnical Engineering Division. Vol. 116. pp. 165-185.

Roscoe. K. H. and Poorooshasb. H. B. (1963). "A Fundamental Principle of Similarity in Model Test for Earth Pressure Problems." Proc. 2nd Asian Conference Soil Mechanics. Vol. 1. pp. 134-140. Japan.

Roscoe. K. H.. Schofield. A. N. and Wroth. C. P. (1958). "On Yielding of Soils." Geotechnique. Vol. 8. No. 1. pp. 22-53.

Rowe. P. W. (1962). "The stress Dilatancy Relation for Static Equilibrium of an Assembly of Particles in Contact." Proceedings of Royal Society. Series A.. 269. pp. 500-527.

Sasitharan. S.. Robertson. P. K.. Sego. D.C. and Morgenstern. N. R. (1994). "State Boundary Surface for Very Loose Sand and its Practical Implications." Canadian Geotechnical Journal. Vol. 31. pp. 321-334.

Schofield. A. N.. Wroth. C. P. (1968). "Critical State Soil Mechanics" McGraw-Hill

Seed. H. B. (1979). "Soil Liquefaction and Cyclic Mobility Evaluation for Level Ground During Earthquakes." Journal of Geotechnical Engineering Division. ASCE. Vol. 105. No. GT2. pp. 201-255.

Seed. H. B. (1987). "Design Problems in Soil Liquefaction." Journal of Geotechnical Engineering. ASCE. Vol. 113. No. 8. August. pp. 827-845.

Seed. H. B. and Idriss. I. M. (1967). "Analysis of Soil Liquefaction. Niigata Earthquake." Journal of the Soil Mechanics and Foundation Engineering Division. ASCE. Vol. 93. No. SM3. May. pp. 83-108.

Seed. H. B. and Idriss. I. M. (1971). "Simplified Procedure for Evaluating Soil Liquefaction Potential." Journal of the Soil Mechanics and Foundations Division. ASCE. Vol. 97. No. SM9, pp. 1249-1273.

Seed. H. B. and Idriss, I. M. (1982). "Ground Motions and Soil Liquefaction During Earthquakes." Earthquake Engineering research Institute Monograph.

Seed. H. B. and Lee. K. L. (1966). "Liquefaction of Saturated Sands During Cyclic Loading." Journal of the soil Mechanics and Foundation Engineering Division. ASCE. Vol. 92. No. SM6. November. pp. 105-134.

Seed. H. B.. Lee. K. L.. Idriss. I. M. and Makdisi. F. I. (1975). "The Slides in the San Fernando Dams During the Earthquake of February 9. 1971." Journal of Soil Mechanics and Foundation Division. ASCE. Vol. 101. No. GT7. pp. 651-688.

Seed. H. B. and Peacock. W. H. (1971). "Test Procedures for Measuring Soil Liquefaction Characteristics." Journal of the Soil Mechanics and Foundations Division. ASCE. Vol. 97. No. SM8.pp. 1099-1119.

Seed. H. B.. Tokimatsu. K.. Harder. L. F. and Chung. R. M. (1985). "Influence of SPT Procedures in Soil Liquefaction Resistance Evaluations." Journal of Geotechnical Engineering. ASCE. Vol. 111. No. 12. pp. 1425-1445.

Seed. R. B. and Harder. L. F. (1990). "SPT-Based Analysis of Cyclic Pore Pressure Generation and Undrained Residual Strength." Proceedings of H.Bolton Seed Memorial Symposium. Vol. 2. pp. 351-376.

Selig. E. T. and Chang. C. S. (1981). "Soil Failure Modes in Undrained Cyclic." Journal of the Geotechnical Engineering Division. ASCE. Vol. 107. No. GT5. May. pp. 539-551.

Skempton. A. W. (1986). "Standard Penetration Test Procedures and the Effects in Sands of Overburden Pressure. Relative Density. Particle Size. Aging and Overconsolidation." Geotechnique. Vol. 36. No. 3. pp. 425-447.

Skopek. P.. Morgenstern. N. R. and Robertson. P. K. (1994). "State Boundary Surface for Very Loose Sand." Submitted to Journal of Geotechnical and Geoenviromental Engineering, ASCE. for Publication.

Sladen. J. A.. D'Hollander. R. D. and Krahn. J. (1985-a). "The Liquefaction of Sands. a Collapse Surface Approach." Canadian Geotechnical Journal. Vol. 22. pp. 564-578.

Sladen. J. A.. D'Hollander. R. D. and Krahn. J. (1985-b). "Back Analysis of the Nerlerk Berm Liquefaction Slides." Canadian Geotechnical Journal. Vol. 22. pp. 579-588.

Stark. T. D. and Mesri. G. (1992). "Undrained Shear Strength of Liquefied Sands for Stability Analysis." Journal of Geotechnical Engineering. ASCE. Vol. 118. No. 11. pp. 1727-1747.

Tatsuoka. F. and Ishihara. K. (1974-a). "Yielding of Sand in Triaxial Compression." Soils and Foundations. Vol. 14. No. 2. June. pp. 63-76.

Tatsuoka. F. and Ishihara. K. (1974-b). "Drained Deformation of Sand Under Cyclic Stresses Reversing Direction." Soils and Foundations. Vol. 14. No. 3. Sept.. pp. 51-65.

Tokimatsu. K. and Yoshimi. Y. (1983). "Empirical Correllation of Soil Liquefaction Based on SPT N-Value and Fine Content." Soils and Foundations. Vol. 23. No. 4. pp. 56-74.

Vaid. Y. P. and Chern. J. C. (1983). "Mechanism of Deformation During Cyclic Undrained Loading of Saturated Sands." Soil Dynamic and Earthquake Engineering. Vol. 2. No. 3. pp. 171-177.

Vaid. Y. P. and Chern. J. C. (1985). "Cyclic and Monotonic Undrained Response of Saturated Sands." Advances in the Art of Testing Soils under Cyclic Conditions. ASCE. Edited by V. Khosla. pp. 120-147.

Vaid. Y. P.. Chung, E. K. and Kuerbis. R. H. (1990). "Stress Path and Steady State." Canadian Geotechnical Journal. Vol. 27. pp. 1-7.

Vaid. Y. P. and Thomas. J. (1995). "Liquefaction and Post Liquefaction Behavior of Sands." Journal of Geotechnical Engineering. Vol. 121. No. 2. pp. 163-173.

Verdugo. R. L. (1992). "Characterization of Sandy Soil Behavior under Large Deformation." Ph.D. Thesis. Tokyo University.

Verdugo. R.. Ishihara. K. (1996). "The Steady State of Sandy Soils" Soils and Foundations. Vol. 36. No. 2. June. pp. 81-91.

Vermeer. P.A. (1978). "A Double Hardening Model for Sand" Geotechnique. Vol. 28. No. 4. pp. 413-433.

Vesic. A. S. and Clough. G. W. (1968). "Behavior of Granular Materials under High Stresses." Journal of Soil Mechanics and Foundation Division. ASCE. Vol. 94. No. SM3. pp. 661-688.

Wang. Z. L.. Dafalias. Y. F. and Shen. C. K. (1990). "Bounding Surface Hypoplasticity Model for Sand." Journal of Engineering Mechanics. ASCE. Vol. 116. No. 5. pp. 983-1001.

Wood. D. M.. Belkheir. K.. Liu. D. F. (1994). "Strain Softening and State Parameter for Sand Modelling" Geotechnique. Vol. 44. No. 2. pp. 335-339.

Yasufuko. N.. Murata. H.. Hyodo. M. (1991). "Yield Characteristics of Anisotropically Consolidated Sand under Low and High Stresses" Soils and Foundations. Vol. 31. No. 1. March. pp. 95-109.

Yoshimine. M. (1996). "Undrained Flow Deformation of Saturated Sand Under Monotonic Loading Conditions." Ph.D. Thesis. Tokyo University.

Zienkiewicz. O. C.. Leung. K. H.. Hinton. E. and Chang. C.T. (1982). "Liquefaction and Permanent Deformation under Dynamic Conditions-Numerical Solution and Constitutive Relations." Soil Mechanics-Transient and Cycle Loads. Edited by G.N. Pande and O.C. Zienkiewicz. Chapter 5. pp. 71-103.

Appendix

AN EXAMPLE FOR CALIBRATION OF THE MODEL

In this appendix, the calibration of the model for Toyoura sand will be described in step by step method. The calibration will be achieved following the procedure which has been described in section 3.11. using the tests which have been mentioned in Table 3.1.

1- Because the results of shear wave velocity and hydrostatic cyclic tests were not available, the shear modulus and bulk modulus (G and B) have been determined using the initial slope measured at the origin of the deviatoric stress-shear strain and mean effective stress-volumetric strain curves obtained in drained triaxial test. For calculation, the test which has been shown in Figures (A.1) to (A.4) (Verdugo and Ishihara. 1996: Verdugo. 1992) and the following equations have been used:

$$G = \frac{\dot{q}}{2\dot{\varepsilon}_d} \qquad \text{(A-1)}$$

$$B = \frac{\dot{p}}{\dot{\varepsilon}_r} \qquad \text{(A-2)}$$

where $\dot{q}$, $\dot{p}$, $\dot{\varepsilon}_d$ and $\dot{\varepsilon}_v$ are increments of deviatoric stress, mean effective stress, shear strain and volumetric strain, respectively. If these increments are taken as equal to what exists in the first segment, this segment will be the elastic zone for the model. Using the values in Table (A.1), we will have $G = 45$ MPa and $B = 30$ MPa.

Because elastic moduli depend on void ratio and mean effective stress, the void ratio and mean effective stress at which G and B have been determined must be kept as e and p. For Toyoura sand these values are 0.963 and 0.4 MPa, respectively.

It is suggested that G and B be normalized for a specific p_0 and e_0. Using normalization, all the parameters which depend on a reference will be defined at a specific value as reference. As a result, application of the model will be easier. In this thesis, $p_0 = p_{atm}$ and $e_0 = 1$ have been used for normalization. Using the following equations, G_0 and B_0 for Toyoura sand will be 21 MPa and 14 MPa respectively.

$$G_0 = G \ (\frac{p_0}{p})^{0.5} \frac{(2.17 - e_0)^2(1+e)}{(2.17 - e)^2(1+e_0)}$$ (A-3)

$$B_0 = B \ (\frac{p_0}{p})^{0.5} \frac{(2.17 - e_0)^2(1+e)}{(2.17 - e)^2(1+e_0)}$$ (A-4)

Equations (A-3) and (A-4) are the same as equations (3-40) and (3-41) but with a new arrangement.

2- The ultimate state line in ($p - e$) plane must be defined for the model. This line can have any shape with any mathematical formulation. For Toyoura sand, based on experimental results (Ishihara, 1993), in the range of interest, a polynomial with order 4 has been considered for this line. The equation is:

$$e_{us} = 0.92649 - 0.12508\,p + 0.043665\,p^2 - 0.012639\,p^3 + 0.00154040\,p^4$$ (A-5)

where e_{u} is void ratio at the ultimate state. Comparison of calculated ultimate state line with experimental observations has been shown in Figure (4.2).

For triaxial extension. Yoshimine (1996) was not interested in the behavior of Toyoura sand at large strains (ultimate state). and he has looked at quasi-steady state conditions. Therefore. only a few results over a small range of stresses and void ratios were available. Based on these few data. ultimate state for triaxial extension is not the same as that reported by Ishihara (1993) for triaxial compression. Therefore. for triaxial extension (based on these data). it was assumed that the ultimate state line is parallel with that in compression with 0.08 shifting to down.

3- m_k is determined by using η_{ue} and η_{uc} . i.e.. the slope of ultimate state lines in $(q - p)$ plane in triaxial extension and compression respectively. and the following equation:

$$m_k = -\frac{\eta_{ue}}{\eta_{uc}} \qquad (A\text{-}6)$$

For Toyoura sand. based on Ishihara (1993) and Yoshimine (1996). η_{ue} and η_{uc} are respectively (-0.90) and 1.26. Therefore. m_k is 0.714.

4- To determine m_c . α . H_c . H_t . $\overline{\eta}_c$ and $\overline{\eta}_t$. the results of one pair of drained triaxial compression and extension tests are used. $(q - \varepsilon_d)$. $(p - \varepsilon_v)$. $(q - p)$ and $(p - e)$ curves are divided to some linear segments so that the slopes of $(q - \varepsilon_d)$ curves for each pair segments in compression and extension are the same. The linear segments for compression have been shown in Figures (A.1) to (A.4). The numerical values also can be found in Table (A.1).

m_c and α are determined by the following equations:

$$m_c = \frac{\eta_c - \eta_E}{1 + m_k} \tag{A-7}$$

$$\alpha = \eta_c - m_c \tag{A-8}$$

where η_c and η_E in the above equations are stress ratio at the initial point of each plastic segment in compression and extension. For Toyoura sand, because the result of drained triaxial extension test was not available, m_c, α and parameters related to extension for each yield surface have been determined by using the method which has been described in section 3.12. d_0 and C_0 were chosen by trial and error such that the best fit was obtained to the test which has been shown in Figure (A.5). Based on this curve fitting, d_0 and C_0 are equal to 0.45 and 6.0, respectively. The values of m_c and α for each yield surface are shown in Table (A.2).

To determine H_c and H_E, after changing the arrangement of equation (3-52), one has:

$$H_c (\text{or } H_E) = \frac{1 - \eta \frac{\dot{p}}{\dot{q}}}{(1 + \frac{2}{9}\eta^2)(\frac{\dot{\varepsilon}_d}{\dot{q}} - \frac{1}{2G})} \tag{A-9}$$

For determining plastic moduli in compression and extension, the values related to each segment in compression and extension must be put in equation (A-9).

The variation of G with void ratio and mean effective stress should be considered by equation (3-40). In each segment, the values of p, e and η are not constant: however, considering the small size of each segment, this much sophistication is not needed and a constant value for these parameters can be considered for each segment in the calibration.

H_c and H_E depend on mean effective stress and void ratio (refer to equation 3-42). Therefore, the calculated H_c and H_E are related to the p and e of each segment.

In step 8. these parameters will be calculated using a unique reference mean effective stress and void ratio (p_0 and e_0). The process of determination of plastic moduli in compression and extension for Toyoura sand has been shown in Table (A.3). As described in sections (3.11) and (3.12). the ratio of ($\dot{\varepsilon}_d/\dot{q}$) is the same in compression and extension for each segment and also ($\dot{p}/\dot{q}$) for extension is equal to ($-2/3$). Because of the lack of data in extension. it was assumed that G for each segment is the same in compression and extension.

$\overline{\eta}_c$ and $\overline{\eta}_E$. which are dilation parameters in compression and extension at a specific state (ψ_c and ψ_E in compression and extension. respectively) and specific position (α_{ij}^0). are determined for each yield surface. using the following equations:

$$\overline{\eta}_c = \cfrac{\eta}{\left[\cfrac{2(\cfrac{\dot{q}}{\dot{p}} - \eta) - \sqrt{9}H_c(1 + \cfrac{2}{9}\eta^2)^{0.5}(\cfrac{\dot{\varepsilon}_v}{\dot{p}} - \cfrac{1}{B})}{\sqrt{9}H_c(1 + \cfrac{2}{9}\eta^2)^{0.5}(\cfrac{\dot{\varepsilon}_v}{\dot{p}} - \cfrac{1}{B}) + 2(\cfrac{\dot{q}}{\dot{p}} - \eta)}\right]^{0.5}} \qquad (A\text{-}10)$$

$$\overline{\eta}_E = \cfrac{-\eta}{\left[\cfrac{2(\eta - \cfrac{\dot{q}}{\dot{p}}) - \sqrt{9}H_E(1 + \cfrac{2}{9}\eta^2)^{0.5}(\cfrac{\dot{\varepsilon}_v}{\dot{p}} - \cfrac{1}{B})}{\sqrt{9}H_E(1 + \cfrac{2}{9}\eta^2)^{0.5}(\cfrac{\dot{\varepsilon}_v}{\dot{p}} - \cfrac{1}{B}) + 2(\eta - \cfrac{\dot{q}}{\dot{p}})}\right]^{0.5}} \qquad (A\text{-}11)$$

Equations (A-10) and (A-11) are a new arrangement of equation (3-53). For using B in the above equations. the variation of B with mean effective stress and void ratio is considered by equation (3-41).

Because dilation parameters depend on state parameter (refer to equation 3-23). state parameters of each segment in compression and extension must be kept as ψ_c and ψ_E .

ψ_c and ψ_E are determined by the following equation:

$$\psi_c \text{ (or } \psi_E \text{)} = e - e_{us} \qquad \text{(A-12)}$$

where e_{us} is void ratio at ultimate state at the same p of each segment in compression or extension. Calculation of $\overline{\eta}_c$ and ψ_c for each yield surface for Toyoura sand has been shown in Table (A.4).

To determine $\overline{\eta}_E$, because of lack of data, it was assumed that for each yield surface:

$$\overline{\eta}_E = m_k \overline{\eta}_c \qquad \text{(A-13)}$$

The results have been shown in Table (A.4)

5- n_H must be determined by curve fitting. This can be done by using one undrained triaxial test. As described in section 4.3, n_H (which shows the rate of variation of plastic modulus with void ratio) has a significant effect on model performance and is determined mostly by stress path. By changing the value of n_H and performing prediction, one must try to obtain the best fit to the experimental results. Based on the author's experience, usually within the first three trials, this parameter is determined. For Toyoura sand, the test with $p_i = 3$ MPa (p_i is initial mean effective stress), which has been shown in Figure (4.16), was used for determination of n_H. The value of this parameters for Toyoura sand is 9.

6- K_α, which shows the rate of variation of dilation parameter with respect to the position of yield surface, is also determined by curve fitting (i.e., changing K_u, performing prediction and comparing with experimental stress path until obtaining the best fit). The results of one undrained monotonic triaxial test on an anisotropically consolidated sample (it is suggested to use either extension test for $K_0 < 1$ or compression

test for $K_0 > 1$) or one undrained cyclic triaxial test can be used for determination of that. For Toyoura sand, using the test which has been shown in Figure 5.15, K_u is equal to 0.1.

7- Finally if one is interested to use isotropic-kinematic hardening in the model, he must determine another parameter (k). This parameter is determined by curve fitting, using one undrained triaxial test or drained triaxial test on dense sand. For typical predictions of the model which have been presented in chapter 3, it was assumed that $k = 2$.

8- Considering the formulation of the model and calibration procedure, one can see that H_{0c}, H_{0l}, $\bar{\eta}_{0c}$ and $\bar{\eta}_{0E}$ depend on a specific reference, i.e., they must be defined at a specific p_0, e_0, ψ_{ref} and α_{ll}^0. Using the following equations, all these parameters can be defined at a unique value of p_0, e_0, ψ_{ref} and α_{ll}^0 (for example $p_0 = p_{atm}$, $e_0 = 1$, $\psi_{ref} = 0$ and $\alpha_{ll}^0 = 0$, which have been used in this thesis). Then these parameters can be used as reference values in prediction.

$$H_0 = \frac{H}{(\frac{p}{p_0})^{0.5}\left[\frac{(2-e)(2+e_0)}{(2-e_0)(2+e)}\right]^{n_H}} \tag{A-14}$$

$$\bar{\eta}_0 = \bar{\eta}\exp\left[\frac{K_\alpha(\alpha_{ll}^0\alpha_{ll}^0 - \alpha_{ll}\alpha_{ll})}{g^2(\theta)m_c^2} + 5(\psi_{ref} - \psi)|\eta^3|\right] \tag{A-15}$$

Equations (A-14) and (A-15) are the same for compression and extension. For determination of plastic modulus and dilation parameter for compression and extension, the parameters related to them must be put in the equations.

In using equation (A-15), one must consider that for triaxial conditions:

$$\alpha_{ll}\alpha_{ll} = \frac{2}{3}\alpha^2 \tag{A-16}$$

$$g(\theta) = 1 \qquad \text{for triaxial compression} \qquad (A\text{-}17)$$

and $\qquad g(\theta) = m_k \qquad$ for triaxial extension $\qquad (A\text{-}18)$

This normalization has been done for Toyoura sand and the results are shown in Table (A.5). In triaxial extension, because of lack of data, the assumption was that state parameters in compression and extension are the same for each segment.

Table A.1. The results of a drained triaxial compression test on Toyoura sand (after Verdugo and Ishihara. 1996: Verdugo. 1992)

q (MPa)	ε_d (%)	p (MPa)	ε_v (%)	e
0	0	0.392	0	0.963
0.063	0.070	0.413	0.071	0.9616
0.116	0.206	0.431	0.153	0.960
0.196	0.843	0.457	0.433	0.9545
0.226	1.111	0.467	0.601	0.9512
0.29	1.854	0.489	0.988	0.9436
0.328	2.397	0.501	1.207	0.9393
0.392	3.438	0.523	1.63	0.9310
0.45	4.689	0.542	2.058	0.9226
0.486	5.55	0.554	2.313	0.9176
0.521	6.624	0.566	2.634	0.9113
0.581	8.785	0.586	3.077	0.9026
0.608	9.99	0.595	3.316	0.8979
0.639	11.432	0.605	3.627	0.8918
0.668	13.072	0.615	3.856	0.8873
0.697	14.836	0.624	4.106	0.8824
0.72	16.56	0.632	4.294	0.8787
0.748	18.744	0.641	4.513	0.8744
0.769	21.047	0.648	4.671	0.8713
0.791	23.993	0.656	4.814	0.8685
0.818	27.522	0.665	4.957	0.8657
0.836	31.378	0.671	5.008	0.8647
0.844	33.304	0.673	5.038	0.8641
0.849	36.396	0.675	5.059	0.8637
0.849	42.47	0.675	5.059	0.8637

Table A.2. Determination of m_c and α for Toyoura sand

YS	η_c	η_E	m_c	α
1	0.153	-0.069	0.129	0.024
2	0.269	-0.121	0.228	0.041
3	0.429	-0.193	0.363	0.066
4	0.484	-0.218	0.410	0.074
5	0.593	-0.269	0.503	0.090
6	0.655	-0.298	0.556	0.099
7	0.750	-0.346	0.639	0.110
8	0.830	-0.391	0.713	0.118
9	0.877	-0.421	0.757	0.120
10	0.920	-0.451	0.802	0.120
11	0.991	-0.508	0.875	0.117
12	1.022	-0.537	0.909	0.113
13	1.056	-0.572	0.950	0.106
14	1.086	-0.606	0.987	0.099
15	1.117	-0.646	1.028	0.089
16	1.139	-0.677	1.060	0.080
17	1.167	-0.720	1.101	0.066
18	1.187	-0.753	1.131	0.055
19	1.206	-0.788	1.163	0.043
20	1.230	-0.835	1.205	0.025
21	1.246	-0.868	1.233	0.013
22	1.254	-0.886	1.249	0.005
23	1.258	-0.895	1.256	0

Table A.3. Determination of plastic moduli for Toyoura sand

YS	$\dot{q}$ (MPa)	$\dot{p}$ (MPa)	$\dot{\varepsilon}_d$ (%)	$\dot{\varepsilon}_v$ (%)	p (MPa)	e	η_t	G (MPa)	H_c (MPa)	η_E	H_E (MPa)
1	0.053	0.018	0.136	0.082	0.431	0.960	0.269	47.02	59.511	-0.121	69.065
2	0.08	0.026	0.637	0.28	0.457	0.9545	0.429	48.99	11.910	-0.193	15.184
3	0.03	0.01	0.268	0.168	0.467	0.9512	0.484	49.88	10.052	-0.218	13.384
4	0.064	0.022	0.743	0.387	0.489	0.9436	0.593	51.88	6.936	-0.269	10.099
5	0.038	0.012	0.543	0.219	0.501	0.9393	0.655	53.0	5.427	-0.298	8.039
6	0.064	0.022	1.041	0.423	0.523	0.9310	0.750	55.12	4.297	-0.346	7.097
7	0.058	0.019	1.251	0.428	0.542	0.9226	0.830	57.12	3.051	-0.391	5.273
8	0.036	0.012	0.861	0.255	0.554	0.9176	0.877	58.37	2.620	-0.421	4.758
9	0.035	0.012	1.074	0.321	0.566	0.9113	0.920	59.79	1.930	-0.451	3.701
10	0.06	0.02	2.161	0.443	0.586	0.9026	0.991	61.96	1.561	-0.508	3.141
11	0.027	0.009	1.205	0.239	0.595	0.8979	1.022	63.05	1.221	-0.537	2.528
12	0.031	0.01	1.442	0.311	0.605	0.8918	1.056	64.40	1.155	-0.572	2.414
13	0.029	0.01	1.64	0.229	0.615	0.8873	1.086	65.54	0.888	-0.606	2.004
14	0.029	0.009	1.764	0.25	0.624	0.8824	1.117	66.70	0.851	-0.646	1.829
15	0.023	0.008	1.724	0.188	0.632	0.8787	1.139	67.65	0.631	-0.677	1.511
16	0.028	0.009	2.184	0.219	0.641	0.8744	1.167	68.74	0.621	-0.720	1.429
17	0.021	0.007	2.303	0.158	0.648	0.8713	1.187	69.56	0.423	-0.753	1.020
18	0.022	0.008	2.946	0.143	0.656	0.8685	1.206	70.39	0.319	-0.788	0.849
19	0.027	0.009	3.529	0.143	0.665	0.8657	1.230	71.29	0.340	-0.835	0.851
20	0.018	0.006	3.856	0.051	0.671	0.8647	1.246	71.76	0.204	-0.868	0.517
21	0.008	0.002	1.926	0.03	0.673	0.8641	1.254	71.95	0.212	-0.886	0.433
22	0.005	0.002	3.092	0.021	0.675	0.8637	1.258	72.12	0.060	-0.895	0.187
23	0	0	6.074	0	0.675	0.8637	1.258	72.12	1E-6	-0.895	1E-6

Table A.4. Determination of dilation parameters for Toyoura sand

YS	B (MPa)	η_c	$\overline{\eta}_c$	ψ_c	$\overline{\eta}_L$
1	31.35	0.269	0.399	0.0803	0.285
2	32.66	0.429	0.682	0.0772	0.487
3	33.25	0.484	1.134	0.0748	0.810
4	34.59	0.593	1.116	0.0692	0.797
5	35.33	0.655	1.033	0.0660	0.738
6	36.75	0.750	1.182	0.0597	0.844
7	38.08	0.830	1.209	0.0530	0.864
8	38.91	0.877	1.203	0.049	0.859
9	39.86	0.920	1.272	0.0437	0.909
10	41.31	0.991	1.223	0.0368	0.874
11	42.03	1.022	1.255	0.0329	0.897
12	42.93	1.056	1.324	0.0276	0.946
13	43.69	1.086	1.299	0.0239	0.892
14	44.47	1.117	1.290	0.0198	0.921
15	45.1	1.139	1.269	0.0168	0.907
16	45.83	1.167	1.289	0.0132	0.920
17	46.37	1.187	1.269	0.0107	0.906
18	46.93	1.206	1.262	0.0086	0.902
19	47.53	1.230	1.277	0.0065	0.912
20	47.84	1.246	1.259	0.0060	0.899
21	47.97	1.254	1.272	0.0056	0.909
22	48.08	1.258	1.265	0.0053	0.904
23	48.08	1.258	1.258	0.0053	0.898

Table A.5. Model parameters for Toyoura sand

$G_0 = 21$ MPa $\qquad B_0 = 14$ MPa $\qquad m_k = 0.714$

$n_H = 9.0$ $\qquad K_\alpha = 0.1$

YS	m_c	α	H_{0c} (MPa)	H_{0E} (MPa)	$\overline{\eta}_{0c}$	$\overline{\eta}_{0E}$
1	0.129	0.024	17.848	20.713	0.395	0.283
2	0.228	0.041	3.253	4.147	0.660	0.480
3	0.363	0.066	2.614	3.480	1.085	0.794
4	0.410	0.074	1.614	2.350	1.036	0.773
5	0.503	0.090	1.187	1.758	0.940	0.710
6	0.556	0.099	0.836	1.381	1.040	0.803
7	0.639	0.11	0.529	0.915	1.037	0.814
8	0.713	0.118	0.425	0.771	1.018	0.806
9	0.757	0.120	0.288	0.553	1.071	0.851
10	0.802	0.120	0.208	0.418	1.021	0.816
11	0.875	0.117	0.153	0.316	1.052	0.839
12	0.909	0.113	0.134	0.280	1.124	0.890
13	0.950	0.106	0.097	0.219	1.071	0.842
14	0.987	0.099	0.087	0.188	1.123	0.875
15	1.028	0.089	0.062	0.148	1.121	0.866
16	1.060	0.080	0.058	0.132	1.160	0.885
17	1.101	0.066	0.038	0.091	1.160	0.877
18	1.131	0.055	0.027	0.073	1.171	0.877
19	1.163	0.043	0.028	0.070	1.202	0.892
20	1.205	0.025	0.017	0.042	1.188	0.881
21	1.233	0.013	0.017	0.035	1.204	0.891
22	1.249	0.005	0.005	0.015	1.200	0.886
23	1.256	0	1E-6	1E-6	1.193	0.881

Figure. A.1. Variation of deviatoric stress versus shear strain in drained triaxial compression test on Toyoura sand.
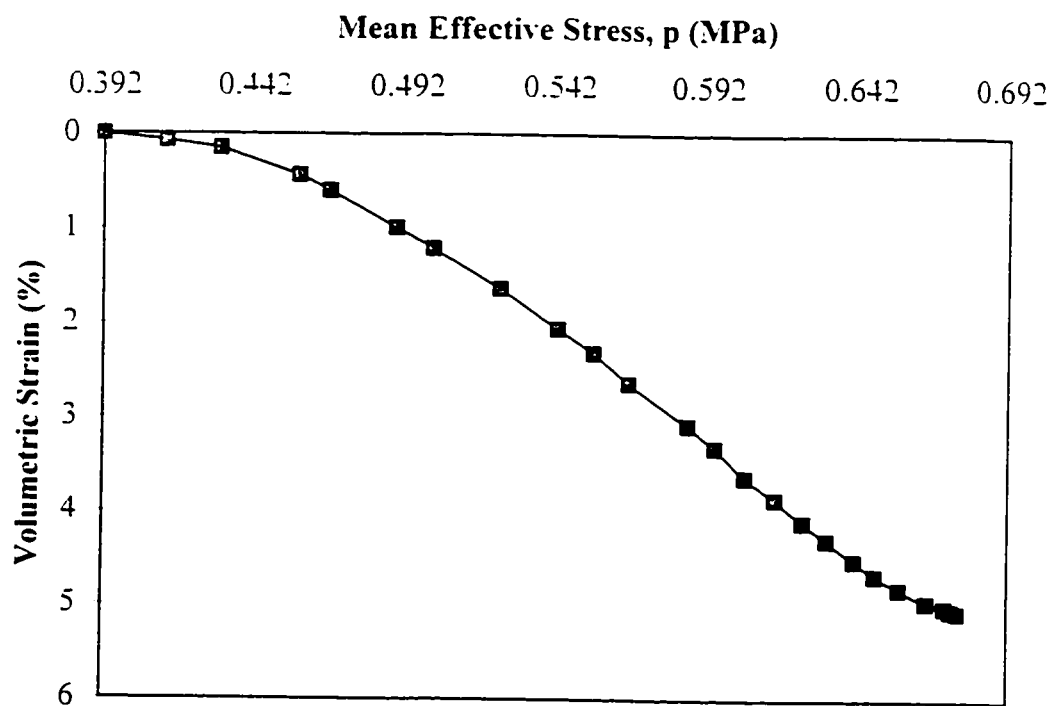

Figure A.2. Variation of mean effective stress versus volumetric strain in drained triaxial compression test on Toyoura sand.
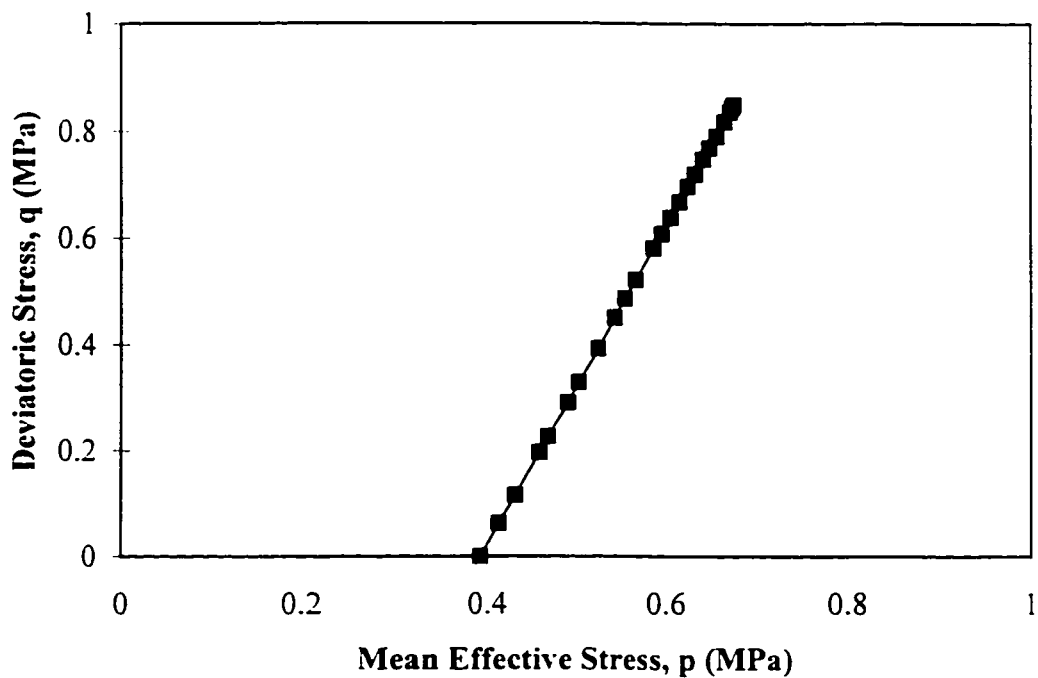
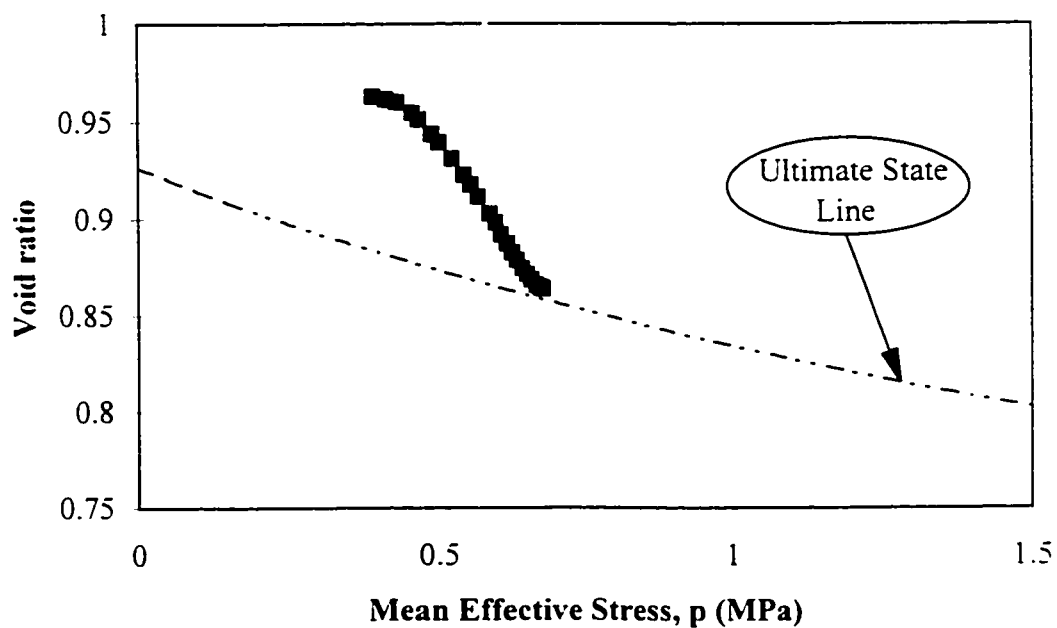**Figure A.3.** Stress path in drained triaxial compression test on Toyoura sand.

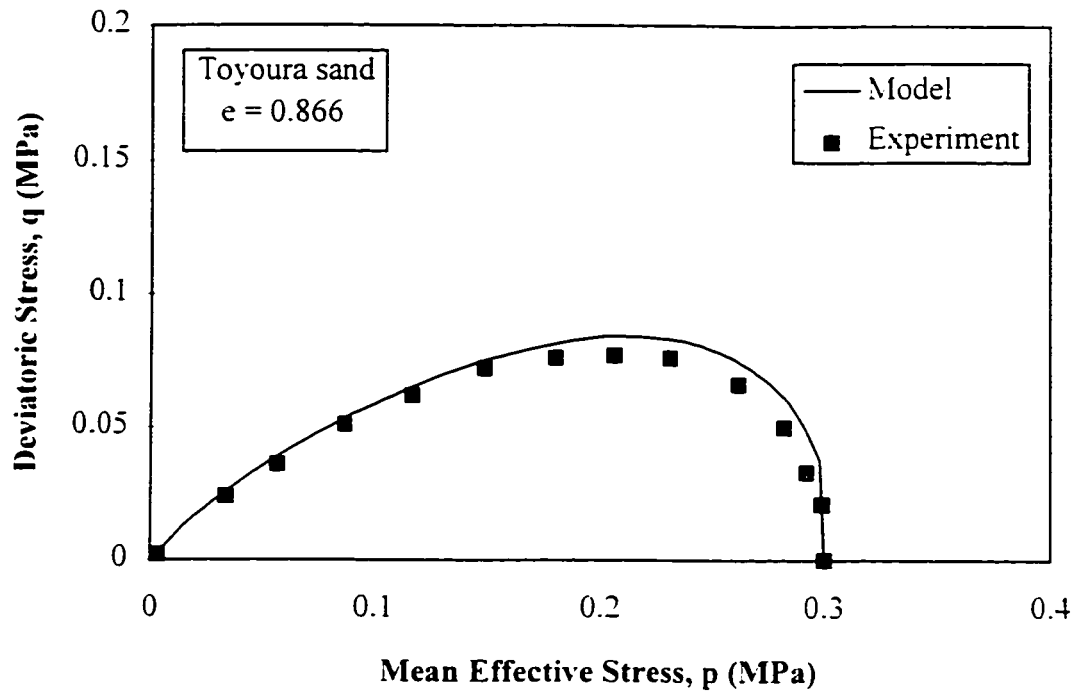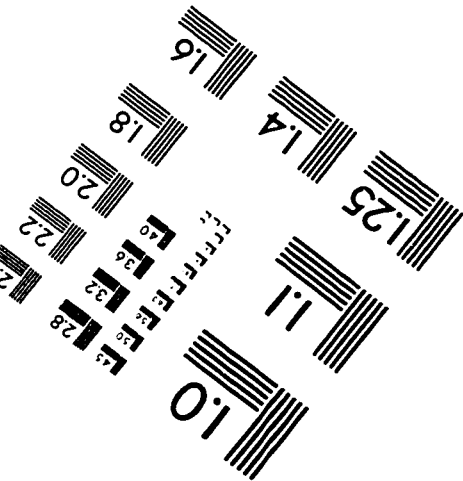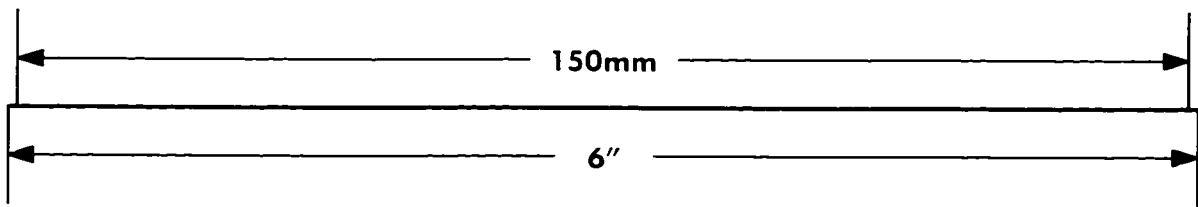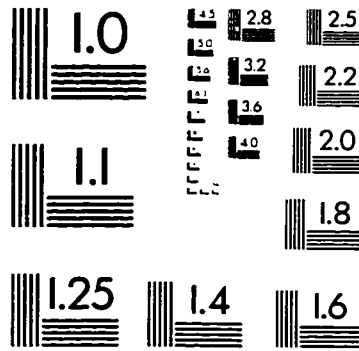**Figure A.4.** Variation of void ratio versus mean effective stress in drained triaxial compression test on Toyoura sand.
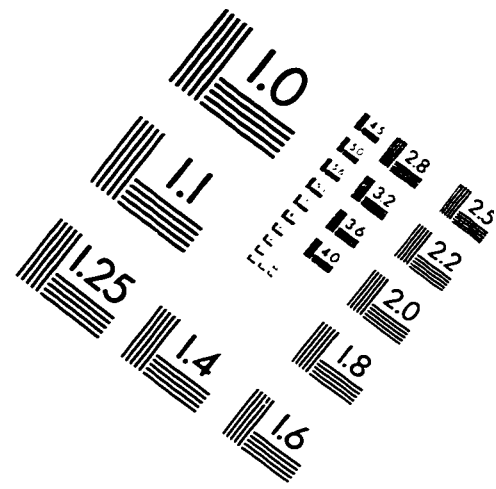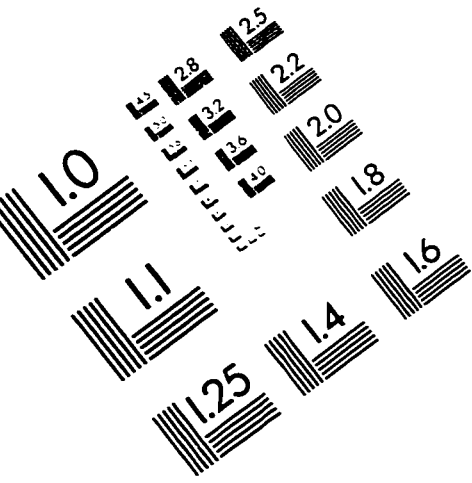
Figure A.5. Curve fittining for determination of parameters of the model in triaxial extension for Toyoura sand.

IMAGE EVALUATION
TEST TARGET (QA-3)

150mm

6"